

Design and Analysis of an adaptive λ -Tracking Controller for powered Gearshifts in automatic Transmissions

Dissertation

zur Erlangung des akademischen Grades

Doktoringenieur

(Dr.-Ing.)

vorgelegt

an der Fakultät Verkehrswissenschaften "Friedrich List"

der Technischen Universität Dresden

von

Peter Loepelmann, M.Sc.

geboren am 18. Februar 1985 in Perleberg

Erstgutachter: Prof. Dr.-Ing. Bernard Bäker

Zweitgutachter: Prof. Dr.-Ing. Hans-Christian Reuss

Datum der öffentlichen Verteidigung: 14. November 2014

Abstract

To meet the continuously increasing goals in vehicle fuel efficiency, a number of measures are taken in automotive powertrain engineering, such as the combination of electric drives and conventional combustion engines in hybrid vehicles or the increase in gear ratios. This development leads to more complex powertrain systems, such as automatic transmissions. At the same time, the need for complex control systems is increased to achieve this desired functionality.

Automatic transmissions are controlled by an electro-hydraulic control unit that governs all operations such as gear shifting and starting. Since most of the control software is designed in the form of open-loop control, most of the operations have to be calibrated manually. Thus, there exists a large number of calibration parameters in the control software that have to be tuned individually for each combination of engine, transmission and vehicle model. This process is therefore time-consuming and costly. Hence, it would be advantageous to reduce the need for calibration and in the end shorten the development process for automatic transmissions by reducing software complexity while maintaining functionality and performance.

The goal of this thesis is to replace parts of the control software responsible for conducting the gearshifts that require extensive tuning by implementing control systems that have no need for calibration: adaptive high-gain λ -tracking controllers. In order to obtain the control parameters, i.e., the feedback gains, without calibration, an adaption law is implemented that continuously computes these parameters during operation of the controller. Thus, calibration is no longer needed. Since the system has to be high-gain-stabilizable, an extensive system analysis is conducted to determine whether an adaptive λ -tracking controller can be implemented. A nonlinear model of the clutch system dynamics is formulated and investigated. As a result, high-gain stability is proven for the system class and validated in simulation. Following the stability analysis, the devised adaptive controller is implemented into the control software running on the series production transmission control unit. Extensive simulations with a comprehensive vehicle model running the extended transmission software are conducted to design and to test the adaptive controllers and their underlying parameters during transmission operation in order to evaluate the control performance. The control software containing the adaptive controller is then implemented in two distinct vehicles with different automatic transmissions equipped with series production control hardware for the purpose of hardware experiments and validation. The resulting reduction of calibration efforts is discussed.

Contents

Glossary	VII
1 Introduction	1
1.1 Motivation	1
1.2 Calibration of Gearshifts	2
1.3 Thesis Outline	7
2 Fundamentals of Adaptive Control	9
2.1 Linear Control Systems	9
2.1.1 System Class	9
2.1.2 Control Architecture	9
2.1.3 Stability of LTI Systems	11
2.1.4 Classic adaptive Controllers	11
2.1.5 Other adaptive Controllers	17
2.1.6 High-gain Feedback Stability	19
2.2 Nonlinear Control Systems	23
2.2.1 System Class and Control Architecture	23
2.2.2 High-Gain Feedback Stability	23
3 System Analysis	29
3.1 Automatic Transmissions with powered Gearshifts	29
3.1.1 FDCT Dual-Clutch Transmission	29
3.1.2 NAG3 Automatic Transmission	31
3.1.3 Shift Quality	32
3.2 System Modeling	33
3.2.1 Hydraulic System	35
3.2.2 Mechanical Subsystem	39
3.3 Stability Analysis	41
3.3.1 System Class	41
3.3.2 Relative Degree	43

3.3.3	Minimum-Phase Property	45
3.3.4	Sign of High-Frequency Gain	49
3.4	Requirements of Control Architecture	50
3.4.1	Feedback Structure	50
3.4.2	Requirements of Adaption Law	51
4	Control Design	53
4.1	Software Integration	53
4.1.1	Adaptive Control during Gearshifts	53
4.1.2	Constrained Shift	54
4.1.3	Release Shift	55
4.1.4	Simulation Environment	56
4.2	Adjustment of Adaptive Controller	57
4.2.1	Integral Control Feedback	57
4.2.2	Scaling of Adaption Dynamics	60
4.2.3	Anti-Windup Measures	62
4.3	Parameter Studies	63
4.3.1	Gain Coefficient κ	65
4.3.2	Gain Coefficient η	67
4.3.3	λ -Neighborhood	68
4.3.4	Coefficient ε	70
4.3.5	Decrease Gain Coefficient σ	70
4.3.6	Waiting Time t_d	72
4.3.7	Initialization k_0	73
4.3.8	Increase Gain Coefficient γ	74
4.4	Counteractive Adaption Law Dynamics	76
4.5	Fully Exponential Adaption Law	80
4.6	Digital Control Integration	84
4.6.1	Hardware Constraints	84
4.6.2	Derivative Feedback Control	86
4.7	Engine Intervention Control	91
5	Vehicle Experiments: Comparative Study	95
5.1	FDCT Dual-Clutch Transmission	96
5.1.1	Traditional Control	97
5.1.2	Adaptive Control	102

5.1.3	Comparison of Shift Duration	109
5.2	NAG3 Automatic Transmission	115
5.2.1	Traditional Control	116
5.2.2	Adaptive Control	121
5.2.3	Comparison of Shift Duration	128
5.3	Exemplary Shifts during Coasting	133
6	Discussion and Conclusions	137
6.1	Summary	137
6.2	Results	138
6.2.1	Stability	139
6.2.2	Control Performance	139
6.2.3	Applicability to Series Production Hardware	140
6.2.4	Reduction of Calibration Efforts	140
6.3	Outlook	141
6.3.1	Adaptive Control Architecture	142
6.3.2	Other Components	144
6.3.3	Evaluation of Calibration Efforts	145
	Bibliography	147
	List of Figures	153
	List of Tables	157
	Acknowledgments	159

Glossary

Some of the notations in this thesis are taken from the mathematical background of the control theory. For example, the error signal is referred to as $e(\cdot)$ if the overall signal is concerned, whereas $e(t)$ refers to a specific value of the control error at time t . This notation is used for other signals as well.

Vectors and matrices are boldfaced. The notation $:=$ is used to define parameters and signals.

$\textcircled{1}, \textcircled{2}, \textcircled{3}, \dots, \textcircled{9}, \textcircled{R}$	engaged gear
$a(\cdot)$	longitudinal acceleration
$\mathbf{A} \in \mathbb{R}^{n \times n}$	state matrix
$\mathbf{A}_B \in \mathbb{R}^{n \times n}$	state matrix of subsystem \textcircled{B}
A_1, A_2	control areas in hydraulic control valve
A_{fric}	surface area of clutch friction pairings
$A_{\text{in}}(\cdot)$	cross section of hydraulic inlet aperture
$A_{\text{out}}(\cdot)$	cross section of hydraulic outlet aperture
A_{pist}	piston surface area
A_S	signal attenuation
$\mathbf{B} \in \mathbb{R}^{n \times m}, \mathbf{b} \in \mathbb{R}^n$	input matrix, input vector
$\mathbf{b}_B \in \mathbb{R}^n$	input vector of subsystem \textcircled{B}
c_{CV}	spring rate of control valve return spring
c_{pist}	spring rate of clutch piston return spring
$\mathbf{C} \in \mathbb{R}^{r \times n}, \mathbf{c} \in \mathbb{R}^r$	output matrix, output vector
$\mathbf{c}_B \in \mathbb{R}^r$	output vector of subsystem \textcircled{B}
C_i	electromagnetic coefficient
C_{hyd}	hydraulic coefficient
$\mathbf{d}(\mathbf{x}(t))$	nonlinear disturbance vector
$\mathbf{d}_A(\mathbf{x}_A)$	nonlinear disturbance vector of subsystem \textcircled{A}
\mathbf{d}_B	disturbance vector of subsystem \textcircled{B}
d_c	viscous damping coefficient of clutch disks
d_{CV}	viscous damping coefficient of control valve piston

d_{pist}	viscous damping coefficient of clutch piston
D_{es}	energy spectral density
D_v	vibration dose value
$e(\cdot)$	error signal
$e_1(\cdot)$	error signal during upshifts
$e_2(\cdot)$	error signal during downshifts
e_ν	error signal, time-discrete
E	Young's modulus of oil
$\mathbf{f}(\mathbf{x}(t))$	nonlinear system state vector
$\mathbf{f}_A(\mathbf{x}_A)$	nonlinear system state vector of subsystem (A)
$\vec{F}_{\text{el}}(\cdot)$	electromagnetic force
$\vec{F}_{\text{friction}}(\cdot)$	viscous friction force
$\vec{F}_{\text{p,Cl}}(\cdot)$	force generated by clutch pressure feedback
$\vec{F}_{\text{spring}}(\cdot)$	return spring force
$\mathbf{g}(\mathbf{x}(t))$	nonlinear system input vector
$\mathbf{g}_A(\mathbf{x}_A)$	nonlinear system input vector of subsystem (A)
$G_{\text{tf}}(\cdot)$	transfer function
G_s	autopower spectrum
$H(\cdot)$	Heaviside function
$\mathbf{h}(\mathbf{x}(t))$	nonlinear system output vector
$\mathbf{h}_A(\mathbf{x}_A)$	nonlinear system output vector of subsystem (A)
$i(\cdot)$	electric current
i_g	current gear ratio
i_{max}	maximum electric current
$I(\cdot)$	integral feedback term
$\mathbf{I}_m \in \mathbb{R}^{m \times m}$	identity matrix of order m
I_ν	integral feedback term, time-discrete
I_0	initial integral feedback value
J_{in}	combined mass moment of inertia at transmission input shaft
J_D	mass moment of inertia of clutch input shaft
J_L	mass moment of inertia of clutch output shaft
J_{out}	combined mass moment of inertia of vehicle mass and output shaft
$k(\cdot)$	common gain factor
k_0	initial common gain factor value
$k_1(\cdot)$	common gain factor during upshifts
$k_2(\cdot)$	common gain factor during downshifts

k_{diff}	gradient of common gain factor, time-discrete
k_P	proportional feedback gain
k_P^*	proportional feedback gain, above which high-gain feedback stabilization is achieved
k_ν	common gain factor, time-discrete
$K(\cdot)$	generalized common gain factor
L_g, L_f	Lie derivatives of $\mathbf{g}(\mathbf{x}(t)), \mathbf{f}(\mathbf{x}(t))$
L_{out}	angular momentum of transmission output shaft
m_{CV}	mass of control valve piston
m_{pist}	mass of clutch piston
$M_{\text{coup}}(\cdot)$	coupling torque
$M_D(\cdot)$	driving torque
$M_{\text{Eng}}(\cdot)$	engine drive torque
$M_L(\cdot)$	load torque
$M_{\text{Veh}}(\cdot)$	combined load torque of vehicle, corresponding to combined drive resistances
n	system order
$n_{\text{Eng}}(\cdot)$	engine speed
n_A, n_B	order of subsystems $\textcircled{A}, \textcircled{B}$
N	filter order
p_a	accelerator pedal value
$p_{\text{Cl}}(\cdot)$	clutch pressure
p_{OS}	oil sump pressure
p_{SP}	system supply pressure
$P(\cdot)$	proportional feedback term
P_ν	proportional feedback term, time-discrete
$Q_{\text{CV}}(\cdot)$	volume current generated by control valve
$Q_d(\cdot)$	hydraulic flow disturbance
$Q_{\text{in}}(\cdot)$	volume current flowing into clutch piston volume
$Q_{\text{out}}(\cdot)$	volume current flowing out of clutch piston volume
r_m	mean friction radius
\vec{r}_s	position vector
$s(\cdot)$	control valve piston position
$s_d \in \mathbb{C}$	complex number for digital controller
s_{hf}	sign of high-frequency gain
$s_{\text{max}}, s_{\text{min}}$	end positions of control valve piston

Glossary

t	time
t_{1-4}	time constants subject to calibration
t_e	time at which the system output signal entered the λ -neighborhood
t_d	waiting time, duration of stay
t_{dur}	desired shift duration
$t_{\text{dur},1}$	desired shift duration during upshifts
$t_{\text{dur},2}$	desired shift duration during upshifts
t_l	time at which a control output limit has been reached
T	digital sampling time
$\mathbf{u} \in \mathbb{R}^m$	control input vector
$u(\cdot)$	control signal
u_ν	control signal, time-discrete
$u_{\text{max}}, u_{\text{min}}$	control signal limits
u_A	control input of subsystem \textcircled{A}
v_1, v_2	maximum velocities of control valve piston
V	volume of clutch piston chamber
$\mathbf{x} \in \mathbb{R}^n$	system state vector
$\mathbf{x}_A, \mathbf{x}_B \in \mathbb{R}^n$	system state vector of subsystems \textcircled{A} , \textcircled{B}
$x(\cdot)$	clutch piston position
$\mathbf{y} \in \mathbb{R}^r$	system output vector
$y(\cdot)$	system output signal
$y_A(\cdot)$	system output signal of subsystem \textcircled{A}
$y_{\text{ref}}(\cdot) \in C^n, \quad n \in \mathbb{N}$	reference trajectory
y_ν	system output signal, time-discrete
$y_{\text{ref},\nu}$	reference trajectory, time-discrete
z	number of friction pairings of clutch disks
z_d	z-transformed complex number
z_k	zeros of subsystem \textcircled{B}
\mathbf{Z}	matrix of zeros of a system
α	flow coefficient
γ	coefficient to influence adaption speed
δ	relative degree
δ_A, δ_B	relative degree of subsystems \textcircled{A} , \textcircled{B}
δ_{eff}	effective relative degree on a macroscopic scale

Δ	term indicating counteracting behavior of proportional and integral feedback terms
Δf	frequency resolution
ΔT	time period for computation of D_{es}
Δ_ν	term indicating counteracting behavior of proportional and integral feedback terms, time-discrete
ε	coefficient for smaller error neighborhood
η	gain coefficient for integral feedback term
κ	gain coefficient for derivative feedback term
λ	error neighborhood
λ_τ	error neighborhood parameter for funnel control
μ	coefficient of sliding friction
ξ, η_I	nonlinear function vectors
ρ	density of oil
σ, σ_d	coefficient for decrease term in adaption laws
σ_i	coefficient for increase term in fully exponential adaption law
$\sigma_f(\cdot)$	adaption coefficient for adaptive fuzzy control
$\Sigma(\cdot)$	generalized integral feedback term
τ	time parameter for funnel control
$\varphi_1(\cdot)$	coordinate of motion, input shaft
$\varphi_2(\cdot)$	coordinate of motion, output shaft
$\dot{\varphi}_{in}(\cdot)$	angular velocity of transmission input shaft during fixed gear
$\dot{\varphi}_{out}(\cdot)$	angular velocity of transmission output shaft
$\phi_i(\mathbf{x}), z_i, a(\mathbf{z}), b(\mathbf{z}), q_i(\mathbf{z})$	nonlinear functions
$\Phi(\mathbf{x})$	nonlinear function vector
$\omega_{rel}(\cdot)$	relative speed of clutch disks
$\omega_{eng}(\cdot)$	engine speed
ω_E	end value of engine speed signal
$\omega_{c,d}$	cut-off frequency
$\omega_{s,d}$	stopband frequency
ω_S	start value of engine speed signal
B05, B06, B08	brakes of NAG3 transmission
CAN	Control Area Network
ECU	electronic control unit
K1, K2	clutches of FDCT transmission

Glossary

K27, K38, K81	clutches of NAG3 transmission
LTI	linear time-invariant
MIMO	multiple-input, multiple-output
PID	proportional, integral, derivative
SiL	software-in-the-loop
SISO	single-input, single-output
TCU	transmission control unit

1 Introduction

First, the motivation for this thesis is provided and an overview of the work is given. Also, the topic of calibration of automotive control software is introduced. The chapter concludes with the problem definition and thesis outline.

1.1 Motivation

The past years have seen a growing concern in reducing the CO₂-emissions and in improving the fuel efficiency of passenger cars and commercial vehicles. To meet the ambitious goals in vehicle fuel consumption, energy efficiency has become of the essence in automotive engineering, especially in the design of powertrain systems (see [Grim 13]). In order to achieve these goals, a number of measures are taken, such as the combination of electric drives and conventional combustion engines in hybrid vehicles (see [TiRE 12]) or the increase in gear ratios in automotive transmissions (see [DöHI 13]). This leads to an increase in overall powertrain efficiency, since the combustion engine can be operated closer to its energy-optimal set point in a wider range of driving situations (see [FiJK 12]). However, this development also leads to more complex powertrain systems, such as in automatic transmissions. At the same time, the need for complex control systems is increased (see [RöBK 12]).

Automatic transmissions are controlled via an electro-hydraulic control unit that conducts all operations such as gear shifting, vehicle pull away and fault diagnosis. Since most of the control software is designed in the form of open-loop control, most of the operations have to be calibrated manually. Thus, some form of a-priori knowledge is required. This is done in order to ensure the desired system performance regarding speed and comfortability in a wide range of driving and operating scenarios. As a result, there is a vast number of calibration parameters in the control software that have to be tuned individually for each combination of engine, transmission and vehicle model.

1.2 Calibration of Gearshifts

Reducing the calibration efforts is a continuing goal in improving the development process for powertrain systems. In order to show the magnitude of the calibration process, a common gearshift procedure is considered.

The automatic transmissions discussed in this thesis are capable of switching gears while providing a continuous torque to the output driveshaft. They are designed with multiple sets of gears to engage different gear ratios. These gear set combinations are engaged with the help of multiple friction clutch actuators that can be operated in a powered state to ensure continuity of drive torque. When switching the gear ratio, one clutch supporting the current gear has to be disengaged while a second clutch, responsible for the next gear, has to be engaged. The friction clutches are electro-hydraulically actuated. The control pressure of a hydraulic fluid, which is controlled via an electrically actuated control valve, exerts a force on the clutch piston in order to push the friction disks together and transmit the drive torque from one side of the clutch to the other. A common powered upshift procedure is carried out as follows:

First, the disengaging clutch is moved into a state with low slippage, so that the current torque is still transmitted. At the same time, the engaging clutch is filled with hydraulic oil and moved to the touch point, where it does not yet transmit any torque. After this state is achieved, the torque handover phase is conducted. The disengaging clutch reduces its pressure and transmitted torque, while the engaging clutch further increases its pressure and its respective ability to transmit the drive torque. At the end of the handover phase, the disengaging clutch is fully released and the engaging clutch is now transmitting the full torque while still being in a slipping state. Now the engine speed has to be reduced to the level that is characteristic for the new gear ratio. To achieve this, the clutch pressure is further increased to act as a break in order to reduce relative speed at the clutch to zero. During this procedure, certain functions in the transmission control software are active to force a certain gradient of the engine speed and to simultaneously reduce the drive torque generated by the combustion engine. After the relative speed at the engaging clutch has been reduced to zero, the gearshift procedure is complete. During the gearshift process, numerous disturbances and uncertainties are present that cannot be measured and accounted for. For example, the current clutch pressure, friction coefficients and actual torque capacities are unknown. Also, there exists a number of varying influences such as temperature, total vehicle mass, as well as wear and tear effects, that have a major effect on the shifting quality in a passenger car. Therefore, tuning the transmission control software is a complex task. During the calibration process, a vast number of pa-

rameters is tuned that are used later during a specific situation. This is done in an effort to ensure the same shifting quality in different driving situations. Figure 1.1 shows some exemplary time constants that have to be tuned during the calibration process. Various

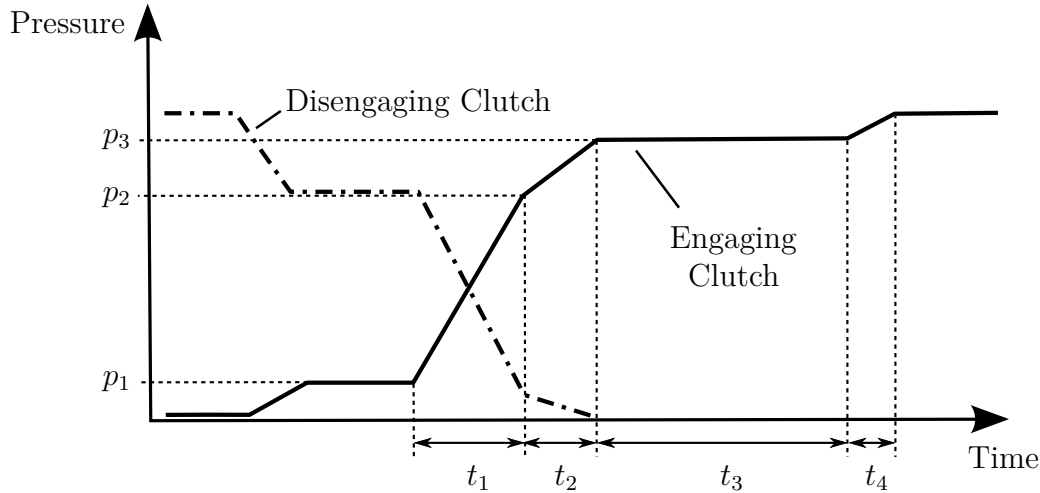


Figure 1.1: Exemplary plot of clutch pressures versus time of a common powered upshift procedure, including some exemplary time constants $t_1 - t_4$ and pressure values $p_1 - p_3$ that are subject to calibration

methods are conceivable to expedite the calibration process.

One possibility is to use a detailed system model for simulation purposes and tune the calibration parameters in a software-in-the-loop (SiL) environment. This set of pre-tuned parameters can be used for the actual calibration process using a vehicle with the actual powertrain hardware. If the system model is sufficiently detailed, this method can contribute to reducing the classic calibration efforts. However, it is a very complex task to obtain a precise system model that can be used for the characterization of a simulated shift procedure. Also, the shifting quality is very subjective and cannot be easily simulated.

Another method is to conduct automated calibration procedures on a test-bench, where the complete powertrain is assembled and can be tested using a number of different load scenarios to assess the shifting quality (see [BSEA 08]). An optimization method would have to be implemented in order to determine the next set of calibration parameters that would improve the shifting quality. Thus, calibration parameters could be tuned automatically. However, this generates the need for a complex and costly test-bench system. Again, the characterization of the shifting quality is quite subjective and therefore not easy to emulate in a sensor evaluation algorithm that would feed into the optimization process. Hence, an automated calibration approach is also not optimal when trying to

reduce the calibration efforts.

A completely different approach is to avoid the calibration process altogether, rather than shortening or automating it. The large number of calibration parameters is due to the fact that most of the transmission control software is designed in the form of open-loop control. This results in the need to specify control values for numerous operation scenarios, such as the time constants $t_1 - t_4$ and pressure constants $p_1 - p_3$ depicted in Fig. 1.1, in order to achieve the desired system behavior. When applying closed-loop control systems, the controller uses a feedback signal of the system output to generate an error value and to compute a suitable control value. Nonetheless, the control parameters also have to be pre-specified and would therefore be part of the calibration process. This deficiency can be overcome by incorporating adaptive controllers into the transmission control software. They use an adaptation law to continuously compute the control parameters and thus eliminate the need for calibration (see [ÅsWi 89], [Ilch 91]). This approach is pursued in this thesis.

In the following, various methods for calibration are examined, as well as strategies to shorten or even to circumvent the calibration process.

When considering gearshift procedures, the main goal is to achieve fast shifts while ensuring shift comfort. This is to be achieved for a wide range of different driving situations. Some exemplary environmental and systemic influences that can change quickly and have a rather large effect on the shifting quality are:

- current engine speed: 600 min^{-1} to 7000 min^{-1} ,
- current engine torque: -70 Nm to 1000 Nm ,
- temperature of transmission oil: -40°C to 100°C ,
- total vehicle mass, including tow load: 1500 kg to 7000 kg ,
- wear and tear of transmission components, such as friction clutch disks or contaminations in the hydraulic fluids.

Therefore, the shifting quality has to be calibrated for each unique set of these conditions.

Manual Calibration

The most common procedure in powertrain engineering is to conduct a manual calibration of the respective system, such as gearshifts in automatic transmissions. Thus, the calibration process benefits from an experienced engineer, who is able to evaluate the shifting

quality while driving and making the appropriate changes in the calibration parameters, if necessary. This is to be repeated for every conceivable system state, e.g. driving situation, that the transmission may encounter. Therefore, this process is very costly and time-consuming.

Automated Calibration

In order to reduce the need for manual calibration, there have been efforts to automatically conduct a calibration of transmission control units with the help of a test-bench (see [Stef07], [BSEA 08], [KKAG 09]). A complete powertrain system can be operated as if it was driving on the road and the calibration parameters can be changed according to a test plan. During the process, the shift quality is evaluated by an algorithm that generates a grade for each shift conducted by the test-bench and changes the calibration parameters in order to optimize the shift quality. Thus, an optimization algorithm is in operation that substitutes the calibration engineer for evaluation of shift quality.

This automated calibration approach is advantageous with respect to reproducibility of system states, since all environmental parameters can be controlled on a test-bench. Therefore, the calibration can be conducted efficiently with less test runs to verify the chosen parameters. However, an automated calibration test-bench is also quite costly and has to run for a certain time for the optimization algorithm to obtain a conclusive shift quality evaluation.

Model-based Calibration

Another possibility is to conduct calibration procedures without any powertrain hardware. Instead, a simulated powertrain environment is used. This requires a detailed model of the powertrain system and the transmission control unit (see [ScKB 05], [Crew 07], [LaKr 10]). If available, this enables the engineer to conduct certain parts of the calibration in a simulation environment, so no costly test-bench or vehicle is needed. However, the need for a detailed system model is difficult to meet. Obtaining a system model with the complexity of a complete vehicle powertrain is a demanding task. Numerous measurements of individual system dynamics would be required for model verification and validation purposes. This is also very time-consuming and therefore not feasible. Also, the evaluation of the shift quality – which is highly subjective – is difficult to do with the help of simulated data.

Adaptive Control

A completely different approach is to avoid calibration altogether. It is required mostly for open-loop controllers, so that they can be operated with the desired performance regarding speed and comfortability during different system states, in this case, driving situations. If closed-loop controllers are applied, they automatically react to changing system parameters and disturbances. However, the control parameters, for example the proportional, integral and derivative gains of a PID-controller, still have to be calibrated. Also, in order to achieve the desired performance in different driving situations, these parameters would have to be calibrated for each individual situation. This deficiency can be overcome with the help of adaptive controllers (see [ÅWi89]). They use an adaptation law to continuously compute the control parameters and are therefore able to quickly react to changes in the system or environmental parameters. This in return enables them to be applied to a system with only partial knowledge of the system parameters. This way, they can contribute to the reduction of the calibration efforts, if they can be incorporated into the transmission control software.

Goal of Thesis

The aim of this thesis is to reduce calibration efforts of automatic transmission control software in replacing traditional open-loop controllers by adaptive high-gain feedback controllers that require very little calibration. Hence, software complexity is supposed to be reduced while functionality has to be maintained. The newly devised controllers are designed and evaluated regarding

- stability of the closed-loop control architecture,
- control performance,
- feasibility of application in series production control hardware, and
- potential to reduce calibration efforts.

In order to achieve sufficient control performance, different feedback structures and various adaptation laws are investigated. The goal is to at least recreate the shift quality and speed achieved by the current traditional control software while reducing the number of calibration parameters. Hence, the advantage gained by reduced calibration efforts is not to be impaired by diminished control performance.

1.3 Thesis Outline

After these introductory remarks (Chapter 1), the theory and state of the art of adaptive control is discussed (Chapter 2). Both linear and nonlinear system theory with regard to adaptive λ -tracking control is discussed. Thus, the tools for analyzing the clutch control system and for designing suitable adaptive controllers are given. The following chapter provides an overview over the automatic transmissions considered in this thesis and forms the theoretical basis of adaptive control for application in automatic transmissions (Chapter 3). A nonlinear system model is obtained via a set of ordinary differential equations and its stability regarding high-gain feedback control is investigated. Based on the discoveries, controller requirements are derived. In Chapter 4, the adaptive control algorithms are designed and integrated into the transmission control software. The control parameters are calibrated and the intricacies of the digital control implementation are discussed. The design process is accompanied by simulations of gearshifts in a SiL environment. The devised adaptive controller is tested in vehicle experiments and compared to simulation in Chapter 5. Two distinct powertrains with two different transmissions are compared while running the same adaptive controller in the control software to conduct gearshifts. Both shift quality and shift speed are investigated. Finally, Chapter 6 concludes the work by evaluating the results. The potential to reduce calibration efforts is discussed and an overview of future work in the field of adaptive control in automatic transmissions is given.

2 Fundamentals of Adaptive Control

In this chapter, the principle of adaptive high-gain feedback control is introduced along with the theoretical background and stability investigation methods for both linear and nonlinear systems. Exemplary adaptive controllers are discussed.

2.1 Linear Control Systems

First, an introduction into linear system theory is given and basic high-gain feedback controllers are considered along with the stability requirements.

2.1.1 System Class

Consider a linear time-invariant (LTI) system:

$$\left. \begin{aligned} \dot{\mathbf{x}}(t) &= \mathbf{A} \mathbf{x}(t) + \mathbf{B} \mathbf{u}(t) \\ \mathbf{y}(t) &= \mathbf{C} \mathbf{x}(t) \end{aligned} \right\} \quad (2.1)$$

where $\mathbf{A} \in \mathbb{R}^{n \times n}$, $\mathbf{B} \in \mathbb{R}^{n \times m}$, $\mathbf{C} \in \mathbb{R}^{r \times n}$, $\mathbf{x} \in \mathbb{R}^n$, $\mathbf{u} \in \mathbb{R}^m$, $\mathbf{y} \in \mathbb{R}^r$. Also, there is no feedthrough matrix, i.e., $\mathbf{D} = 0$.

This constitutes the standard case of a multiple-input, multiple-output (MIMO) system with state matrix \mathbf{A} , input matrix \mathbf{B} and output matrix \mathbf{C} .

For single-input, single-output (SISO) systems, \mathbf{A} is also a matrix, whereas \mathbf{b} and \mathbf{c} are mere vectors, denoted by small letters. Furthermore, $y(\cdot)$ and $u(\cdot)$ become scalar functions of time.

2.1.2 Control Architecture

In order to influence a system of the form (2.1), a controller has to be implemented that determines the control input $u(\cdot)$. There are two basic designs of control systems: open- and closed-loop control. An open-loop controller only uses information from the reference signal $y_{\text{ref}}(\cdot)$ to generate a control value. Open-loop controllers are unable to react to any

disturbances that act on the system. If a reaction is required, the disturbances have to be predetermined and accounted for in the controller design.

A closed-loop controller incorporates a feedback structure into the system. This enables the controller to use information from the system state vector, as well as the reference signal to generate a control signal $u(\cdot)$ (see Fig. 2.1).

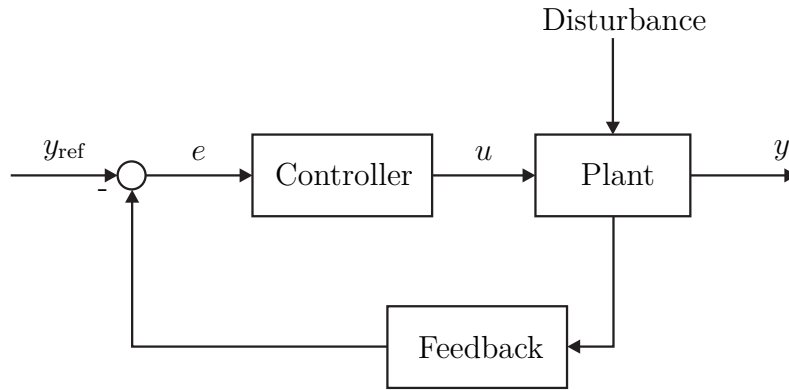


Figure 2.1: Closed-loop control structure

A closed-loop system is able to automatically react to disturbances acting on the system. However, sensors are needed to measure one or more system states and generate the feedback loop.

In the thesis at hand, output feedback control is considered. It consists of a single output value $y(\cdot) \in \mathbb{R}$ being measured and fed back into a controller for the computation of an error value $e(\cdot)$ that is used to generate a single control input value $u(\cdot)$. Thus, a SISO system is controlled, as shown in the following example:

$$\left. \begin{aligned} \dot{\mathbf{x}}(t) &= \mathbf{A} \mathbf{x}(t) + \mathbf{b} u(t) \\ y(t) &= \mathbf{c} \mathbf{x}(t) \end{aligned} \right\} \quad (2.2)$$

$$\left. \begin{aligned} e(t) &= y(t) - y_{\text{ref}}(t) \\ u(t) &= -k_P e(t) \end{aligned} \right\} \quad (2.3)$$

where $k_P > 0$, $\mathbf{A} \in \mathbb{R}^{n \times n}$, $\mathbf{b} \in \mathbb{R}^n$, $\mathbf{c} \in \mathbb{R}^n$, $\mathbf{x} \in \mathbb{R}^n$, $u \in \mathbb{R}$, $y \in \mathbb{R}$, $k_P \in \mathbb{R}$.

Note that the sign of $u(\cdot)$ is dependent on the sign of the high-frequency gain, which is discussed in Section 2.1.6. The controller has to counteract the system's dynamics in order to reduce the error signal $e(\cdot)$. At this point, it is assumed that a negative control value $u(\cdot)$ causes the system output and thus the error signal to be reduced.

This constitutes a simple proportional feedback controller for further considerations.

2.1.3 Stability of LTI Systems

For LTI systems of the form (2.1), there are multiple methods to investigate their stability. In the thesis at hand, the root locus plot is discussed.

Consider the distribution of the poles and zeros of the system's transfer function (see [Unbe08]). Asymptotic stability is achieved if all of the poles have negative real parts, i.e., the poles are located in the left-half open complex plane. As long as the system's poles are distributed in this manner, the controller does not need to stabilize the system. If the poles are distributed in a way that some are located on the right-half open complex plane, the controller has to be designed in such a way that the closed-loop system is stabilized, i.e., the poles are moved to left-half complex plane. A feedback controller of the form (2.3) is able to relocate all poles, depending on the proportional gain k_P . The trajectories the poles take while the feedback gain is increased is given in the root locus plot. While increasing the feedback gain, the poles move along individual trajectories on the complex plane. The shape of the trajectories is dependent on the underlying system dynamics. They end in the location of the zeros of the system, which means that for $k_P \rightarrow +\infty$, the poles are located directly on the zeros. If there are more poles than zeros, which is the case for deterministic systems, the extra poles may move anywhere on the complex plane. If however there is only one more pole than zeros in the system, this extra pole always moves towards $-\infty$ for $k_P \rightarrow +\infty$ and is therefore relocated to the stable region of the complex plane.

A feedback controller that is able to stabilize the system has to be designed with a certain proportional gain $k_P \geq k_P^*$ that achieves the relocation of the poles towards a stable distribution in the complex plane. The value k_P^* denotes the minimal gain at which stability is achieved. This can be determined for instance with the help of the root locus plot. However, precise knowledge of the system and its parameters is required.

2.1.4 Classic adaptive Controllers

If little or nothing is known of the system parameters, classic control design methods fail. They rely on the knowledge of the transfer function or the time constants of the system to design a suitable controller that achieves the desired performance and closed-loop stability, as mentioned above. The case of unknown system parameters may arise if the system is very complex and a sufficient model is unavailable, or if the parameters are subject to sudden and significant changes. Adaptive controllers are a way of dealing with these problems (see Fig. 2.2). The principle of adaptive control was first investigated for autopilot systems in high-performance aircrafts (see [ÅsWi89]). These controllers used

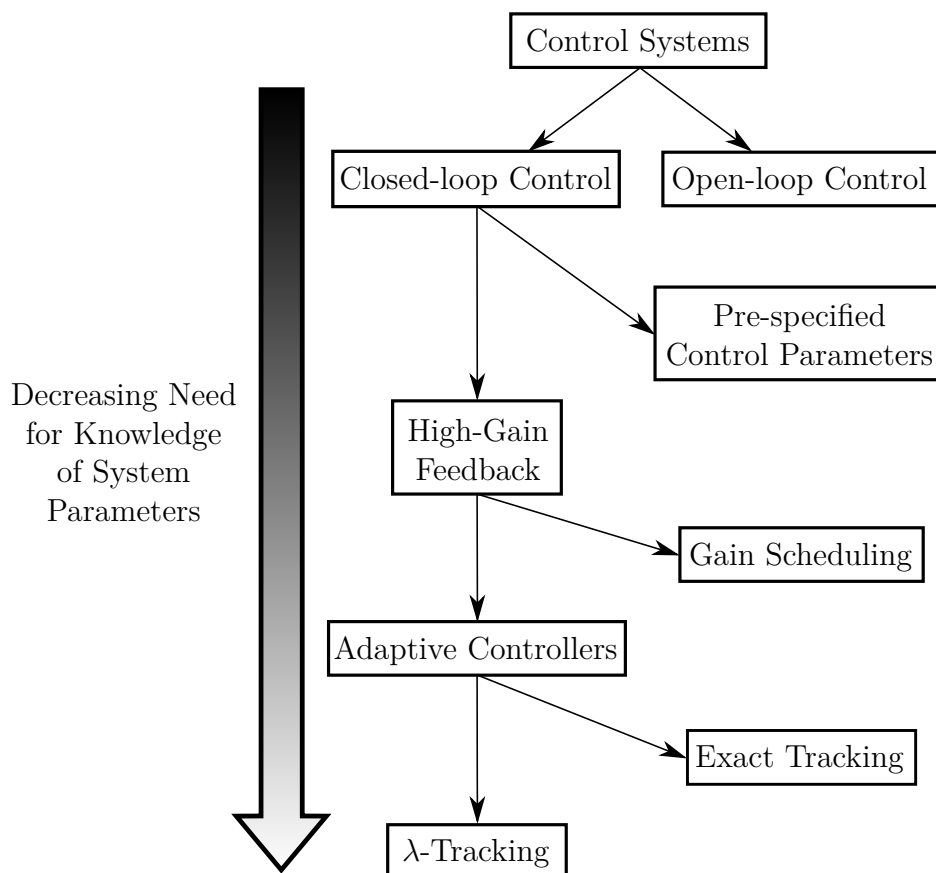


Figure 2.2: Classification of control systems

a gain scheduling method in order to switch control parameters such as proportional or derivative gains according to the current system state to account for drastic changes in system parameters, such as air pressure. The first adaptive controller based on high-gain feedback was introduced by Willems and Byrnes (see [WiBy 84]), where an adaption law was introduced that continuously computes the control gain, rather than pre-specifying it. In [Nuss 84], the controller was extended by a so-called Nussbaum function that eliminates the need to know the sign of the high-frequency gain of the system, which had been a prerequisite before. It was shown that the system can be stabilized in this manner. However, better control performance is achieved if the sign is known (see Section 2.1.6 for further details).

Adaptive λ -tracking control has been investigated in different areas. Among them are the control of mechanical systems, such as servo systems (see [IISc 07], [HaES 08]), manipulator robots (see [HaES 08]) or the locomotion of biologically inspired robots (see [BeZi 06]). Also, the adaptive control of the concentration of an anesthetic in a patient during surgery has been demonstrated (see [Bull 00]). Furthermore, adaptive λ -tracking is able to control

pH values in a biogas reactor (see [IPL97]). All of these examples suggest that the principle of λ -tracking control is applicable to a wide range of scenarios and is therefore worthwhile to investigate for the purpose of this work.

A classic adaptive controller, taken from [IRy94], is:

$$\left. \begin{aligned} e(t) &= y(t) - y_{\text{ref}}(t) \\ u(t) &= -k(t) e(t) \\ \dot{k}(t) &= \max\{0, |e(t)| - \lambda\}^2, \quad k(0) = 0 \end{aligned} \right\} \quad (2.4)$$

where $\lambda \geq 0$.

This constitutes a first-order controller, since there is a differential equation of first order in the adaptor of controller (2.4).

The controller works as follows: The proportional gain of the controller is not constant, but a function of time, which means that it is not pre-specified by the designer. During operation, the gain $k(\cdot)$ is determined by the adaptor (2.4). If the system output $y(t)$ is outside the error neighborhood, i.e., $|e(t)| > \lambda$, the gain is increased by the square of that distance. If the system output is inside the λ -neighborhood, the gain is kept constant, since the adaption law now states $\dot{k}(t) = 0$. This constitutes λ -tracking with a dead-zone behavior (see Fig. 2.3). The adaptor ensures that the gain $k(\cdot)$ is increased until

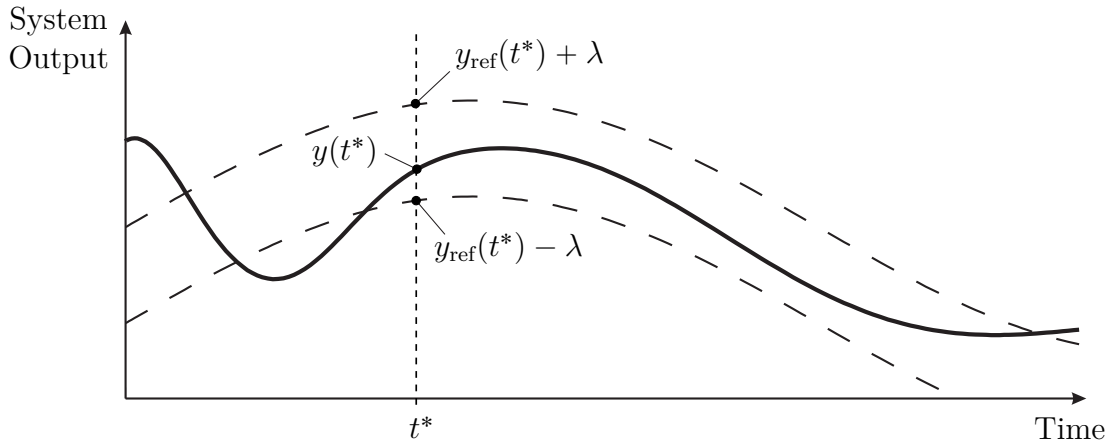


Figure 2.3: Principle of λ -tracking

the control goal is achieved, i.e., until the gain reached the level $k(t) \geq k_p^*$ necessary for stabilization. Afterwards, the gain may only be increased further, but not reduced.

Scheduling and Boost of Increase Term

In order to increase the control performance, various extensions to the adaptor's increase behavior have been investigated (see [BeSt09], [BeSt10], [LoBe11], [BeLo12]).

First, the adaptor's behavior was amplified by the introduction of a factor $\gamma > 1$:

$$\dot{k}(t) = \gamma (\max \{0, |e(t)| - \lambda\})^2 \quad (2.5)$$

where $\lambda \geq 0, \gamma > 1$.

Since γ can be chosen arbitrarily large, the increase of $k(\cdot)$ can be amplified at will. This improves the control performance considerably. However, there are no restrictions to prevent the gain factor from overshooting, since the adaptor's dynamics are unbounded. Thus, $k(\cdot)$ may become unnecessarily large.

Another extension deals with the nature of the quadratic function in the adaptor. If the system output is far away from the λ -neighborhood, the square of that distance contributes well to the increase term. If however the system output is close, but still outside the λ -neighborhood, the adaptor's dynamics are unsatisfactory. A small number (< 1), if squared, results in an even smaller number, so the increase of the gain factor $k(\cdot)$ will be quite slow if $\lambda < |e(t)| < 1 + \lambda$. To overcome this deficiency, different increase terms are introduced for different regions of the error value $e(t)$ (see [BeSt 09]):

$$\dot{k}(t) = \begin{cases} \gamma (|e(t)| - \lambda)^2, & \text{if } 1 + \lambda < |e(t)| \\ \gamma (|e(t)| - \lambda)^{\frac{1}{2}}, & \text{if } \lambda \leq |e(t)| \leq 1 + \lambda \\ 0, & \text{if } |e(t)| < \lambda \end{cases} \quad (2.6)$$

where $\lambda \geq 0, \gamma > 1$.

This adaptor changes the increase term from a quadratic to a square-root function, while $y(\cdot)$ approaches the λ -neighborhood. Thus, small values of the control error $|e(t)|$ are not decreased further by the quadratic function. This leads to an overall improved control performance.

σ -Modification and Decrease Term

At this point, there is no possibility to decrease the gain factor $k(\cdot)$. However, this may be necessary: Consider the case that a strong disturbance acts on the system, which leads to the system output repeatedly exiting the λ -neighborhood. This results in an increase of the control gain to achieve the control goal. If the disturbance subsides, or is replaced by one with a considerably smaller amplitude, the control goal is still achieved, but the gain factor $k(\cdot)$ is now higher than necessary for this situation. Hence, the control system becomes unnecessarily stiff and the control actuator uses more energy to quickly

change the control input of the system. This might be unfavorable behavior, since saving energy is usually desired. The control gain should therefore be as high as necessary and as low as possible. Thus, the adaptor has to include the ability to reduce the control gain. In [LoBe 11], multiple adaptors capable of doing so have been investigated. One possibility is to include the increase and decrease behavior into one equation, as proposed in [IoKo 83]:

$$\dot{k}(t) = -\sigma k(t) + \gamma (\max\{0, |y(t)| - \lambda\})^2 \quad (2.7)$$

where $\lambda \geq 0, \gamma > 1, \sigma > 0$.

This is known as σ -modification. Note that it was originally designed for a stabilizing controller only. For λ -tracking, $|y(t)|$ has to be replaced by $|e(t)|$.

This controller leads to a rather chaotic behavior of the system, since increase and decrease terms may be active simultaneously. Also, decrease of the gain factor starts as soon as the system output enters the λ -neighborhood. As pointed out in [MaPo 96], it may be advantageous to wait a pre-specified time t_d for which the λ -neighborhood has to be observed before the reduction of the gain factor begins. This can be incorporated into the known scheduling scheme of adaptor (2.6), as in the following example (see [BeSt 10]):

$$\dot{k}(t) = \begin{cases} \gamma (|e(t)| - \lambda)^2, & \text{if } |e(t)| > 1 + \lambda \\ \gamma (|e(t)| - \lambda)^{\frac{1}{2}}, & \text{if } \lambda \leq |e(t)| \leq 1 + \lambda \\ 0, & \text{if } |e(t)| < \lambda \quad \wedge \quad t - t_e < t_d \\ -\sigma, & \text{if } |e(t)| < \lambda \quad \wedge \quad t - t_e \geq t_d \end{cases} \quad (2.8)$$

where $\lambda \geq 0, \gamma > 1, \sigma > 0, t_d > 0$, and t_e denotes the time at which the system output last entered the λ -neighborhood.

In this case, $k(\cdot)$ would be decreased linearly after the system output had spent the pre-specified time t_d inside the λ -neighborhood. If it is left afterwards, the usual increase terms of the adaptor take over.

Although this design satisfies all the needs for the decrease capability, the linear reduction term is not optimal. In [LoBe 11], a reduction term is proposed that combines an

exponential decrease term with deceleration behavior:

$$\dot{k}(t) = \begin{cases} \gamma (|e(t)| - \lambda)^2, & \text{if } |e(t)| > 1 + \lambda \\ \gamma (|e(t)| - \lambda)^{\frac{1}{2}}, & \text{if } \lambda \leq |e(t)| \leq 1 + \lambda \\ 0, & \text{if } |e(t)| < \lambda \quad \wedge \quad t - t_e < t_d \\ -\sigma \left(1 - \frac{|e(t)|}{\lambda}\right) k(t), & \text{if } |e(t)| < \lambda \quad \wedge \quad t - t_e \geq t_d \end{cases} \quad (2.9)$$

where $\lambda \geq 0, \gamma > 1, \sigma > 0, t_d > 0$.

Now, the decrease term is a function of $k(t)$ and $e(t)$. This way, the decrease rate is dependent on the overall magnitude of $k(t)$. Also, the decrease of $k(\cdot)$ is stalled when the system output approaches the border of the λ -neighborhood from within. This helps to avoid exiting the λ -neighborhood due to the decrease behavior.

Modification of λ -Neighborhood

In order to enforce that the specified λ -neighborhood is obeyed, a smaller $\varepsilon\lambda$ -neighborhood is used in the adaption law, with $0 < \varepsilon \leq 1$ (see [LoBe 11], [BeLo 12]). Thus, ε -safe λ -tracking is introduced:

$$\dot{k}(t) = \begin{cases} \gamma (|e(t)| - \varepsilon\lambda)^2, & \text{if } |e(t)| > 1 + \varepsilon\lambda \\ \gamma (|e(t)| - \varepsilon\lambda)^{\frac{1}{2}}, & \text{if } \varepsilon\lambda \leq |e(t)| \leq 1 + \varepsilon\lambda \\ 0, & \text{if } |e(t)| < \varepsilon\lambda \quad \wedge \quad t - t_e < t_d \\ -\sigma \left(1 - \frac{|e(t)|}{\varepsilon\lambda}\right) k(t), & \text{if } |e(t)| < \varepsilon\lambda \quad \wedge \quad t - t_e \geq t_d \end{cases} \quad (2.10)$$

where $\lambda \geq 0, \gamma > 1, \sigma > 0, t_d > 0, 0 < \varepsilon \leq 1$.

This way, the likelihood of the system output leaving the $\varepsilon\lambda$ -neighborhood is as high as leaving the λ -neighborhood with adaptor (2.9). However, since $\varepsilon\lambda < \lambda$, the system is less likely to leave the λ -neighborhood with adaptor (2.10).

By incorporating all the modifications to classic adaptors discussed in this section into

one adaptive controller, the following is obtained:

$$\left. \begin{aligned} e(t) &= y(t) - y_{\text{ref}}(t) \\ u(t) &= -k(t) e(t) \\ \dot{k}(t) &= \begin{cases} \gamma (|e(t)| - \varepsilon\lambda)^2, & \text{if } |e(t)| > 1 + \varepsilon\lambda \\ \gamma (|e(t)| - \varepsilon\lambda)^{\frac{1}{2}}, & \text{if } \varepsilon\lambda \leq |e(t)| \leq 1 + \varepsilon\lambda \\ 0, & \text{if } |e(t)| < \varepsilon\lambda \quad \wedge \quad t - t_e < t_d \\ -\sigma \left(1 - \frac{|e(t)|}{\varepsilon\lambda}\right) k(t), & \text{if } |e(t)| < \varepsilon\lambda \quad \wedge \quad t - t_e \geq t_d \end{cases} \end{aligned} \right\} \quad (2.11)$$

where $\lambda \geq 0, \gamma > 1, \sigma > 0, t_d > 0, 0 < \varepsilon \leq 1$.

This denotes the basic adaptive controller from literature that will be used for the following considerations.

Note that replacing open-loop controllers with a closed-loop control structure requires the implementation of sensors to create a feedback loop. In the case of the automatic transmissions considered in this work, additional sensors are not required, since speed sensors providing angular velocities of the clutches' input and output shafts are already present in the transmissions' design.

2.1.5 Other adaptive Controllers

There are various principles to design adaptive controllers. In this section, alternatives are presented and the corresponding adaption laws are considered, to provide a more detailed overview of adaptive control systems.

Funnel Control

In the previous section, an introduction into first-order controllers is given. They incorporate a differential equation into the adaption law, so there exists an equation for $\dot{k}(t)$. It is also conceivable to use explicit equations for $k(t)$ and thus create zero-order controllers. One example of zero-order controllers that is subject to current research is funnel control (see [IIRS 02], [IISc 07], [Schu 09]). It works as follows:

The adaptor generates an upper limit for the error value $|e(t)|$ that is not supposed to be left. This limit function is designed in the form of a funnel, so that an arbitrarily large error value at the beginning will evolve towards the pre-specified λ -neighborhood and never leave the error funnel in the process (see Fig. 2.4). As depicted, the error value is supposed to evolve inside the funnel function, described by the terms $\pm \frac{1}{\varphi(t)}$. This is

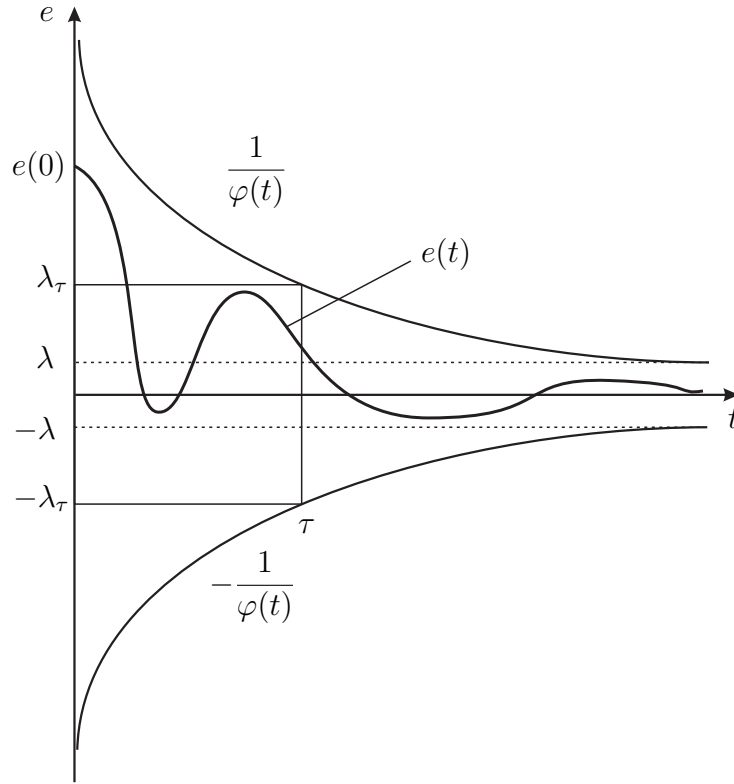


Figure 2.4: Principle of funnel control with limit functions $\pm \frac{1}{\varphi(t)}$ ([IISc 07])

achieved with the following controller (see [IIRS 02]):

$$\left. \begin{aligned} e(t) &= y(t) - y_{\text{ref}}(t) \\ u(t) &= -k(t)e(t) \\ k(t) &= \frac{1}{1 - \varphi(t)|e(t)|} \\ \varphi(t) &= \frac{t}{\lambda(t - \tau) + \lambda_\tau \tau} \end{aligned} \right\} \quad (2.12)$$

where $\lambda_\tau > \lambda > 0, \tau > 0$.

The controller works as follows: If the error value $|e(t)|$ approaches the border of the funnel function, the control gain $k(t)$ is increased. It may be increased arbitrarily high, since the equation yields $k(t) \rightarrow +\infty$ for $|e(t)| \rightarrow \frac{1}{\varphi(t)}$. Thus, the system output is kept inside the funnel at all times. For $t \rightarrow +\infty$, the funnel function equals the λ -neighborhood. Note that the unbounded increase of $k(\cdot)$ results in a stiff system.

Some problems arise when a funnel controller of type (2.12) is applied. First of all, the system output will oscillate inside the prescribed funnel. The gain factor is always decreased to $k(t) = 1$, if $|e(t)| = 0$. An appropriate control gain is achieved only if

$|e(t)| > 0$. Hence, the control gain also oscillates. Furthermore, this leads to a stiff closed-loop system, since strong and sudden changes of the control gain occur. This kind of irregular behavior is unfavorable for most control applications. Therefore, funnel control is not considered in this thesis.

Adaptive Fuzzy Control

Another possibility of designing adaptors for high-gain feedback controllers is the usage of fuzzy systems. Instead of differential equations, a fuzzy system computes the current gain factor $k(t)$. Thus, linguistic rules can be incorporated into the adaptive controller, which can be advantageous in transferring expert knowledge about a system into the adaptor.

Remark 2.1 *Note that in the case presented here, the fuzzy inference system is used to compute the gain of an underlying proportional controller. This is contrary to traditional fuzzy controllers, where the control output $u(t)$ is the result of the fuzzy system. Thus, the approach taken here is only partly a fuzzy controller.*

In [BeLo 12], the following adaptive fuzzy controller is proposed:

$$\left. \begin{aligned} e(t) &= y(t) - y_{\text{ref}}(t) \\ u(t) &= -k(t) e(t) \\ \dot{k}(t) &= \sigma_f(t) k(t) \\ \sigma_f(t) &= \text{Fuzzy Controller}(e(t), t, t_d, \varepsilon, \lambda) \\ k(0) &= 1 \end{aligned} \right\} \quad (2.13)$$

with $\lambda \geq 0, t_d > 0, 0 < \varepsilon \leq 1$.

The controller incorporates a first-order adaptive controller with locally exponential behavior. The rate of the exponential increase or decrease is determined via a fuzzy inference system. A rule set is devised that is supposed to generate the desired control behavior. As discussed in [BeLo 12], this approach may lead to slow control dynamics. However, it is conceivable to revisit the adaptive fuzzy controller and modify the adaption law as well as the underlying rule set to the clutch control system at hand.

2.1.6 High-gain Feedback Stability

For adaptive controllers, a number of requirements have to be met by the system in order to ensure stability of the closed-loop system. Following the previous remarks on the root-locus plot, these requirements are now discussed.

As shown in [Sont98] and [Schr10], the following conditions have to be met for the application of an adaptive high-gain feedback controller:

- the relative degree of the system equals one,
- the system is minimum-phase and
- the sign of the high-frequency gain is known.

Relative Degree

The relative degree δ of a system gives the derivative order of the system's output $y(\cdot)$ that the control input $u(\cdot)$ directly acts on. It therefore denotes the lowest number of integrators that the input signal has to overcome on its path towards the system output. For LTI systems, the relative degree is also the difference of the number of poles and zeros of the system's transfer function. The relative degree is determined as follows:

Begin with $\delta = 1$ and compute:

$$\mathbf{CA}^{\delta-1}\mathbf{B} \tag{2.14}$$

If $\mathbf{CA}^{\delta-1}\mathbf{B} = 0$, increase δ by 1 and recompute. Repeat the process until $\det(\mathbf{CA}^{\delta-1}\mathbf{B}) \neq 0$. After the process is finished, δ equals the relative degree of the system.

The condition of $\delta = 1$ implies, there can only be one more pole than zeros in the system. As mentioned above, one surplus pole always moves towards $-\infty$ on the complex plane while increasing the feedback gain, and is therefore stabilized.

As shown in [Sont98], this condition can be relaxed. If a system contains more than one surplus pole, i.e., if the relative degree is greater than 1, the feedback structure can be modified to stabilize the system. If derivatives of the system output up to the order $\delta - 1$ are included in the feedback structure, additional zeros can be incorporated into the closed-loop system. This way, the relative degree of the system is lowered. For example, a system with relative degree 2 can be controlled via high-gain feedback if a derivative term is introduced into the feedback structure. Therefore, an adaptive PD-feedback controller is able to stabilize and control a system with $\delta = 2$.

Minimum-Phase Property

A system is called minimum-phase, if it has stable zero dynamics. For LTI systems, this means that all of the zeros are located in the left-half open complex plane, i.e., if they

have negative real parts. The zeros are computed with the help of the Rosenbrock matrix (see [DrHa 99]):

$$\det \begin{bmatrix} \mathbf{A} - \mathbf{Z}\mathbf{I}_m & \mathbf{B} \\ \mathbf{C} & 0 \end{bmatrix} = 0 \quad (2.15)$$

$$\mathbf{Z}_{ij} \leq 0 \quad (2.16)$$

The need for this requirement is quite obvious when considering the root-locus plot (see Fig. 2.5): When changing the proportional feedback gain of a closed-loop system, all of the poles are relocated along certain trajectories, which end in the zeros of the system. If a high-gain feedback controller is supposed to be applied, it has to be ensured that at some level of $k(t) \geq k_P^*$, all of the poles are moved to the left-half open complex plane, where closed-loop stability is achieved, called the stable region of the complex plane. This is not possible if any zeros are located on the right-half open complex plane, as the root-locus trajectories would not reach the stable region for $k(t) \rightarrow +\infty$. Therefore, the minimum-phase condition is imperative for high-gain feedback control of a system. This behavior is

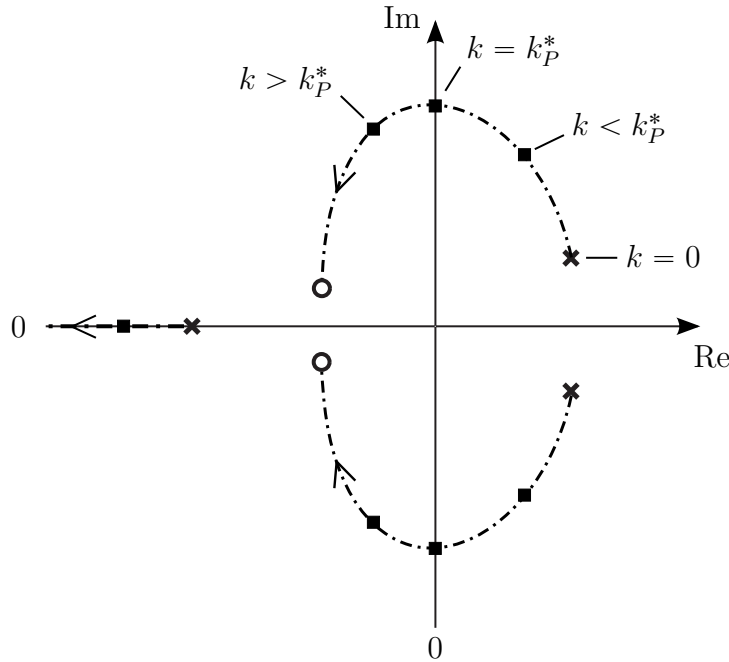


Figure 2.5: Root locus plot of an LTI system with feedback stabilization and different settings for the proportional feedback gain $k(\cdot)$

depicted in Fig. 2.5. For $k = 0$, i.e., without feedback control, the system has an unstable pair of poles in the right-half complex plane, a stable pole in the left-half complex plane and a pair of zeros in the left-half complex plane. Thus, the system is minimum-phase. If

the proportional feedback gain is increased, the unstable poles move along the root locus trajectories. If the feedback gain increases beyond a certain value k_P^* , the unstable poles are relocated in the stable region of the complex plane. For $k(t) \rightarrow +\infty$, the poles would be located directly on the zeros of the system, and thus effectively achieving cancellation of the system dynamics.

Sign of High-Frequency Gain

The sign of the high-frequency gain of the system has to be known in order to apply an adaptive controller. It denotes the direction of the actuator that is operated via the control signal $u(\cdot)$. This could be the direction of the mechanical torque of an electric motor resulting from a positive electric current, for example. In engineering applications, this knowledge is usually present.

The adaptive controllers discussed so far require the system to react in such a way that an increase of the control signal $u(\cdot)$ results in an increase of the system output signal $y(\cdot)$. This coincides with the spectrum of the gain matrix \mathbf{CAB} having only eigenvalues in the right-half open complex plane:

$$\text{spec}(\mathbf{CAB}) \in \mathbb{C}_+ \quad (2.17)$$

In case of SISO systems, \mathbf{cAb} becomes a number. Thus, the sign of the high-frequency gain is positive. If the sign is negative, i.e., if the eigenvalues of the gain matrix are located in the left-half open complex plane, the control signal has to reverse its sign as well for the controller to be operational. Hence, the controller equations are extended:

$$\left. \begin{aligned} e(t) &= s_{\text{hf}} \cdot (y(t) - y_{\text{ref}}(t)) \\ u(t) &= k(t) e(t) \\ s_{\text{hf}} &:= \begin{cases} -1, & \text{if } \text{spec}(\mathbf{CAB}) \in \mathbb{C}_+ \\ 1, & \text{if } \text{spec}(\mathbf{CAB}) \in \mathbb{C}_- \end{cases} \end{aligned} \right\} \quad (2.18)$$

Note that this notation changes the sign of the error signal $e(\cdot)$, not the control signal $u(\cdot)$. However, this has the same effect, since $u(t) \propto e(t)$. Also, by reversing the definition of s_{hf} with regard to the spectrum of the gain matrix, the sign of $u(t)$ has been reversed to $u(t) = k(t) e(t)$ as well.

2.2 Nonlinear Control Systems

In the following, nonlinear systems theory and high-gain feedback stability of nonlinear systems are discussed. This background is necessary if the system at hand exhibits nonlinear dynamics, such as in hydraulics, which is to be expected in automatic transmissions.

2.2.1 System Class and Control Architecture

As before, the focus of this thesis lies on SISO systems. For nonlinear SISO systems, a different form of representation has to be chosen:

$$\left. \begin{aligned} \dot{\mathbf{x}}(t) &= \mathbf{f}(\mathbf{x}(t)) + \mathbf{g}(\mathbf{x}(t)) \cdot u(t) \\ y(t) &= \mathbf{h}(\mathbf{x}(t)) \end{aligned} \right\} \quad (2.19)$$

where $\mathbf{x} \in \mathbb{R}^n$, $\mathbf{f} \in C^l(\mathbb{R}^n, \mathbb{R}^n)$, $\mathbf{g} \in C^l(\mathbb{R}^n, \mathbb{R}^n)$, $\mathbf{h} \in C^q(\mathbb{R}^n, \mathbb{R})$, $l \in \mathbb{N}_0$, $q \in \mathbb{N}$, $y \in \mathbb{R}$, $u \in \mathbb{R}$. This denotes a general nonlinear SISO system with a linear input-affine control signal $u(\cdot)$.

In order to act on the system to achieve the desired behavior, an adaptive output feedback controller of the form (2.18) is applied to system (2.19):

$$\begin{aligned} \dot{\mathbf{x}}(\mathbf{t}) &= \mathbf{f}(\mathbf{x}(\mathbf{t})) + \mathbf{g}(\mathbf{x}(\mathbf{t})) \cdot u(t) \\ y(t) &= \mathbf{h}(\mathbf{x}(\mathbf{t})) \\ e(t) &= s_{\text{hf}} \cdot (y(t) - y_{\text{ref}}(t)) \\ u(t) &= k(t) e(t) \\ k(t) &= \text{Adaptor} \end{aligned}$$

2.2.2 High-Gain Feedback Stability

There are various methods to investigate the stability of nonlinear systems, such as the Lyapunov Stability or the Describing Function (see [Isid 95], [Khal 96], [Föll 98], [Sont 98]). However, all of these methods rely on the knowledge of the system parameters, which is not feasible when dealing with uncertain systems. Therefore, a stability criterion has to be found that is able to analyze uncertain systems and at the same time provides a conclusion whether a nonlinear system can be stabilized by high-gain feedback, i.e., if adaptive λ -tracking controllers can be applied. To this end, the requirements for adaptive control of LTI-SISO systems are revisited:

- relative degree: $\delta = 1$,

- system is minimum-phase, i.e., has stable zero dynamics,
- known sign of the high-frequency gain.

If it is possible to find a corresponding set of conditions that apply to nonlinear SISO systems of the form (2.19), the stability of adaptive control with λ -tracking can be investigated.

Sign of High-frequency Gain

Again, this condition is easy to meet. For almost every engineering problem, the sign of the high-frequency gain is known. If not, a Nussbaum function can be incorporated into the controller to overcome this problem (see [Nuss84]), in which case the sign is adapted along with the common gain factor. The same considerations as in Section 2.1.6 apply.

Relative Degree

The relative degree δ of a nonlinear system is now defined as follows (see [Niva90] and [Isid95]):

$$L_g L_f^k \mathbf{h}(\mathbf{x}) = 0, \text{ for all } \mathbf{x} \text{ in the vicinity of } \mathbf{x}_0 \text{ and for all } k < \delta - 1 \quad (2.20)$$

$$L_g L_f^{\delta-1} \mathbf{h}(\mathbf{x}_0) \neq 0 \quad (2.21)$$

where

$$L_g \mathbf{h}(\mathbf{x}) := \frac{\partial \mathbf{h}}{\partial \mathbf{x}} \mathbf{g}(\mathbf{x}) \quad (2.22)$$

$$L_f \mathbf{h}(\mathbf{x}) := \frac{\partial \mathbf{h}}{\partial \mathbf{x}} \mathbf{f}(\mathbf{x}) \quad (2.23)$$

$$L_f^2 \mathbf{h}(\mathbf{x}) := \frac{\partial L_f \mathbf{h}(\mathbf{x})}{\partial \mathbf{x}} \mathbf{f}(\mathbf{x}) \quad (2.24)$$

$$L_g L_f \mathbf{h}(\mathbf{x}) := \frac{\partial (L_f \mathbf{h}(\mathbf{x}))}{\partial \mathbf{x}} \mathbf{g}(\mathbf{x}) \quad (2.25)$$

Therefore, this condition can be investigated for nonlinear systems.

Minimum-Phase Property

For nonlinear systems, it is not trivial to determine if the system has stable zero dynamics, i.e., if it is minimum-phase. An analogy to the location of the zeros of an LTI system in the left-half open complex plane has to be found.

In [Isid95], a method for investigating nonlinear systems regarding their zero dynamics is

proposed. First, the system (2.19) at hand has to undergo a coordinate transformation, which results in a system form that is known in literature as the *Byrnes-Isidori Normal Form*.

Consider a system of form (2.19) with a relative degree $\delta < n$, i.e., less than the system order, which results in the existence of zero dynamics. Now, a new set of functions $\phi_i(\mathbf{x})$ can be generated:

$$\phi_1(\mathbf{x}) = \mathbf{h}(\mathbf{x}) \quad (2.26)$$

$$\phi_2(\mathbf{x}) = L_f \mathbf{h}(\mathbf{x}) \quad (2.27)$$

$$\vdots$$

$$\phi_\delta(\mathbf{x}) = L_f^{\delta-1} \mathbf{h}(\mathbf{x}) \quad (2.28)$$

These functions are easy to find. However, to complete the mapping, $n - \delta$ more functions are required:

$$\Phi(\mathbf{x}) = \begin{pmatrix} \phi_1(\mathbf{x}) \\ \vdots \\ \phi_\delta(\mathbf{x}) \\ \phi_{\delta+1}(\mathbf{x}) \\ \vdots \\ \phi_n(\mathbf{x}) \end{pmatrix} \quad (2.29)$$

Let $z_i = \phi_i(\mathbf{x})$. Then z_δ can be expressed as follows:

$$\dot{z}_\delta = L_f^\delta \mathbf{h}(\mathbf{x}) + L_g L_f^{\delta-1} \mathbf{h}(\mathbf{x}) u \quad (2.30)$$

Now, \mathbf{x} has to be expressed as a function of \mathbf{z} , which yields:

$$\mathbf{x} = \Phi^{-1}(\mathbf{z}) \quad (2.31)$$

$$a(\mathbf{z}) := L_g L_f^{\delta-1} \mathbf{h}(\Phi^{-1}(\mathbf{z})) \quad (2.32)$$

$$b(\mathbf{z}) := L_f^\delta \mathbf{h}(\Phi^{-1}(\mathbf{z})) \quad (2.33)$$

$$\dot{z}_\delta = b(\mathbf{z}) + a(\mathbf{z}) u \quad (2.34)$$

Moreover, if the functions $\phi_{\delta+1}(\mathbf{x}), \dots, \phi_n(\mathbf{x})$ can be chosen so that $L_g \phi_i(\mathbf{x}) = 0$, then

$$\dot{z}_i = q_i(\mathbf{z}) = L_f \phi_i(\Phi^{-1}(\mathbf{z})) \quad \text{for } \delta + 1 \leq i \leq n \quad (2.35)$$

Thus, the transformation into the Byrnes-Isidori Normal Form is complete:

$$\begin{aligned}
 \dot{z}_1 &= z_2 \\
 \dot{z}_2 &= z_3 \\
 &\vdots \\
 \dot{z}_{\delta-1} &= z_\delta \\
 \dot{z}_\delta &= b(\mathbf{z}) + a(\mathbf{z})u \\
 \dot{z}_{\delta+1} &= q_{\delta+1}(\mathbf{z}) \\
 &\vdots \\
 \dot{z}_n &= q_n(\mathbf{z})
 \end{aligned} \tag{2.36}$$

Now, the investigation of the system's zero dynamics is possible according to [Isid 95]. Again, the system is rewritten as follows:

$$\begin{aligned}
 \dot{z}_1 &= z_2 \\
 \dot{z}_2 &= z_3 \\
 &\vdots \\
 \dot{z}_{\delta-1} &= z_\delta \\
 \dot{z}_\delta &= b(\boldsymbol{\xi}, \boldsymbol{\eta}_I) + a(\boldsymbol{\xi}, \boldsymbol{\eta}_I)u \\
 \dot{\boldsymbol{\eta}}_I &= q(\boldsymbol{\xi}, \boldsymbol{\eta}_I),
 \end{aligned} \tag{2.37}$$

where

$$\boldsymbol{\xi} = \begin{pmatrix} z_1 \\ \vdots \\ z_\delta \end{pmatrix} \tag{2.38}$$

$$\boldsymbol{\eta}_I = \begin{pmatrix} z_{\delta+1} \\ \vdots \\ z_n \end{pmatrix} \tag{2.39}$$

In order to obtain the zero dynamics of the system, the problem of zeroing the output signal is considered. This is the case when the internal dynamics of the system are acting in such a way that the resulting output signal is zero, much like a specific frequency of an input signal, that corresponds to a zero in the transfer function, acting on an LTI system.

Since the system output is $y(t) = z_1(t)$, this yields

$$\dot{z}_1(t) = \dot{z}_2(t) = \cdots = \dot{z}_\delta(t) = 0 \quad (2.40)$$

$$\boldsymbol{\xi} = \mathbf{0} \quad (2.41)$$

Thus, the zero dynamics of the system are given as:

$$\dot{\boldsymbol{\eta}}_I = q(0, \boldsymbol{\eta}_I(t)) \quad (2.42)$$

The solution of the differential equation (2.42) can be used to obtain a suitable input signal $u(\cdot)$ to generate the zeroing of the output. It is therefore essential in investigating the minimum-phase property of a system (see [Isid 95] for further details).

Note that the transformation into the normal form (2.36) is difficult, especially obtaining the functions $\dot{z}_{\delta+1}, \dots, \dot{z}_n$.

In [BuAl 00], the possibility of designing a state observer for λ -tracking control of nonlinear systems with higher relative degree is proposed. If the system can be transformed into the Byrnes-Isidori Normal Form, this control architecture may be applied.

3 System Analysis

In this chapter, the actual powertrain system is considered. An introduction into the available automatic transmissions is given and shift quality is discussed. A system model is derived that is used for stability analysis based on the theory given in the previous chapter. Requirements for the adaptive control architecture are formulated.

3.1 Automatic Transmissions with powered Gearshifts

The investigations in this thesis focus on automatic transmissions capable of facilitating powered gearshifts common in modern automotive powertrains. Note that these transmissions can be applied regardless of the drive architecture, be it a conventional internal combustion engine or a hybrid drive, extended by one or more electric motors. In both cases, the transmission changes gears in the same manner.

In this thesis, two exemplary systems are considered: a traditional automatic transmission with multiple planetary gear sets for rear-wheel drive and a dual-clutch transmission for front-wheel drive. Both are used in passenger cars and vans of Mercedes-Benz and are referred to as the NAG3 and FDCT, respectively.

3.1.1 FDCT Dual-Clutch Transmission

The FDCT transmission (commercial designation: 7G-DCT, depicted in Fig. 3.1) consists of two input driveshafts, that connect to one common output driveshaft via multiple spur gear sets. Each of the input shafts holds gear sets for different gear ratios. The first shaft, connected to the first of the two clutches, can engage the odd-numbered gear ratios, i.e., 1st, 3rd, 5th and 7th gear. The second shaft, connected to the second clutch, is responsible for engaging the even-numbered gear ratios, i.e., 2nd, 4th and 6th gear (see Table 3.1). To change gears, the desired ratio is selected on the disengaged shaft with the help of hydraulically actuated gear selector forks and the shaft is then engaged via the corresponding clutch. At the same time, the old gear is disengaged by opening the respective clutch of the previously active shaft.

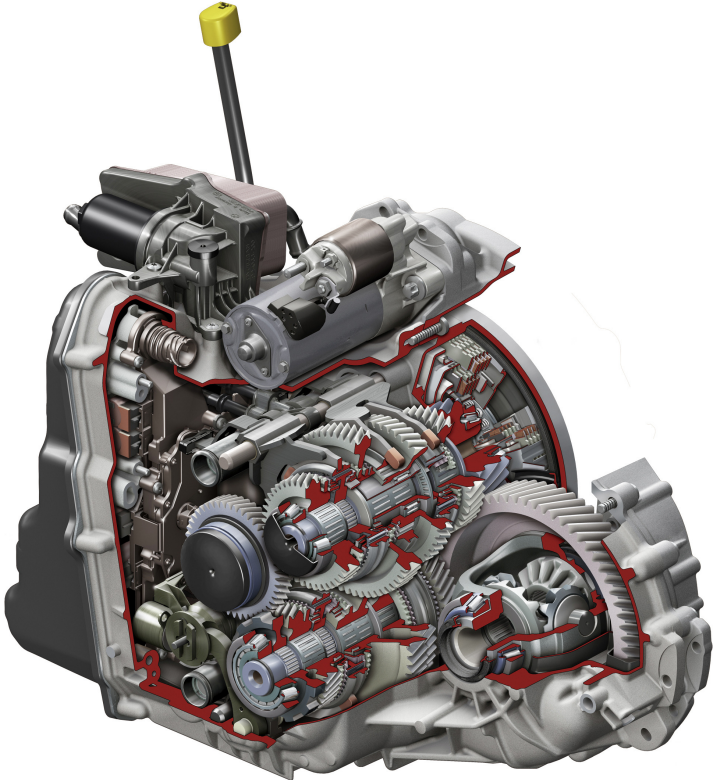


Figure 3.1: FDCT dual-clutch transmission ([Daim 11], © by Daimler AG)

Thus, a smooth gearshift procedure with a continued drive torque can be performed.

Table 3.1: Gearshift pattern of FDCT transmission

Gear	K1	K2	Selector Fork Setting
①	●		1
②		●	2
③	●		3
④		●	4
⑤	●		5
⑥		●	6
⑦	●		7
Ⓡ		●	R

The engaged clutch is marked with a filled circle for the respective gear. Also, the selector fork has to select the desired gear on the respective input shafts of the transmission. For example, in order to drive in 5th gear, clutch K1 has to be engaged while the selector fork is set to 5th gear as well, engaging the correct spur gear set.

3.1.2 NAG3 Automatic Transmission

The NAG3 transmission (commercial designation: 9G-TRONIC) has four standard planetary gear sets that can be engaged and switched with the help of six hydraulically actuated friction clutches, three of which act as brakes. Different combinations of engaged and dis-

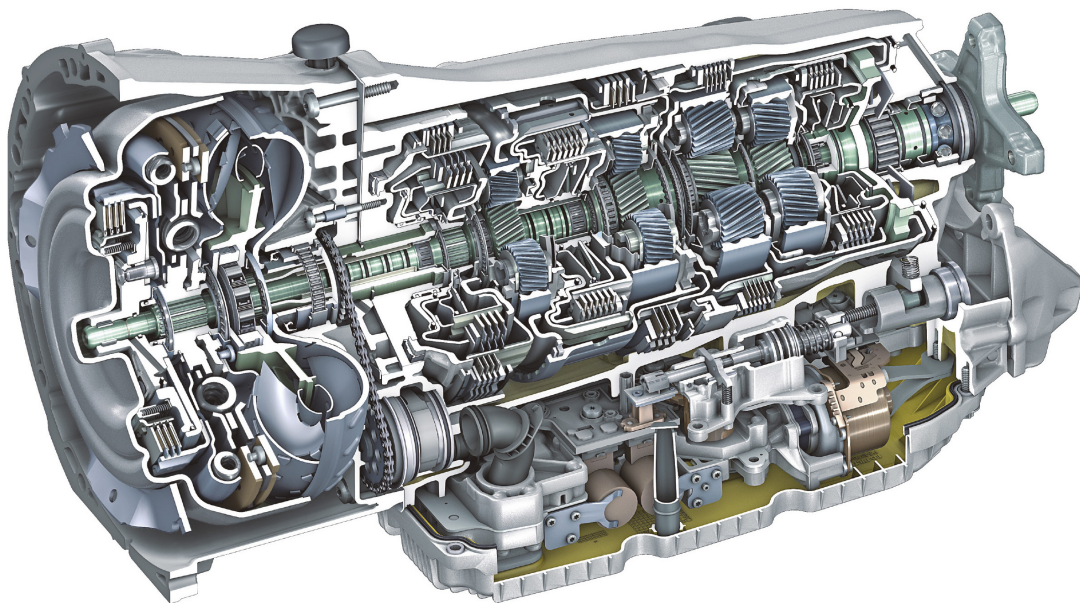


Figure 3.2: NAG3 automatic transmission ([Daim 13], © by Daimler AG)

engaged actuators enable the transmission to select different gear ratios; nine forward gears and one reverse gear (see Table 3.2). The actuator combinations of previous and next gears only differ in two clutch states, one of which is disengaged, while the other has to be engaged. For example, shifting from first to second gear means disengaging

brake B05 while engaging clutch K81. Thus, the transition from one gear to the other is essentially the same as with the FDCT transmission: One clutch is disengaged while a second clutch is engaged at the same time. By implementing a suitable control scheme that involves overlapping the hydraulic pressures of both participating clutches, a smooth and torque-continuous gearshift can be performed.

Table 3.2: Gearshift pattern of NAG3 transmission

Gear	K81	B05	B08	K38	K27	B06
①		●		●		●
②	●			●		●
③	●	●				●
④		●			●	●
⑤	●	●			●	
⑥	●			●	●	
⑦		●		●	●	
⑧			●	●	●	
⑨		●	●		●	
Ⓜ		●	●			

Again, clutches marked with filled circles are engaged in the respective gear, while the others are disengaged.

3.1.3 Shift Quality

An important aspect of gearshift control in automatic transmissions is ensuring a high level of shift quality, i.e., shift comfort. Driver and passengers are not supposed to perceive any uncomfortable longitudinal accelerations during gearshifts, apart from the change in acceleration due to changed transmission output torque. Thus, any shift control strategy has to consider shift comfort.

It is not trivial to identify the levels of acceleration and jerk that are perceived as uncomfortable by the vehicle passengers, since they are dependent on both amplitude and frequency of the acceleration signal. Various metrics have been developed to characterize and compare different acceleration signals and their corresponding control strategies, for

example the vibration dose value D_v and the energy spectral density D_{es} (see [DGWJ 05]):

$$D_v = \sqrt[4]{\int_{t_1}^{t_2} a^4(t) dt} \quad (3.1)$$

$$D_{es} = \frac{G_s(2\pi f)}{\Delta f} \Delta T \quad (3.2)$$

where $a(\cdot)$ is the longitudinal vehicle acceleration, $G_s(2\pi f)$ is the autopower spectrum of $a(\cdot)$, Δf is the frequency resolution and $\Delta T = t_2 - t_1$ is the time period chosen for the calculation of D_{es} .

These metrics have been used to assess the shift comfort of powertrain state changes, for example engine starts, in hybrid electric vehicles (see [Kuan 06], [GoWE 09]). However, they are only helpful in comparing specific acceleration scenarios, they provide no objective criteria for the shift comfort. In the cited publications, the ideal scenario is that the start-up procedure of the internal combustion engine has no effect on the powertrain, i.e., the longitudinal acceleration remains unchanged. During a gearshift, this is not feasible. Due to the change in transmission output torque, the vehicle acceleration changes as well. Thus, the aforementioned metrics (3.1) and (3.2) have to be adapted in order to be useful during gearshift procedures. For instance, a specific form of an "ideal" acceleration signal $a(\cdot)$ may be defined to serve as a basis for comparing different gearshifts. However, this setting is very subjective and therefore arbitrary. Also, different acceleration scenarios during gearshifts may differ drastically in subjective shift comfort, but yield similar values of the metrics. Thus, assessing shift comfort with the metrics (3.1) and (3.2) is unfeasible. Nonetheless, there is one possibility of roughly evaluating the shift comfort: avoiding oscillations in the engine speed signal. If oscillations occur, they will most likely induce unfavorable jerks in the powertrain as well. Moreover, they can be heard by the vehicle's passengers and the shift procedure is perceived as being faulty. Hence, avoiding engine speed oscillations contributes to good shift quality. An in-depth investigation of the longitudinal acceleration during shifts – apart from the consideration of engine speed oscillations – is beyond the scope of this thesis.

3.2 System Modeling

After the introductory remarks on automatic transmissions in the previous section, a system model is derived in the following that serves as a basis for stability investigations. To this end, a single friction clutch is modeled (see Fig. 3.3). The system consists of

an electro-hydraulic and a mechanical subsystem. The transmission control unit (TCU) generates an electric current in a hydraulic control valve that is connected to the supply pressure line and the oil sump for releasing hydraulic pressure. The control valve generates a control pressure at its outlet, which acts on the clutch piston and generates a force, that, if sufficiently high, compresses the release springs and starts to close the clutch. Thus, the clutch disks are pushed against one another, which in return enables the clutch to transmit a torque. If the pressure is increased further, the clutch stops to slip and the friction disks stick together. Thus, the complete drive torque is transmitted without any losses. For simplification purposes, only one disk is depicted in Fig. 3.3 for the clutch's input and output shaft, respectively. Usually, multiple friction disks are involved to increase the capability of torque transmission. Note that the system model is essentially the same for

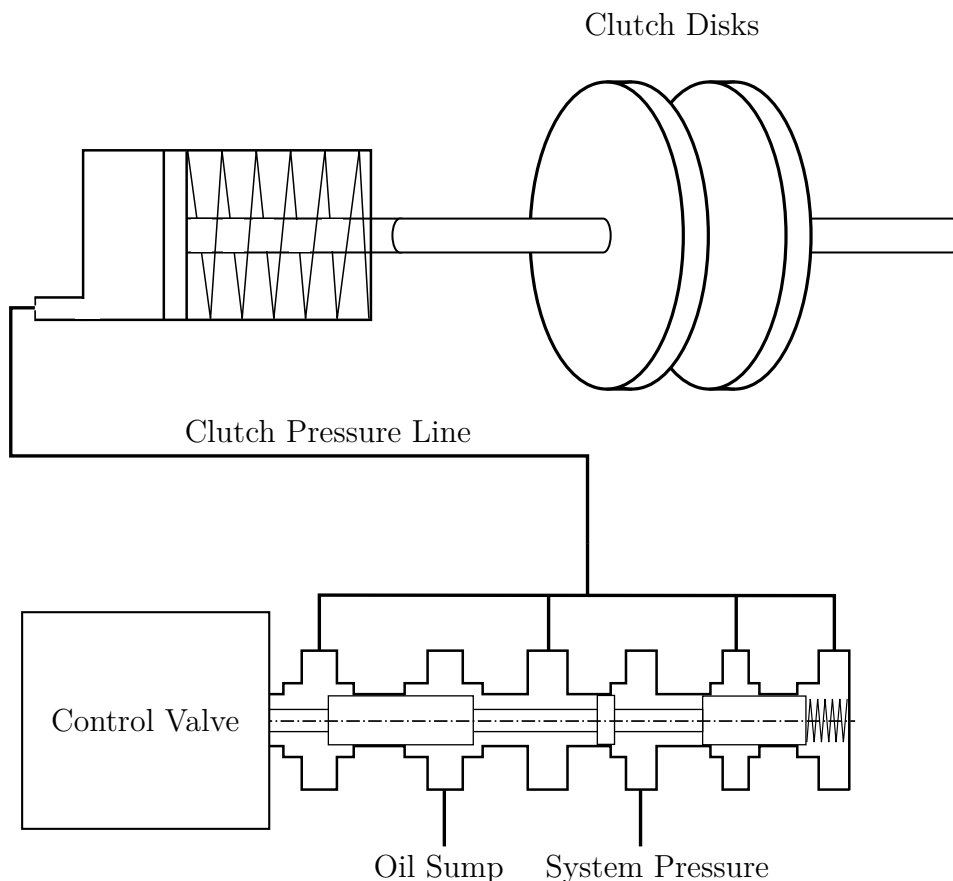


Figure 3.3: Clutch control system overview

both the FDCT and NAG3 transmissions. Both have hydraulically actuated clutches that swap transmitting the drive torque during a gearshift. Also, the hydraulic control system

is the same in both transmissions: Each clutch actuator has a control valve that directly connects to the clutch piston chamber for setting the desired hydraulic pressure. As far as the control system theory is concerned, both transmissions are the same, except for different values of the system parameters. The modeling of the clutch system is divided into the hydraulic and mechanical subsystem.

3.2.1 Hydraulic System

The essential element in the hydraulic system is the control valve, as depicted in Fig. 3.4.

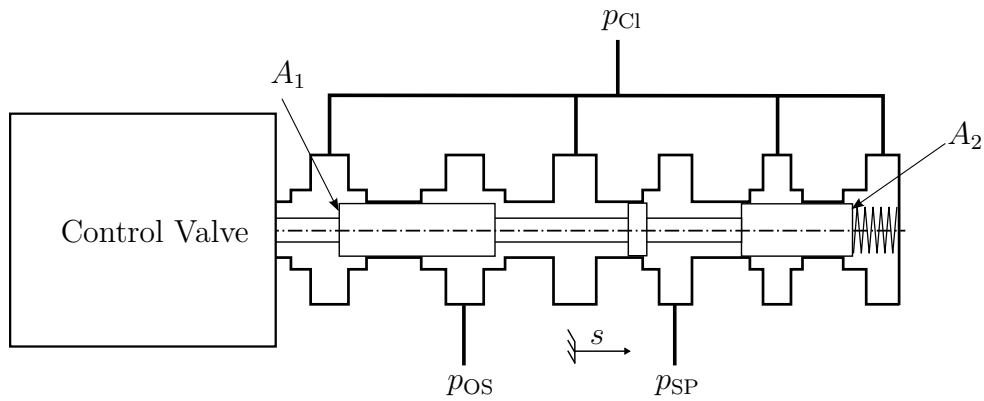


Figure 3.4: Hydraulic control valve with inlets and outlets

There are three main hydraulic ports: The valve outlet line to the clutch piston, the inlet line from the system pressure level and the outlet line to the oil sump. Also, the output pressure is fed back to the control valve in order to generate a hydraulic feedback loop. Thus, an equilibrium of forces exists at the valve piston, consisting of electromagnetic force, spring force and hydraulic force, resulting from the hydraulic pressure acting on the control surface areas A_1 and A_2 . The piston is at rest, if the generated output pressure p_{CL} corresponds to the electric current i of the control valve. If there are disturbances in the clutch pressure, the equilibrium of forces is no longer present and the valve piston moves either to the left to open the outlet line to the oil sump, or it moves to the right to open the inlet line to the system pressure. Hence, the output pressure is hydraulically controlled. By controlling the electric current i of the control valve, the valve set point can be chosen, which corresponds to different output pressures. The control valve can therefore be modeled as follows:

$$m_{CV} \ddot{r}_s = \vec{F}_{el} + \vec{F}_{p,Cl} + \vec{F}_{spring} + \vec{F}_{friction} \quad (3.3)$$

$$\vec{e}_s : \quad m_{CV} \ddot{s} = C_i i - (A_2 - A_1) p_{CL} - c_{CV} s - d_{CV} \dot{s}, \quad (3.4)$$

where

- \vec{r}_s – position vector
- \vec{F}_{el} – electromagnetic force
- $\vec{F}_{friction}$ – viscous friction force
- $\vec{F}_{p,Cl}$ – force generated by clutch pressure feedback
- \vec{F}_{spring} – spring force
- m_{CV} – mass of valve piston
- s – location of valve piston
- i – electric current
- C_i – electromagnetic coefficient
- p_{Cl} – clutch pressure
- A_1, A_2 – control surface areas
- c_{CV} – spring rate of valve return spring
- d_{CV} – viscous damping coefficient of valve piston

Model Assumption 3.1 *Friction forces exceeding the viscous damping term are neglected at this point, since their modeling is very complex and dependent on various assumptions. Also, stick-slip friction is counteracted in the considered transmissions by adding a dithering component to the electric current signal $i(\cdot)$ acting on the valve piston. Thus, the piston is in constant oscillation around its set point and static friction forces are negligible.*

The control pressure p_{Cl} exiting the control valve exerts a force on the clutch piston. However, the piston chamber has to be filled first by the hydraulic current Q_{CV} , before

any pressure in the clutch piston is generated. Figure 3.5 depicts a schematic of the hydraulic clutch subsystem.

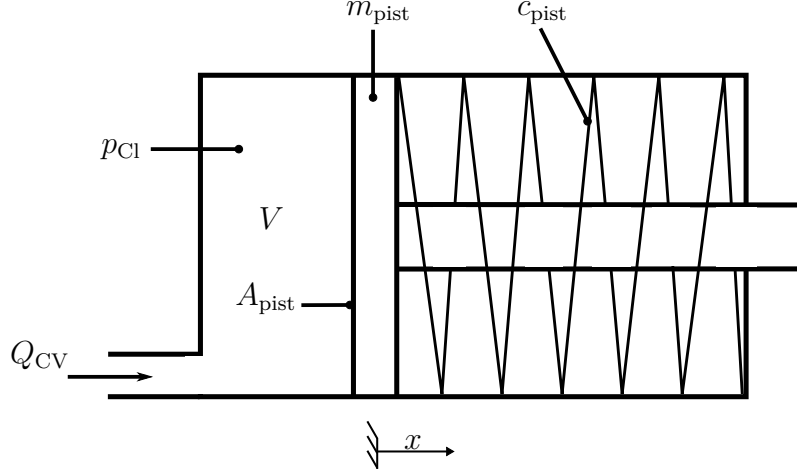


Figure 3.5: Hydraulic clutch subsystem

If the clutch piston is in motion, there is also a displacement current that is required to keep the pressure constant. The hydraulic current that flows from the control valve into the clutch piston is modeled as follows:

$$Q_{CV} = Q_{in} + Q_{out} \quad (3.5)$$

$$Q_{CV} = \alpha \sqrt{\frac{2}{\rho}} A_{in}(s) \sqrt{p_{SP} - p_{Cl}} - \alpha \sqrt{\frac{2}{\rho}} A_{out}(s) \sqrt{p_{Cl} - p_{OS}} \quad (3.6)$$

$$A_{in}(s) := C_{hyd} H(s) s \quad (3.7)$$

$$A_{out}(s) := -C_{hyd} H(-s) s \quad (3.8)$$

where

- Q_{CV} – volume current of control valve
- α – flow coefficient
- ρ – density of oil
- $A_{in}(s)$ – cross section of inlet aperture
- $A_{out}(s)$ – cross section of outlet aperture
- C_{hyd} – hydraulic constant

- $H(\cdot)$ – Heaviside function
- p_{SP} – system supply pressure
- p_{Cl} – clutch pressure
- p_{OS} – pressure of oil sump

Inlet and outlet of the valve piston are therefore modeled as apertures with variable cross sections, which depend on the valve piston position. The hydraulic current follows accordingly. The equations for the aperture cross section are modeled in a way that only one of them is open at a time. At $s = 0$, i.e., if the piston is in the equilibrium position, both apertures are closed.

Model Assumption 3.2 *The dynamic apertures of the control valve are dominant in the clutch pressure line. Other hydraulic apertures may exist in the hydraulic system to influence the oil's dynamics by suppressing pressure oscillations, for example. However, these dynamics and the related apertures are not included in the system model, since they are negligible while the clutch is in operation. They become significant during filling or emptying the clutch piston chamber at the beginning or end of a shift procedure. However, these phases are not considered in this work (see Sections 4.1.2 and 4.1.3 for further details).*

The hydraulic current flowing into the clutch generates a force acting on the clutch piston, which in the end causes its movement. This is modeled as follows:

$$p_{Cl} = \frac{E}{V} \int_{(t)} Q_{CV}(t) - \underbrace{A_{pist} \dot{x}(t)}_{Q_d(t)} dt \quad (3.9)$$

$$\vec{e}_x : \quad m_{pist} \ddot{x} = A_{pist} p_{Cl} - c_{pist} x - d_{pist} \dot{x} \quad (3.10)$$

where

- E – Young's modulus of oil
- A_{pist} – piston surface area
- x – clutch piston position
- V – volume of clutch piston chamber
- Q_d – hydraulic flow disturbance

- m_{pist} – mass of clutch piston
- c_{pist} – spring rate of clutch return spring
- d_{pist} – viscous damping coefficient of clutch piston

Model Assumption 3.3 *Note that the term $Q_d(t) = A_{\text{pist}} \dot{x}(t)$, denoting the hydraulic displacement current caused by the movement of the clutch piston, is modeled as a disturbance signal. Its magnitude is bounded, since $A_{\text{pist}} = \text{const.}$ and $\lim_{t \rightarrow +\infty} |\dot{x}(t)| \ll +\infty$ because of friction and piston position end stops. Also, this influence is very small, since the clutch piston does not move a long distance and the resulting speeds $\dot{x}(\cdot)$ are small as well.*

Centrifugal hydraulic pressure is not present, because of counteractive measures taken by mechanical design. Consider the clutch piston chamber during operation: The piston rotates with a certain angular velocity, which exerts a centrifugal force on the hydraulic oil in the clutch piston chamber. Thus, an additional axial force acting on the clutch piston surface area is created by increased hydraulic pressure. This nonlinear clutch pressure amplification is counteracted by an additional oil chamber opposite to the clutch piston chamber (see [NaBL07]). This design causes the centrifugal pressure to act on both sides of the clutch piston and the forces are canceled out. Thus, centrifugal hydraulic pressures are compensated in the transmission designs considered here and are not part of the system model.

This concludes the modeling of the hydraulic clutch subsystem.

3.2.2 Mechanical Subsystem

The mechanical subsystem is modeled as opposing rotating disks. There is a drive torque acting on the input side and a load torque acting on the output side of the clutch, as depicted in Fig. 3.6. The goal is to control the relative speed between the clutch disks in order to either close the clutch or to control the slipping state by setting a specific relative speed. To achieve this, a coupling torque is generated between the disks. It is dependent on the clutch pressure acting on the friction disks. The slipping clutch is modeled as follows:

$$\vec{e}_x : \quad J_D \ddot{\varphi}_1 = M_D - M_{\text{coup}} - d_c \dot{\varphi}_1 \quad (3.11)$$

$$\vec{e}_x : \quad J_L \ddot{\varphi}_2 = -M_L + M_{\text{coup}} - d_c \dot{\varphi}_2 \quad (3.12)$$

$$M_{\text{coup}} = z r_m \mu (A_{\text{fric}} p_{\text{Cl}} - c_{\text{pist}} x) \quad (3.13)$$

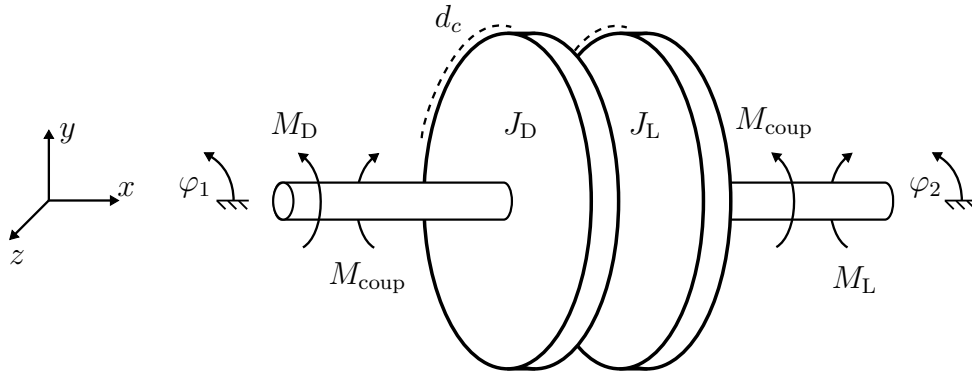


Figure 3.6: Mechanical clutch subsystem

where

- J_D – mass moment of inertia on the input shaft
- J_L – mass moment of inertia on the output shaft
- M_D – driving torque
- M_L – load torque
- φ_1 – coordinate of motion, input shaft
- φ_2 – coordinate of motion, output shaft
- M_{coup} – coupling torque
- z – number of friction pairings of multiple clutch disks
- r_m – mean friction radius
- μ – coefficient of sliding friction
- A_{fric} – surface area of friction pairing
- d_c – viscous damping coefficient of clutch disks

Model Assumption 3.4 *The coefficient of friction μ is assumed to be constant. This is physically not correct, since μ depends on oil temperature and relative speed. However, a more precise model is not necessary here, as the varying friction coefficient is treated as a disturbance acting on the system.*

This concludes the modeling of the electro-hydraulically actuated friction clutch system in slipping state. The case of the closed clutch is not considered, since there is no influence on the system by controlling the clutch pressure when $\omega_{\text{rel}} = \dot{\varphi}_1 - \dot{\varphi}_2 = 0$. However, if the clutch pressure is lowered far enough to generate slip between the clutch disks, the relative speed can be controlled again via the control valve. Therefore, equations (3.4) – (3.13) provide a suitable system model:

$$\left. \begin{aligned}
 m_{\text{CV}} \ddot{s} &= C_i i - (A_2 - A_1) p_{\text{Cl}} - c_{\text{CV}} s - d_{\text{CV}} \dot{s} \\
 Q_{\text{CV}} &= \alpha \sqrt{\frac{2}{\rho}} A_{\text{in}}(s) \sqrt{p_{\text{SP}} - p_{\text{Cl}}} - \alpha \sqrt{\frac{2}{\rho}} A_{\text{out}}(s) \sqrt{p_{\text{Cl}} - p_{\text{OS}}} \\
 A_{\text{in}}(s) &:= C_{\text{hyd}} H(s) s \\
 A_{\text{out}}(s) &:= -C_{\text{hyd}} H(-s) s \\
 p_{\text{Cl}} &= \frac{E}{V} \int_{(t)} Q_{\text{CV}}(t) - \underbrace{A_{\text{pist}} \dot{x}(t)}_{Q_d(t)} dt \\
 m_{\text{pist}} \ddot{x} &= A_{\text{pist}} p_{\text{Cl}} - c_{\text{pist}} x - d_{\text{pist}} \dot{x} \\
 J_D \ddot{\varphi}_1 &= M_D - M_{\text{coup}} - d_c \dot{\varphi}_1 \\
 J_L \ddot{\varphi}_2 &= -M_L + M_{\text{coup}} - d_c \dot{\varphi}_2 \\
 M_{\text{coup}} &= z r_m \mu (A_{\text{fric}} p_{\text{Cl}} - c_{\text{pist}} x)
 \end{aligned} \right\} \quad (3.14)$$

3.3 Stability Analysis

In this section, the stability of the previously derived system model (3.14) is investigated in order to assess the feasibility of adaptive λ -tracking control.

3.3.1 System Class

Since there are nonlinear equations in the system model, the system representation has to be chosen accordingly:

$$\begin{aligned}
 \dot{\mathbf{x}}(t) &= \mathbf{f}(\mathbf{x}(t)) + \mathbf{g}(\mathbf{x}(t)) \cdot u(t) \\
 y(t) &= \mathbf{h}(\mathbf{x}(t)) + \mathbf{d}(\mathbf{x}(t))
 \end{aligned}$$

with the disturbance vector $\mathbf{d}(\mathbf{x}(t))$. The system state vector is:

$$\begin{aligned}
 \mathbf{x} &= \left(x_1 \ x_2 \ x_3 \ x_4 \ x_5 \ x_6 \ x_7 \right)^{\text{T}} \\
 &= \left(s \ \dot{s} \ p_{\text{Cl}} \ x \ \dot{x} \ \dot{\varphi}_1 \ \dot{\varphi}_2 \right)^{\text{T}}
 \end{aligned} \quad (3.15)$$

After a series of elementary conversions, the system model (3.14) is transformed into the complete nonlinear state-space system:

$$\dot{\mathbf{x}}(t) = \mathbf{f}(\mathbf{x}(t)) + \mathbf{g}(\mathbf{x}(t)) \cdot u(t) \quad (3.16)$$

$$y(t) = h(\mathbf{x}(t)) + \mathbf{d}(\mathbf{x}(t)) \quad (3.17)$$

$$\mathbf{f}(\mathbf{x}(t)) = \begin{pmatrix} x_2 \\ -\frac{A_2 - A_1}{m_{CV}} x_3 - \frac{c_{CV}}{m_{CV}} x_1 - \frac{d_{CV}}{m_{CV}} x_2 \\ \frac{E \alpha C_{hyd} \sqrt{2}}{V \sqrt{\rho}} \left(H(x_1) x_1 \sqrt{p_{SP} - x_3} + H(-x_1) x_1 \sqrt{x_3 - p_{OS}} \right) \\ x_5 \\ \frac{A_{pist}}{m_{pist}} x_3 - \frac{c_{pist}}{m_{pist}} x_4 - \frac{d_{pist}}{m_{pist}} x_5 \\ -\frac{z r_m \mu A_{fric}}{J_D} x_3 + \frac{z r_m \mu c_{pist}}{J_D} x_4 - \frac{d_c}{J_D} x_6 \\ \frac{z r_m \mu A_{fric}}{J_L} x_3 - \frac{z r_m \mu c_{pist}}{J_L} x_4 - \frac{d_c}{J_L} x_7 \end{pmatrix} \quad (3.18)$$

$$\mathbf{g}(\mathbf{x}(t)) = \left(0 \quad \frac{C_i}{m_{CV}} \quad 0 \quad 0 \quad 0 \quad 0 \quad 0 \right)^T \quad (3.19)$$

$$h(\mathbf{x}(t)) = x_6 - x_7 \quad (3.20)$$

$$\mathbf{d}(\mathbf{x}(t)) = \left(0 \quad 0 \quad -Q_d \quad 0 \quad 0 \quad \frac{M_D}{J_D} \quad -\frac{M_L}{J_L} \right)^T \quad (3.21)$$

with constants

$$\begin{aligned} & A_1, A_2, c_{CV}, m_{CV}, d_{CV}, E, \alpha, C_{hyd}, V, \rho, p_{SP}, p_{OS}, \\ & A_{pist}, m_{pist}, c_{pist}, d_{pist}, z, r_m, \mu, A_{fric}, d_c, J_D, J_L, C_i > 0 \end{aligned} \quad (3.22)$$

and with the Heaviside function $H(\cdot)$.

Note that as discussed in Model Assumption 3.3, the disturbance signal $Q_d(\cdot)$ is bounded and can therefore be compensated by a feedback controller. Thus, it can be neglected when investigating the system dynamics.

3.3.2 Relative Degree

Using the algorithm given in Section 2.2.2, the relative degree of the nonlinear clutch system can be determined:

$$L_g L_f^0 h(\mathbf{x}) = L_g h(\mathbf{x}) = 0 \quad (3.23)$$

$$L_g L_f^1 h(\mathbf{x}) = 0 \quad (3.24)$$

$$L_g L_f^2 h(\mathbf{x}) = 0 \quad (3.25)$$

$$L_g L_f^3 h(\mathbf{x}) = -\frac{\sqrt{2} C_{\text{hyd}} E A_{\text{fric}} \mu C_i \alpha r_m z (J_D + J_L)}{\sqrt{\rho} J_D J_L V m_{\text{CV}}} \cdot \left(\sqrt{x_3 - p_{\text{OS}}} + H(x_1) \sqrt{p_{\text{SP}} - x_3} - H(x_1) \sqrt{x_3 - p_{\text{OS}}} \right) \quad (3.26)$$

The term in parentheses from (3.26) is crucial, since all other constants are by definition greater than zero:

$$0 \neq \sqrt{x_3 - p_{\text{OS}}} + H(x_1) \sqrt{p_{\text{SP}} - x_3} - H(x_1) \sqrt{x_3 - p_{\text{OS}}} \quad (3.27)$$

In order to check if the term is $\neq 0$ for all \mathbf{x} , two cases are considered.

First Case: $x_1 < 0$

In case of $x_1 < 0$, the clutch is emptied by opening the control valve output towards the oil sump, so the clutch pressure is lowered. Thus, the equation (3.27) now merely states:

$$\sqrt{x_3 - p_{\text{OS}}} \neq 0 \text{ with } x_3 \not\leq p_{\text{OS}} \quad (3.28)$$

Thus, $L_g L_f^3 h(\mathbf{x}) \neq 0$ holds as long as the clutch pressure x_3 is not equal or less than the oil sump pressure p_{OS} . This state is not reached during operation, since it is impossible to reduce the clutch pressure below the oil sump pressure, which is the lowest pressure level in the system. The clutch pressure may be as low as the oil sump pressure in an extreme case, however it is not necessary to reduce it further. Hence, it is of no consequence that there exists no control over the system in this case.

Second Case: $x_1 \geq 0$

If $x_1 > 0$, the control valve fills the clutch with hydraulic oil from the supply pressure line. Equation (3.27) now states:

$$\sqrt{p_{\text{SP}} - x_3} \neq 0 \text{ with } x_3 \not\geq p_{\text{SP}} \quad (3.29)$$

Hence, $L_g L_f^3 h(\mathbf{x}) \neq 0$ holds as long as the clutch pressure does not equal or is exceeding the system supply pressure. This is not achieved during operation, since pressure levels above the supply pressure are neither feasible nor required. Thus, if $x_3 = p_{\text{SP}}$, a state is reached where it is not possible to influence the system towards overcoming this limitation. However, this is never required and thus of no consequence.

In conclusion, $L_g L_f^3 h(\mathbf{x}) \neq 0$ for all \mathbf{x} under the assumptions discussed above. Therefore, the computation of the relative degree of the system results in

$$\delta = 4. \quad (3.30)$$

Note that the system model (3.16) – (3.21) includes certain simplifications that have not been discussed so far, notably the end stops of the control valve piston. Hence, the hydraulic subsystem has limitations regarding its system dynamics:

- The position of the control valve piston is limited by end stops:

$$s_{\min} \leq x_1(t) \leq s_{\max} \quad \forall t \quad (3.31)$$

- Also, the control input, i.e., the electric current of the control valve, is bounded:

$$0 \leq u(t) \leq i_{\max} \quad \forall t \quad (3.32)$$

- Finally, since the acceleration of the control valve piston is limited by the force generated by the bounded electric current, and the viscous damping caused by friction in the control valve, the velocity of the piston is also bounded:

$$-v_1 \leq x_2(t) \leq v_2 \quad \forall t \quad (3.33)$$

The limitations above are not modeled in the system (3.16)-(3.21). Nonetheless, the system dynamics are effected by them, notably the relative degree. As stated in Section 2.1.6,

it can be viewed as the least number of integrators that the input signal has to overcome towards the system output. As discussed above, the position and the velocity of the control valve piston are limited, which corresponds to limits in their respective integrators. If the limits are reached, the integrators cease to contribute to the system dynamics. They become mere constants and reduce the set of differential equations. Thus, the system dynamics are reduced by the number of saturated integrators, i.e., 2. The relative degree is reduced by 2 as well while the saturation is in effect. If the respective system states diverge towards infinity from an unsaturated state, the limitations will quickly stop this behavior and reliably reduce the effective relative degree to $\delta_{\text{eff}} = \delta - 2 = 2$. Thus, the system has an effective relative degree of 2 on a macroscopic scale.

3.3.3 Minimum-Phase Property

As discussed in Section 2.2.2, system (3.16) – (3.21) has to be transformed into the Byrnes-Isidori Normal Form in order to investigate its zero dynamics. The functions $\phi_1, \dots, \phi_\delta$ are obtained with the help of the presented algorithm (2.26) – (2.28) using a computer algebra system (MuPAD Symbolic Math Toolbox for MATLAB R2010b, by SciFace Software, version 5.5.0, 2010):

$$\phi_1(\mathbf{x}) = x_6 - x_7 \quad (3.34)$$

$$\phi_2(\mathbf{x}) = -\frac{z r_m \mu A_{\text{fric}} (J_D + J_L)}{J_D J_L} x_3 + \frac{z r_m \mu A_{\text{fric}} (J_D + J_L)}{J_D J_L} x_4 - \frac{d_c}{J_D} x_6 + \frac{d_c}{J_L} x_7 \quad (3.35)$$

$$\begin{aligned} \phi_3(\mathbf{x}) = & \frac{d_c(d_c x_6 + z r_m \mu A_{\text{fric}} x_3 - z r_m \mu c_{\text{pist}} x_4)}{J_D^2} \\ & - \frac{d_c(d_c x_7 + z r_m \mu A_{\text{fric}} x_3 - z r_m \mu c_{\text{pist}} x_4)}{J_L^2} + \frac{z r_m \mu c_{\text{pist}}(J_D + J_L)}{J_D J_L} x_5 \\ & + \frac{E z r_m \mu A_{\text{fric}}(J_D + J_L)}{J_D J_L V \sqrt{\rho}} \\ & \cdot \left(A_{\text{pist}} \rho x_5 + \sqrt{2} C_{\text{hyd}} \alpha x_1 (H(x_1) - 1) \sqrt{x_3 - p_{\text{OS}}} \right. \\ & \quad \left. - \sqrt{2} C_{\text{hyd}} \alpha x_1 H(x_1) \sqrt{p_{\text{SP}} - x_3} \right) \end{aligned} \quad (3.36)$$

$$\begin{aligned}
 \phi_4(\mathbf{x}) = & -\frac{d_c^2(d_c x_6 + z r_m \mu A_{\text{fric}} x_3 - z r_m \mu c_{\text{pist}} x_4)}{J_D^3} \\
 & + \frac{d_c^2(d_c x_7 + z r_m \mu A_{\text{fric}} x_3 - z r_m \mu c_{\text{pist}} x_4)}{J_L^3} \\
 & - \frac{E}{V \sqrt{\rho}} \left(A_{\text{pist}} \sqrt{\rho} x_5 + \sqrt{2} C_{\text{hyd}} \alpha x_1 (H(x_1) - 1) \sqrt{x_3 - p_{\text{OS}}} \right. \\
 & \quad \left. - \sqrt{2} C_{\text{hyd}} \alpha x_1 H(x_1) \sqrt{p_{\text{SP}} - x_3} \right) \\
 & \cdot \left(\frac{z r_m \mu A_{\text{fric}} d_c}{J_D^2} + \frac{z r_m \mu A_{\text{fric}} d_c}{J_L^2} \right. \\
 & \quad + \frac{\sqrt{2} E C_{\text{hyd}} \alpha z r_m \mu (J_D + J_L) (-\sqrt{p_{\text{SP}} - x_3})}{2 J_D J_L \sqrt{\rho} \sqrt{x_3 - p_{\text{OS}}} \sqrt{p_{\text{SP}} - x_3}} x_1 \\
 & \quad \left. + \frac{\sqrt{2} E C_{\text{hyd}} \alpha z r_m \mu (J_D + J_L) (H(x_1) (\sqrt{x_3 - p_{\text{OS}}} + \sqrt{p_{\text{SP}} - x_3}))}{2 J_D J_L \sqrt{\rho} \sqrt{x_3 - p_{\text{OS}}} \sqrt{p_{\text{SP}} - x_3}} x_1 \right) \\
 & - \frac{z r_m \mu c_{\text{pist}} d_c (J_D^2 + J_L^2)}{J_D^2 J_L^2} x_5 \\
 & - \frac{z r_m \mu (V c_{\text{pist}} + A_{\text{fric}} A_{\text{pist}} E) (J_D + J_L) (c_{\text{pist}} x_4 - A_{\text{pist}} x_3 + d_{\text{pist}} x_5)}{J_D J_L V m_{\text{pist}}} \\
 & - \frac{\sqrt{2} A_{\text{fric}} C_{\text{hyd}} E \alpha z r_m \mu (J_D + J_L)}{J_D J_L V \sqrt{\rho}} \\
 & \cdot \left(\sqrt{x_3 - p_{\text{OS}}} + H(x_1) (-\sqrt{x_3 - p_{\text{OS}}} + \sqrt{p_{\text{SP}} - x_3}) \right) x_2
 \end{aligned} \tag{3.37}$$

The generation of the functions $\phi_{\delta+1}, \dots, \phi_n$, necessary to obtain the complete mapping $\Phi(\mathbf{x})$, is very difficult. Moreover, the inverse $\Phi^{-1}(\mathbf{z})$ is required to find the corresponding functions $\dot{z}_1, \dots, \dot{z}_n$ to complete the Byrnes-Isidori Normal Form, which is even more difficult to find. The Heaviside- and square-root-functions in (3.34) – (3.37) hinder the generation of a transformation matrix $\Phi(\mathbf{x})$ or its inverse $\Phi^{-1}(\mathbf{z})$. Thus, the algorithm discussed in Section 2.2.2 is not feasible here.

However, a different approach can be taken. It is possible to split the nonlinear system into its hydraulic and mechanical subsystems, respectively. Thus, a nonlinear subsystem with the hydraulic model and a linear subsystem with the mechanical model can be created. Their dynamics are independent, so a separate stability analysis can be performed for each subsystem. There exists only one signal – $x_3(\cdot)$, i.e., the current clutch pressure p_{Cl} – that is fed from the hydraulic to the mechanical subsystem:

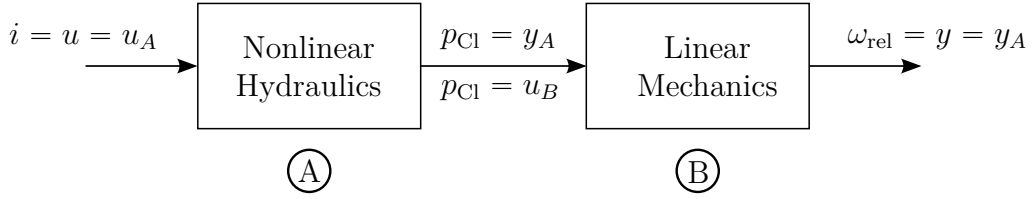


Figure 3.7: Splitting the system into a nonlinear and a linear subsystem

First, consider the hydraulic Subsystem (A). The electric current is the input signal, the clutch pressure is the output signal of this subsystem:

$$\dot{\mathbf{x}}_A(t) = \mathbf{f}_A(\mathbf{x}_A(t)) + \mathbf{g}_A(\mathbf{x}_A(t)) \cdot u_A(t) \quad (3.38)$$

$$y_A(t) = h_A(\mathbf{x}_A(t)) + d_A(\mathbf{x}_A(t)) \quad (3.39)$$

$$\mathbf{f}_A(\mathbf{x}_A(t)) = \begin{pmatrix} x_2 \\ -\frac{A_2 - A_1}{m_{CV}} x_3 - \frac{c_{CV}}{m_{CV}} x_1 - \frac{d_{CV}}{m_{CV}} x_2 \\ \frac{E \alpha C_{hyd} \sqrt{2}}{V \sqrt{\rho}} \left(H(x_1) x_1 \sqrt{p_{SP} - x_3} + H(-x_1) x_1 \sqrt{x_3 - p_{OS}} \right) \end{pmatrix} \quad (3.40)$$

$$\mathbf{g}_A(\mathbf{x}_A(t)) = \begin{pmatrix} 0 \\ \frac{C_i}{m_{CV}} \\ 0 \end{pmatrix} \quad (3.41)$$

$$h_A(\mathbf{x}_A(t)) = x_3 \quad (3.42)$$

$$d_A(\mathbf{x}_A(t)) = -Q_d \quad (3.43)$$

Note that the additional hydraulic flow $Q_d(\cdot)$, modeled as a disturbance signal, is not part of the subsystems dynamics, as discussed in Model Assumption 3.3. The relative degree of the first subsystem can be computed:

$$L_g L_f^0 h_A(\mathbf{x}_A) = L_g h_A(\mathbf{x}_A) = 0 \quad (3.44)$$

$$L_g L_f^1 h_A(\mathbf{x}_A) = 0 \quad (3.45)$$

$$L_g L_f^2 h_A(\mathbf{x}_A) = -\frac{C_{hyd} E A_{fric} \mu C_i \alpha r_m z (J_D + J_L)}{\sqrt{\rho} J_D J_L V m_{CV}} \cdot \left(\sqrt{x_3 - p_{OS}} + H(x_1) \sqrt{p_{SP} - x_3} - H(x_1) \sqrt{x_3 - p_{OS}} \right) \quad (3.46)$$

Equation (3.46) is the same as (3.26). Thus, the same remarks apply and the computation of the relative degree terminates at $L_g L_f^2 h_A(\mathbf{x}_A)$. Hence, the hydraulic Subsystem (A) has a relative degree of $\delta_A = 3$.

Consider the system order of Subsystem $\textcircled{\text{A}}$, i.e., $n_A = 3$. For any zero dynamics to exist in a system, the relative degree has to be less than the system order, i.e., $\delta < n$ (see [Isid 95]). Since the relative degree equals the system order in this case, i.e., $\delta_A = n = 3$, there exist no zero dynamics. Hence, the existence of any unstable zero dynamics can be ruled out.

Consider the linear mechanical Subsystem $\textcircled{\text{B}}$, with the clutch pressure p_{C1} acting as the input, and the relative speed of the clutch system ω_{rel} being the output signal, in form of a linear state-space notation:

$$\dot{\mathbf{x}}_B(t) = \mathbf{A}_B \mathbf{x}_B(t) + \mathbf{b}_B u_B(t) \quad (3.47)$$

$$y_B(t) = \mathbf{c}_B \mathbf{x}_B(t) + \mathbf{d}_B \quad (3.48)$$

$$\mathbf{A}_B = \begin{pmatrix} 0 & 1 & 0 & 0 \\ -\frac{c_{\text{pist}}}{m_{\text{pist}}} & -\frac{d_{\text{pist}}}{m_{\text{pist}}} & 0 & 0 \\ \frac{z r_m \mu c_{\text{pist}}}{J_D} & 0 & -\frac{d_c}{J_D} & 0 \\ -\frac{z r_m \mu c_{\text{pist}}}{J_L} & 0 & 0 & -\frac{d_c}{J_L} \end{pmatrix} \quad (3.49)$$

$$\mathbf{b}_B = \begin{pmatrix} 0 \\ \frac{A_{\text{pist}}}{m_{\text{pist}}} \\ -\frac{z r_m \mu A_{\text{fric}}}{J_D} \\ \frac{z r_m \mu A_{\text{fric}}}{J_L} \end{pmatrix} \quad (3.50)$$

$$\mathbf{c}_B = \begin{pmatrix} 0 & 0 & 1 & -1 \end{pmatrix} \quad (3.51)$$

$$\mathbf{d}_B = \begin{pmatrix} 0 \\ 0 \\ M_D \\ -M_L \end{pmatrix} \quad (3.52)$$

With Subsystem $\textcircled{\text{B}}$, linear system analysis methods can be applied. The location of the system's zeros is computed with the help of the Rosenbrock matrix:

$$\det \begin{bmatrix} \mathbf{A}_B - z_k \mathbf{I} & \mathbf{b}_B \\ \mathbf{c}_B & 0 \end{bmatrix} = 0 \quad (3.53)$$

$$z_1 = -\frac{2 d_c}{J_D + J_L} \quad (3.54)$$

$$z_{2,3} = -\frac{d_{\text{pist}}}{2 m_{\text{pist}}} \pm \sqrt{\frac{d_{\text{pist}}^2}{4 m_{\text{pist}}^2} - \frac{c_{\text{pist}}}{m_{\text{pist}}} + \frac{A_{\text{pist}} c_{\text{pist}}}{A_{\text{fric}} m_{\text{pist}}}} \quad (3.55)$$

To ensure that the subsystem is minimum-phase, all zeros have to be located in the left-half open complex plane, i.e., have negative real parts:

$$0 > -\frac{d_{\text{pist}}}{2 m_{\text{pist}}} \pm \sqrt{\frac{d_{\text{pist}}^2}{4 m_{\text{pist}}^2} - \frac{c_{\text{pist}}}{m_{\text{pist}}} + \frac{A_{\text{pist}} c_{\text{pist}}}{A_{\text{fric}} m_{\text{pist}}}} \quad (3.56)$$

$$A_{\text{fric}} > A_{\text{pist}} \quad (3.57)$$

As long as the system is designed so that $A_{\text{fric}} > A_{\text{pist}}$, which is the case with the transmissions considered here (see [Daim 11] and [Daim 13]), Subsystem (B) is in fact minimum-phase, since all zeros are negative, i.e., $z_{1,2,3} < 0$. Note that the subsystem is of system order $n_B = 4$, therefore, its relative degree is $\delta_B = 1$.

To conclude, the findings of investigating both Subsystems (A) and (B) individually are:

- The relative degree of the complete nonlinear system is $\delta_A + \delta_B = \delta = 4$, which is the same result found in (3.26).
- The hydraulic Subsystem (A) does not have any zero dynamics.
- The mechanical Subsystem (B) has three zeros, all of which are stable if $A_{\text{fric}} > A_{\text{pist}}$, which is the case in the systems at hand. Thus, Subsystem (B) is minimum-phase.
- In conclusion, the complete nonlinear system (3.16)-(3.21) is minimum-phase.

The findings discussed above are consistent with the effective relative degree of $\delta_{\text{eff}} = 2$. The reduced relative degree applies only on a macroscopic scale, if restrictions are considered that are not part of the mathematical system model. As far as the system's zeros are concerned, the relative degree is still $\delta = 4$.

3.3.4 Sign of High-Frequency Gain

As discussed above, the sign of the high-frequency gain denotes the direction of action of the control output actuator. In the case of the clutch system, a distinction concerning the shift type has to be made: During powered upshifts, a positive control error signal $e(t)$ requires the respective clutch to be pressurized more, resulting in a reduction of the engine speed and in turn reducing the error signal as well. Thus, the sign is positive. During powered downshifts, the existence of a positive tracking error requires the pressure of the engaging clutch to be lowered. Thus, the sign is negative in this case. Similar considerations are made for unpowered up- and downshifts, respectively. For each shift type, the sign of the high-frequency gain s_{hf} is determined, as shown in Table 3.3.

Table 3.3: Sign of high-frequency gain

Shift Type	Upshift	Downshift
Powered Shift	$s_{\text{hf}} = 1$	$s_{\text{hf}} = -1$
Unpowered Shift	$s_{\text{hf}} = -1$	$s_{\text{hf}} = 1$

The coefficient s_{hf} is included in the controller's error signal computation, to correct for changing signs of the high-frequency gain. Hence, the sign of the error signal $e(t)$ changes accordingly, which results in a change of sign for the individual feedback terms and the subsequent control output $u(t)$ as well:

$$e(t) = s_{\text{hf}} \cdot (y(t) - y_{\text{ref}}(t)) \quad (3.58)$$

The definition given in Table 3.3 replaces the previous one from (2.18) in Section 2.1.6.

3.4 Requirements of Control Architecture

In this section, the conclusions of the stability analysis are drawn and a suiting architecture for adaptive λ -tracking controllers is devised.

3.4.1 Feedback Structure

As discussed in Section 2.1.6, the effective relative degree of $\delta_{\text{eff}} = 2$ requires a derivative feedback term, in order to reduce the relative degree of the closed-loop system to $\delta_{\text{eff}} - 1 = 1$. Thus, the basic adaptive controller (2.11) has to be extended by a derivative feedback term, adapted from [BeSt 10]:

$$e(t) = s_{\text{hf}} \cdot (y(t) - y_{\text{ref}}(t)) \quad (3.59)$$

$$u(t) = k(t) e(t) + \kappa k(t) \dot{e}(t) \quad (3.60)$$

$$\dot{k}(t) = \begin{cases} \gamma (|e(t)| - \varepsilon\lambda)^2, & \text{if } |e(t)| > 1 + \varepsilon\lambda \\ \gamma (|e(t)| - \varepsilon\lambda)^{\frac{1}{2}}, & \text{if } \varepsilon\lambda \leq |e(t)| \leq 1 + \varepsilon\lambda \\ 0, & \text{if } |e(t)| < \varepsilon\lambda \quad \wedge \quad t - t_e < t_d \\ -\sigma \left(1 - \frac{|e(t)|}{\varepsilon\lambda}\right) k(t), & \text{if } |e(t)| < \varepsilon\lambda \quad \wedge \quad t - t_e \geq t_d \end{cases} \quad (3.61)$$

where $\lambda \geq 0, \gamma > 1, \sigma > 0, t_d > 0, 0 < \varepsilon \leq 1, \kappa > 0$.

The common gain factor $k(\cdot)$, as calculated by the adaption law, affects both the proportional and derivative feedback gains of the controller. The coefficient κ can be used to set

a ratio between the two and thus generate a dominant proportional feedback by choosing $0 < \kappa < 1$, for example. For $\kappa > 1$, the derivative term would become dominant. As shown in [BeLo 12], it is sensible to choose a small value for κ . The mere existence of the derivative feedback ensures stability of the closed-loop system. Setting a small value for κ reduces noise generated by the differentiated term $\dot{e}(\cdot)$. Also, a strong derivative feedback acts as a damping element in the closed-loop system and increases settling time of the controller. In conclusion, $0 < \kappa < 1$ is recommended.

Note that the generation of the error signal $e(\cdot)$ does not require additional sensors. The angular velocity of the clutch disks is available, since speed sensors are already present in the transmissions considered here. The hardware setup does not have to be extended.

3.4.2 Requirements of Adaption Law

As discussed above in Section 2.1.4, the adaptor is supposed to be able to increase, but also decrease the common gain factor $k(\cdot)$, if necessary. This creates a much more energy-efficient control architecture, since the energy put into the system by the controller is kept as low as possible and as high as necessary.

Also, a low gain factor produces weaker reactions to the change of the error signal $e(\cdot)$. While at first this may seem unfavorable, since the control goal will not be reached as fast as possible, it also achieves a smoother transition of the system while reducing $e(\cdot)$ below the error neighborhood λ . Thus, the powertrain experiences less jolts that may be perceived as being uncomfortable by the driver and passengers, caused by sudden changes in hydraulic clutch pressure. It is essential that any reactions generated by the controller, and thus by the adaption law, ensure continued driving comfort. The controllers devised in this thesis are not supposed to cause any regression in shift comfort. This has to be observed when choosing and designing adaptive controllers and their underlying adaption laws.

This concludes the analysis of the hydraulic clutch system regarding high-gain feedback stability. An adaptive λ -tracking controller can be implemented.

4 Control Design

After the high-gain feedback stability of the clutch control system has been established in the previous chapter, this chapter focuses on the actual adaptive controllers and their underlying adaption laws that are designed and implemented into the FDCT and NAG3 control software, respectively. Control structure and adaption laws are discussed and evaluated using a SiL simulation setup. Also, some remarks on digital control systems are made.

Note that the existing transmission control software is extended, which runs on a series production control unit. Thus, *no special prototyping hardware* is used.

4.1 Software Integration

For both the FDCT and NAG3 transmissions, the clutch control algorithms are designed as digital controllers that are integrated into the control software. Thus, the continuous control algorithms discussed so far are transformed into a time-discrete set of equations. The details of the resulting digital adaptive controller are discussed in Section 4.6.

The software modules responsible for conducting the gearshift procedures are extended by the adaptive control architecture. Software switches are included to select the traditional or the adaptive controllers in order to facilitate comparative experiments.

4.1.1 Adaptive Control during Gearshifts

As discussed above, powered gearshifts follow two distinct procedures that are divided into specific phases: the constrained and the release shifts, respectively. Depending on the current driving state, one of the two is selected:

Table 4.1: Classification of shift procedures

Table 4.1: Classification of shift procedures		
Accelerating		Coasting
Upshift	Constrained Shift	Release Shift
Downshift	Release Shift	Constrained Shift

During constrained shifts, for example shifting up while accelerating, the engine speed is forced against its current gradient: to reduce speed while accelerating and to increase speed while coasting. In release shifts, the opposite is the case, the engine speed is changed towards the direction of its current gradient, for instance while shifting down during acceleration. The constrained and release shift procedures are performed differently (see [Förs 91], [RöWa 95]).

The clutch controller is designed to control the engine speed during a shift, i.e., $y(t) := n_{\text{eng}}(t)$. In case of a torque converter without an engaged lock-up clutch, the torque converter output speed is controlled. For simplification, it is referred to as the engine speed for further considerations. Thus, the reference trajectory $w(\cdot)$ is the desired progression of the engine speed and the control signal $u(\cdot)$ effects the corresponding pressure of the clutch that is responsible for setting the engine speed by increasing or decreasing its relative speed accordingly. Hence, the relative speed of the controlled clutch is proportional to the engine speed for a specific gear change. This speed mapping is carried out by the transmission control software by selecting the proper gear ratios and clutch speeds.

Note that independent gain factors $k_{1,2}(\cdot)$ are used for up- and downshift procedures, respectively. It is also conceivable to use only one gain factor, or even to distinguish between individual gearshifts. For example, the gain factor for shifts from 1st to 2nd gear may be saved and adapted independently from the gain factor during shifts from 2nd to 3rd gear. In this thesis, the controller distinguishes only between up- and downshifts and therefore uses two individually saved gain factors. More extensive investigations are necessary to determine if more gain factors are favorable or even if the reduction to one overall gain factor is feasible. Since it has no effect on controller performance and is useful for simplification, the individual gain factors $k_{1,2}(\cdot)$ are generally referred to as $k(\cdot)$. A distinction is made whenever necessary.

4.1.2 Constrained Shift

Constrained shifts are carried out as follows: The disengaging clutch reduces its pressure to a value that is just high enough to transmit the current torque. At the same time, the engaging clutch increases its pressure from near-zero to a value that is just below the ability to transmit any torque. After this state has been achieved, both clutch pressures – and thus their ability to transmit torque – are overlapped: The engaging clutch increases its pressure while the disengaging clutch reduces its pressure. After this torque handover, the disengaging clutch is emptied to a near-zero pressure. Note that up to this point, the engine speed is still at the value corresponding to the previous gear. Now, the engaging

clutch increases its pressure for a time to force the engine speed towards its new set point corresponding to the target gear ratio. This phase is performed with the help of an engine speed controller and is marked with a gray box in plots (see Fig. 4.1). After the engine speed has been set, the shift procedure is complete.

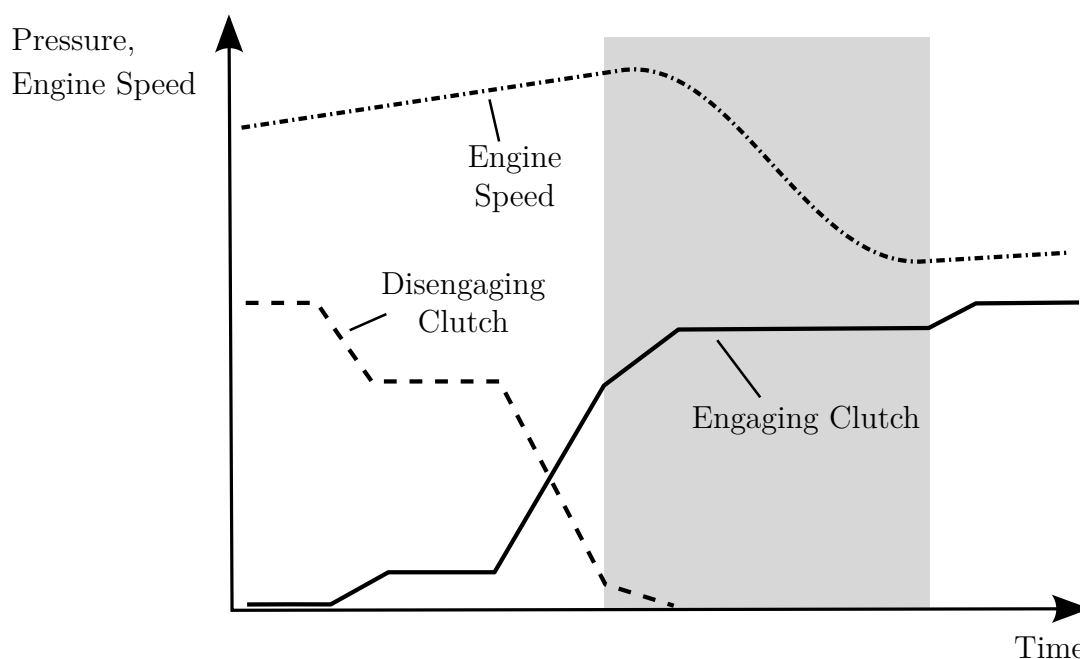


Figure 4.1: Exemplary constrained shift procedure

The adaptive controllers discussed in this thesis are designed to perform the speed control phase of the shift procedure. They are implemented instead of the traditional speed controller.

4.1.3 Release Shift

At first, release shifts are set up the same way as constrained shifts: The disengaging clutch reduces its pressure as far as possible in order to barely transmit the current drive torque, whereas the engaging clutch increases its pressure to a level where no torque is transmitted yet. At this point, the disengaging clutch reduces pressure even further for a time, so that the engine speed may converge to the value corresponding to the target gear. Thus, the engine dynamics are released for a short period of time. During this phase, which is again marked with a gray box in plots, the engine speed controller is in operation. After the desired speed value has been reached, the disengaging clutch increases its pressure again to hold the current speed. Now, the hydraulic clutch pressures are overlapped in the same way as before during constrained shifts. After the disengaging

clutch has been fully emptied, the engaging clutch now fully transmits the torque. Since the engine speed has been set before, the shift procedure is now complete (see Fig. 4.2). Again, the phase where the engine speed is set is carried out with speed controllers. They are replaced by the adaptive controllers discussed in this thesis, overtaking the control task.

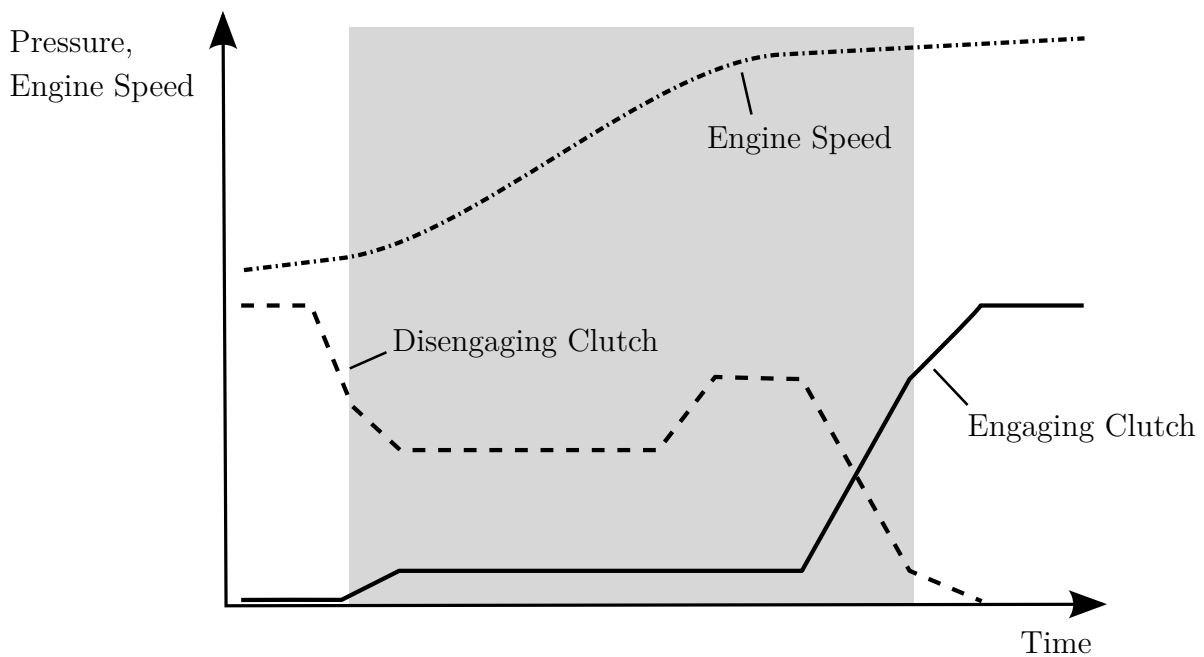


Figure 4.2: Release shift procedure

4.1.4 Simulation Environment

In order to quickly evaluate control designs, a SiL simulation environment using the software Silver (by QTronic, Version 2.5.5, 2013) is used. It incorporates a vehicle model, a comprehensive transmission hardware model and a simulated TCU that runs the actual control software. With this setup, the control software including the adaptive controller can be simulated and virtual experiments can be conducted.

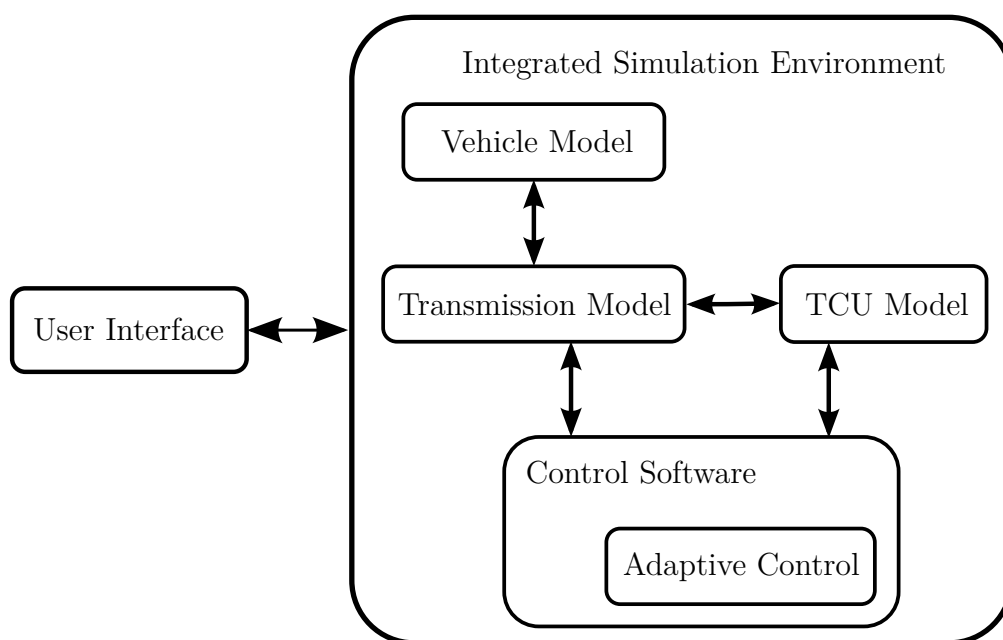


Figure 4.3: Software-in-the-Loop simulation setup

The mathematical models that the simulation environment is based on have been developed independently, prior to this thesis. They have been shown to be sufficiently accurate and reliable by extensive validation on test-benches and are used in multiple research and development departments at Daimler AG.

4.2 Adjustment of Adaptive Controller

In this section, some extensions are made to the adaptive controller (3.59) – (3.61) to account for specific system properties of the clutch control system at hand and to enhance control performance.

4.2.1 Integral Control Feedback

So far, only a PD-feedback structure has been considered, where the derivative feedback is needed for stability reasons. However, it is also advantageous to investigate integral feedback terms. Traditionally, integral feedback is responsible for the elimination of steady-state errors and has been used in the context of high-gain feedback control before

(see [WUDZ04]). Thus, the control structure is extended (see [LoBe11]):

$$e(t) = s_{\text{hf}} \cdot (y(t) - y_{\text{ref}}(t)) \quad (4.1)$$

$$u(t) = k(t) e(t) + \kappa k(t) \dot{e}(t) + \eta k(t) \int_0^t e(\tau) d\tau \quad (4.2)$$

$$\dot{k}(t) = \begin{cases} \gamma (|e(t)| - \varepsilon\lambda)^2, & \text{if } |e(t)| > 1 + \varepsilon\lambda \\ \gamma (|e(t)| - \varepsilon\lambda)^{\frac{1}{2}}, & \text{if } \varepsilon\lambda \leq |e(t)| \leq 1 + \varepsilon\lambda \\ 0, & \text{if } |e(t)| < \varepsilon\lambda \quad \wedge \quad t - t_e < t_d \\ -\sigma \left(1 - \frac{|e(t)|}{\varepsilon\lambda}\right) k(t), & \text{if } |e(t)| < \varepsilon\lambda \quad \wedge \quad t - t_e \geq t_d \end{cases} \quad (4.3)$$

$$k(0) = k_0 \quad (4.4)$$

where $\lambda \geq 0, \gamma > 1, \sigma > 0, t_d > 0, 0 < \varepsilon \leq 1, \kappa > 0, \eta > 0$.

The coefficient η is used to set a ratio between proportional and integral feedback terms. At first, it is set to $\eta = 1$.

There is another benefit in using an integral feedback term. Consider the control output at the beginning of the speed control phase during the shift procedure: First, the error signal and its time derivative are zero, i.e., $e(0) = \dot{e}(0) = 0$. Thus, a PD-feedback controller would result in a control output signal of $u(0) = 0$ as well and therefore reduce the current clutch pressure towards zero. This is caused by the lack of any feed-forward control, which has been specifically excluded to avoid calibration. This unfavorable behavior is depicted in Fig. 4.4. The top plot shows the reference and actual speed signals, respectively. At the beginning of each speed control phase, the engine accelerates away from the reference trajectory, which coincides with the control output signal $u(t)$ being zero at the beginning (see time indexes 61.7 s and 65.8 s in the center plot, respectively). This causes the clutch pressure to be decreased, as is depicted in the pressure signals in the bottom plot of Fig. 4.4 around the same time. Note that the clutch pressure signals do not show actual clutch pressures, since the sensors are placed in some distance from the clutch pistons. However, they can be consulted for qualitative investigations. Also, since the control output signal $u(\cdot)$ is the electric current of the hydraulic control valve $i(\cdot)$, its unit is $[u] = \text{mA}$.

To avoid this unwanted decrease, the controller needs to set a certain pressure value in the clutch when taking over control from the previous open-loop control algorithms. Ideally, it is initialized in a way that would generate the same control output signal as before, so there would be a continuous handover from one shift phase to the other.

The integral term can be used to achieve this behavior. Its integrator may be initialized

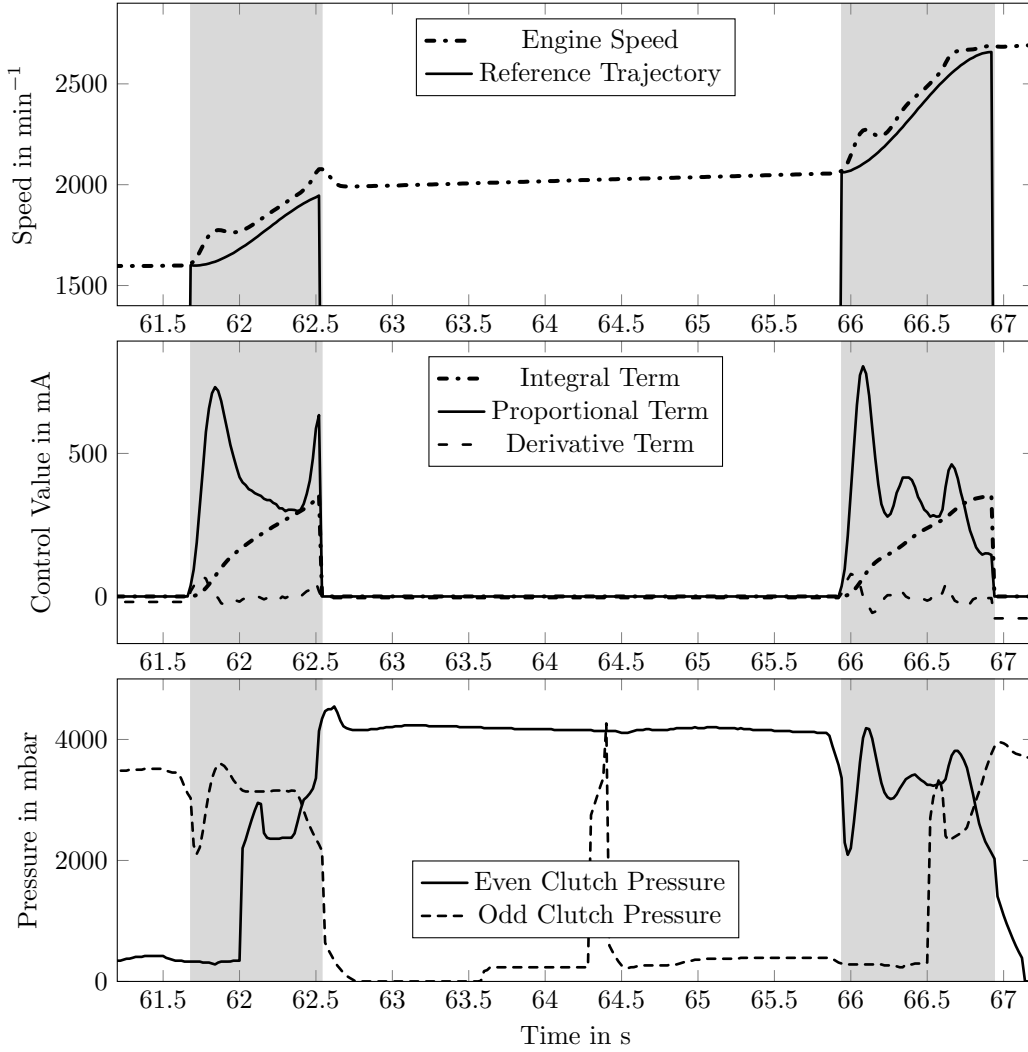


Figure 4.4: SiL simulation of exemplary downshift procedures without control initialization in FDCT transmission

to a starting value that corresponds to the previous pressure setting. From this point on, the control behavior is governed by the adaptive controller only.

The integral term is therefore set to an initial value I_0 , which is obtained from the previously set clutch pressure:

$$I_0 \propto u(-0) \propto p_{Cl}(-0) \quad (4.5)$$

$$\eta k(t) \int_{-t}^0 e(\tau) d\tau \stackrel{\dagger}{=} I_0 \quad (4.6)$$

The resulting control behavior is tested in simulation. As depicted in Fig. 4.5, the initial

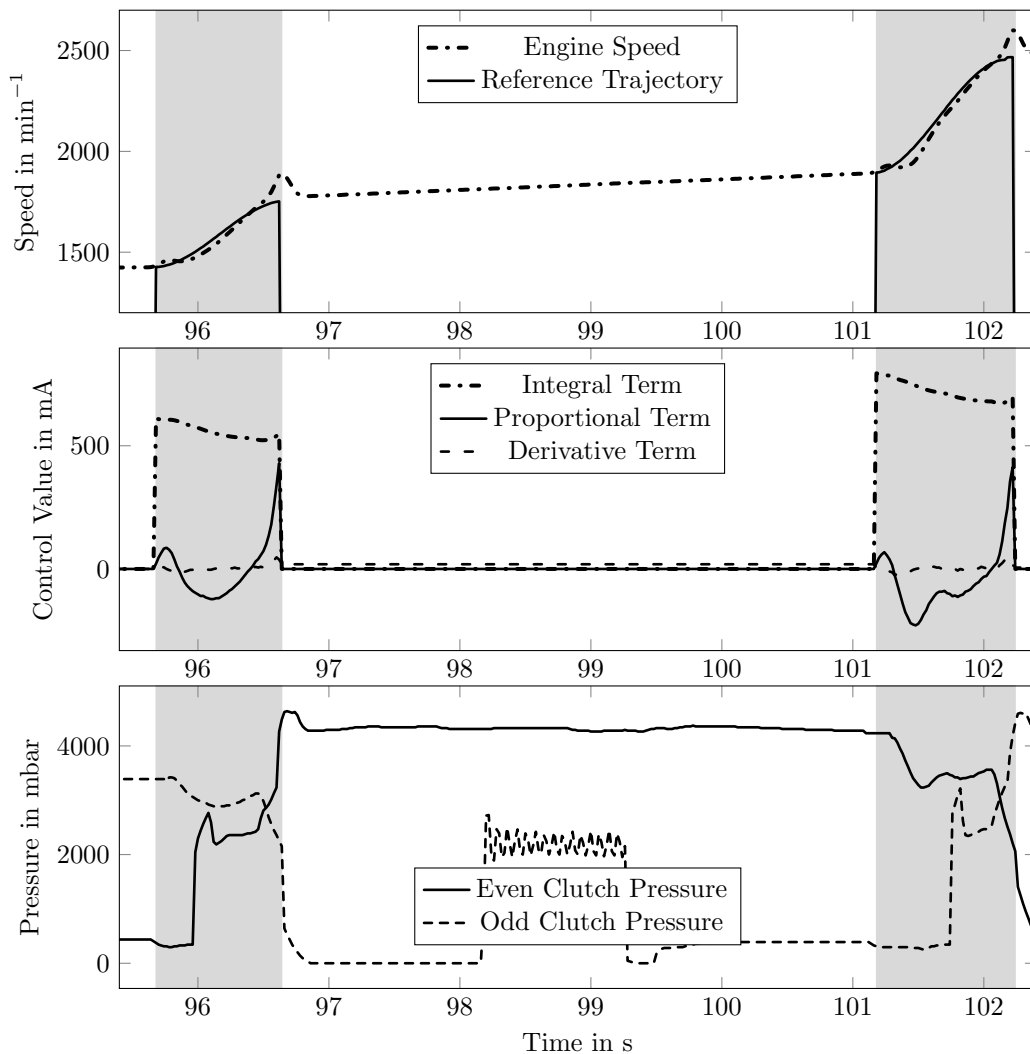


Figure 4.5: SiL simulation of exemplary downshift procedures with control initialization of the integral feedback term in FDCT transmission

control output is no longer zero at the beginning of the speed control phase, due to the initialization of the integral term. Thus, there is no corresponding drop in the clutch pressure signal and the shift procedure is carried out much faster and with a smoother overall clutch pressure signal, which helps to keep sudden longitudinal accelerations low and shift comfort high.

4.2.2 Scaling of Adaption Dynamics

Consider a typical control scenario, where the adaption law has to increase the common gain factor $k(\cdot)$ during a shift procedure. For demonstration purposes, a simulation of one upshift procedure during vehicle pull away is carried out. As depicted in the exemplary

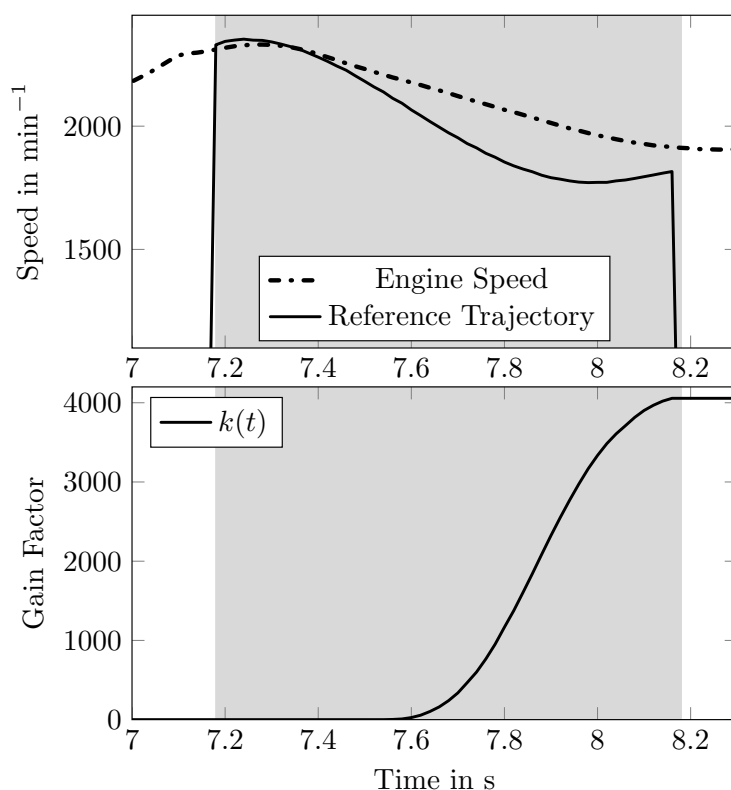


Figure 4.6: SiL simulation of an exemplary adaption of $k(\cdot)$ from 0 to ca. 4000 during upshift procedure with increase coefficient $\gamma = 0.5$

simulation in Fig. 4.6, the gain factor $k(\cdot)$ is increased from 0 to ca. 4000 during one upshift procedure. However, this value is much too high. Investigations of the traditional clutch control software revealed that a feasible gain level is $k = [0.2, 2]$, and thereby four orders of magnitude smaller than the adapted value in Fig. 4.6. Thus, the adaption law has to be scaled down to achieve lower levels of $k(\cdot)$ with corresponding adaption dynamics. To this end, the increase coefficient γ is reduced by four orders of magnitude as well, which indicates a calibration requirement. This is not necessary for the decrease term, since its dynamics are proportional to the absolute value of $k(\cdot)$. With the modification of γ , the resulting common gain factor, as computed during the exemplary upshift procedure, is now ca. $k = 0.4$, as depicted in Fig. 4.7.

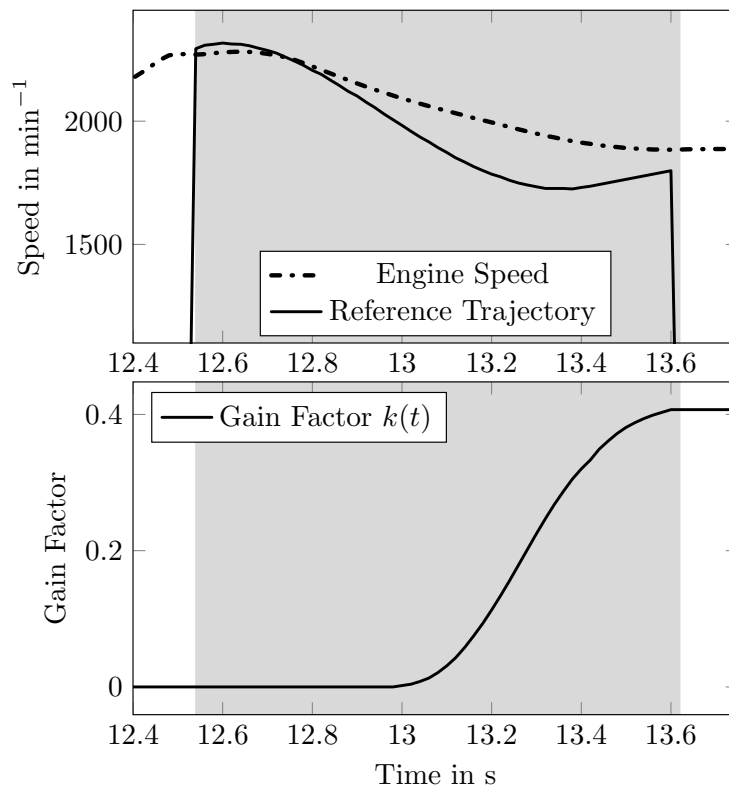


Figure 4.7: SiL simulation of an exemplary adaption of $k(\cdot)$ from 0 to ca. 0.4 during an upshift procedure, with increase coefficient $\gamma = 5 \cdot 10^{-5}$

4.2.3 Anti-Windup Measures

The underlying principle of PID-control relies on the fact that the control output $u(\cdot)$ is not limited. Thus, arbitrarily large control values can be assumed by the control output actuator to react to changes in the error signal; caused for example by disturbances or changes in the reference signal. However, any physical control system is limited in some respects. This is also the case with the clutch control system at hand, where the primary actuator, in this case the hydraulic control valve, can only be set to a maximum electric current. If engaged, it sets the clutch pressure to the highest system pressure available. Thus, the control output is bounded. This effect has to be taken into consideration when designing the feedback architecture, especially the integral feedback term. In case the maximum control value is reached, the integral feedback term continues to accumulate the existing error signal, although no further action can be exerted by the control output. The same is true for the lower bound, i.e., if no pressure is present in the clutch piston. This windup behavior has to be corrected by anti-windup measures.

The same considerations apply for the adaption law, which is of integral form itself, i.e., a first-order adaptive controller. When the bounded output value is reached and the error

signal is still outside the λ -neighborhood, i.e., $e(t) \geq \lambda$, any increase of the common gain factor $k(\cdot)$ has no effect on the control performance. Hence, anti-windup measures have to be included in the adaption law as well.

Therefore, both the integral feedback term and the adaption law are equipped with an algorithm observing the control output. If the limits are reached, the respective terms are frozen. This way, their values are kept constant until the limitations are left again:

$$\int_0^t e(\tau) d\tau : \quad \Sigma(t) = \begin{cases} \int_0^t e(\tau) d\tau & , \text{ if } u(t) < u_{\max} \wedge u(t) > u_{\min} \\ \Sigma(t_l) & , \text{ if } u(t) \geq u_{\max} \vee u(t) \leq u_{\min} \end{cases} \quad (4.7)$$

$$k(t) : \quad K(t) = \begin{cases} \int_0^t \dot{k}(\tau) d\tau & , \text{ if } u(t) < u_{\max} \wedge u(t) > u_{\min} \\ k(t_l) & , \text{ if } u(t) \geq u_{\max} \vee u(t) \leq u_{\min} \end{cases} \quad (4.8)$$

where t_l denotes the time where either an upper or lower bound of the control value was reached most recently. This extension avoids windup-behavior of both the adaptor and the integral feedback. It is implemented for all adaptive controllers from this point on. However, it is not restated in the equations describing the control dynamics to improve readability.

Note that during limited control operation, where the adaption law and the integral feedback are halted, the controller is essentially reduced to a fixed output value. The stability considerations made before in Section 2.1.6 are based on an unbounded control output signal $u(\cdot)$. This condition no longer applies during anti-windup limitation. Throughout that time, no stabilization can be conducted by the adaptive controller. However, it is reasonable to assume that the system is physically designed in such a way that it exhibits stable behavior under these circumstances, which are not exclusive to the adaptive control architecture but may occur during traditional control operation as well. Both simulation and experimental results support this assumption, since no instability has been observed during limited operation of the controller.

4.3 Parameter Studies

So far, the adaptive controller (4.1) – (4.4) has not been investigated regarding the dynamics of both the adaption law and the underlying PID-controller. The control parameters and those governing the adaption law have been found using a series of simulations and thus obtaining a suitable set of values that achieve the control goal for the system at hand. They are discussed in this section.

Note that the underlying structure of a high-gain feedback λ -tracking controller can be designed with tools from traditional control design theory found in literature, for instance selecting a PID-controller, as it is done here. However, there exists no theory of how to design the controller's adaption law regarding its parameters. This is an intuitive process that the designer has to complete when setting up a new controller for a system. This trial-and-error method is carried out with the help of simulation tools. This constitutes a small drawback in the attempt to reduce calibration efforts. However, since there is only a small number of parameters, this calibration process can be completed quickly.

It is important to point out that the evaluation of the adaptor's dynamics is rather difficult and relies on the application and its requirements, in order to decide which of the control goals are more important than others. For instance, a very fast reaction to changes in the system's dynamics may cause a sudden and strong increase in the common gain factor $k(\cdot)$ that might lead to uncomfortable system reactions or tendency to induce oscillations. These choices are discussed in the following.

First, the FDCT transmission is considered and serves as a basis for control design. The following parameters have been chosen based on simulation results:

Table 4.2: Standard set of adaptive control parameters

Parameter	Value	Remark
κ	0.01	Gain coefficient of derivative feedback term
η	1.0	Gain coefficient of integral feedback term
λ	50.0	parameter defining error-neighborhood, in min^{-1}
ε	1.0	Coefficient for smaller λ -neighborhood
γ	$2 \cdot 10^{-5}$	Coefficient for increase of common gain factor
σ	0.2	Coefficient for exponential decrease of common gain factor
t_d	0.5	Time frame before decrease is activated, in s
k_0	0.6	Initial value of common gain factor

This constitutes the standard parameter set. It is suitable to achieve the control goal of performing the desired shift procedures. Figure 4.8 shows some exemplary up- and downshifts that have been conducted in simulation with controller (4.1) – (4.4) and the parameters from Table 4.2. As depicted in Fig. 4.8, shifts are conducted successfully and without oscillations. This forms the basis for the following considerations, where each parameter is discussed in detail with the help of simulated gearshifts of the FDCT transmission.

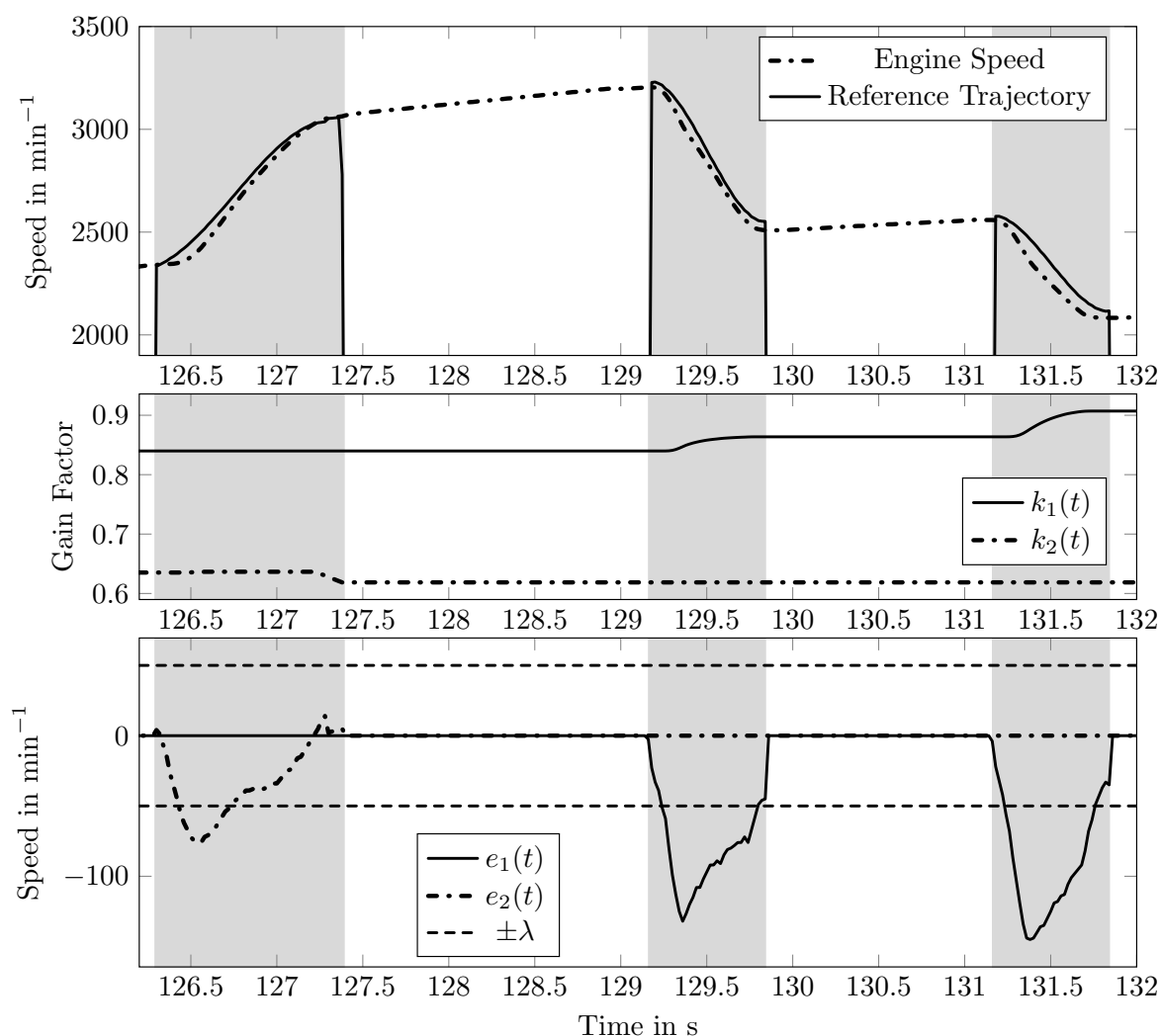


Figure 4.8: SiL simulation of exemplary up- and downshift procedures with standard parameters from Table 4.2, FDCT transmission

4.3.1 Gain Coefficient κ

The parameter κ is set to 0.01 to ensure an existing derivative feedback for stability reasons and at the same time reduce its influence on the overall control output $u(\cdot)$ by choosing a value much smaller than 1. A large derivative feedback may lead to damping of the control signal and may therefore counteract the action by the proportional feedback. Moreover, the derivative term may introduce noise into the control system, since any noise already present in the system output signal is amplified by the time derivative. This may also cause instability in the closed-loop system. Figure 4.9 shows the system's tendency to oscillate with a higher setting for κ .

Since the controller is implemented in the form of a discrete control algorithm with a

pre-specified frequency, it is desirable to reduce any discretization effects on the system as far as possible. Thus, a smaller value of $\kappa = 0.01$ is chosen. The discretization effects are discussed further in Section 4.6.2.

With a smaller setting of $\kappa = 0.01$, the closed-loop system shows no oscillations, as shown in Fig. 4.10. It is therefore a favorable setting.

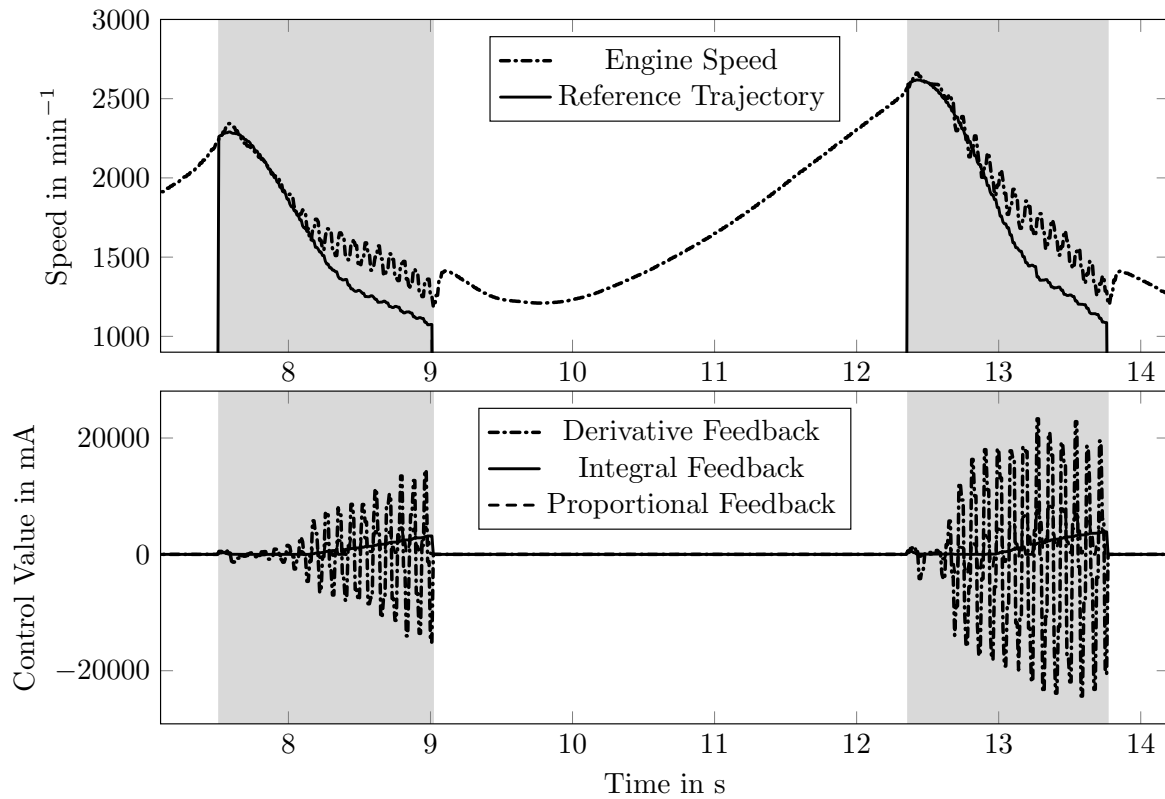


Figure 4.9: Upshifts exhibiting strong control output oscillations due to noise amplification by derivative feedback term, $\kappa = 0.1$

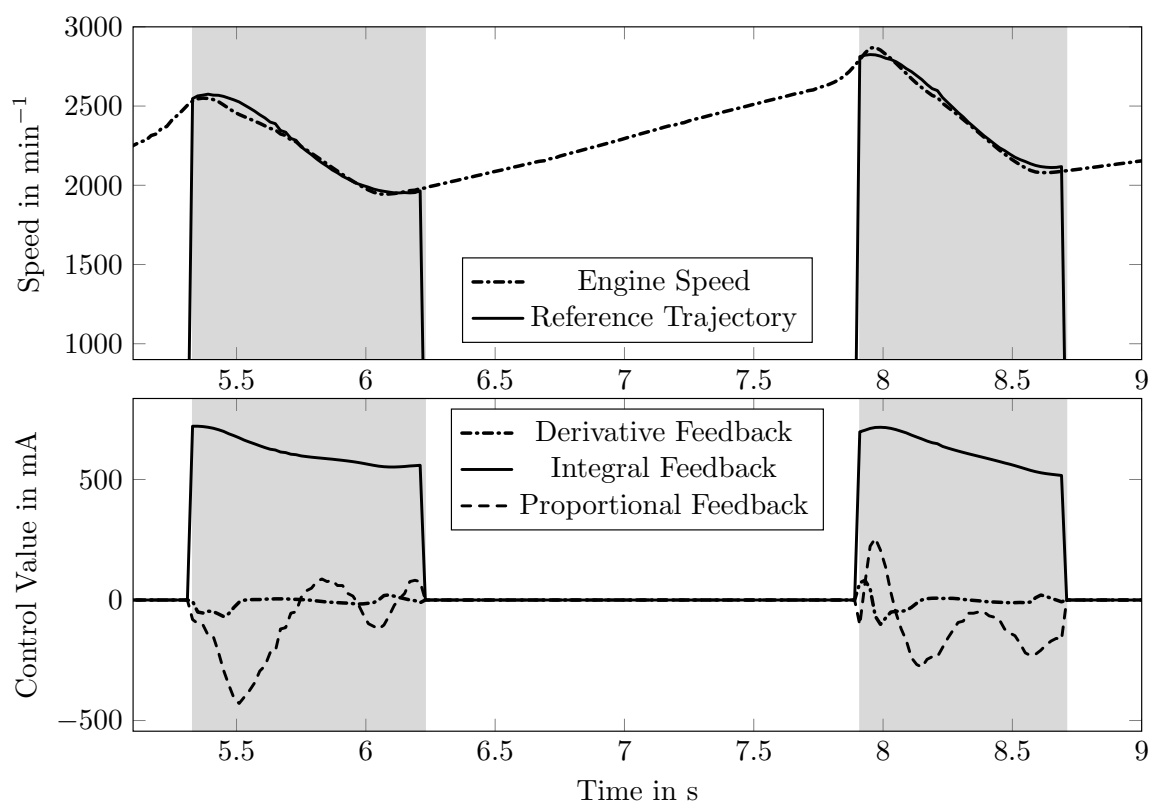


Figure 4.10: Upshifts without control output oscillations due to reduced derivative coefficient $\kappa = 0.01$

4.3.2 Gain Coefficient η

The parameter η is kept at 1. Thus, the proportional and integral feedback terms have equal influence on the control output signal $u(\cdot)$. A stronger integral term with $\eta > 1$ may lead to a loss in short-term control reactions generated by the proportional feedback. On the other hand, a setting of $\eta < 1$ may not be sufficient in reducing steady-state errors. Figure 4.11 shows three downshift procedures with varying settings of η . The integral gain coefficient of $\eta = 0.1$ is not sufficient to eliminate the steady-state error over the course of the shift procedure, since the λ -neighborhood is not reached (Fig. 4.11, left column). If η is increased to 1, the control goal is achieved before the shift procedure ends (Fig. 4.11, center column). A setting of $\eta = 2$ does not significantly improve the control performance, so this higher setting is not necessary (Fig. 4.11, right column). The λ -neighborhood is only reached marginally faster than with $\eta = 1$. Also, a dominant integral feedback term with $\eta \gg 1$ may lead to slow control dynamics. Thus, the setting of $\eta = 1$ achieving good control performance in conjunction with faster control dynamics is chosen.

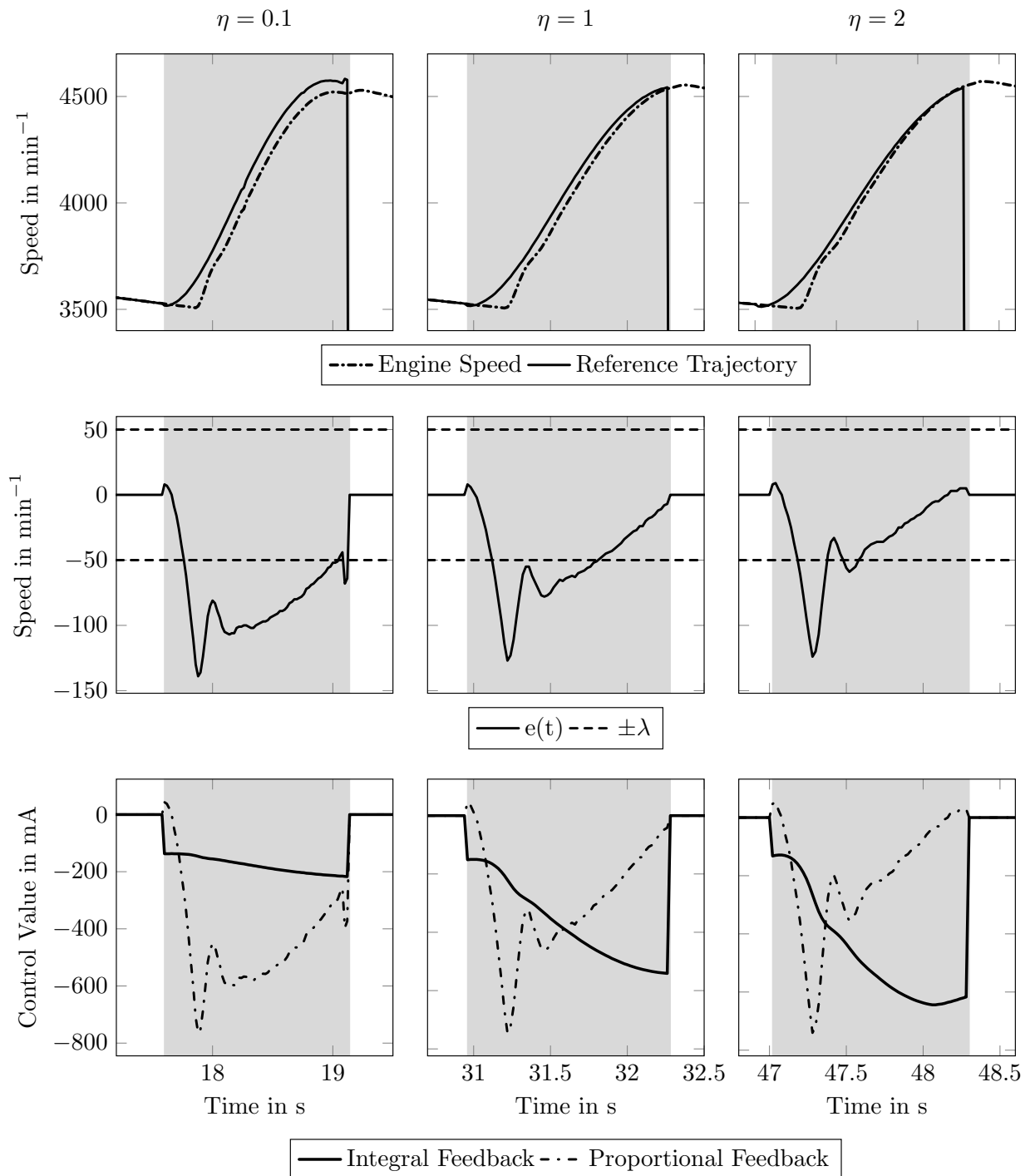


Figure 4.11: Downshift procedures with integral gain coefficients of $\eta = \{0.1, 1, 2\}$

4.3.3 λ -Neighborhood

The error neighborhood λ has to be large enough to safely encompass any error signal noise without causing a reaction by the adaption law and at the same time be small enough so

that the desired control performance is achieved. If λ is smaller than the noise amplitude, the adaptive controller will track the noise of the error signal $e(\cdot)$, (see [BeSt 10]), which is to be avoided. Also, a certain tracking error is desired. The adaptive clutch controller is implemented without any feed-forward control. Thus, there is no mechanism that would allow the controller to perform a perfect gearshift with an error signal of $e(t) \equiv 0 \forall t$. In addition to the pre-initialized fixed-value integral feedback term, the controller has to generate a time-dependent control value in order to follow the desired reference trajectory $w(\cdot)$, which is generated by the proportional and derivative feedback terms. Hence, the existence of a tracking error is necessary and therefore has to be included in the λ -neighborhood.

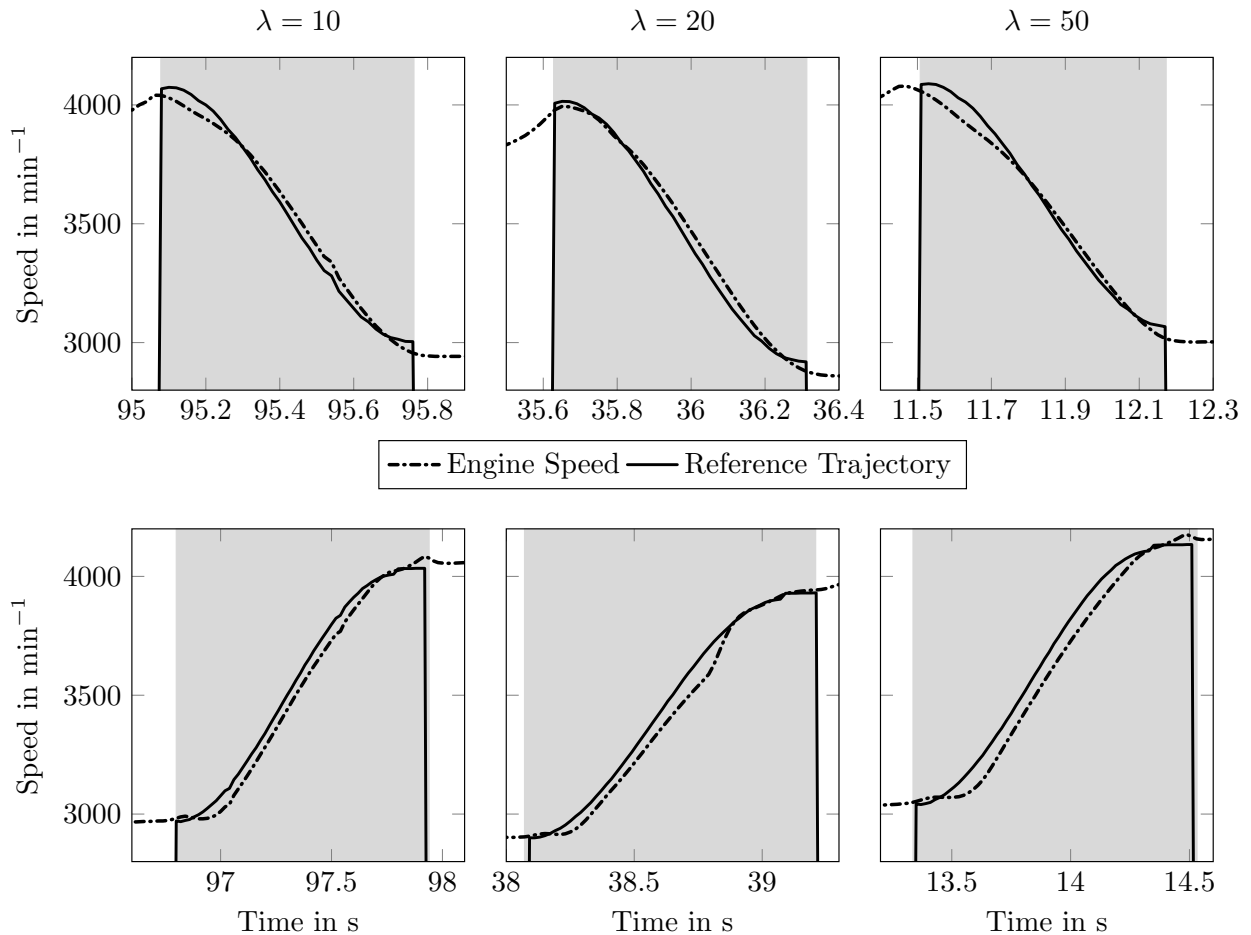


Figure 4.12: Upshift (top row) and downshift (bottom row) procedures with $\lambda = \{10, 20, 50\}$

As shown in Fig. 4.12, there is no qualitative difference between the investigated settings of λ with regards to the control performance. With $\lambda = 50$, the tracking error is marginally larger in downshift procedures (bottom row). However, the upshift procedures (top row)

show no tendency if a higher or lower setting of λ is favorable. In order to safely encompass any noise in the λ -neighborhood and also to allow for a tracking error, $\lambda = 50$ has been chosen and proven suitable for the control dynamics.

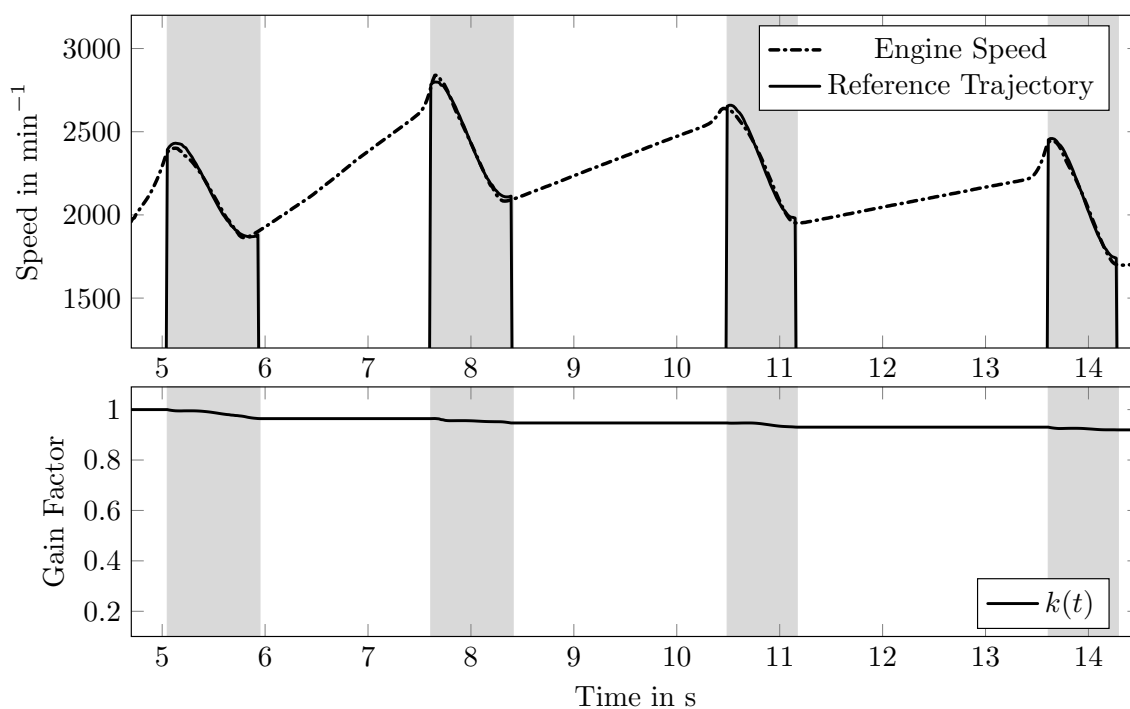
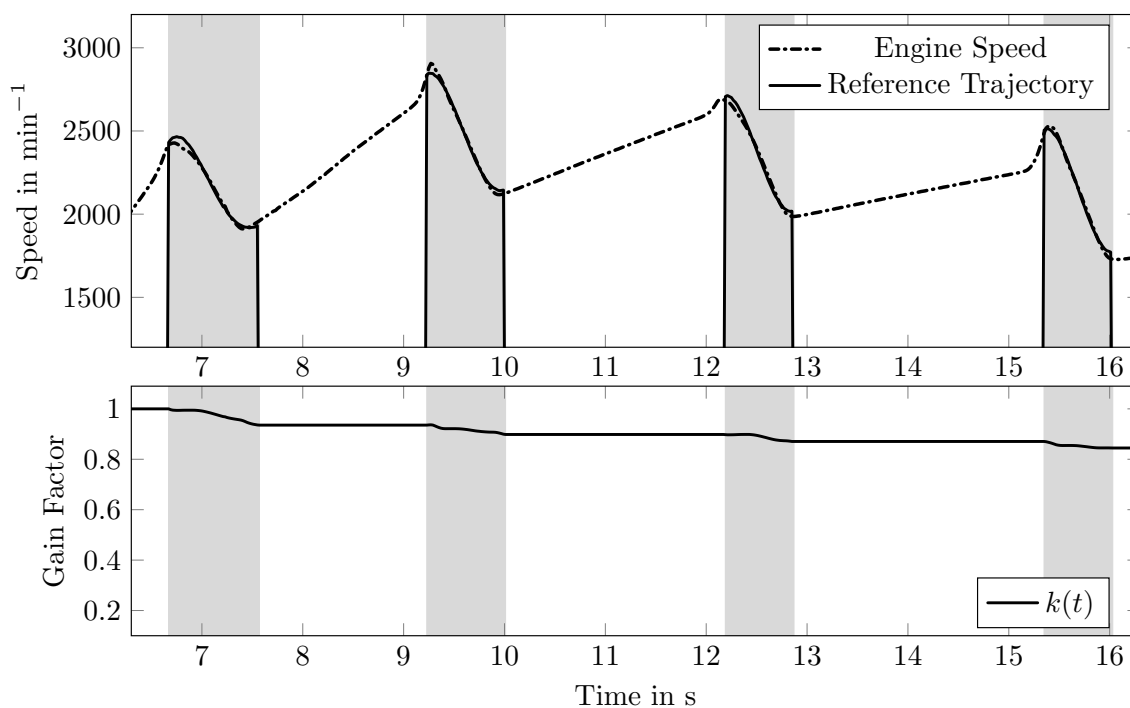
Remark 4.1 *In literature, much smaller values for λ are used, for example $\lambda = 0.2$ in [BeZi 06] and [BeLo 12]. However, the value of the λ -neighborhood is dependent on the order of magnitude of the system output $y(\cdot)$. In the cited publications, the system output lies within $y \in [-2, 2]$ and thus λ is set to ca. 5% of this range, i.e., $\lambda = 0.2$. The output signal of the transmission system considered here ranges between $y \in [600, 7000]$ and the λ -neighborhood is set to $\lambda = 50$, which is ca. 1% of the range. Thus, a feasible and comparatively small value for λ is chosen.*

4.3.4 Coefficient ε

As discussed above in Section 4.3.3, the effect on the control dynamics caused by decreasing the λ -neighborhood is insignificant. Thus, setting a value $\varepsilon < 1$ does not contribute to improve the control performance. Thus, the value $\varepsilon = 1$ is kept.

4.3.5 Decrease Gain Coefficient σ

The coefficient σ denotes the rate of decay for the exponential decrease term of the adaption law. Its purpose is to ensure that the common gain factor $k(\cdot)$ is reduced after exceeding the required level, since an overshoot is to be expected. The gain factor is supposed to be as high as necessary and as low as possible to minimize the control energy input and reduce stiffness of the underlying controller. At this point, four upshifts during vehicle pull away are simulated, with an initially high setting of $k_0 = 1$ and a waiting time of $t_d = 0$ s in order to investigate the behavior of the decrease term and the influence of the coefficient σ . As depicted in Fig. 4.13, the decrease behavior of the common gain factor $k(\cdot)$ is rather weak with a setting of $\sigma = 0.1$. Over the course of four upshifts, $k(\cdot)$ is only decreased by approximately 10%. A stronger decrease is advisable.

Figure 4.13: Upshift procedures during vehicle pull away with $\sigma = 0.1$ Figure 4.14: Upshift procedures during vehicle pull away with $\sigma = 0.2$

With $\sigma = 0.2$, the decrease of $k(\cdot)$ is much more dynamic, as depicted in Fig. 4.14. During the four subsequent upshifts, the gain factor is reduced by ca. 17%.

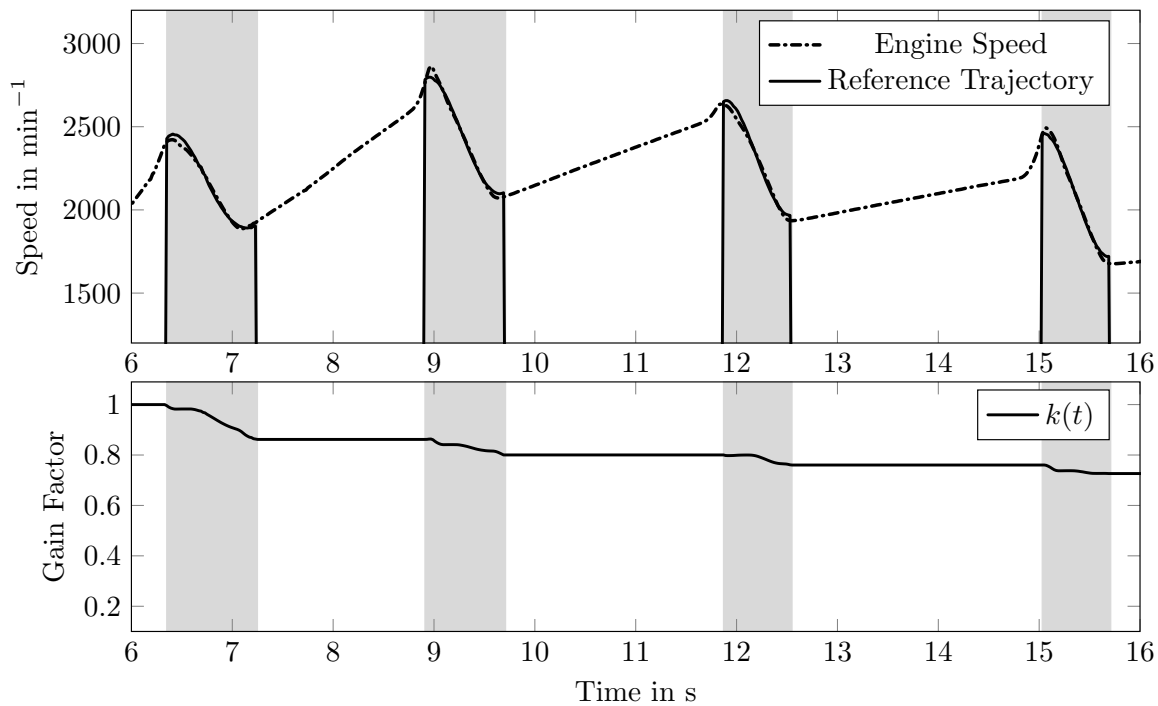


Figure 4.15: Upshift procedures during vehicle pull away with $\sigma = 0.4$

If the coefficient σ is set to 0.4, the decrease of $k(\cdot)$ is even stronger, as shown in Fig. 4.15. Although sufficient control performance is achieved, the common gain factor $k(\cdot)$ is decreased significantly to about 75% its former value over the course of four upshifts.

Note that the setting of σ to achieve the desired adaption performance is closely related to the setting of the waiting time t_d (discussed in the following section). One may choose to wait a longer time before engaging a stronger decrease coefficient. On the other hand, an adaption law where the decrease term is activated sooner and is accompanied by a smaller decrease coefficient, may also be suitable. For the purpose of this thesis, a moderate setting of $\sigma = 0.2$ is chosen.

4.3.6 Waiting Time t_d

The parameter t_d denotes the time span that has to pass after the system output $y(\cdot)$ entered the λ -neighborhood and before the decrease term of the adaption law is activated. Its goal is to avoid any oscillating behavior of the increase and decrease of the common gain factor $k(\cdot)$, as observed with the σ -modification (2.7). Note that the adaption process is reinitialized at the beginning of each shift procedure. Thus, the waiting time is specified with respect to a single shift duration. As discussed above, t_d and σ have to be set in accordance to achieve the desired control dynamics. In this thesis, the decrease term is

aimed at reducing $k(\cdot)$ on a macroscopic time scale. Thus, a rather long waiting time of $t_d = 0.5$ together with a decay coefficient of $\sigma = 0.2$ is chosen. The usual duration for a shift procedure is between 0.7 s and 1 s. Thus, the common gain factor $k(\cdot)$ is only decreased after the control goal has been achieved for a long time, i.e., for the most part of a shift procedure. Hence, the decrease term is subordinate to the increase term.

4.3.7 Initialization k_0

In between shift procedures, the common gain factor $k(\cdot)$ is saved. Thus, one shift procedure is initialized with the level of $k(\cdot)$ with which the previous shift ended. At engine shutdown, the gain factor would have to be saved to the non-volatile memory of the TCU to be available at startup. However, since this feature is not implemented at this point, a value of $k_0 = 0.6$ is used as initialization for the very first shift procedure after startup of both vehicle and simulation set-ups (see Fig. 4.16).

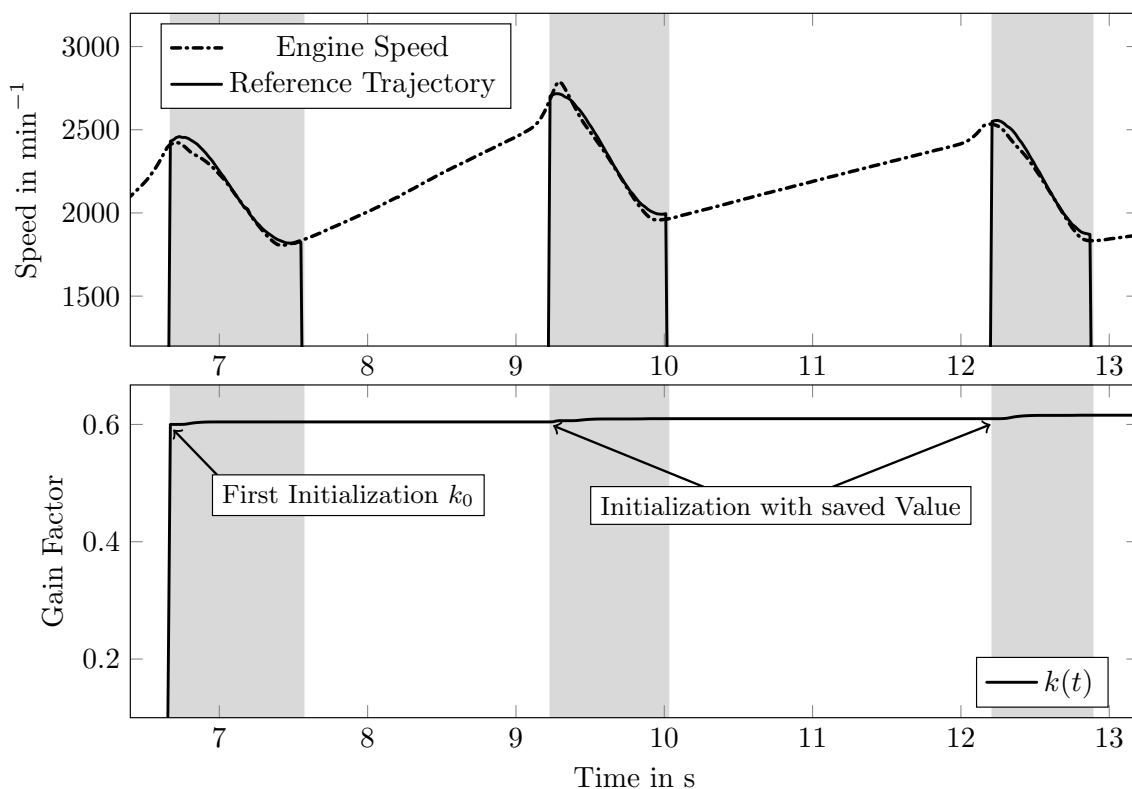


Figure 4.16: Upshift procedures during vehicle pull away with initialization of common gain factor $k(\cdot)$

4.3.8 Increase Gain Coefficient γ

The parameter γ plays a decisive role in the adaptor's increase dynamics. The adaption behavior is supposed to be fast enough so that the control goal is achieved during a single shift procedure. The following simulations show a series of upshifts during vehicle pull away with the corresponding adaption of the common gain factor $k(\cdot)$. In order to generate a clear reaction by the adaptor, the initial value for the gain factor is reduced to $k_0 = 0.1$ during these simulations. A value of $k_0 = 0$ is not feasible, since it would inhibit the initialization of the integral feedback term expressed in (4.6). As depicted in Fig. 4.17, the adaptor shows a strong reaction to the system output $y(\cdot)$ being outside the λ -neighborhood between $t = 7.5$ s and $t = 8.3$ s by drastically increasing the common gain factor $k(\cdot)$. Finally, around $t = 8.4$, the shift is successfully completed. However, during the following upshifts, the gain factor is increased further, indicating that the adaption during the previous shift procedure is not complete. Thus, the gain coefficient γ may be increased.

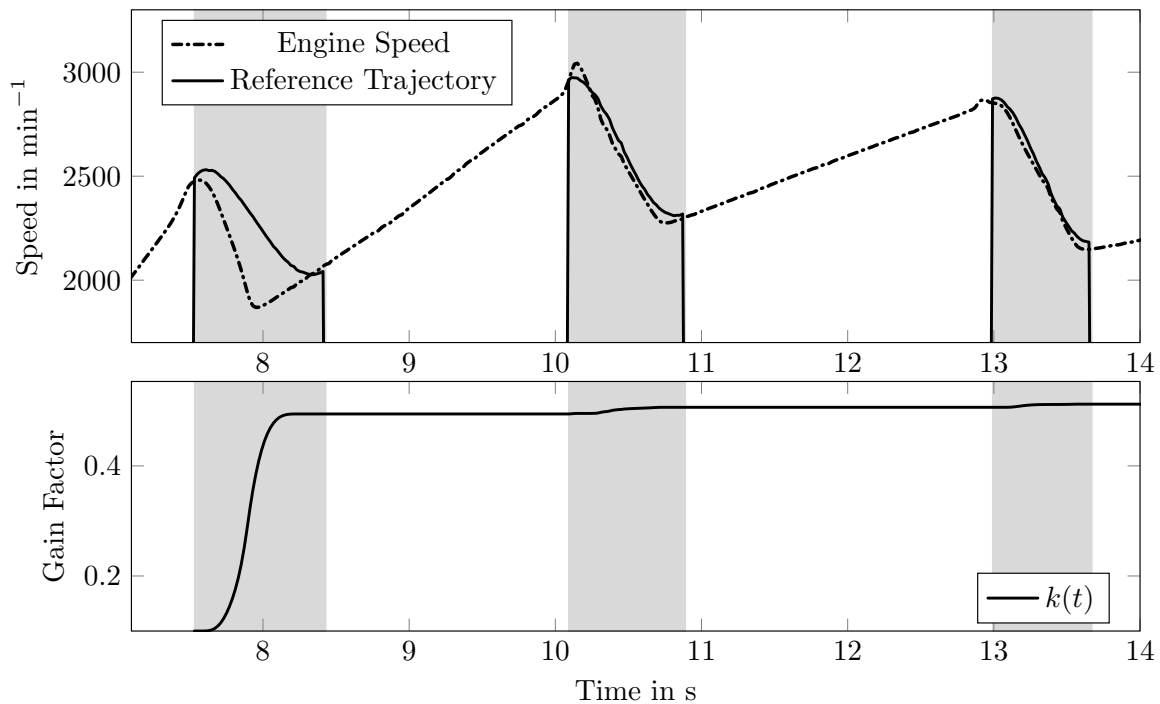


Figure 4.17: Upshift procedures during vehicle pull away with $\gamma = 1 \cdot 10^{-5}$

The same vehicle pull away maneuver including three upshift procedures was performed in simulation as shown in Fig. 4.18, now with a higher setting of $\gamma = 2 \cdot 10^{-5}$. The first strong reaction by the adaptor during the first shift procedure is comparable to the one in Fig. 4.17. However, the gain factor $k(\cdot)$ is increased much further, to ca. 1.1. During

the following upshifts, no additional adaption is required, and thus the gain factor is kept constant while the shifts are performed successfully.

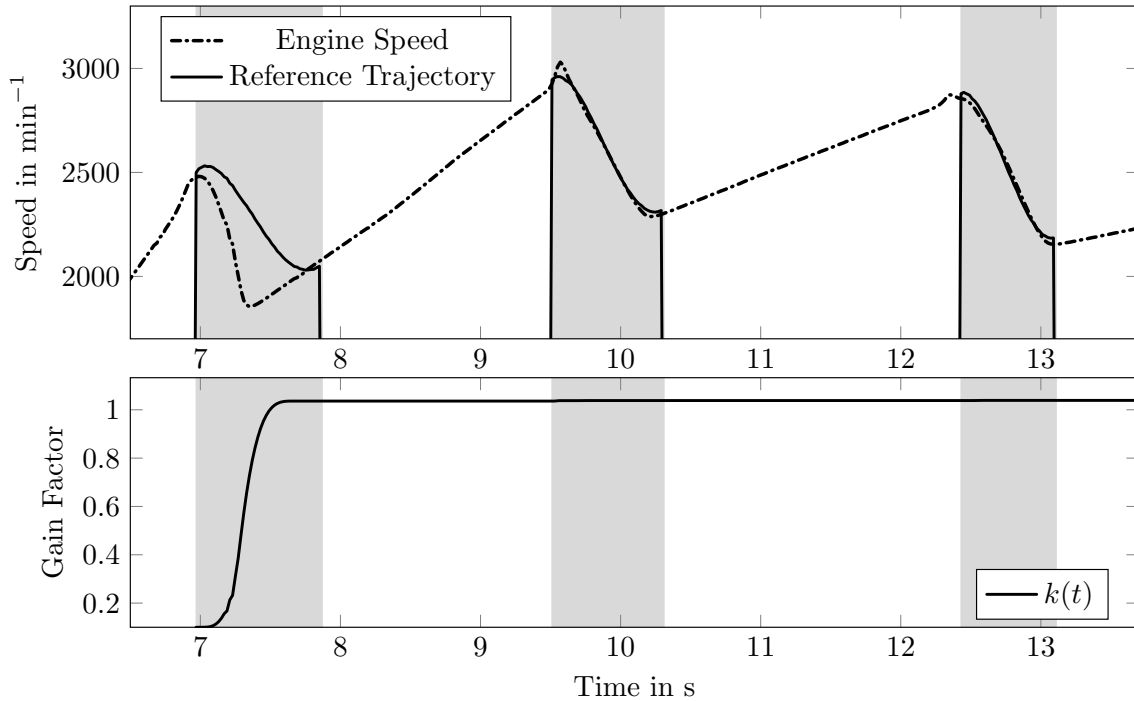


Figure 4.18: Upshift procedures during vehicle pull away with $\gamma = 2 \cdot 10^{-5}$

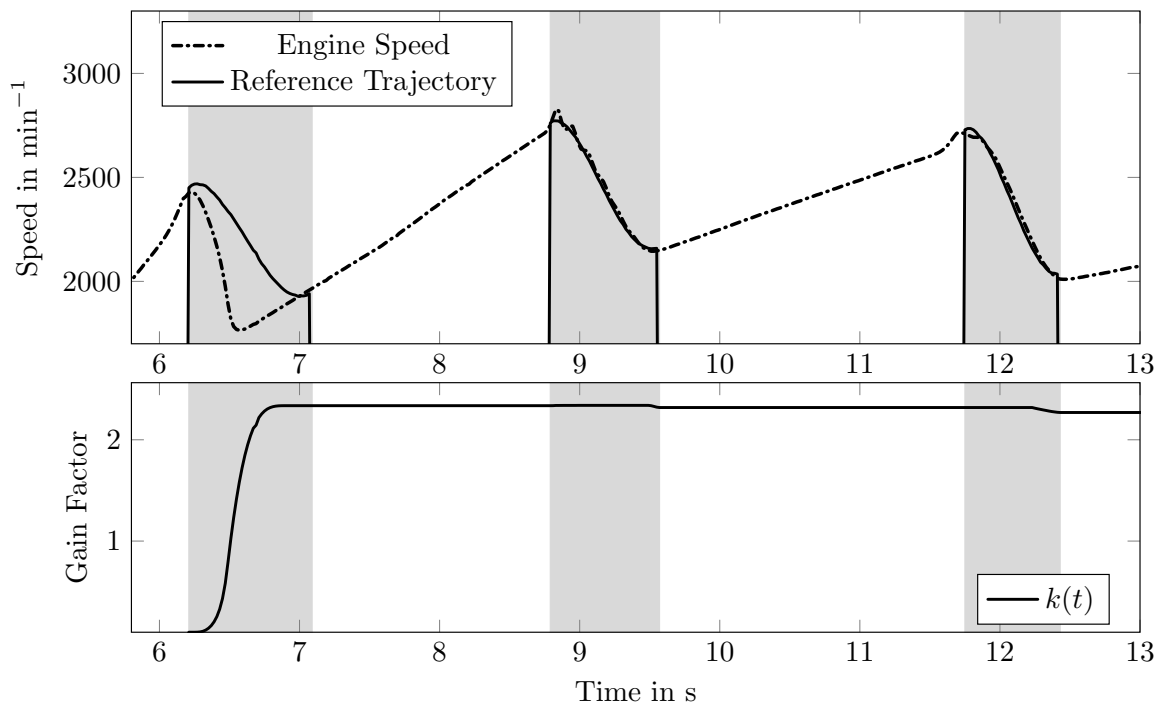


Figure 4.19: Upshift procedures during vehicle pull away with $\gamma = 4 \cdot 10^{-5}$

For comparison purposes, the gain coefficient γ is increased to $4 \cdot 10^{-5}$ and the same maneuver is conducted in simulation, as shown in Fig. 4.19. The control performance is comparable to the one in Fig. 4.18. However, the common gain factor $k(\cdot)$ is increased even higher during the first shift procedure. In fact, during the following upshifts, it is decreased again. Thus, the initial adaption between $t = 6.2\text{s}$ and $t = 6.8\text{s}$, leads to a value of $k(\cdot)$ that is higher than necessary. Although the control goal is achieved nonetheless, this higher setting of $\gamma = 4 \cdot 10^{-5}$ is not necessary and may cause sudden and uncomfortable reactions by the clutch system in later shifts, due to intense gain factor adaption. Thus, $\gamma = 2 \cdot 10^{-5}$ is chosen.

Note that the strong decrease of the engine speed during the first upshift in Figs. 4.17 – 4.19, where the first sizable increase of the gain factor $k(\cdot)$ is conducted, is implausible at first. Since the control feedback gain is still small at this point ($k_0 = 0.1$), the engine speed is expected to increase due to insufficient control output values. However, the strong decrease of engine speed suggests a high control output. This is caused by the sudden increase of the gain factor in conjunction with the pre-initialized integral feedback term and is an unfavorable behavior of the adaption law. This effect is discussed further in Section 4.4.

4.4 Counteractive Adaption Law Dynamics

In some instances, unusually long downshift procedures occur that are not consistent with the desired control performance, as shown in Fig. 4.20. This is the result of a nearly constant control output signal that is too low to achieve the desired control dynamics and thus perform the shift procedure in the desired time frame. At first, this behavior seems contradictory to the existence of an integral feedback term, which is responsible for the reduction of steady-state errors. Note that due to the small value of κ , the derivative feedback does not contribute to the control dynamics significantly and can be neglected for the following considerations.

The engine speed signal is lower than the reference trajectory for the most part of the shift procedure (see Fig. 4.20, top). Thus, the controller is expected to react to this system state by reducing the clutch pressure and therefore releasing the engine to accelerate. Instead, the control output signal $u(\cdot)$ remains nearly constant. This is due to the counteracting behavior of integral and proportional feedback terms: The correct behavior of reducing the control output can be observed in the proportional term. However, the integral term increases its value – contrary to the desired behavior – which cancels out the reaction of the proportional term. Thus, the overall control output shows almost no reaction

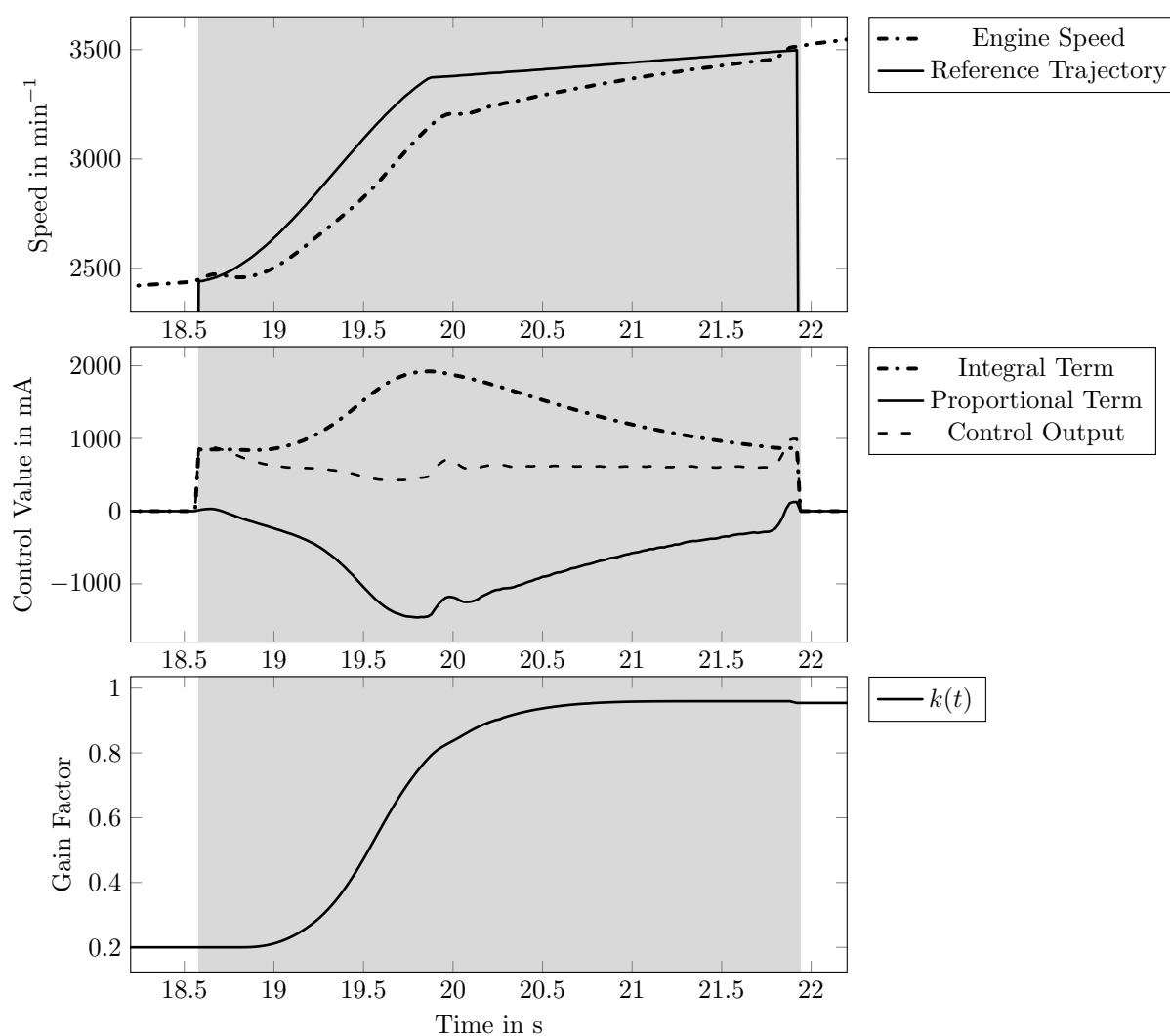


Figure 4.20: Simulation of long downshift procedure from 5th to 4th gear with counteracting proportional and integral feedback terms

(see Fig. 4.20, center). The integral term is increased because of its positive initialization value that is amplified by the strong increase of the common gain factor $k(\cdot)$, caused by the adaption law (see Fig. 4.20, bottom). Thus, an unwanted interaction between the dynamics of the adaption law and the control dynamics are the cause of this faulty behavior. The adaption law's increase of $k(\cdot)$ is much faster than the integral term's decrease, caused by the negative error signal $e(\cdot)$. This dynamics mismatch has to be avoided. Whenever a strong increase of the gain factor coincides with a pre-existing integral term, for instance set by initialization or resulting from previous control action, the controller's response is unsuited to achieve the control goal.

To overcome this deficiency, the counteracting behavior has to be detected and, during

this state, the adaption law has to be muted. Thus, the adaptive controller is extended to:

$$e(t) = s_{\text{hf}} \cdot (y(t) - y_{\text{ref}}(t)) \quad (4.9)$$

$$u(t) = k(t) e(t) + \kappa k(t) \dot{e}(t) + \eta k(t) \int_0^t e(\tau) d\tau \quad (4.10)$$

$$\dot{k}(t) = \begin{cases} \gamma (|e(t)| - \varepsilon\lambda)^2, & \text{if } (|e(t)| > 1 + \varepsilon\lambda \wedge \bar{\Delta}) \\ \gamma (|e(t)| - \varepsilon\lambda)^{\frac{1}{2}}, & \text{if } (\varepsilon\lambda \leq |e(t)| \leq 1 + \varepsilon\lambda \wedge \bar{\Delta}) \\ 0, & \text{if } (|e(t)| < \varepsilon\lambda \wedge t - t_e < t_d) \vee \Delta \\ -\sigma \left(1 - \frac{|e(t)|}{\varepsilon\lambda}\right) k(t), & \text{if } (|e(t)| < \varepsilon\lambda \wedge t - t_e \geq t_d \wedge \bar{\Delta}) \end{cases} \quad (4.11)$$

$$\begin{aligned} \Delta := & (P(t) I(t) < 0) \wedge (\dot{P}(t) \dot{I}(t) < 0) \wedge (I(t) \dot{I}(t) > 0) \\ & \wedge (P(t) \dot{P}(t) > 0) \end{aligned} \quad (4.12)$$

$$P(t) := k(t) e(t) \quad (4.13)$$

$$I(t) := \eta k(t) \int_0^t e(\tau) d\tau \quad (4.14)$$

$$k(0) = k_0 \quad (4.15)$$

where $\lambda \geq 0, \gamma > 1, \sigma > 0, t_d > 0, 0 < \varepsilon \leq 1, \kappa > 0, \eta > 0$. With these modifications,

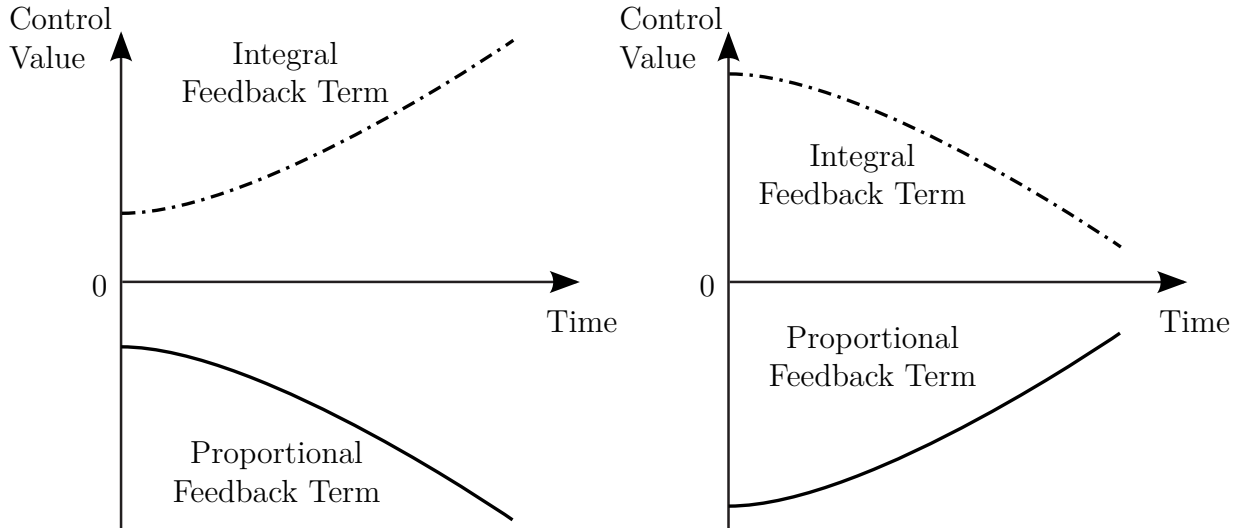


Figure 4.21: Unwanted behavior of counteracting integral and proportional terms (left), and acceptable control behavior (right)

the controller (4.9) – (4.15) deactivates the adaption of the common gain factor, if the

proportional and integral terms show diverging and counteracting behavior. The term Δ denotes the case when integral and proportional terms, as well as their time derivatives, have opposing signs and are not converging towards zero (see Fig. 4.21, left). It is not sufficient to only detect opposing signs of the feedback signals and of their respective derivatives. If that was the case, the control behavior depicted in Fig. 4.21 (right) would also cause the adaption law to be muted. However, this is not desired here and has to be excluded in the formulation for muting term Δ by adding the condition that proportional and integral feedback terms are diverging from zero. If $\Delta = 1$, the adaption law switches to $\dot{k}(t) = 0$, i.e., keeping the common gain factor constant.

The extended controller is tested in simulation with the same downshift procedure as before. The simulation results in Fig. 4.22 show that the control goal is now achieved

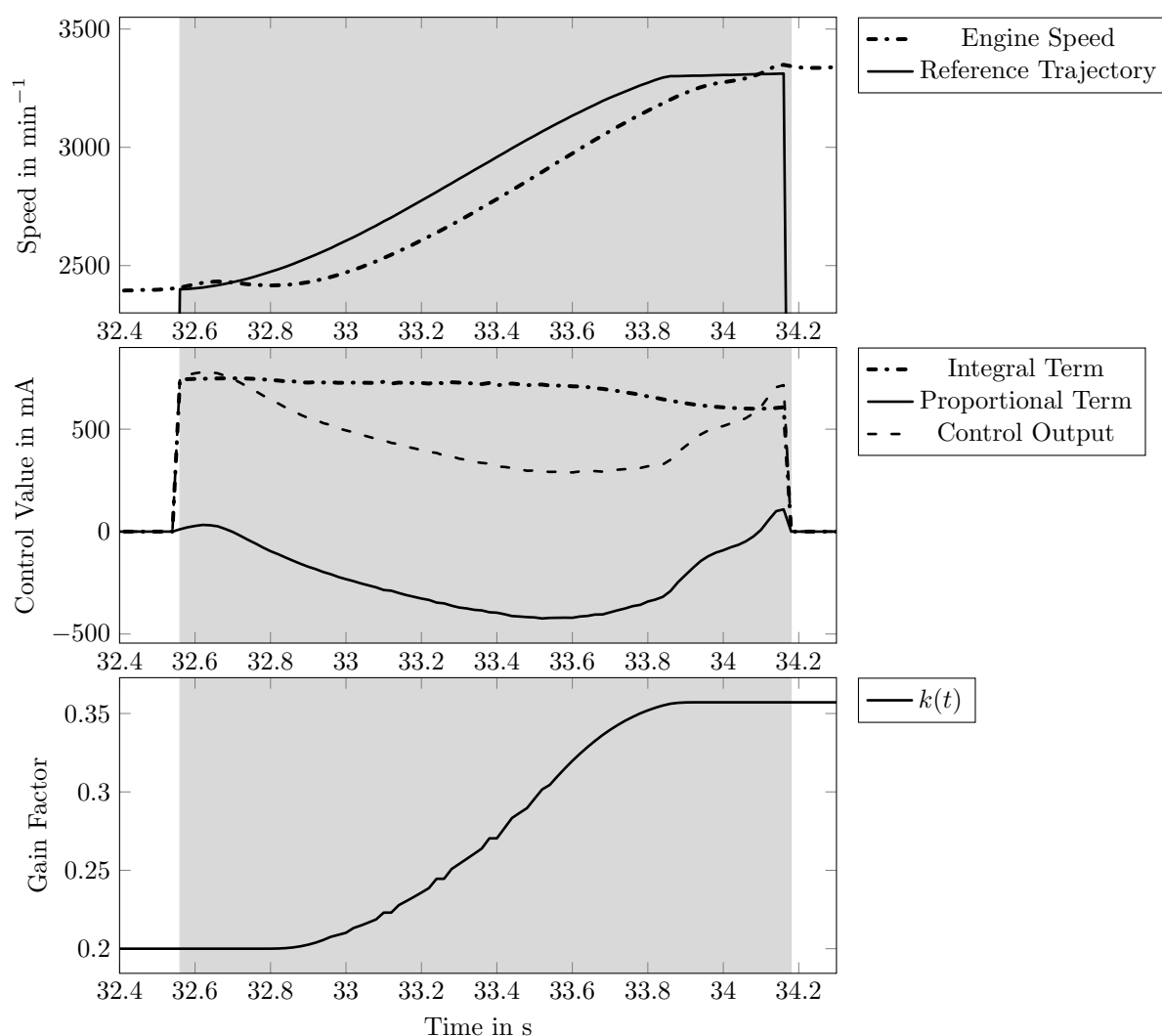


Figure 4.22: Simulation of downshift procedure from 5th to 4th gear with muted adaption law and no counteracting feedback terms

using the extended adaptive controller. The adaptor's muting behavior avoids the counteracting behavior of integral and proportional feedback terms. Thus, the overall control output signal is now longer constant but shows a suitable reaction. As a result, the shift procedure is carried out in a much shorter time frame and the final value of $k(\cdot)$ is much lower due to stalled increase dynamics.

Note that the controller does not exhibit its full potential in terms of shift duration. The shifts depicted here are merely examples to demonstrate the counteraction of integral and proportional feedback terms. For details regarding shift speed, please refer to Sections 5.1.3 and 5.2.3.

4.5 Fully Exponential Adaption Law

So far, only one adaptor for the adaptive PID-controller has been discussed. It was extended to arrive at controller (4.9) – (4.15) and achieves the desired control performance. It is however conceivable to choose different adaption laws. In this section, the following adaptive controller with PID-feedback is considered:

$$e(t) = s_{\text{hf}} \cdot (y(t) - y_{\text{ref}}(t)) \quad (4.16)$$

$$u(t) = k(t) e(t) + \kappa k(t) \dot{e}(t) + \eta k(t) \int_0^t e(\tau) d\tau \quad (4.17)$$

$$\dot{k}(t) = \begin{cases} -\sigma_i \left(1 - \frac{|e(t)|}{\varepsilon\lambda}\right) k(t), & \text{if } |e(t)| \geq \varepsilon\lambda \\ 0, & \text{if } |e(t)| < \varepsilon\lambda \quad \wedge \quad t - t_e < t_d \\ -\sigma_d \left(1 - \frac{|e(t)|}{\varepsilon\lambda}\right) k(t), & \text{if } |e(t)| < \varepsilon\lambda \quad \wedge \quad t - t_e \geq t_d \end{cases} \quad (4.18)$$

$$k(0) = k_0 \quad (4.19)$$

where $\lambda \geq 0, \gamma > 1, \sigma_i > 0, \sigma_d > 0, t_d > 0, 0 < \varepsilon \leq 1, \kappa > 0, \eta > 0, k_0 > 0$.

This controller uses exponential terms for both increase and decrease of the common gain factor $k(\cdot)$. Individual gain coefficients σ_i and σ_d can be assigned to distinguish between the increase and decrease dynamics. This adaptor design is simpler than the one with the standard adaptive controller (4.9) – (4.15).

Note that the same considerations made for the standard adaptive controller (4.9) – (4.15) in Section 4.4 apply here as well. Thus, the exponential adaptive controller is extended

by the correction term Δ :

$$e(t) = s_{\text{hf}} \cdot (y(t) - y_{\text{ref}}(t)) \quad (4.20)$$

$$u(t) = k(t) e(t) + \kappa k(t) \dot{e}(t) + \eta k(t) \int_0^t e(\tau) d\tau \quad (4.21)$$

$$\dot{k}(t) = \begin{cases} -\sigma_i \left(1 - \frac{|e(t)|}{\varepsilon\lambda}\right) k(t), & \text{if } (|e(t)| \geq \varepsilon\lambda \wedge \bar{\Delta}) \\ 0, & \text{if } (|e(t)| < \varepsilon\lambda \wedge t - t_e < t_d) \vee \Delta \\ -\sigma_d \left(1 - \frac{|e(t)|}{\varepsilon\lambda}\right) k(t), & \text{if } (|e(t)| < \varepsilon\lambda \wedge t - t_e \geq t_d \wedge \bar{\Delta}) \end{cases} \quad (4.22)$$

$$\begin{aligned} \Delta := & (P(t) I(t) < 0) \wedge (\dot{P}(t) \dot{I}(t) < 0) \wedge (I(t) \dot{I}(t) > 0) \\ & \wedge (P(t) \dot{P}(t) > 0) \end{aligned} \quad (4.23)$$

$$P(t) := k(t) e(t) \quad (4.24)$$

$$I(t) := \eta k(t) \int_0^t e(\tau) d\tau \quad (4.25)$$

$$k(0) = k_0 \quad (4.26)$$

where $\lambda \geq 0, \gamma > 1, \sigma_i > 0, \sigma_d > 0, t_d > 0, 0 < \varepsilon \leq 1, \kappa > 0, \eta > 0, k_0 > 0$.

With the extensions, adaptive controller (4.20) – (4.26) has the same abilities as controller (4.9) – (4.15):

- ability to increase common gain factor $k(\cdot)$,
- ability to decrease common gain factor $k(\cdot)$,
- dead-zone behavior with error neighborhood λ ,
- full PID-feedback structure to ensure stability, elimination of steady-state errors and initialization, and
- avoidance of counteracting proportional and integral feedback terms with ability to mute the adaption law.

In order to investigate if the exponential increase behavior exhibits favorable dynamics compared to the standard increase term, comparative simulations are carried out, where a series of three shift procedures is conducted.

The parameters given in Table 4.3 are used, obtained from Table 4.2 and extended by the setting for σ_i that was derived from simulation experiments. Note that the scaling with

a factor of 10^{-5} for the increase coefficient σ_i is not included here. Since the dynamics of the exponential increase and decrease terms is dependent on the absolute value of $k(\cdot)$, rescaling is not necessary, as long as a suitable starting value k_0 is chosen. The up-

Table 4.3: Adaptive control parameters for fully exponential adaption law

Parameter	Value	Remark
κ	0.01	Gain coefficient of derivative feedback
η	1.0	Gain coefficient of integral feedback
λ	50.0	Parameter for λ -neighborhood, in min^{-1}
ε	1.0	Coefficient for smaller λ -neighborhood
σ_i	0.3	Coefficient for exponential increase of common gain factor
σ_d	0.2	Coefficient for exponential decrease of common gain factor
t_d	0.5	Waiting time before decrease is activated, in s
k_0	0.6	Initial value of common gain factor

and downshift procedures depicted in Fig. 4.23 show smooth control performance by the exponential adaption law in controller (4.20) – (4.26). These results are comparable to the ones depicted in Fig. 4.8. Hence, as far as these exemplary gearshifts are concerned, both adaption laws have the same qualitative results.

For the purpose of this thesis, controller (4.9) – (4.15) is used. Other adaption laws are not investigated at this point. Some preliminary investigations involving the adaptive fuzzy controller from [BeLo 12] have not resulted in promising control performance. Hence, the adaptor in form of a fuzzy controller is not considered further here.

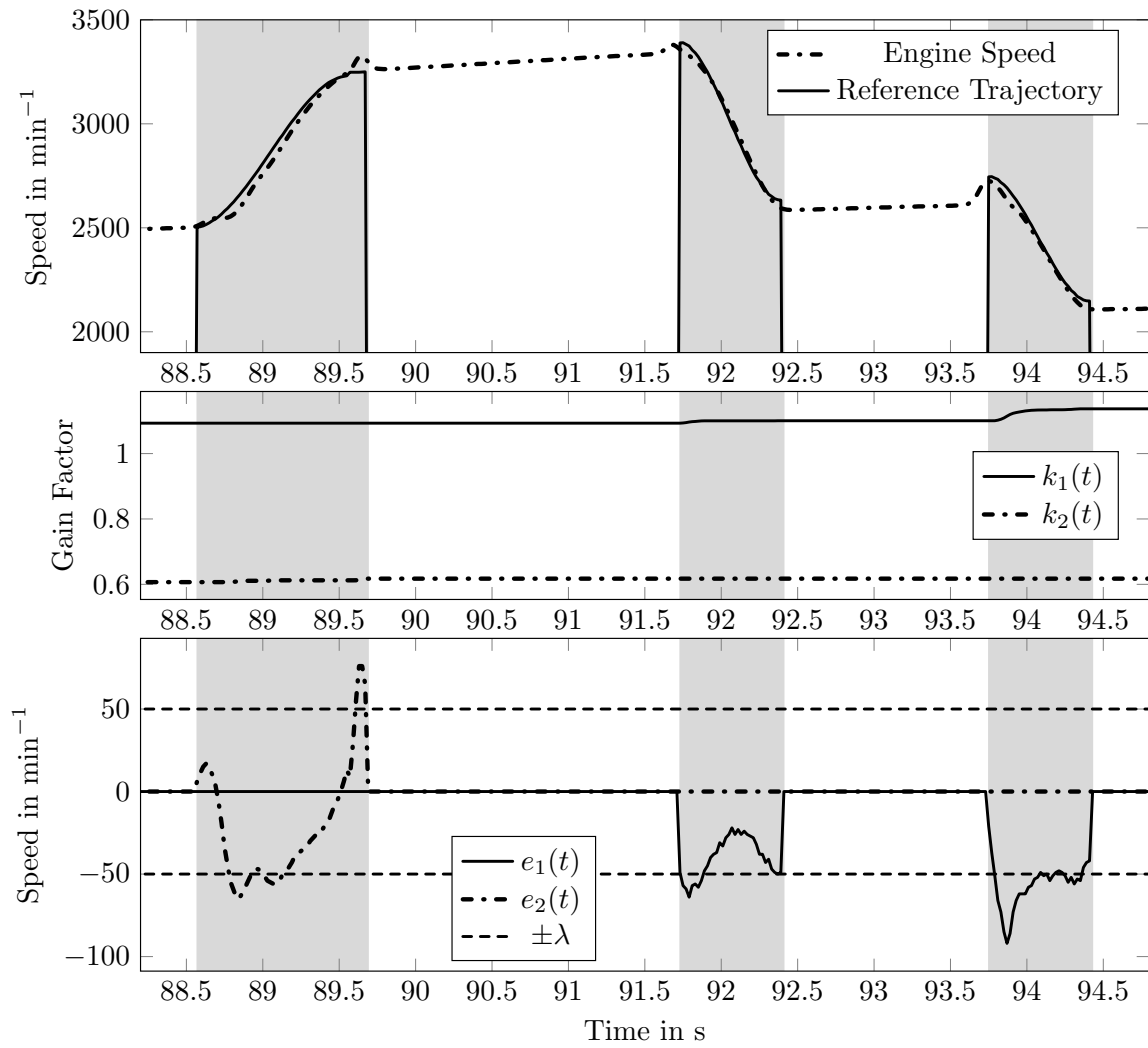


Figure 4.23: Simulation of exemplary shifts with fully exponential adaption law, FDCT transmission

4.6 Digital Control Integration

The details of transforming time-continuous adaptive controllers into time-discrete digital algorithms are investigated in this section. Limitations and the resulting requirements concerning the control design are discussed.

4.6.1 Hardware Constraints

An important requirement that has to be met by the adaptive controller is the ability to function in today's series production control hardware. In order to demonstrate the capabilities of the control concept, any powerful rapid-prototyping control hardware is to be avoided. Instead, the constraints imposed on the control system by the TCU have to be considered.

Limitation of Processing Performance

Since series production components in the automotive industry have to be low-cost to allow for mass production, computing time comes at a premium. This results in TCUs that use most of their processing time and thus have limited margins for extended functionality. If any additional functions are to be implemented, it is essential to design computationally fast algorithms to do so. Thus, any steps that have high demands on computing time are not feasible in this context, for example optimization algorithms.

Sampling Time of the Digital Control Setup

So far, the control architectures discussed in this thesis have been stated in time-continuous form. It is obvious that for integration into the TCU software, they have to be formulated as digital control algorithms. Thus, the adaptive controllers are transformed into digital control equations feasible for software implementation.

The transformation is carried out by converting the controller's differential equations into

difference equations using standard single-step discretization (see [LaZ06], [Lunz10]):

$$e_\nu = s_{\text{hf}} \cdot (y_\nu - y_{\text{ref},\nu}) \quad (4.27)$$

$$u_\nu = k_\nu e_\nu + \kappa k_\nu \frac{e_\nu - e_{\nu-1}}{T} + \eta k_\nu T \sum_{\nu=0}^{\nu} e_\nu \quad (4.28)$$

$$k_\nu = (k_{\nu-1} + k_{\text{diff}}) T \quad (4.29)$$

$$k_{\text{diff}} = \begin{cases} \gamma (|e_\nu| - \varepsilon\lambda)^2, & \text{if } (|e_\nu| > 1 + \varepsilon\lambda \wedge \bar{\Delta}_\nu) \\ \gamma (|e_\nu| - \varepsilon\lambda)^{\frac{1}{2}}, & \text{if } (\varepsilon\lambda \leq |e_\nu| \leq 1 + \varepsilon\lambda \wedge \bar{\Delta}_\nu) \\ 0, & \text{if } (|e_\nu| < \varepsilon\lambda \wedge t - t_e < t_d) \vee \Delta_\nu \\ -\sigma \left(1 - \frac{|e_\nu|}{\varepsilon\lambda}\right) k_\nu, & \text{if } (|e_\nu| < \varepsilon\lambda \wedge t - t_e \geq t_d \wedge \bar{\Delta}_\nu) \end{cases} \quad (4.30)$$

$$\begin{aligned} \Delta_\nu := & (P_\nu I_\nu < 0) \wedge \left(\frac{(P_\nu - P_{\nu-1})(I_\nu - I_{\nu-1})}{T} < 0 \right) \wedge \left(I_\nu \frac{I_\nu - I_{\nu-1}}{T} > 0 \right) \\ & \wedge \left(P_\nu \frac{P_\nu - P_{\nu-1}}{T} > 0 \right) \end{aligned} \quad (4.31)$$

$$P_\nu := k_\nu e_\nu \quad (4.32)$$

$$I_\nu := \eta k_\nu T \sum_{\nu=0}^{\nu} e_\nu \quad (4.33)$$

$$k_{\nu=0} = k_0 \quad (4.34)$$

where $\lambda \geq 0, \gamma > 1, \sigma > 0, t_d > 0, 0 < \varepsilon \leq 1, \kappa > 0, \eta > 0$ and sampling time $T > 0$.

Note that the sampling time is pre-specified within the TCU software setup at $T = 10$ ms. This is a strong side-condition to the capabilities of the time-discrete adaptive controller (4.27) – (4.34). The stability of any time-discrete controller is closely tied to its sampling time. Here, it is fixed by the control hardware. According to literature (see [WöBr05], [Lunz10]), it is possible to choose a sampling time that is fast enough in order to generate quasi-continuous digital controllers. This requires the fastest time constant in the system's dynamics to be sampled ten times during its transition, which would lead to a sampling time of one tenth of the fastest time constant. Thus, a quasi-continuous controller is achieved and the time-continuous form is sufficient for the control design.

However, this is not the case here. For instance, the hydraulic control valve can change its position much faster than $10T = 100$ ms, so these dynamics cannot be fully controlled. Nonetheless, this is not necessary. As discussed in Section 3.3.2, the underlying fast dynamics of the control valve are limited by its end stops. Thus, they cannot contribute to any instability of the system and, therefore, are not required to be controlled. Hence, a slow sampling time is feasible.

Moreover, since the control architecture currently present in the series production TCU is able to control the transmission's clutch systems, it is legitimate to assume that the sampling time is sufficient for this application. At this point, no further investigations aimed at reducing the sampling time and thus improving the control capabilities are carried out. Simulations and vehicle experiments have shown promising results suggesting that the implemented sampling time is in fact sufficient. No anomalies concerning stability have been observed that can be linked to time discretization effects.

4.6.2 Derivative Feedback Control

As discussed in Section 3.4.1, a derivative feedback term is required to ensure stability of the closed-loop system. Due to hardware constraints, the sampling time of $T = 10$ ms has to be obeyed. This generates noise in the derivative feedback term that may lead to uncomfortable control behavior due to sudden peaks of the control output signal.

Filtering of Derivative Feedback Action

In order to reduce noise in the controller, filtering of the derivative feedback term is advisable. For the purpose of this thesis, a Butterworth filter is implemented. Its design, following the bilinear z-transform, is carried out according to [IfJe 93] and [Meye 11]. First, the order of the filter is determined. The design parameters are set to exemplary values:

$$\begin{aligned} \text{Signal attenuation: } A_S &= 10 \text{ dB} \\ \text{Cut-off frequency: } \omega_{c,d} &= 2\pi \cdot 10 \text{ Hz} \\ \text{Stopband frequency: } \omega_{s,d} &= 2\pi \cdot 15 \text{ Hz} \end{aligned}$$

With the following equations:

$$N \geq \frac{\lg\left(\frac{1}{\delta_S} - 1\right)}{2 \lg\left(\frac{\omega_{s,a}}{\omega_{c,a}}\right)} \quad (4.35)$$

$$\omega_{c,a} = \frac{2}{T} \tan\left(\frac{\omega_{c,d} T}{2}\right) \quad (4.36)$$

$$\omega_{s,a} = \frac{2}{T} \tan\left(\frac{\omega_{s,d} T}{2}\right) \quad (4.37)$$

$$\delta_S = 10^{-\frac{A_S}{20}} \quad (4.38)$$

where $\omega_{c,d}, \omega_{c,a}$ are the cut-off frequencies and $\omega_{s,d}, \omega_{s,a}$ are the stopband frequencies for the digital and pre-warped analog filters, respectively.

The filter order is computed as $N \geq 0.85$. Thus, a first-order Butterworth filter is chosen, i.e., $N = 1$. It is of the following form:

$$G_{\text{tf}}(\omega) = \frac{1}{1 + \frac{\omega}{\omega_c}} \quad (4.39)$$

$$G_{\text{tf}}(z_d) = \frac{1 + z_d^{-1}}{\left(1 + \frac{2}{\omega_{c,a} T}\right) + \left(1 - \frac{2}{\omega_{c,a} T}\right) z_d^{-1}} \quad (4.40)$$

Thus, for the exemplary design parameters, the computation yields:

$$G_{\text{tf}}(z_d) = \frac{1 + z_d^{-1}}{4.077 - 2.078 z_d^{-1}} \quad (4.41)$$

where $z_d = e^{s_d T}$, $s_d \in \mathbb{C}$.

The filter (4.41) is applied to the differentiated error signal $\dot{e}(\cdot)$, resulting in a smoother form of the derivative feedback term. This is verified in simulation with controller (4.9) – (4.15), where the coefficient κ is set to 1 in order to better demonstrate the effect on the derivative feedback term.

As shown in Fig. 4.24, the filtering of the derivative feedback term is successfully carried out with the exemplary design parameters. The dashed line, depicting the derivative term, is much smoother in the bottom plot, whereas the solid line, depicting the proportional term, is almost the same in both instances, since the shift procedure is very similar except for minor differences due to slightly different control behavior caused by the modified derivative feedback term.

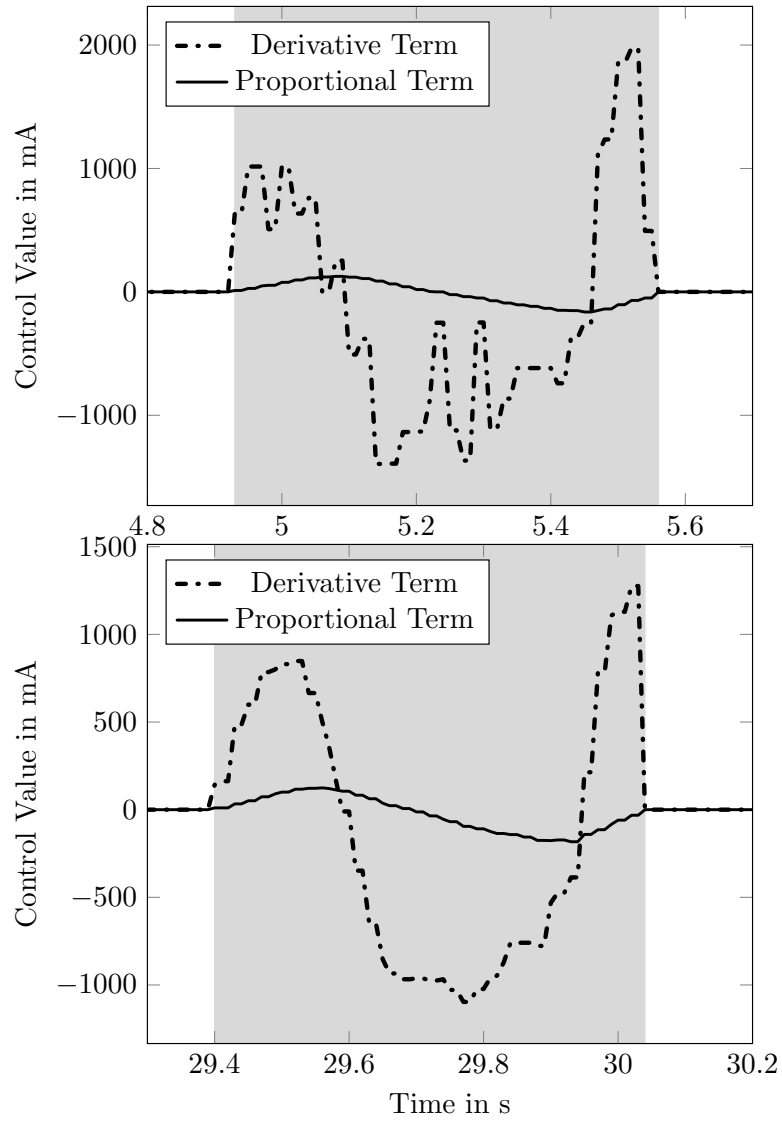


Figure 4.24: Derivative feedback term during shift procedure without (top) and with (bottom) filter (4.41) applied; $\kappa = 1$

Reference Trajectory Planning

Due to the nature of the derivative feedback term, sudden changes in the error signal $e(\cdot)$ result in even stronger peaks in $\dot{e}(\cdot)$. Even with filtering, this effect cannot be neglected. It is therefore essential to avoid any such discontinuities in the error signal.

A major contribution to this unfavorable behavior results from abrupt changes in the reference signal $y_{\text{ref}}(\cdot)$, that have an immediate effect on the error signal $e(\cdot)$ and its derivative. Thus, it is imperative to ensure a continuous form of $y_{\text{ref}}(\cdot)$ and $\dot{y}_{\text{ref}}(\cdot)$. Unfortunately, this is not the case in the reference signal present in the current control software of the FDCT transmission (see Fig. 4.25). Since there exists no derivative feedback in the traditional clutch controller, this is of no concern there. However, the adaptive controllers in this thesis require a reference signal that has a continuous first derivative to avoid strong reactions, and possibly oscillations, that may be induced by the derivative feedback term:

$$y_{\text{ref}}(\cdot) \in C^n, \quad n \in \mathbb{N} \quad (4.42)$$

To achieve a continuous reference signal, a new algorithm is implemented that generates a

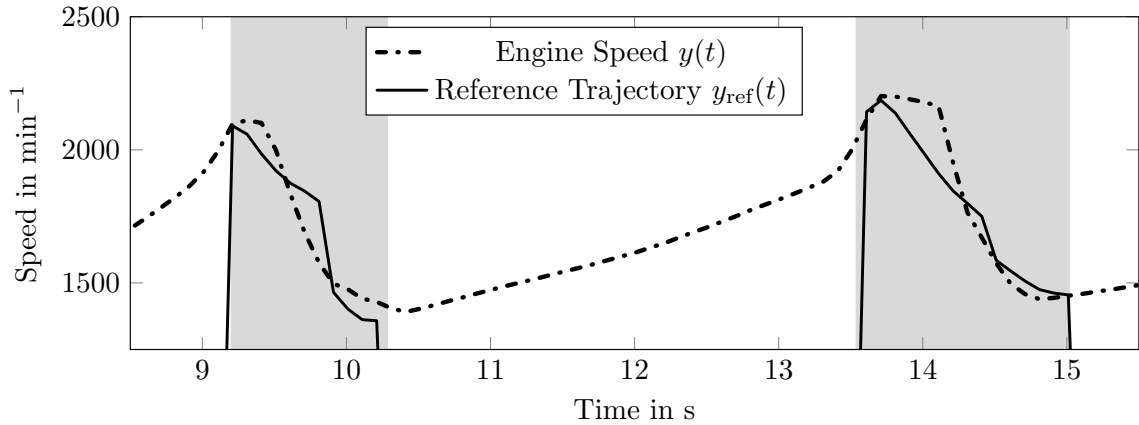


Figure 4.25: Exemplary simulation of traditional shift procedures with discontinuous steps in the set point trajectory $y_{\text{ref}}(\cdot)$

3rd-order polynomial signal. Thus, the start and end speeds as well as their gradients can be specified, together with the desired shift duration (see Fig. 4.26). Also, the reference signal's derivative is generated for use in the derivative feedback term:

$$y_{\text{ref}}(t) = \frac{\dot{\omega}_S + \dot{\omega}_E}{t_{\text{dur}}^2} t^3 + 2 \frac{\omega_S - \omega_E}{t_{\text{dur}}^3} t^3 + 3 \frac{\omega_E - \omega_S}{t_{\text{dur}}^2} t^2 - \frac{\dot{\omega}_S + \dot{\omega}_E}{t_{\text{dur}}} t^2 + \dot{\omega}_S t + \omega_S \quad (4.43)$$

$$\dot{y}_{\text{ref}}(t) = 3 \frac{\dot{\omega}_S + \dot{\omega}_E}{t_{\text{dur}}^2} t^2 + 6 \frac{\omega_S - \omega_E}{t_{\text{dur}}^3} t^2 + 6 \frac{\omega_E - \omega_S}{t_{\text{dur}}^2} t - 2 \frac{\dot{\omega}_S + \dot{\omega}_E}{t_{\text{dur}}} t + \dot{\omega}_S \quad (4.44)$$

with the parameters

- ω_S – start speed
- ω_E – end speed
- $\dot{\omega}_S$ – start speed gradient
- $\dot{\omega}_E$ – end speed gradient
- t_{dur} – shift duration

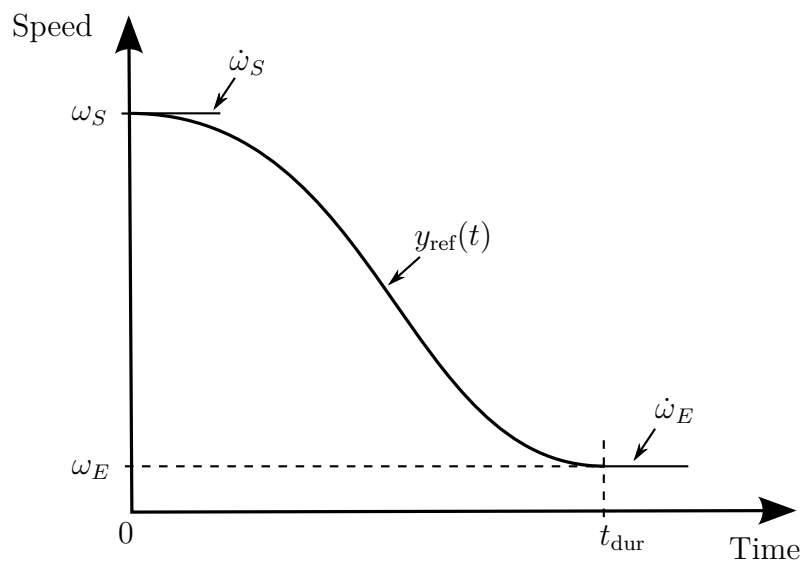


Figure 4.26: Generation of a C^∞ -continuous reference trajectory $y_{\text{ref}}(\cdot)$ in form of a 3rd-order polynomial, with parameters $\omega_S, \dot{\omega}_S, \omega_E, \dot{\omega}_E, t_{\text{dur}}$

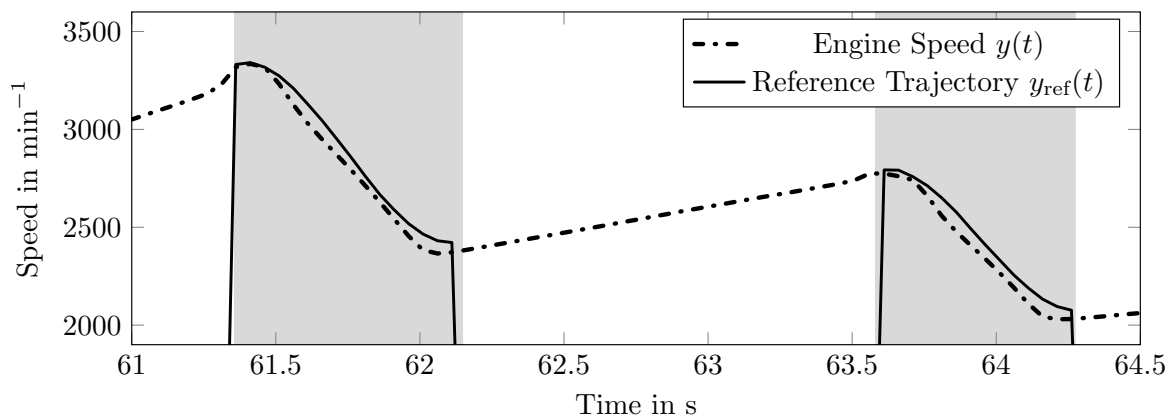


Figure 4.27: Exemplary simulation of adaptively controlled shift procedures with set point trajectory $y_{\text{ref}}(\cdot)$ as 3rd-order polynomial with $t_{\text{dur}} = 0.7$ s

Thus, a smooth signal $y_{\text{ref}}(\cdot) \in C^\infty$ is generated and condition (4.42) is obeyed.

The start and end speed values are determined by the current shift procedure and may vary during the shift, corresponding to the vehicle's acceleration. The start gradient $\dot{\omega}_S$ is taken from the actual speed gradient signal in order to achieve a smooth transition into the speed control phase. The end gradient is set to $\dot{\omega}_E = 0$, whereas the shift duration parameter t_{dur} can be set by the designer. Shorter time spans make for a quicker shift procedure, whereas a longer shift duration may achieve a more comfortable shift. The setting is therefore subject to calibration. An example for the resulting reference signal during shifts is depicted in Fig. 4.27. There are no discontinuities present in the reference signal and the system output signal $y(\cdot)$ is able to follow smoothly. The duration t_{dur} has been set according to simulation results. A value of $t_{\text{dur}} = 0.7\text{ s}$ is common for most shift procedures. Nonetheless, the designer may choose shorter times for faster, sportier shifts or longer times for more comfortable shifts.

4.7 Engine Intervention Control

When designing gearshift controllers, a significant contribution to shift speed and comfort is the engine intervention algorithm.

Consider a powered upshift procedure: The reduction of the engine speed creates an additional torque in the powertrain that is transmitted to the driveshaft. This is a result of the deceleration of the combined moment of inertia at the transmission input shaft:

$$\dot{\vec{L}}_{\text{out}} = J_{\text{out}} \ddot{\varphi}_{\text{out}} = \sum_n \vec{M}_n \quad (4.45)$$

$$\vec{e}_x : \quad J_{\text{out}} \ddot{\varphi}_{\text{out}} = -M_{\text{Veh}} + i_g (M_{\text{Eng}} - J_{\text{in}} \ddot{\varphi}_{\text{in}}) \quad (4.46)$$

$$\ddot{\varphi}_{\text{out}} = \frac{-M_{\text{Veh}} + i_g M_{\text{Eng}} - i_g J_{\text{in}} \ddot{\varphi}_{\text{in}}}{J_{\text{out}}} \quad (4.47)$$

where

- L_{out} – angular momentum of transmission output shaft
- J_{in} – combined mass moment of inertia at transmission input shaft
- J_{out} – combined mass moment of inertia of vehicle mass and output shaft
- $\dot{\varphi}_{\text{in}}$ – angular velocity of transmission input shaft during fixed gear
- $\dot{\varphi}_{\text{out}}$ – angular velocity of transmission output shaft

- M_{Eng} – engine drive torque
- M_{Veh} – combined load torque of vehicle, corresponding to combined drive resistances
- i_g – current gear ratio

Exemplary simulations of powered upshift procedures are conducted with the NAG3 transmission and the adaptive controller in operation to demonstrate the effect of engine intervention control on the powertrain dynamics. For more details regarding this powertrain and for extensive simulations and vehicle experiments, please refer to Section 5.2.

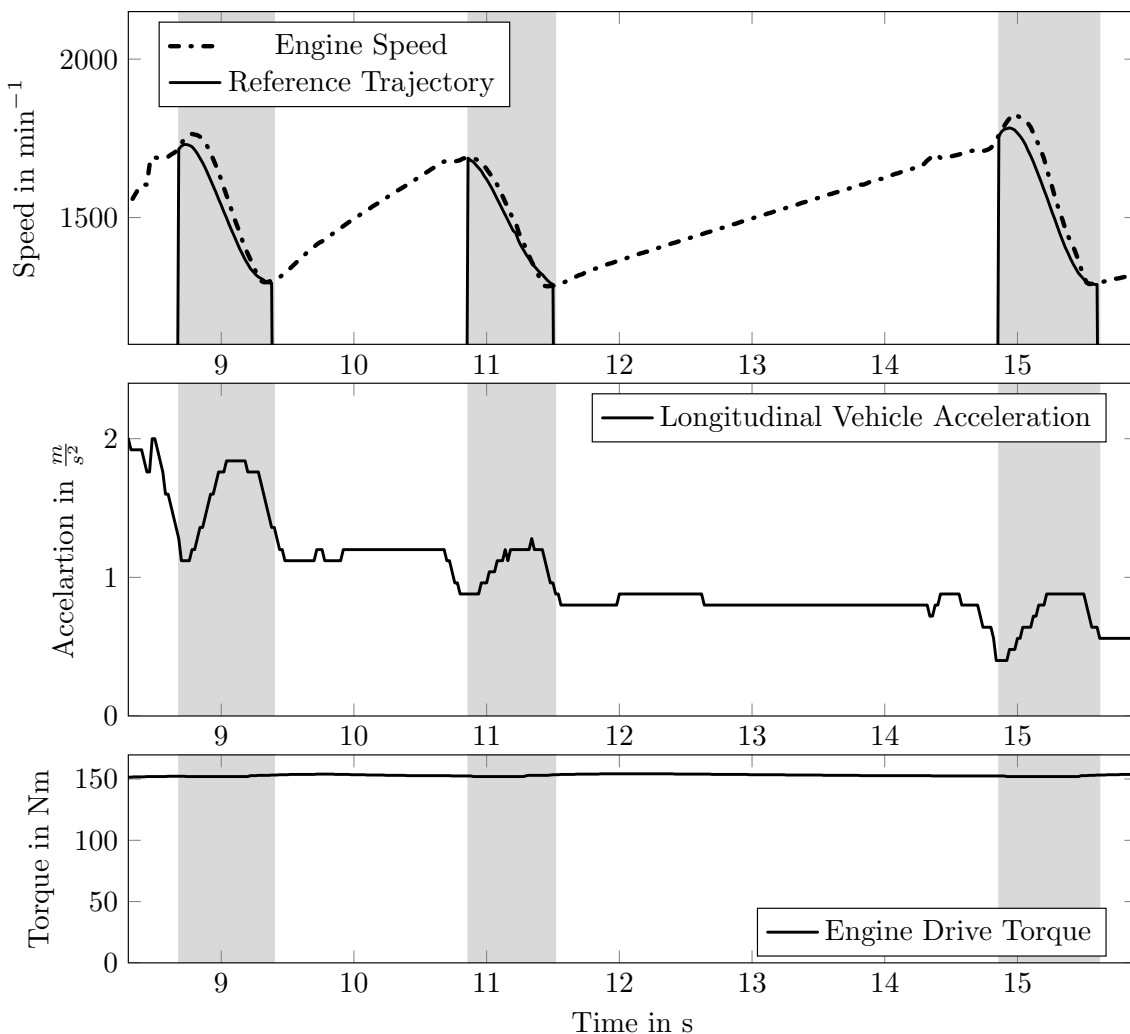


Figure 4.28: SiL simulation of adaptively controlled upshifts without engine torque reduction in NAG3 transmission, $p_a = 30\%$

First, a series of adaptively controlled upshift procedures with an exemplary accelerator pedal setting of $p_a = 30\%$ is conducted in simulation without engine intervention control.

The term $-i_g J_{in} \ddot{\varphi}_{in}$ creates a positive torque at the transmission output, if $\ddot{\varphi}_{in}$ is negative, for instance during upshifts, where the engine speed is reduced (see Fig. 4.28). This leads to an unfavorable jerk in the powertrain, causing a positive longitudinal acceleration in the vehicle, as depicted in Fig. 4.28 (center), around $t = 9.1$ s, $t = 11.3$ s and $t = 15.3$ s. Note that this additional torque is dominant in low gear ratios, where $i_g \gg 1$. In higher gears, as i_g decreases, the additional torque does not affect the powertrain dynamics as much.

This behavior can be counteracted by reducing the engine drive torque M_{Eng} accordingly during the speed controlled shift phase. This is done by the TCU requesting a reduction of drive torque which is then conducted by the engine control unit. However, this feature has been deactivated at this point for comparison purposes. The engine torque stays constant over the course of the three upshift procedures. After the engine intervention algorithm has been reactivated, the three upshifts are carried out anew in simulation, as shown in Fig. 4.29. Now, the reduction of the engine torque is clearly visible during the shift procedures (Fig. 4.29, bottom plot). As a result, the strong additional longitudinal acceleration of the vehicle is avoided (center plot). However, the acceleration signal still shows some oscillations and is therefore not ideal. This is due to the fact that the algorithm computing a suitable engine intervention request is based on the traditional clutch control architecture and is therefore not fully compatible with the adaptive controller.

At this point, no further investigations are made into the generation of a suitable engine intervention control algorithm for adaptively controlled shift procedures. The avoidance of longitudinal jerks by controlling both the engine torque and clutch torque is beyond the scope of this thesis and requires a multiple-input, multiple-output (MIMO) control design. For the purpose of this work, the traditional engine intervention control algorithm is deactivated.

Note that for powered downshifts, similar considerations concerning an additional torque in the powertrain apply. However, in this case the torque is negative, since part of the engine's drive torque is used to accelerate the engine during downshifts, for example. Thus, it is possible to generate a compensatory torque in the engine to avoid this negative jerk and also to facilitate engine speed matching during downshifts. Again, this feature is not discussed here and therefore deactivated.

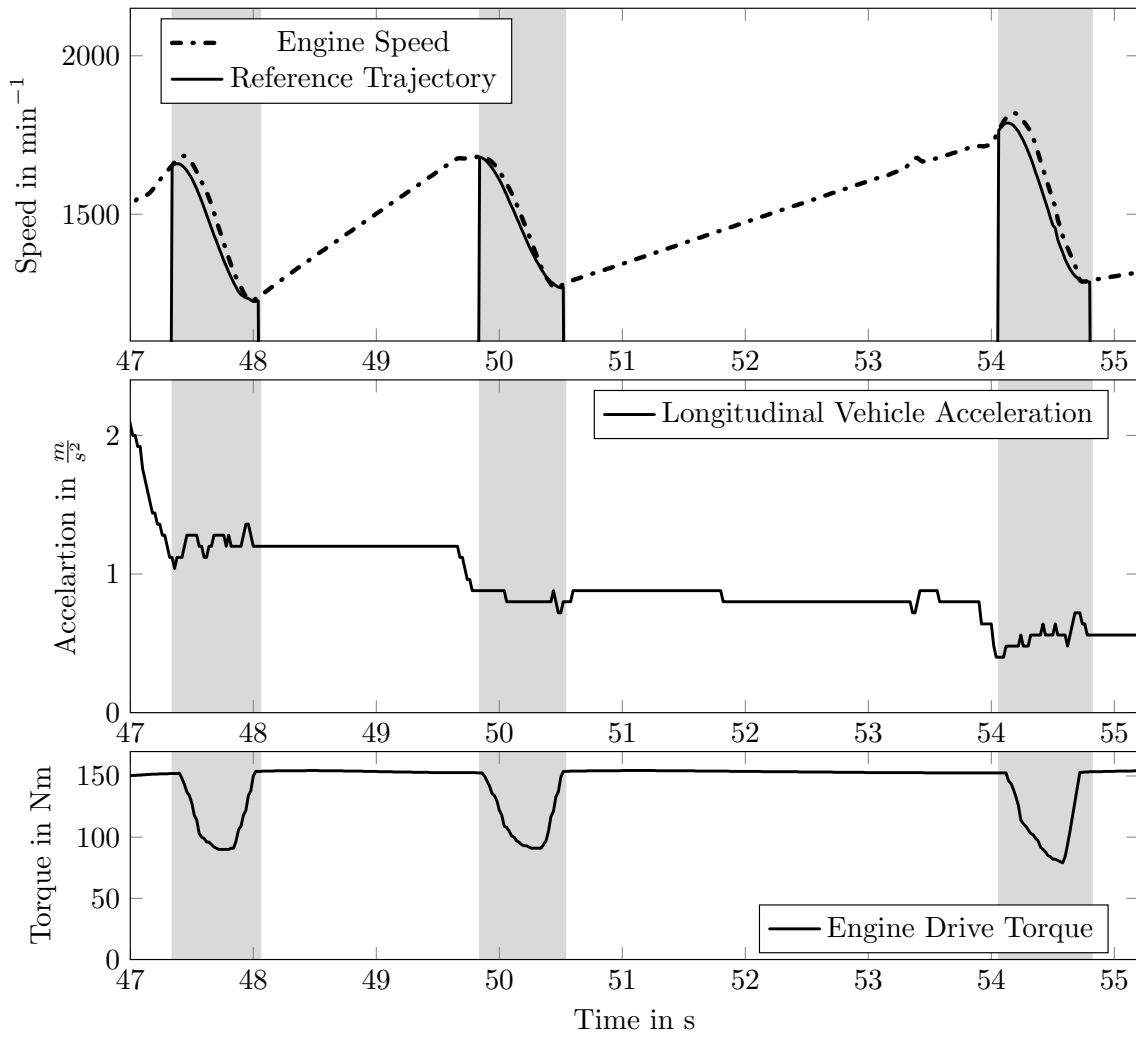


Figure 4.29: SiL simulation of adaptively controlled upshifts with engine torque reduction in NAG3 transmission, $p_a = 30\%$

This concludes the design process of the adaptive λ -tracking controller. Its performance is yet to be evaluated in comparison to the traditional control software.

5 Vehicle Experiments: Comparative Study

In this chapter, the adaptive controller (4.9) – (4.15) designed in Chapter 4 is tested in vehicle operation in simulation and on a test track using actual *series production control hardware*. Thus, the simulation results from the previous chapter are validated and the applicability of adaptive λ -tracking control in two distinct powertrains is demonstrated. It was not possible to conduct vehicle tests under different environmental conditions – such as extreme cold – in controlled, reproducible experiments due to the lack of testing facilities. Hence, before any experiments were conducted, the vehicle was warmed up to ensure the same conditions for all measurements, for instance the temperatures of engine coolant, engine oil, transmission oil and catalytic converter.

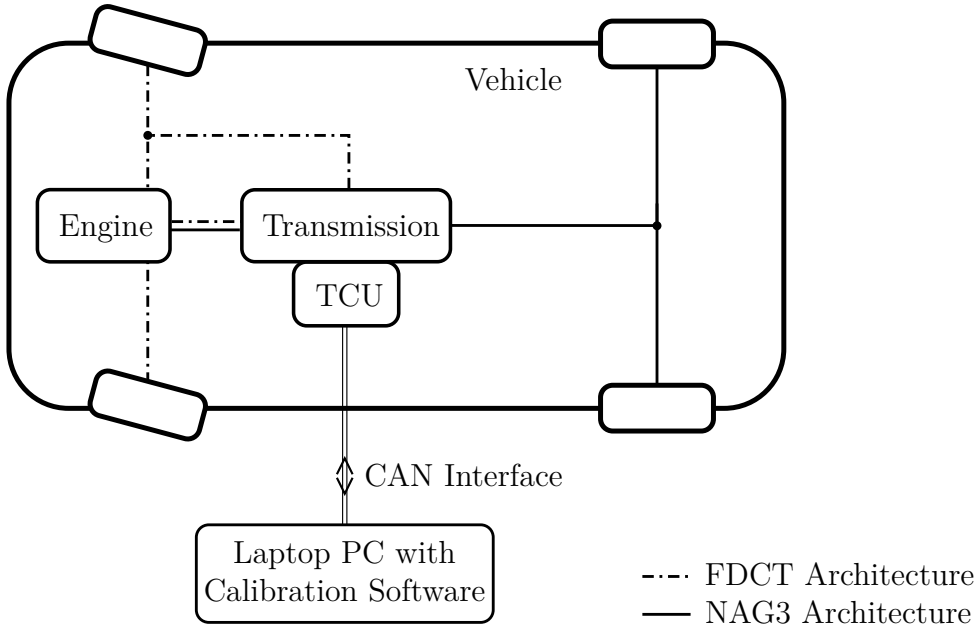


Figure 5.1: Vehicle experimental setup

The control software runs on the transmission control unit, as it would in a series production transmission. Measurements are conducted by recording the software’s variables

with the help of a standard Laptop computer connected to the TCU via the Controller Area Network (CAN) protocol, using the software CANape (by Vector Informatik, version 10.0 SP2, 2011). With the help of the same data link, the calibration parameters can be set (see Fig. 5.1). Note that due to the different powertrain layouts for the FDCT and NAG3 transmissions, the schematic in Fig. 5.1 shows both front- and rear-wheel drive, depending on the transmission.

5.1 FDCT Dual-Clutch Transmission

First, the adaptive controller is tested with the FDCT dual-clutch transmission in a Mercedes-Benz B-Class vehicle with a 90 kW gasoline engine.

A series of driving maneuvers are carried out to test the adaptively controlled shift procedures under different circumstances. They have been chosen for their ability to be conducted in both simulation and vehicle experiment on a test track. Since the length of the available track and maximum vehicle speed are limited, driving maneuvers requiring high speeds are not feasible.

The following maneuvers are conducted:

- Vehicle pull away from standstill with an accelerator pedal value of $p_a = 50\%$. Three subsequent upshifts can be investigated during this maneuver: $\textcircled{1} \rightarrow \textcircled{2} \rightarrow \textcircled{3} \rightarrow \textcircled{4}$
This is also used to evaluate shift duration during upshifts.
- Powered up- and downshifts during vehicle acceleration with $p_a = 50\%$ between 3rd and 4th gear. Thus, constrained and release shifts can be tested: $\textcircled{4} \rightarrow \textcircled{3} \rightarrow \textcircled{4} \rightarrow \textcircled{3} \rightarrow \textcircled{4}$
- Powered up- and downshifts during vehicle acceleration with $p_a = 50\%$ between 4th and 5th gear: $\textcircled{5} \rightarrow \textcircled{4} \rightarrow \textcircled{5} \rightarrow \textcircled{4} \rightarrow \textcircled{5}$
Again, constrained and release shifts are conducted. This is done for comparison purposes and to eliminate any effects specific to the shifts during the previous maneuver.
- In order to evaluate shift duration during downshifts, the vehicle is accelerated to $80 \text{ km} \cdot \text{h}^{-1}$ and put into 7th gear. Now, three downshifts to 4th gear are conducted during vehicle acceleration with $p_a = 50\%$: $\textcircled{7} \rightarrow \textcircled{6} \rightarrow \textcircled{5} \rightarrow \textcircled{4}$

Note that this selection does not constitute a comprehensive shift analysis. Many and more different shift procedures would have to be tested in order to fully investigate control performance for every conceivable driving scenario, which is beyond the scope of this

thesis. Instead, these maneuvers were chosen to test functionality, stability and speed of adaptively controlled gearshifts and at the same time to be conducted easily on the available test track.

The same parameters as before are used for the adaption law, given in Table 4.2.

5.1.1 Traditional Control

For comparison purposes and to assess traditional control performance, a set of traditionally controlled shifts is conducted. This is done in both simulation and vehicle experiment.

In Fig. 5.2, the vehicle is accelerated from standstill with a continuous accelerator pedal

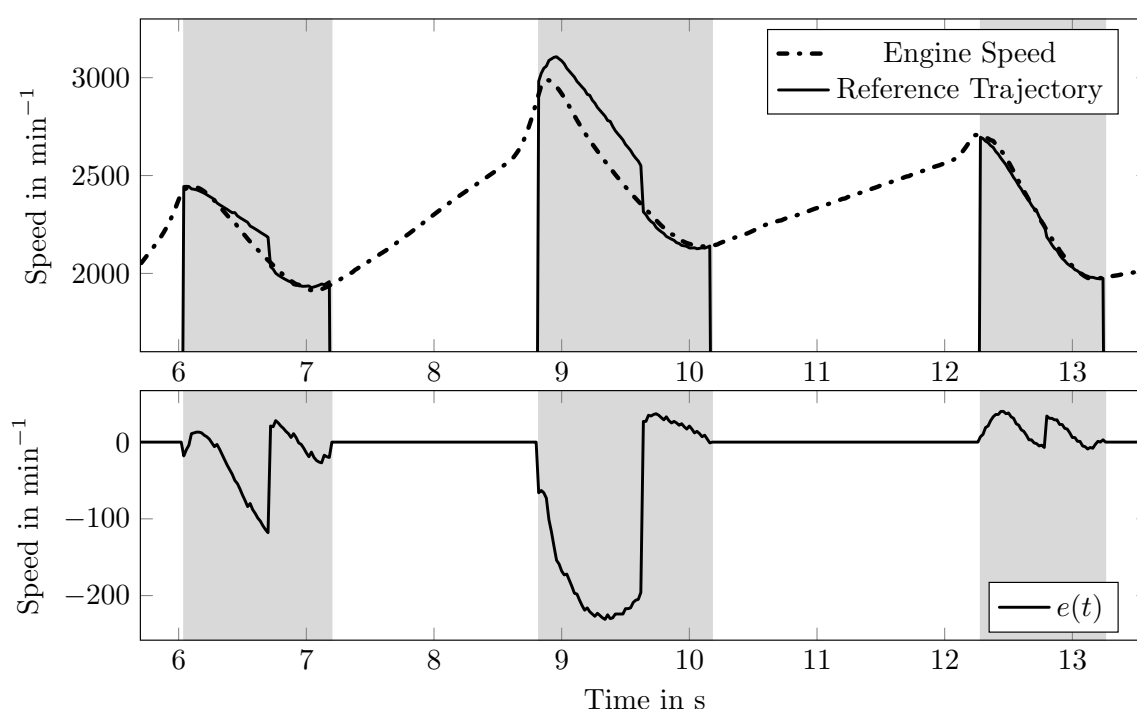


Figure 5.2: FDCT: SiL simulation of ①→②→③→④ maneuver, traditional control

value of 50% in simulation. Thus, three upshifts are carried out from 1st over 2nd and 3rd to 4th gear. The engine speed signal shows a smooth form, whereas the reference trajectory is reinitialized during each shift procedure. As a result, the error value $e(\cdot)$ is virtually eliminated towards the end of each shift. The shift duration ranges from 1 s to 1.4 s.

Figure 5.3 shows the same maneuver in a vehicle experiment. The smoothness of the engine speed signal is comparable to the one in simulation. The discontinuities in the reference trajectory are still present, but not as extensive as in simulation. Also, the shifts occur at different engine speed levels. The upshift from 1st to 2nd gear begins at

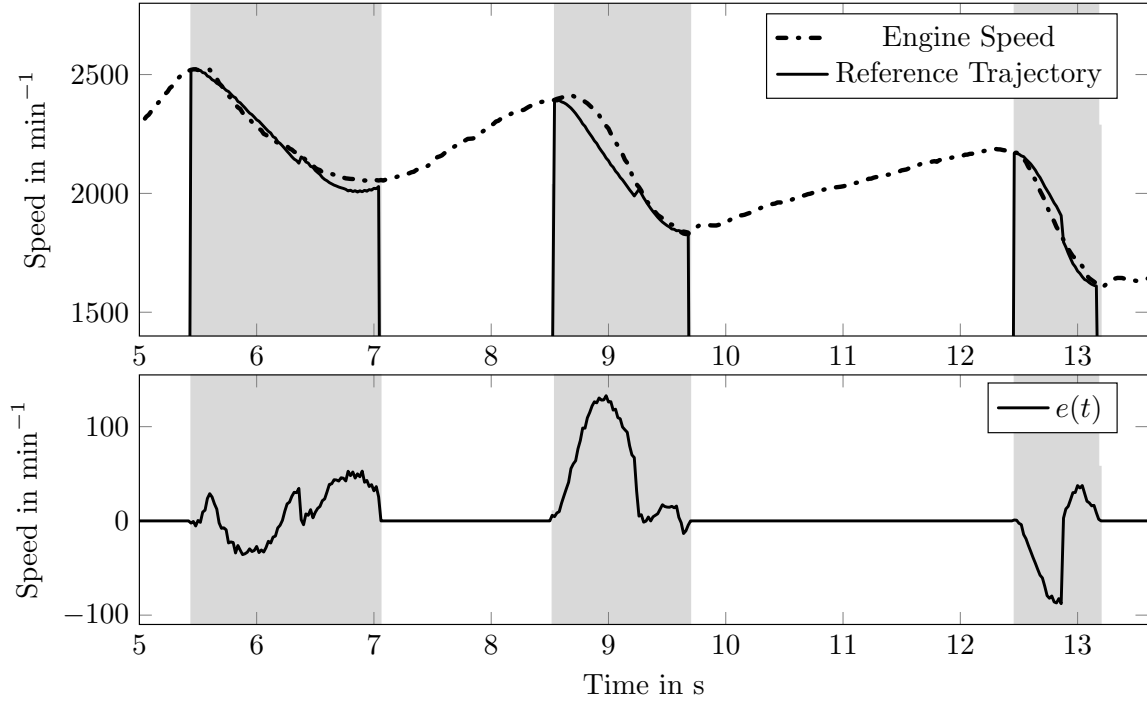


Figure 5.3: FDCT: Vehicle experiment of ①→②→③→④ maneuver, traditional control

ca. 2500 min^{-1} in both cases, whereas the shift from 2nd to 3rd gear begins later in simulation than during the vehicle experiment; at 2900 min^{-1} and 2400 min^{-1} , respectively. Also, the shift from 3rd to 4th gear begins at 2700 min^{-1} in simulation and at 2200 min^{-1} in the actual vehicle. The shifts are initiated by the control software's gear selection algorithm. In order to achieve comparable results, the vehicle test conditions were chosen as close to the simulation parameters as possible. Why shifts are initiated differently is unknown at this point. However, since the focus lies on the gearshift procedures itself, the algorithm responsible for gear selection and shift initiation is not discussed further. The shift duration in vehicle experiments ranges from 0.9 s to 1.5 s, which is comparable to the simulation results. Figure 5.4 shows two down- and two upshift procedures between 3rd and 4th gear during vehicle acceleration with a constant accelerator pedal value of 50%. Note that the clutch control software distinguishes between up- and downshifts in the computation of the error signals. Thus, both error signals $e_{1,2}(\cdot)$ are plotted, where $e_1(\cdot)$ refers to the error signal during upshifts, and $e_2(\cdot)$ denotes the error signal during downshifts.

During upshifts, the engine speed signal follows a smooth form. However, during downshifts, it exhibits some oscillations towards the end of the respective shift procedure. The reference trajectory is followed roughly, although towards the end of downshifts, the engine speed veers away. As a result, the shift is concluded with an increased error signal.

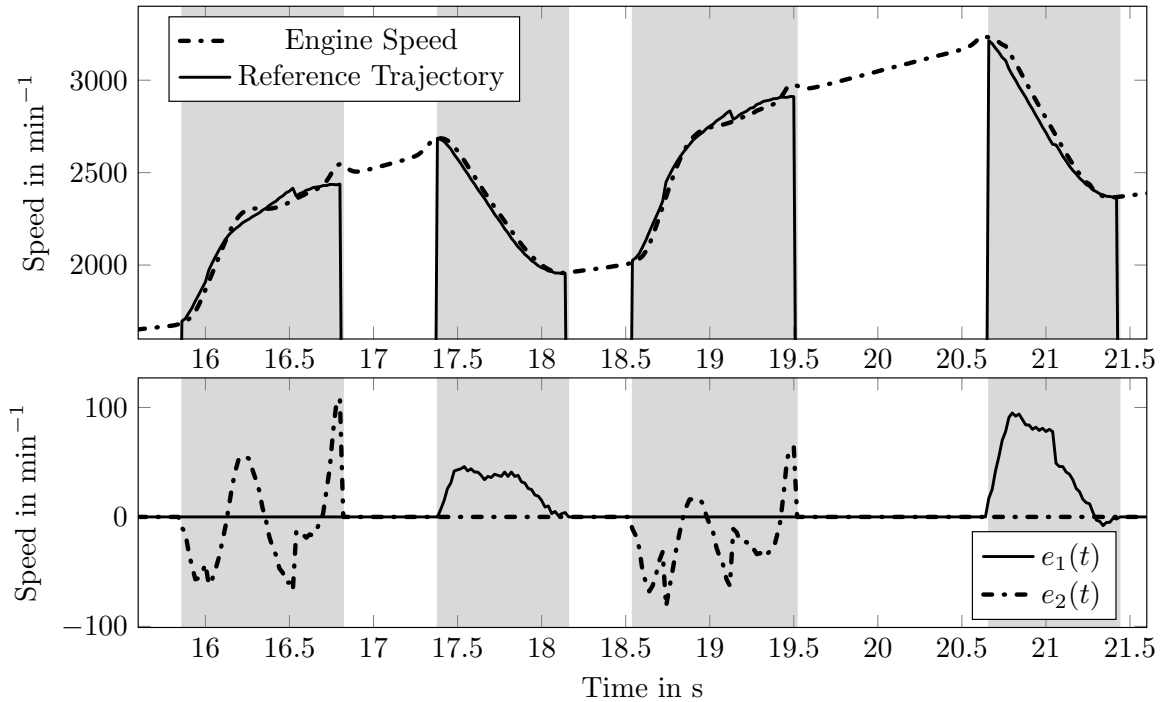


Figure 5.4: FDCT: SiL simulation of ④→③→④→③→④ maneuver, traditional control

Shift duration is ca. 0.8 s during upshifts, and ca. 1 s during downshifts.

Figure 5.5 shows the same maneuver, carried out in the vehicle. Both up- and downshift procedures achieve a control performance comparable to the one in simulation. However, the engine speed signal shows only minor oscillations in the vehicle. During upshifts, the error signal $e_1(\cdot)$ is fairly small towards the end of the shifts (ca. 10 min^{-1}). For downshifts, the error signal $e_2(\cdot)$ is not reduced at the end of the shift. Instead, the engine speed signal veers away from the reference trajectory, causing values of ca. -150 min^{-1} and -120 min^{-1} for $e_2(\cdot)$, respectively.

Downshifts last ca. 1.5 s, whereas upshifts take ca. 0.7 s. In simulation, downshifts are conducted faster and upshifts take a bit longer. Another set of consecutive up- and downshifts is simulated during vehicle acceleration, as depicted in Fig. 5.6, this time between 4th and 5th gear. Again, the upshifts produce a smooth engine signal, whereas oscillations occur during downshifts. As before in Fig. 5.4, the error value is almost eliminated towards the end of upshifts, and is not reduced considerably at the end of downshift procedures. Shift duration is ca. 0.6 s during upshifts, and ca. 1 s during downshifts.

The shift procedures during the same driving maneuver are repeated in the vehicle and shown in Fig. 5.7. The upshift procedures are comparable to the simulation results regarding control performance. However, the experimental data differs somewhat from the simulation results during downshifts. Again, there is a considerable tracking error of ca.

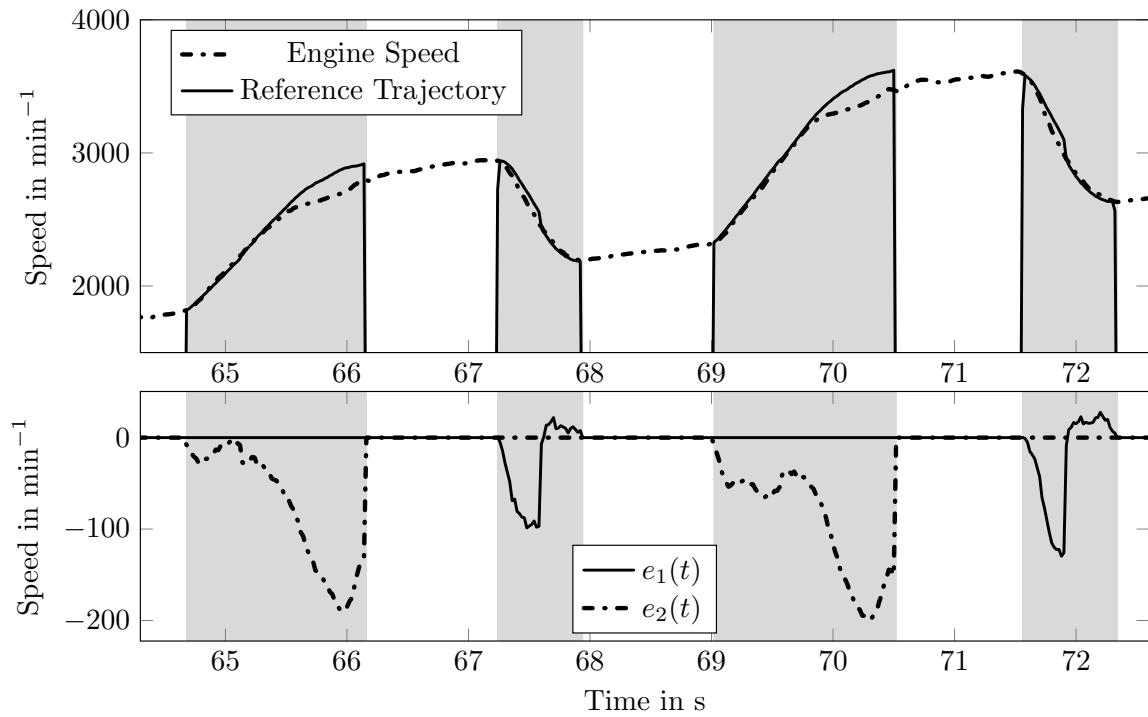


Figure 5.5: FDCT: Vehicle experiment of ④→③→④→③→④ maneuver, traditional control

50 min⁻¹ at the end of each downshift. Unlike the simulation results, the vehicle experiment shows a positive error value.

Downshifts last from 1 s to 1.2 s, upshifts take ca. 0.7 s. In simulation, shift speed is slightly faster.

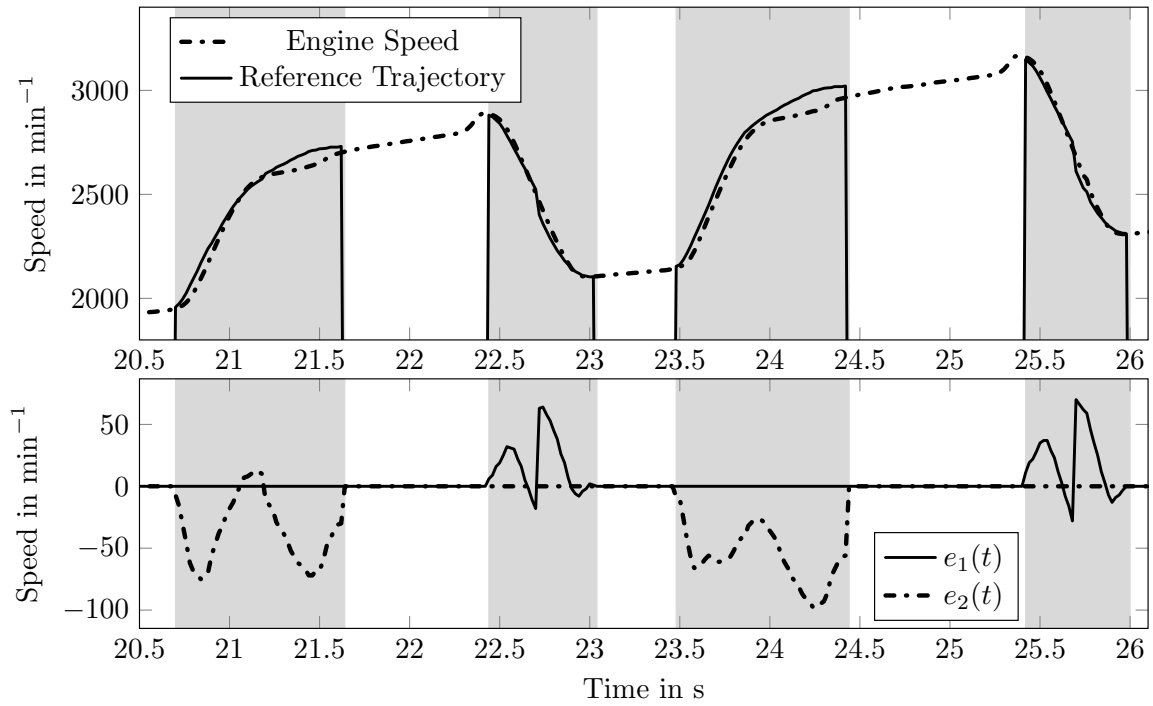


Figure 5.6: FDCT: SiL simulation of ⑤→④→⑤→④→⑤ maneuver, traditional control

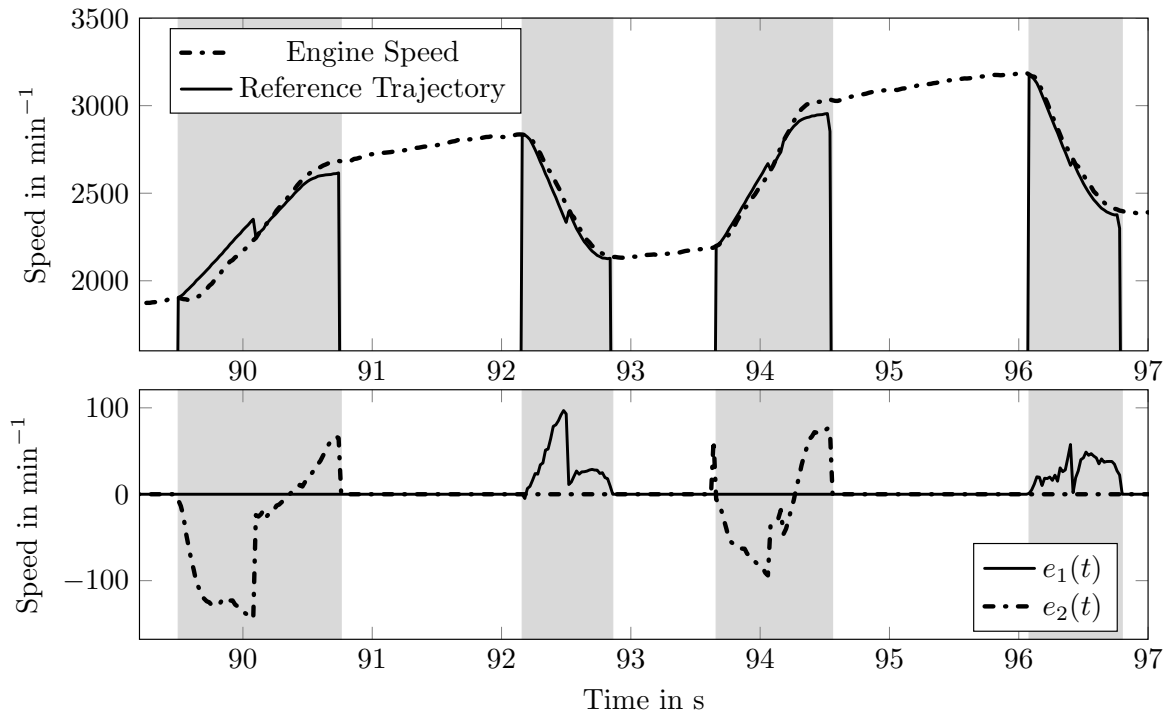


Figure 5.7: FDCT: Vehicle experiment of ⑤→④→⑤→④→⑤ maneuver, traditional control

5.1.2 Adaptive Control

In this section, the simulations and vehicle experiments are carried out anew, this time with the adaptive controller in operation.

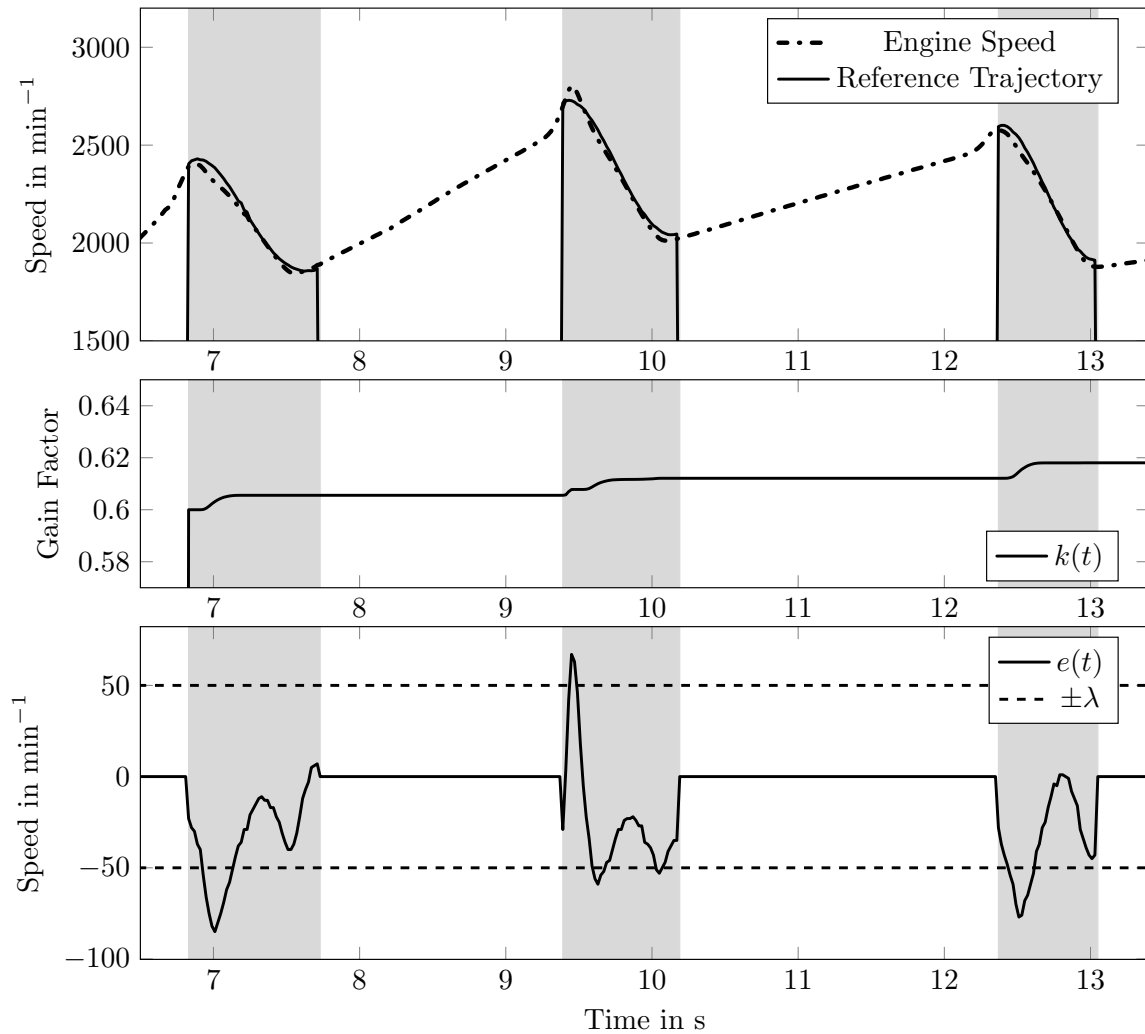


Figure 5.8: FDCT: SiL simulation of ①→②→③→④ maneuver, adaptive control

Shift durations have been set to $t_{\text{dur},1} = 0.9\text{s}$ for upshifts and $t_{\text{dur},2} = 1.0\text{s}$ for downshifts. As with the traditional control software before, the vehicle is accelerated with a constant accelerator pedal value of 50%, which results in a series of three consecutive upshifts, as depicted in Fig. 5.8. Both the engine speed and the reference trajectory show a smooth form. The error signal $e(\cdot)$ leaves the λ -neighborhood occasionally, which causes the adaption law to react and the gain factor $k(\cdot)$ to be increased. Towards the end of each upshift, the error signal is reduced sufficiently below λ , and thus the control goal is achieved. Shift duration ranges from 0.7s to 0.9s. Note that just before the shifts begin,

there is a sudden and unexpected increase in engine speed. The reason for this behavior is unknown.

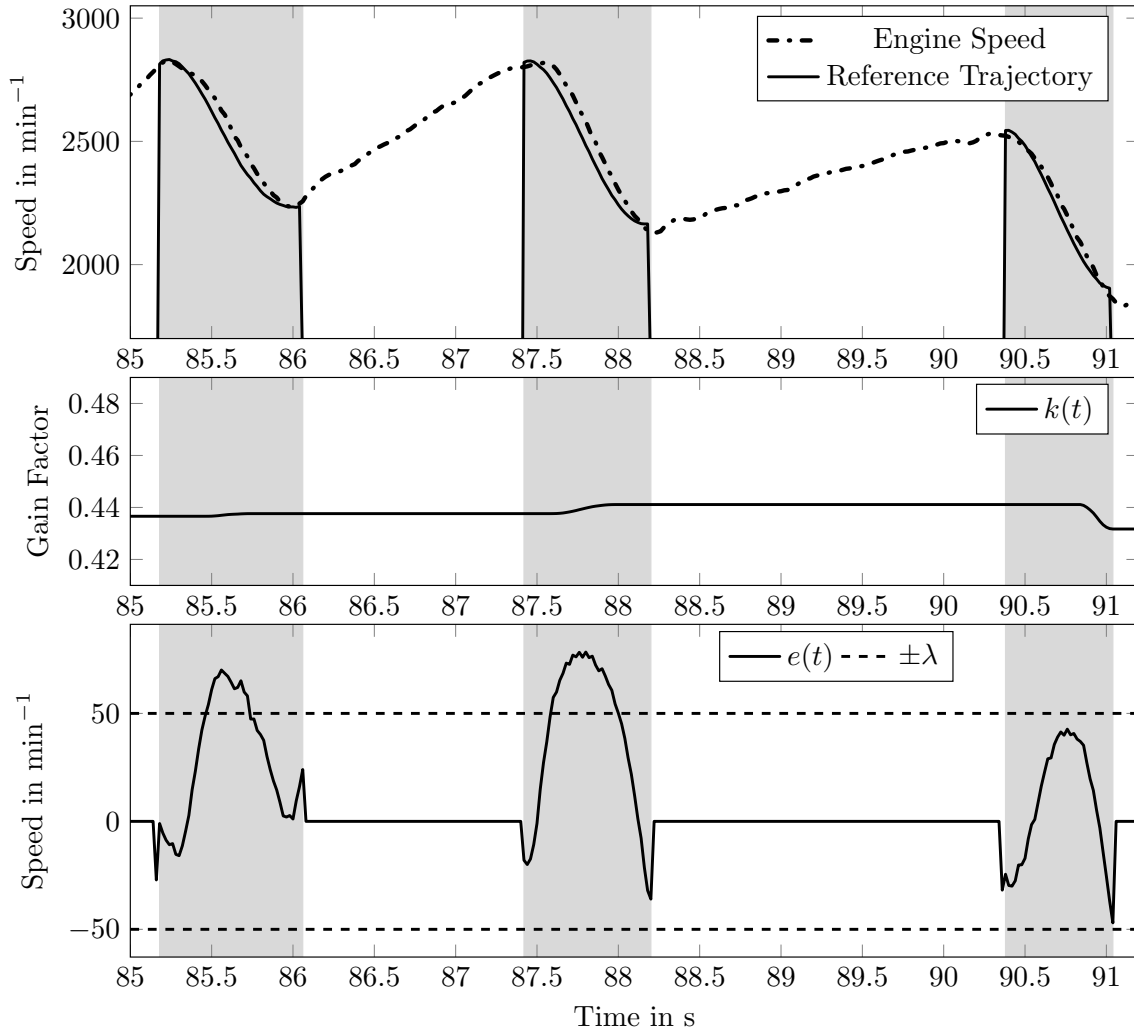


Figure 5.9: FDCT: Vehicle experiment of ①→②→③→④ maneuver, adaptive control

The maneuver is repeated in vehicle experiment, as depicted in Fig. 5.9. The engine speed signal smoothly follows the reference trajectory, and the control goal of $e(t) \leq \lambda$ as achieved for the most part of every shift as well as at the end. Minor increases of the gain factor $k(\cdot)$ are caused by the adaption law, as well as a small decrease during the third shift, resulting from $e(t) \leq \lambda$ over the duration of the procedure. As before during traditional clutch control, the shifts are initiated at different engine speed levels, when vehicle experiments are compared to the simulation results in Fig. 5.8. Again, this is not discussed further. Shift duration ranges from 0.7s to 0.9s, which was the same during simulation.

The unexpected increase of the engine speed just before the shift procedure begins, as

observed in simulation, is not present here. The system exhibits the expected behavior regarding the transition from fixed gear driving to gear shifting. Thus, the simulation generates false system dynamics in these cases.

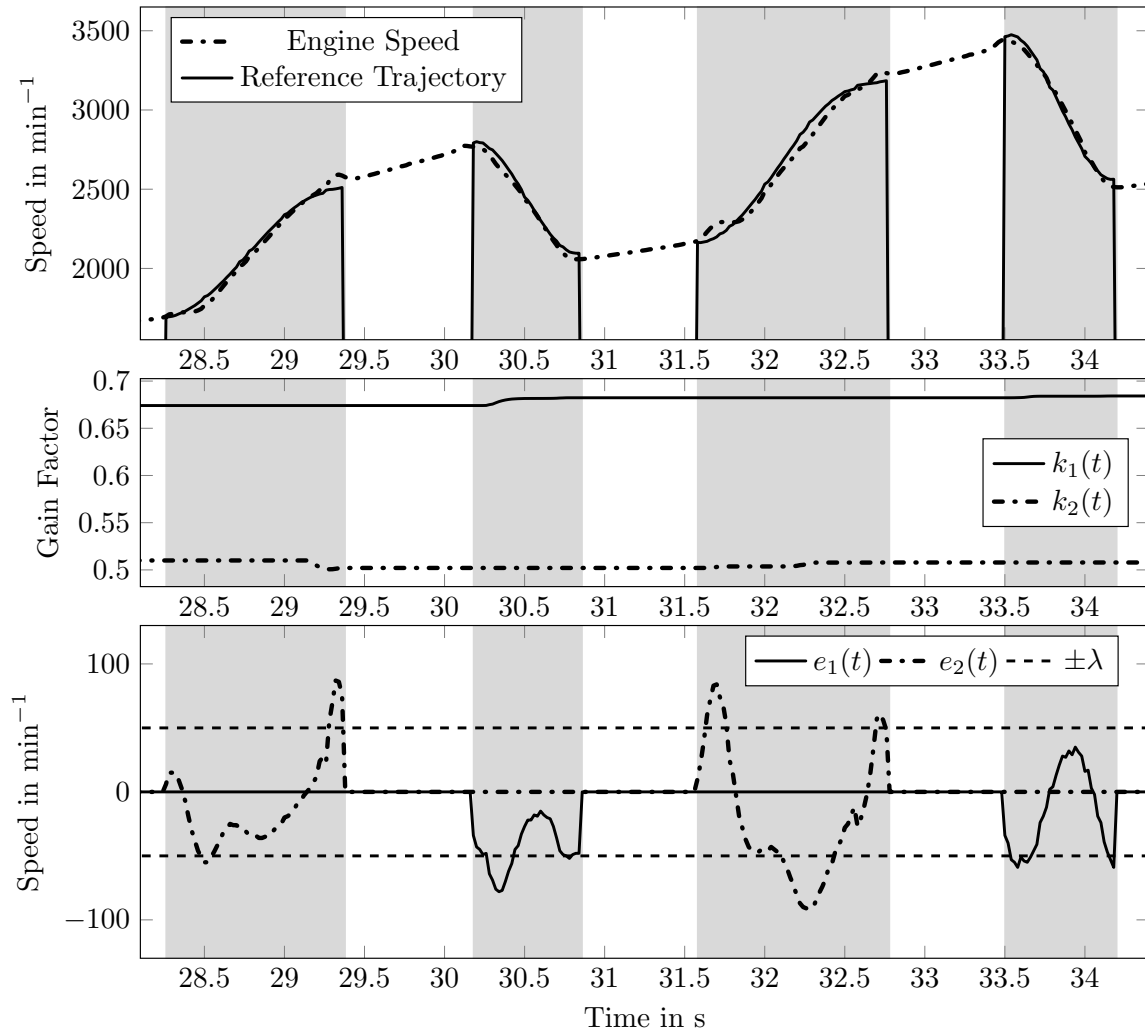


Figure 5.10: FDCT: SiL simulation of ④→③→④→③→④ maneuver, adaptive control

The simulation results of consecutive down- and upshifts between 3rd and 4th gear during vehicle acceleration with a constant accelerator pedal value of 50% are depicted in Fig. 5.10. Again, the adaptive controller causes a smooth reaction of the system output, i.e., the engine speed signal. Only minor oscillations at the beginning and at the end of the downshifts are observed. The engine speed signal veers away from the reference trajectory at the end of downshifts, causing the error signal $e_2(\cdot)$ to jump and leave the λ -strip. During upshifts, the control goal of $e_1(t) \leq \lambda$ is barely achieved once and not achieved during the second procedure. However, these are not substantial violations, and thus the

adaption law's reaction causes only a minor increase of the gain factors $k_{1,2}(\cdot)$. The shifts are completed over a shift duration of 0.7 s for upshifts and ca. 1.1 s for downshifts.

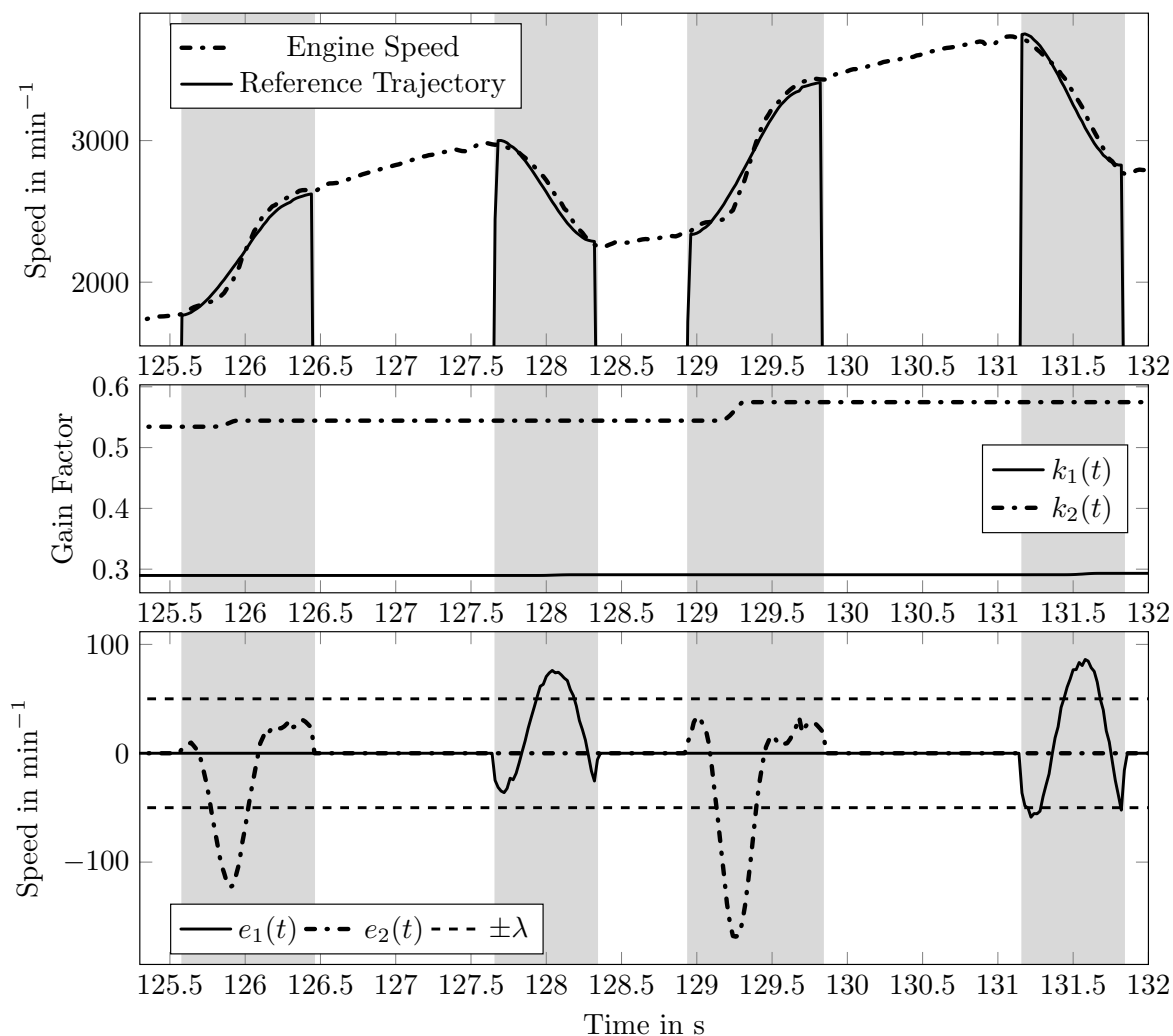


Figure 5.11: FDCT: Vehicle experiment of ④→③→④→③→④ maneuver, adaptive control

In Fig. 5.11, experimental data of the same up- and downshift maneuvers is shown. Downshifts are performed with a smooth engine speed signal and the control goal is achieved during the end of the respective shift procedure, with $e_2(t) \leq \lambda$. Upshifts are performed smoothly as well, although the error signal $e_1(\cdot)$ is not reduced below λ towards the end of the second upshift. Again, small increases of the gain factors $k_{1,2}(\cdot)$ are observed where the λ -neighborhood is left. In comparison to the simulation results in Fig. 5.10, larger error values are generated during vehicle experiments. However, overall shift performance is comparable or better. The engine speed does not suddenly veer away from the reference trajectory at the end of downshifts. Shift duration is ca. 1 s for downshifts, and ca. 0.7 s

during upshifts. In simulation, downshifts lasted ca. 0.1 s longer, whereas upshifts took the same time.

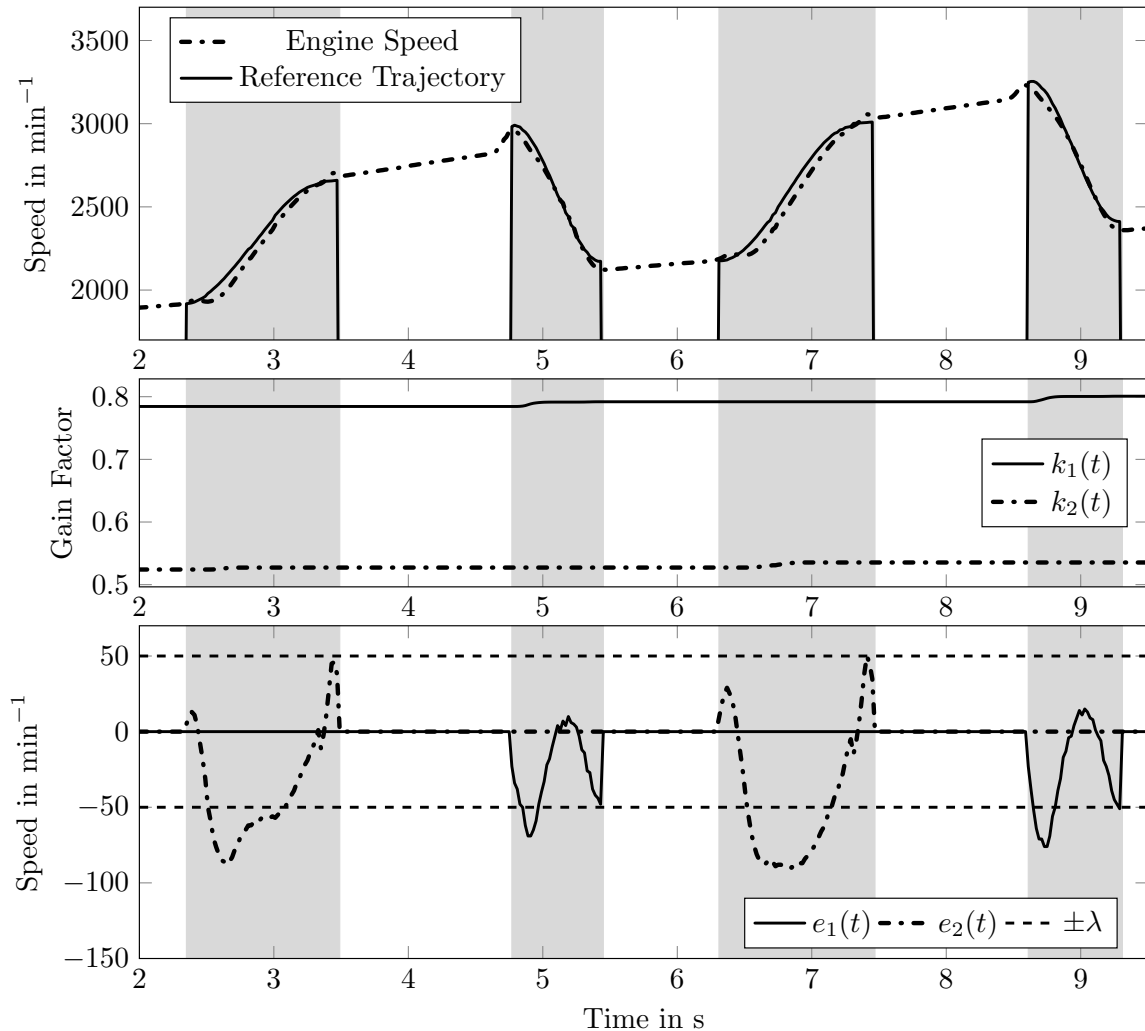


Figure 5.12: FDCT: SiL simulation of ⑤→④→⑤→④→⑤ maneuver, adaptive control

Figure 5.12 shows the simulation results of consecutive down- and upshifts between 4th and 5th gear, during vehicle acceleration. Again, a smooth engine speed signal is achieved during all shift procedures. During downshifts, the control goal of $e_2(t) \leq \lambda$ is achieved towards the end of each shift; the error signal does not veer away from the reference trajectory as much as in Fig. 5.10. During upshifts, the control goal is barely achieved; the corresponding error signal $e_1(\cdot)$ is marginally smaller than the λ -strip. Shift duration is ca. 0.7 s during upshifts, and ca. 1.1 s during downshifts.

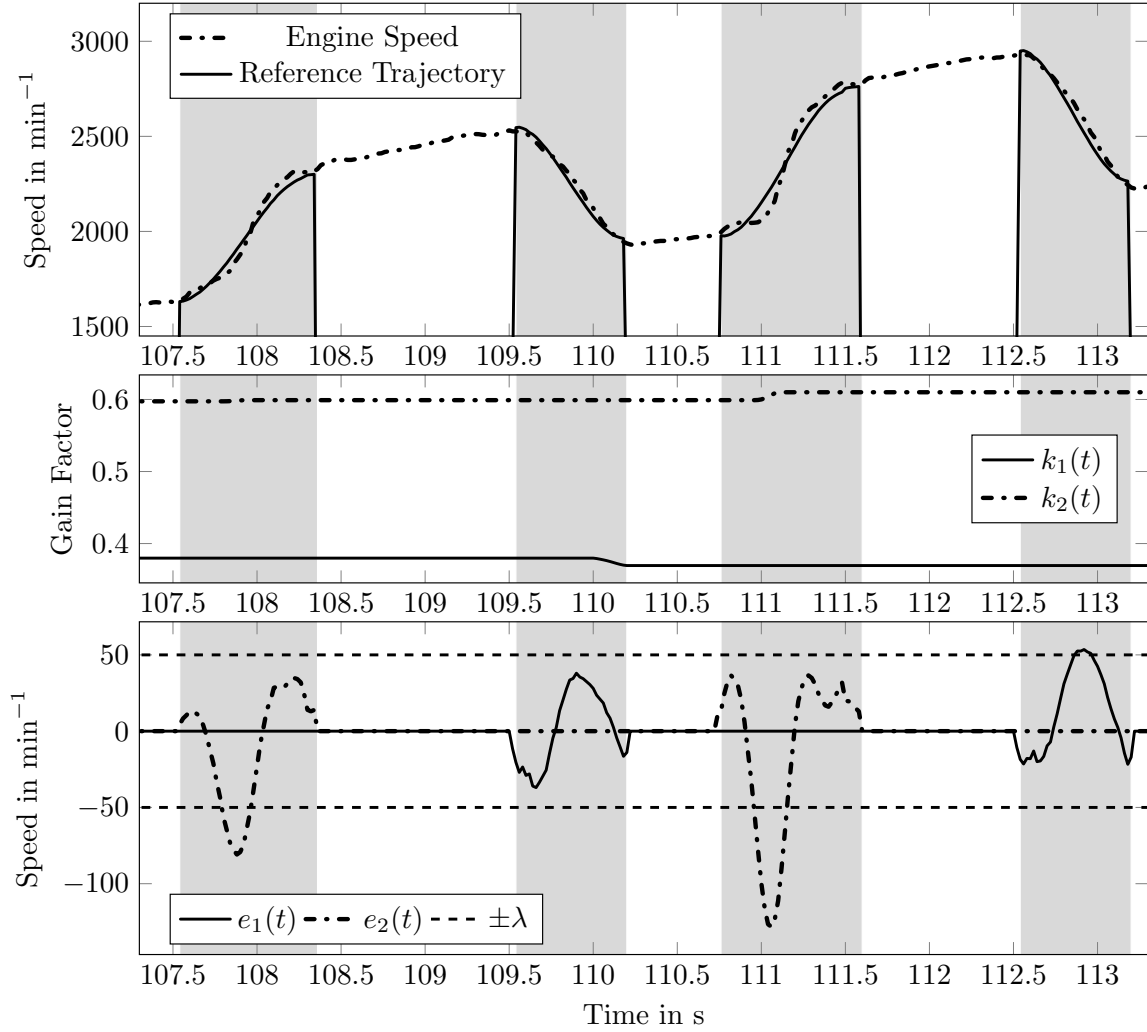


Figure 5.13: FDCT: Vehicle experiment of ⑤→④→⑤→④→⑤ maneuver, adaptive control

The results of the vehicle experiment are given in Fig. 5.13. The engine speed signal shows a smooth form, with minor oscillations during downshift procedures. All shifts are conducted with the control goal of $e_{1,2}(t) \leq \lambda$ achieved at the end of each shift. Some adjustments are made to the gain factors $k_{1,2}(\cdot)$ by the adaption law, including phases of increase and decrease. Compared to the simulation results in Fig. 5.12, control performance is comparable during downshifts, and better during upshifts, with the error signal $e_1(\cdot)$ assuming smaller values and almost remaining inside the λ -neighborhood. Shift duration is ca. 0.9s for downshifts, and ca. 0.7s during upshifts. Compared to simulation, upshift duration is the same, whereas downshifts are conducted faster in the vehicle.

Discussion

Three distinct driving maneuvers have been investigated with both traditional and adaptive control of gearshifts in simulation as well as in vehicle experiments: vehicle pull away from standstill, up- and downshifts between 3rd and 4th and between 4th and 5th gears during vehicle acceleration. Thus, both release and constrained shifts were conducted. The following findings were made:

- The simulation results are comparable to the vehicle experiments, for both traditional and adaptive control of the shift procedures. However, there are some discrepancies. The simulation shows a sudden increase of the engine speed just before upshifts. This cannot be confirmed by experiments. Also, the duration of shift procedures differs between simulation and vehicle experiment. This deviation is clearly observed during traditionally controlled shifts, whereas it is not as significant during adaptive control (see Table 5.1).

Table 5.1: Comparison of shift duration for FDCT transmission

Traditional Control	Simulation	Vehicle
①→②→③→④	1.0 s – 1.4 s	0.9 s – 1.5 s
③→④	0.8 s	0.7 s
④→③	1.0 s	1.5 s
④→⑤	0.6 s	0.7 s
⑤→④	1.0 s	1.0 s – 1.2 s
Adaptive Control		
①→②→③→④	0.7 s – 0.9 s	0.7 s – 0.9 s
③→④	0.7 s	0.7 s
④→③	1.1 s	1.0 s
④→⑤	0.7 s	0.7 s
⑤→④	1.1 s	0.9 s

Thus, the prediction quality of the simulation setup regarding shift duration is inadequate for traditionally controlled gearshifts. During adaptive control, the simulation results are more reliable.

- The adaptive control architecture achieves a smoother form of the resulting engine speed signal with less oscillations than the traditional control setup, in both simulation and vehicle experiment.

- During adaptive control, shift duration is equal to or even shorter than with traditional control.
- The adaptive controller achieves comparable or lower values for the error signals $e_{1,2}(\cdot)$ over the course of the shift procedures.
- The subjective assessment of shift quality during adaptive control in vehicle experiments is comparable to the traditional controller.

In conclusion, the shift quality regarding smoothness of the engine speed, evolution of tracking error and shift duration is comparable or better with the adaptive controller than with the traditional control setup.

5.1.3 Comparison of Shift Duration

In order to test the adaptive control architecture and evaluate its dynamic capabilities, more gearshifts are conducted with a focus on shift duration. This is carried out by setting the duration of the reference trajectory t_{dur} during adaptive control.

Comparison of Upshift Duration

First, a series of upshifts during vehicle pull away with a constant accelerator pedal value of 50 % is conducted.

As shown in Fig. 5.2, the traditional controller achieves shift durations from 1 s to 1.4 s. The corresponding vehicle experiment data shows slightly different shift speeds, ranging from 0.9 s to 1.5 s, as shown in Fig. 5.3. The adaptively controlled shifts conducted in simulation, as given in Fig. 5.9, result in a shift duration from 0.7 s to 0.9 s. These shift speeds are confirmed by vehicle experiment, as depicted in Fig. 5.9. Thus, the adaptive controller already achieves faster shifts than the traditional control setup. Now, the desired shift duration is reduced to $t_{\text{dur},1} = 0.7$ s in order to test controller performance.

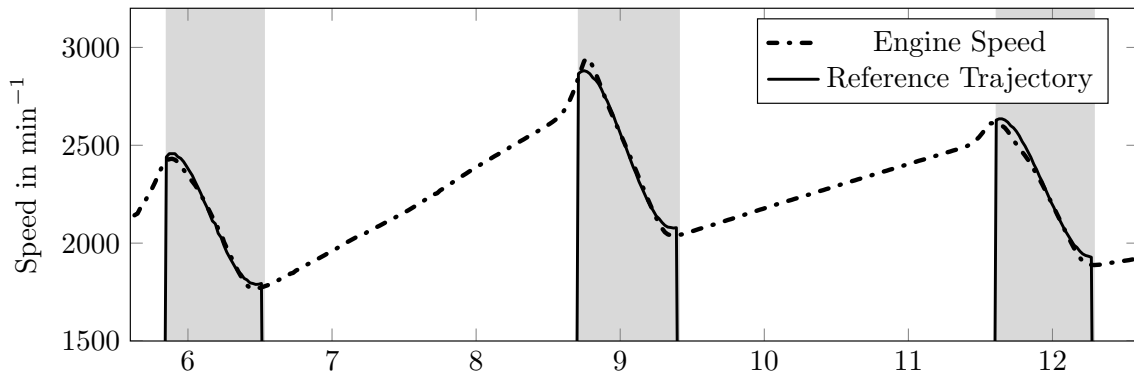


Figure 5.14: FDCT: SiL simulation of ①→②→③→④ maneuver, adaptive control with $t_{dur,1} = 0.7$ s

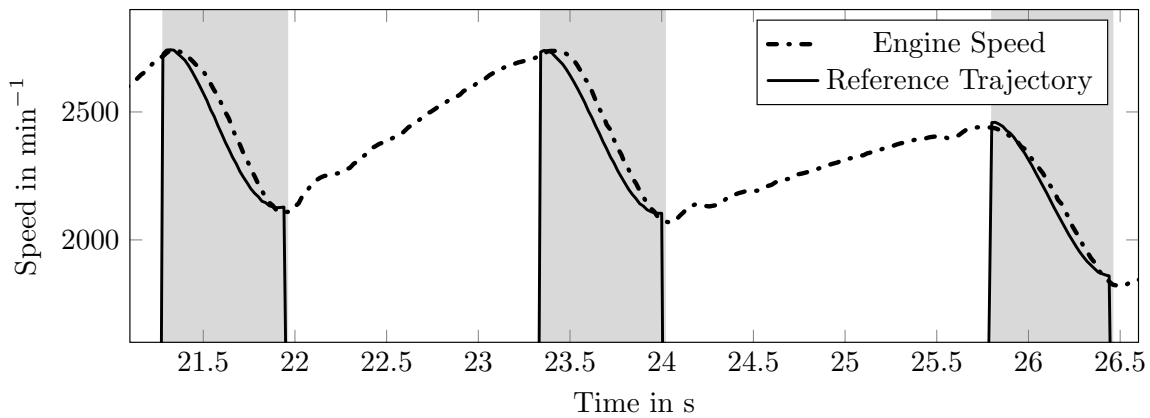


Figure 5.15: FDCT: Vehicle experiment of ①→②→③→④ maneuver, adaptive control with $t_{dur,1} = 0.7$ s

With the adaptive controller, shift durations equal 0.7 s during simulation, as depicted in Fig. 5.14. This is confirmed by the vehicle experiment in Fig. 5.15. Thus, the desired shift duration is lowered further. The shift duration is set to $t_{dur} = 0.5$ s and the simulation and vehicle experiment is conducted anew using adaptive control. During simulation, as shown in Fig. 5.16, the shifts are carried out in the specified time without oscillations. The vehicle experiment in Fig. 5.17 shows the shifts being conducted in the same time span of 0.5 s. However, some oscillations are present in the engine speed signal and the tracking error is quite large. This suggests that the adaptive controller reaches the limits of its capabilities at $t_{dur} = 0.5$ s. Thus, the shift duration is not reduced further.

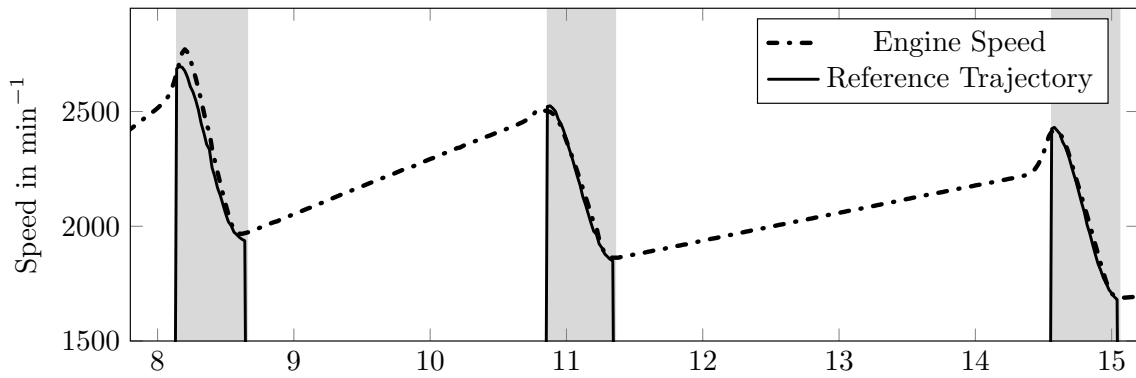


Figure 5.16: FDCT: SiL simulation of ①→②→③→④ maneuver, adaptive control with $t_{dur,1} = 0.5$ s

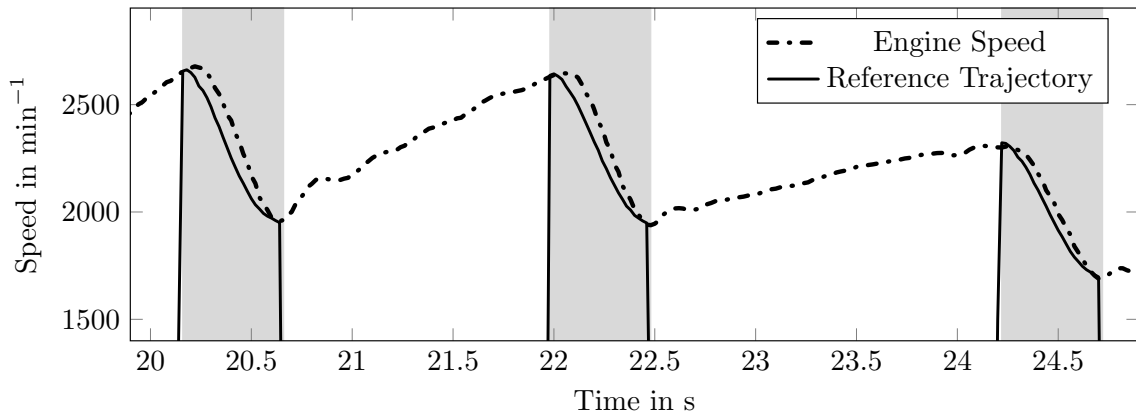


Figure 5.17: FDCT: Vehicle experiment of ①→②→③→④ maneuver, adaptive control with $t_{dur,1} = 0.5$ s

Comparison of Downshift Duration

The control performance evaluation is continued with a series of downshift procedures from 7th to 4th gear during vehicle acceleration with a constant accelerator pedal value of 50%. First, for comparison purposes, the downshifts are conducted using traditional control. In

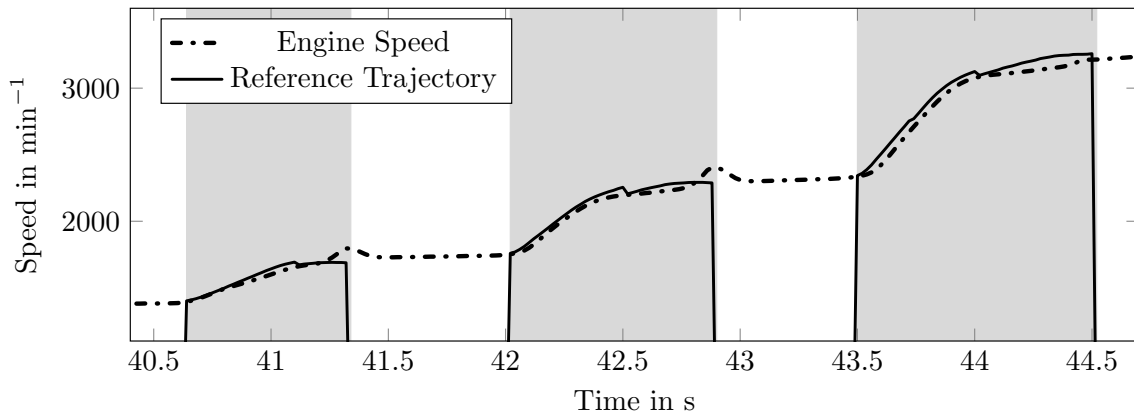


Figure 5.18: FDCT: SiL simulation of ⑦→⑥→⑤→④ maneuver, traditional control

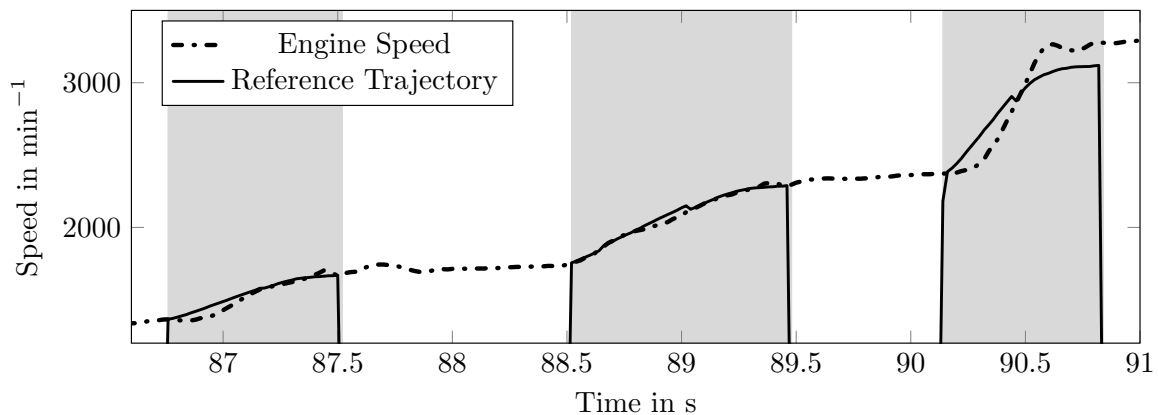


Figure 5.19: FDCT: Vehicle experiment of ⑦→⑥→⑤→④ maneuver, traditional control

simulation, as shown in Fig. 5.18, the shift duration achieved by the traditional controller ranges from 0.7 s to 1 s. These time spans are confirmed by the vehicle experiment, shown in Fig. 5.19.

Now the adaptive controller is used for the powered downshifts. First, the shift duration is set to $t_{\text{dur},2} = 1$ s. In simulation, the shifts are conducted successfully in that time frame (see Fig. 5.20). The results are validated by the vehicle experiment, depicted in Fig. 5.21, where the same duration is achieved.

For the next set of downshifts, the desired shift duration is reduced to $t_{\text{dur},2} = 0.7$ s. In simulation, the shifts are barely completed in time of $t_{\text{dur},2} = 0.7$ s, ranging from 0.75 s

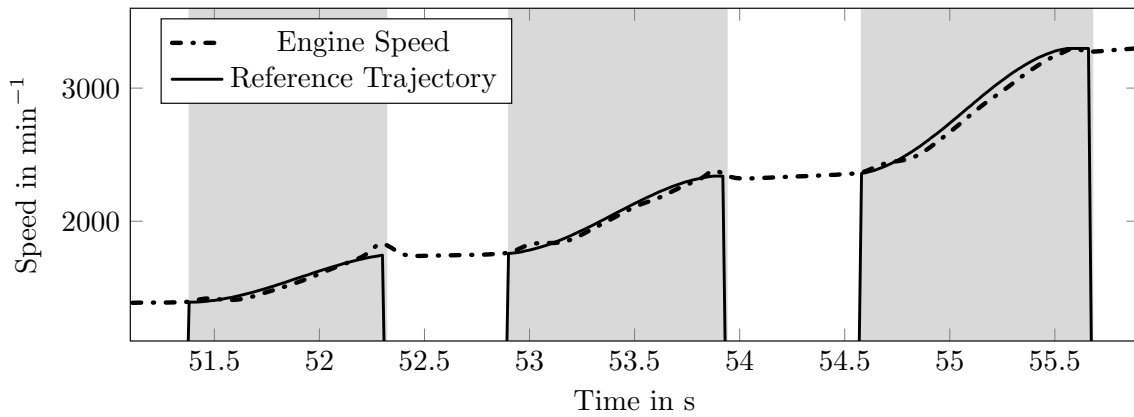


Figure 5.20: FDCT: SiL simulation of ⑦→⑥→⑤→④ maneuver, adaptive control with $t_{\text{dur},2} = 1$ s

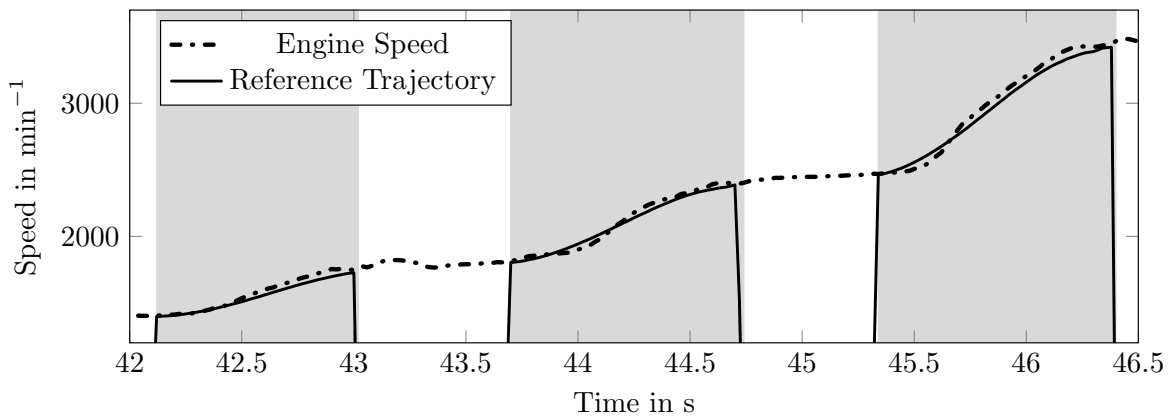


Figure 5.21: FDCT: Vehicle experiment of ⑦→⑥→⑤→④ maneuver, adaptive control with $t_{\text{dur},2} = 1$ s

to 0.9 s (see Fig. 5.22). In vehicle experiments, shown in Fig. 5.23, shifts are carried out faster, with shift duration ranging from 0.75 s to 0.8 s and thus almost achieving the desired setting of $t_{\text{dur},2}$. This behavior suggests that the controller has reached its limits. Downshifts cannot be conducted faster using the adaptive controller.

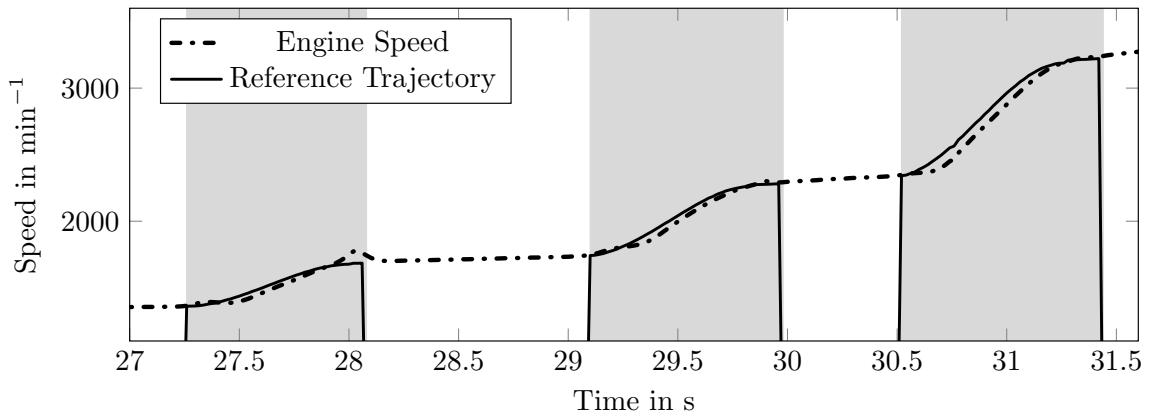


Figure 5.22: FDCT: SiL simulation of ⑦→⑥→⑤→④ maneuver, adaptive control with $t_{dur,2} = 0.7$ s

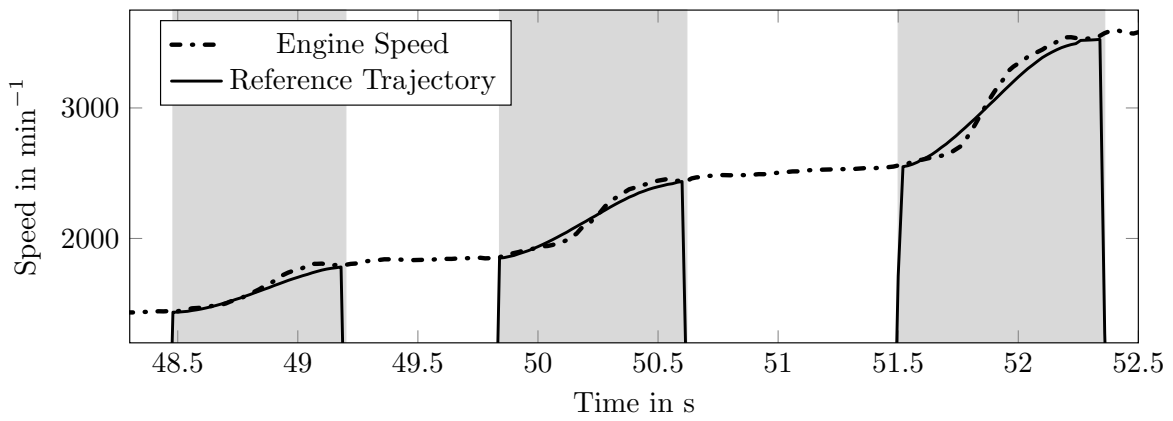


Figure 5.23: FDCT: Vehicle experiment of ⑦→⑥→⑤→④ maneuver, adaptive control with $t_{dur,2} = 0.7$ s

Discussion

The investigation of shift time performance shows that the adaptive controller is able to conduct up- and downshifts in the same time as the traditional control algorithm, or faster. This was shown using both simulation and vehicle experiments.

Table 5.2: Comparison of up- and downshift duration for FDCT transmission

Traditional Control	Simulation	Vehicle
①→②→③→④	1.0 s – 1.4 s	0.9 s – 1.5 s
⑦→⑥→⑤→④	0.7 s – 1.0 s	0.7 s – 1.0 s
Adaptive Control		
①→②→③→④	0.50 s	0.50 s
⑦→⑥→⑤→④	0.75 s	0.75 s

Again, the simulation provides more reliable results when the adaptive controller is in operation (see Table 5.2). Shift duration varies during traditional control operation, whereas shifting times during adaptive control are predicted reliably.

Faster upshifts are achieved with the adaptive controller, where a duration of 0.5 s can be reproduced, compared to at least 0.9 s with the traditional controller in the cases considered here. Therefore, the adaptive controller achieves better performance. During downshifts, the adaptive controller generates a shift duration of 0.75 s, which is a little slower than the fastest traditionally controlled downshift procedures. Thus, controller performance is comparable between traditional and adaptive control in the evaluated cases.

5.2 NAG3 Automatic Transmission

To demonstrate the adaptive capabilities of controller (4.9) – (4.15), it is implemented into a completely different powertrain system with unknown parameters. For this purpose, a Mercedes-Benz E-Class vehicle with a 185 kW Diesel engine mounted to the NAG3 transmission is used and the controller is tested in both simulations and vehicle experiments. The same driving maneuvers as before with the FDCT transmission are conducted. However, they are changed to some extent to account for the different powertrain dynamics. Since the engine is much more powerful, the accelerator pedal values are reduced:

- Vehicle pull away from standstill with an accelerator pedal value of $p_a = 40\%$:
①→②→③→④

- Powered up- and downshifts during vehicle acceleration with $p_a = 30\%$ between 3rd and 4th gear: ④→③→④→③→④
- Powered up- and downshifts during vehicle acceleration with $p_a = 30\%$ between 4th and 5th gear: ⑤→④→⑤→④→⑤
- Powered downshifts from 8th to 4th gear with $p_a = 40\%$:
⑧→⑦→⑥→⑤→④

Note that for the dynamics of the adaption law, the same parameters from the FDCT controller are used (see Table 4.2), except for the first initial value k_0 , which is reduced to 0.1. With the NAG3 transmission, the system output signal $y(\cdot)$ is the angular velocity of the output shaft of the torque converter. However, since the lock-up clutch is engaged during the shifts considered here and for simplification purposes, the engine speed signal is kept as designation of the system output signal.

5.2.1 Traditional Control

In order to generate a basis for shift performance evaluation, a series of traditionally controlled shifts is conducted in both simulation and vehicle experiment. The simulation

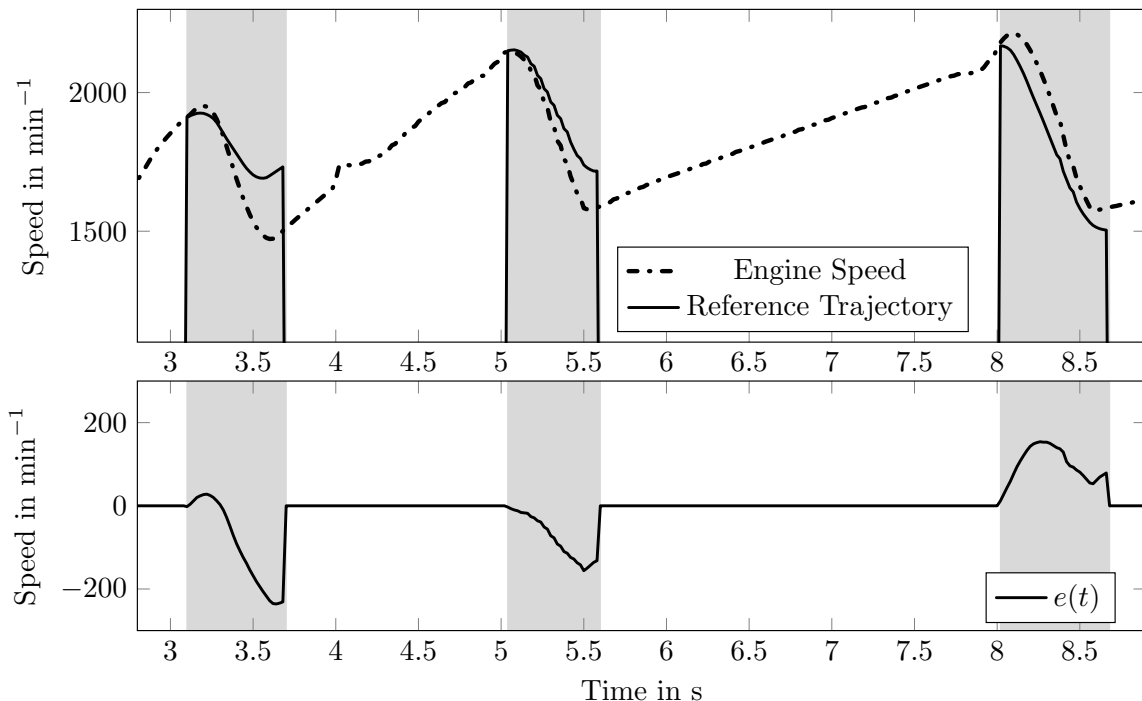


Figure 5.24: NAG3: SiL simulation of ①→②→③→④ maneuver, traditional control

results depicted in Fig. 5.24 show three consecutive traditionally controlled upshifts during

vehicle pull away, from 1st over 2nd and 3rd to 4th gear, with an accelerator pedal value of $p_a = 40\%$. Shifts are carried out without oscillations and in a time period of 0.5 s to 0.7 s. However, control performance is rather poor, considering there are large values of the error signal $e(\cdot)$ that are not reduced towards the end of the shifts. Only during the third upshift procedure, the engine speed signal roughly follows the setpoint trajectory and the tracking error is somewhat reduced. The maneuver is repeated in vehicle experiment, as

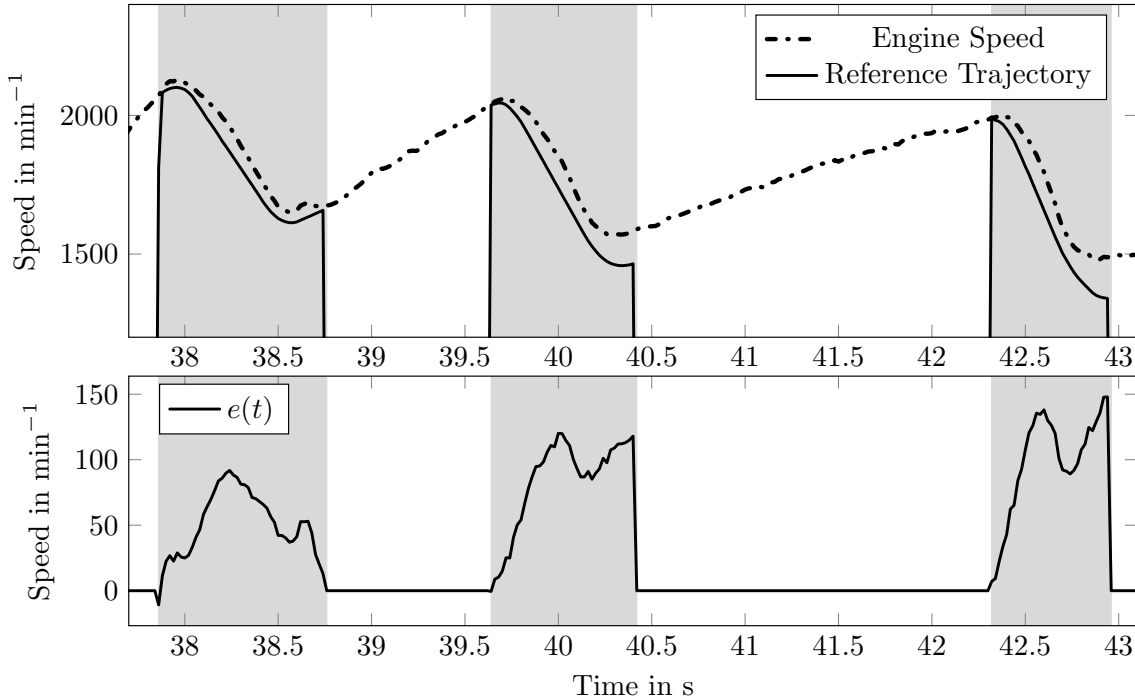


Figure 5.25: NAG3: Vehicle experiment of ①→②→③→④ maneuver, traditional control

depicted in Fig. 5.25. Compared to the simulation results in Fig. 5.24, some oscillations towards the end of the first upshifts are observed. Also, the error signal $e(\cdot)$ is positive at all times, whereas it also assumes negative values during simulation, and again reaches considerable values. Shift duration ranges from 0.6 s to 0.9 s, which is up to 0.2 s slower than in simulation. A series of up- and downshifts is conducted between 3rd and 4th gear in simulation, as depicted in Fig. 5.26. Shifts are carried out with a smooth engine speed signal with durations of ca. 0.3 s for downshifts and ca. 0.7 s during upshifts. However, there are large values of the error signals $e_{1,2}(\cdot)$, since the set point trajectory is practically not followed during downshifts and only roughly followed during upshifts.

In vehicle experiment, the up- and downshifts are also conducted smoothly (see Fig. 5.27). However, compared to the simulation results depicted in Fig. 5.26, there are much larger error signal values $e_2(\cdot)$ during downshifts, whereas the error signal $e_1(\cdot)$ during upshifts is smaller. Thus, better tracking of the reference trajectory is achieved during upshift

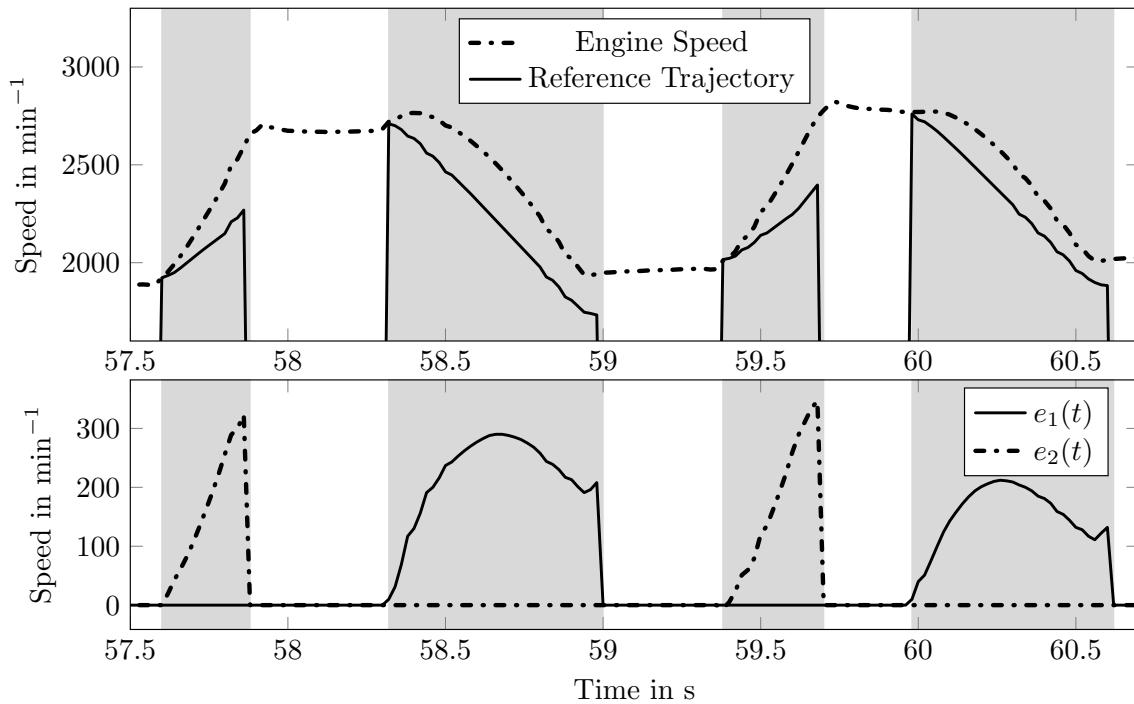


Figure 5.26: NAG3: SiL simulation of ④→③→④→③→④ maneuver, traditional control

procedures. Downshifts take ca. 0.3s to be conducted, whereas upshift duration is ca. 0.5s and therefore ca. 0.2s faster than in simulation. During simulation of up- and downshifts between 4th and 5th gear (see Fig. 5.28), the same observations as before during shifts between 3rd and 4th gear are made. Shifts are carried out smoothly with large error signal values, especially while shifting down. Again, shift duration is ca. 0.3s for down- and ca. 0.7s for upshifts. The vehicle experiment results are shown in Fig. 5.29. Compared to simulation, the error signals are larger during downshifts and relatively small during upshifts with good tracking of the reference signal. Also, shift duration is ca. 0.3s while shifting down and ca. 0.5s for upshifts, which makes upshifts ca. 0.2s faster compared to simulation.

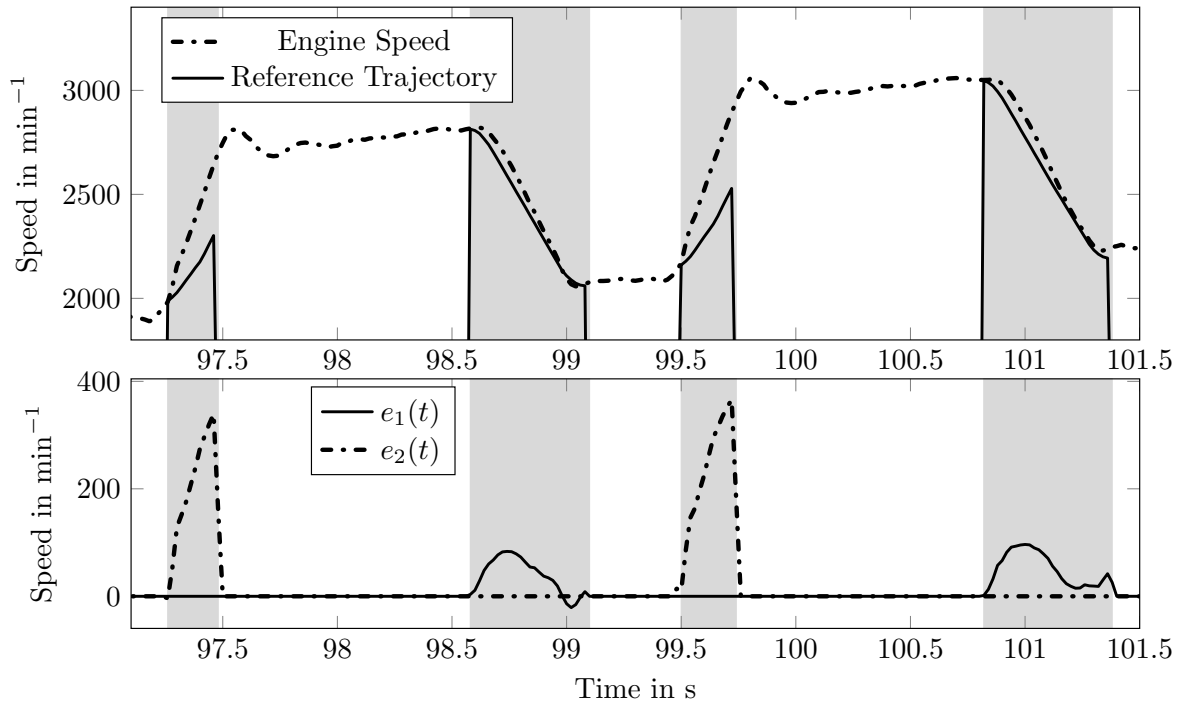


Figure 5.27: NAG3: Vehicle experiment of ④→③→④→③→④ maneuver, traditional control

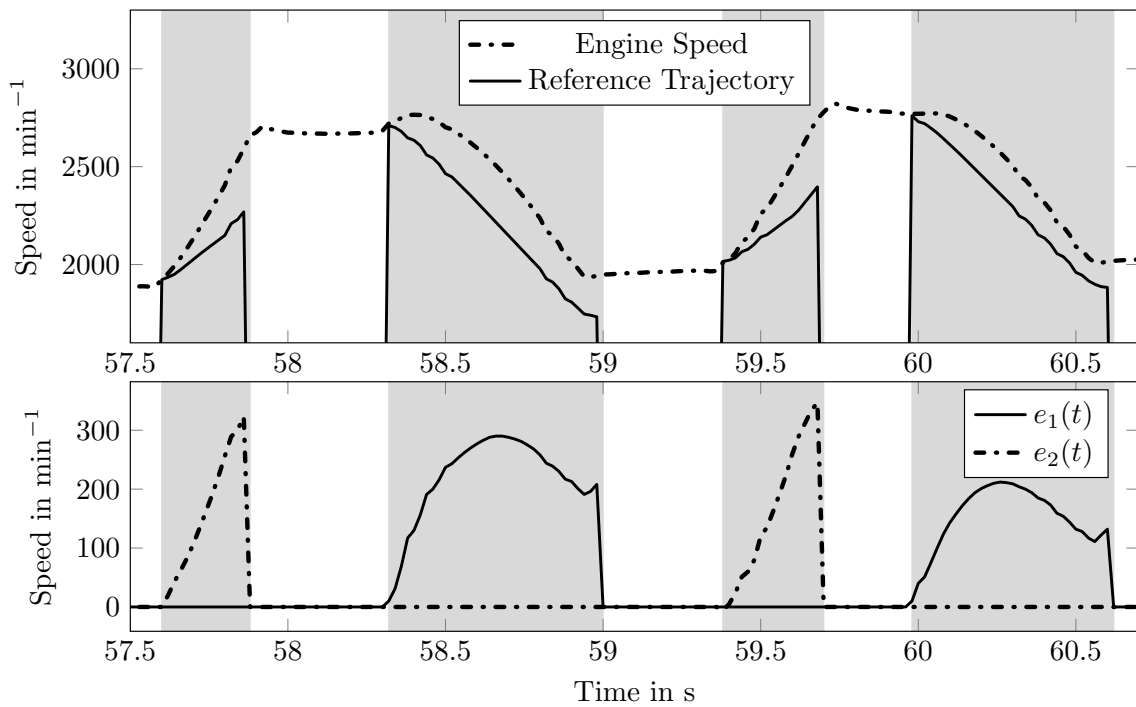


Figure 5.28: NAG3: SiL simulation of ⑤→④→⑤→④→⑤ maneuver, traditional control

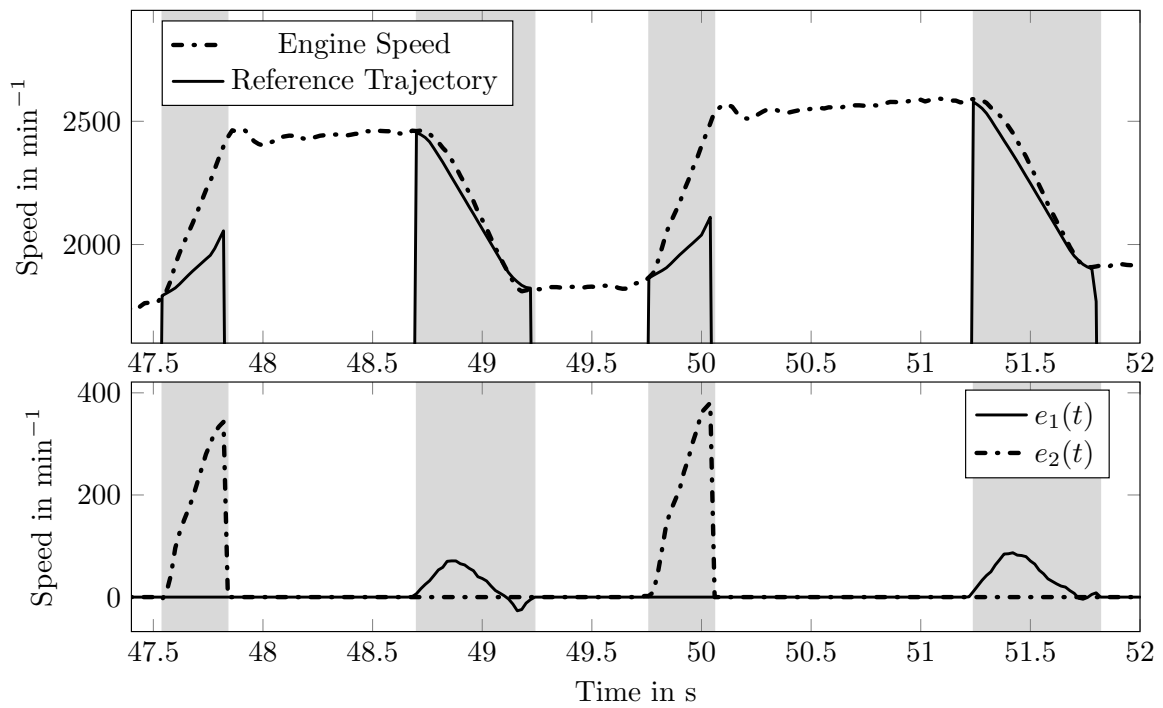


Figure 5.29: NAG3: Vehicle experiment of ⑤→④→⑤→④→⑤ maneuver, traditional control

5.2.2 Adaptive Control

The driving maneuvers are now conducted with the adaptive controller (4.9) – (4.15) in operation during shift procedures. Shift durations are set to $t_{\text{dur},1} = 0.7\text{ s}$ for upshifts and $t_{\text{dur},2} = 0.4\text{ s}$ for downshifts. The simulation results of adaptively controlled upshifts

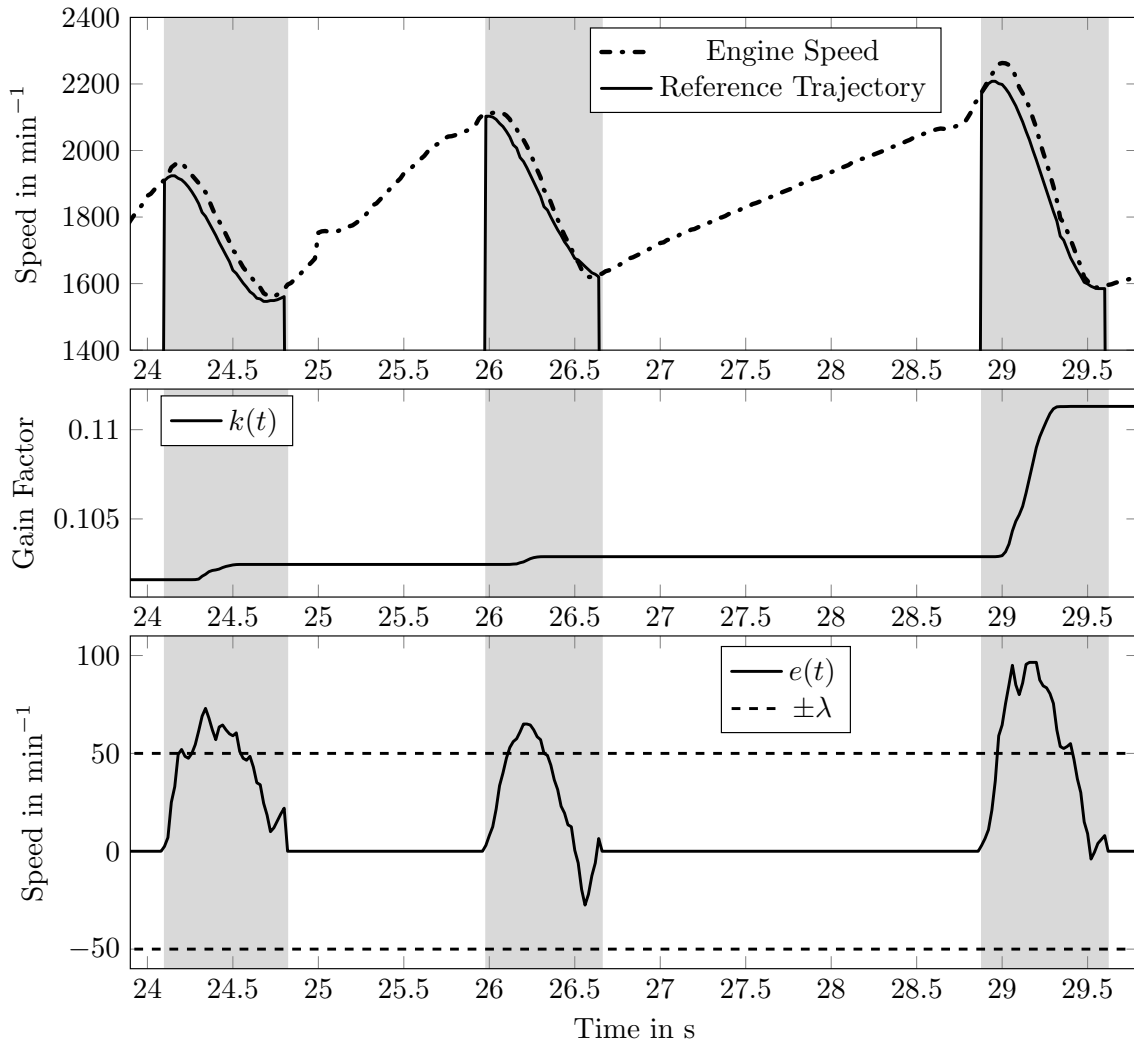


Figure 5.30: NAG3: SiL simulation of ①→②→③→④ maneuver, adaptive control

during vehicle pull away show a smooth form of the engine speed signal, as depicted in Fig. 5.30. The error signal $e(\cdot)$ is reduced to $e(t) < \lambda$ at the end of each shift procedure, which demonstrates good control performance. The adaptive behavior of the controller is clearly visible in the increase of the common gain factor $k(\cdot)$, whenever the λ -neighborhood is left. Shift duration is ca. 0.7s for each shift. The maneuver is carried out in vehicle experiment, as depicted in Fig. 5.31. Shifts are performed mostly with a smooth engine speed signal, except for some small oscillations. The control goal is achieved with the

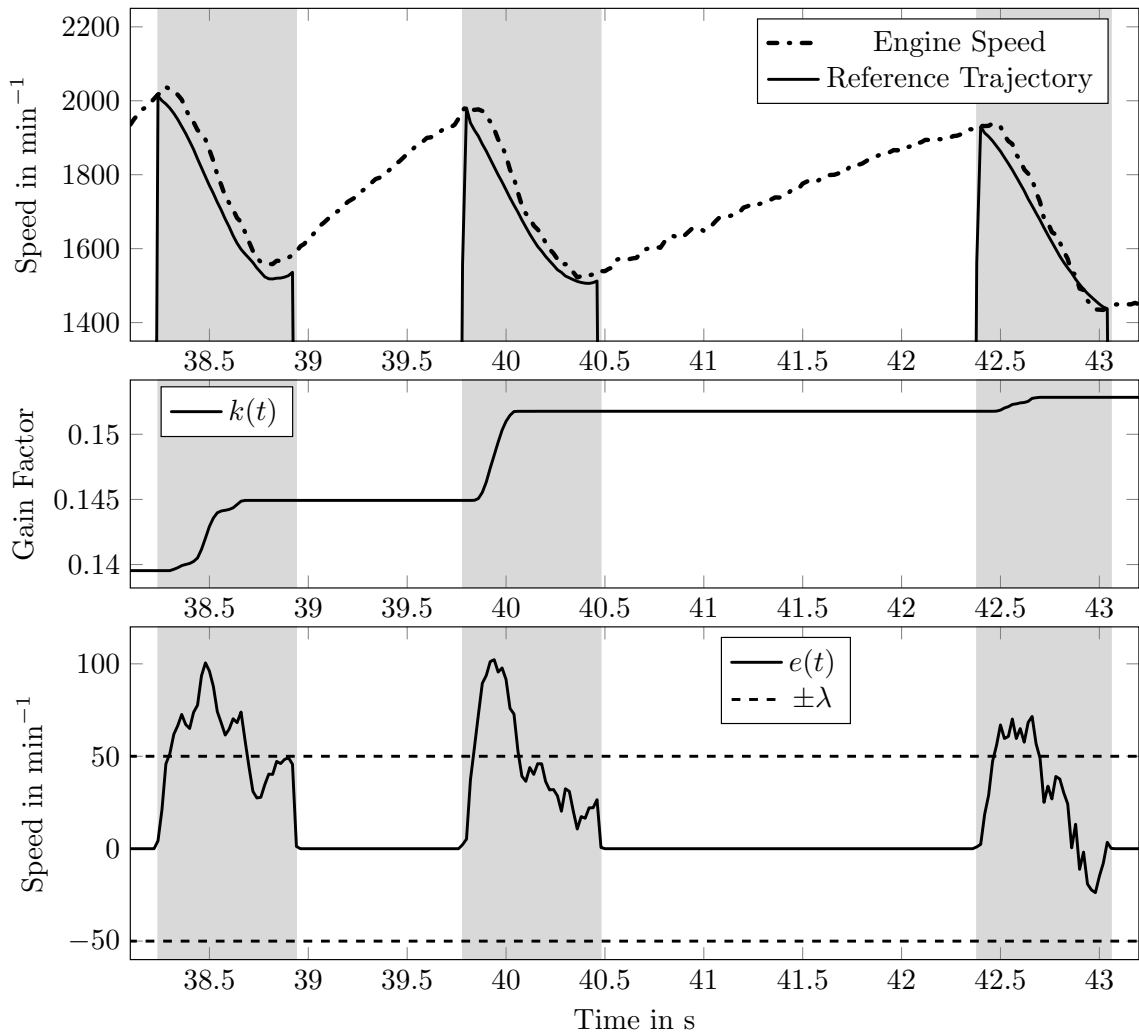


Figure 5.31: NAG3: Vehicle experiment of ①→②→③→④ maneuver, adaptive control

error signal $e(\cdot)$ being smaller than λ at the end of each shift, which take ca. 0.7s to complete. Thus, shift duration and control performance is comparable to the simulation results. The up- and downshifts conducted between 3rd and 4th gear during adaptive control also show a smooth engine speed signal in simulation (see Fig. 5.32). The error signals $e_{1,2}(\cdot)$ are always reduced below λ at the end of the shifts, and thus the control goal is achieved. Downshifts take ca. 0.3s, whereas upshifts last ca. 0.5s. The vehicle experiment results of adaptively controlled up- and downshifts between 3rd and 4th gear are shown in Fig. 5.33. The shifts are conducted smoothly for the most part. Apart from some oscillations after downshifts, control performance is comparable to the simulation results in Fig. 5.32. Note that during downshifts, the error signal is mostly inside the λ -neighborhood, which denotes better control performance than during simulation. Shift duration in the vehicle is ca. 0.4s during downshifts compared to 0.3s in simulation, and

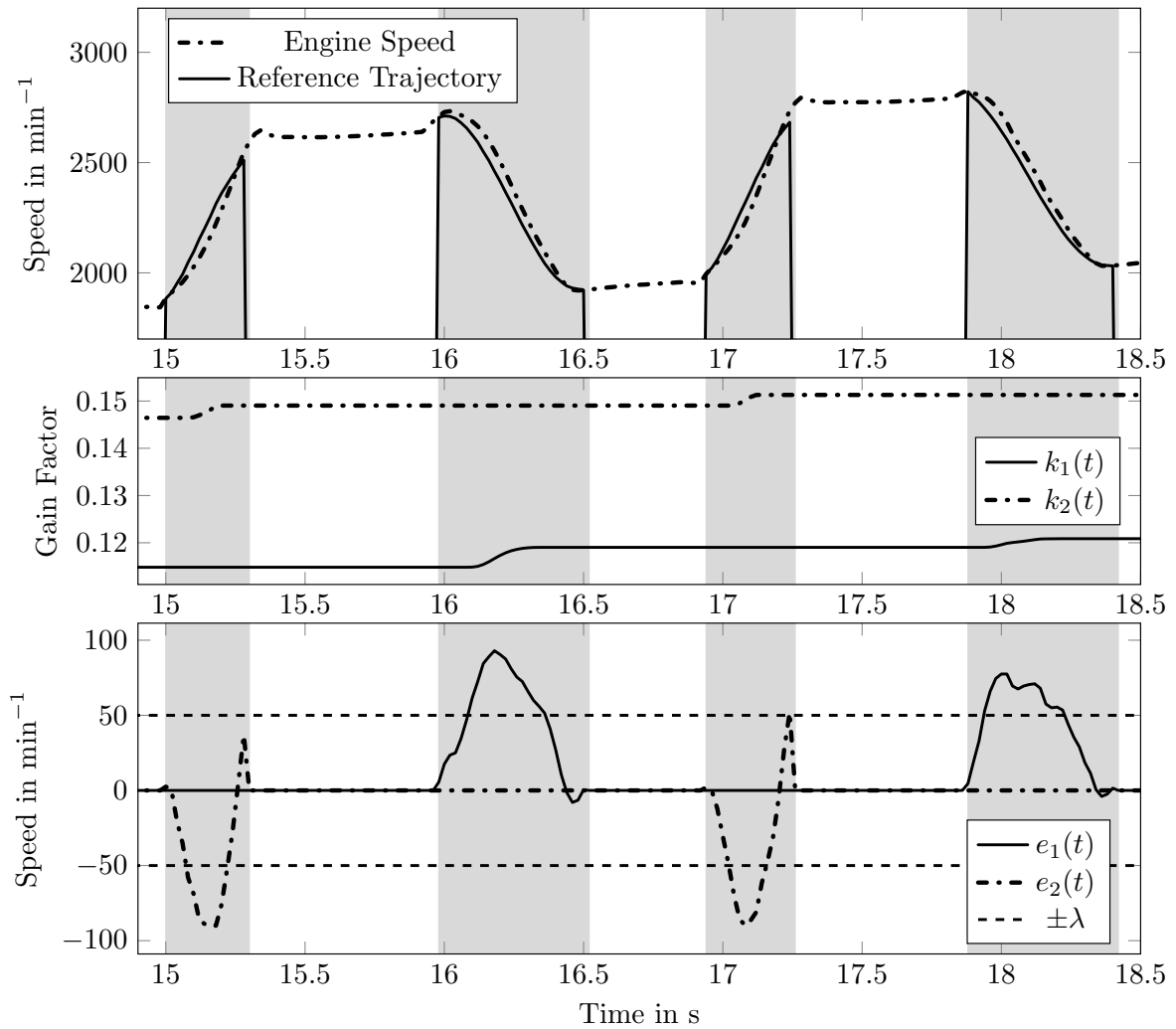


Figure 5.32: NAG3: SiL simulation of ④→③→④→③→④ maneuver, adaptive control

ca. 0.5s during upshifts in both vehicle experiment and simulation. The simulation results of adaptively controlled shifts between 4th and 5th gear, as depicted in Fig. 5.34, also show smooth system behavior while achieving the control goal of $e(t) < \lambda$ at the end of each shift procedure. In this case, shift duration is ca. 0.4s for down- and ca. 0.5s for upshifts.

In Fig. 5.35, the vehicle experiment data is shown. Again, shifts are performed smoothly except for some oscillations after downshift procedures. This is comparable to the simulation results. Note that during downshifts, the error signal is inside the λ -neighborhood all the time. However, no decrease of the gain factor $k_2(\cdot)$ is initiated, since the waiting time $t_d = 0.5$ s is never reached during one shift procedure. Downshifts take ca. 0.4s to complete, whereas upshifts are conducted within 0.5s, the same as during simulation.

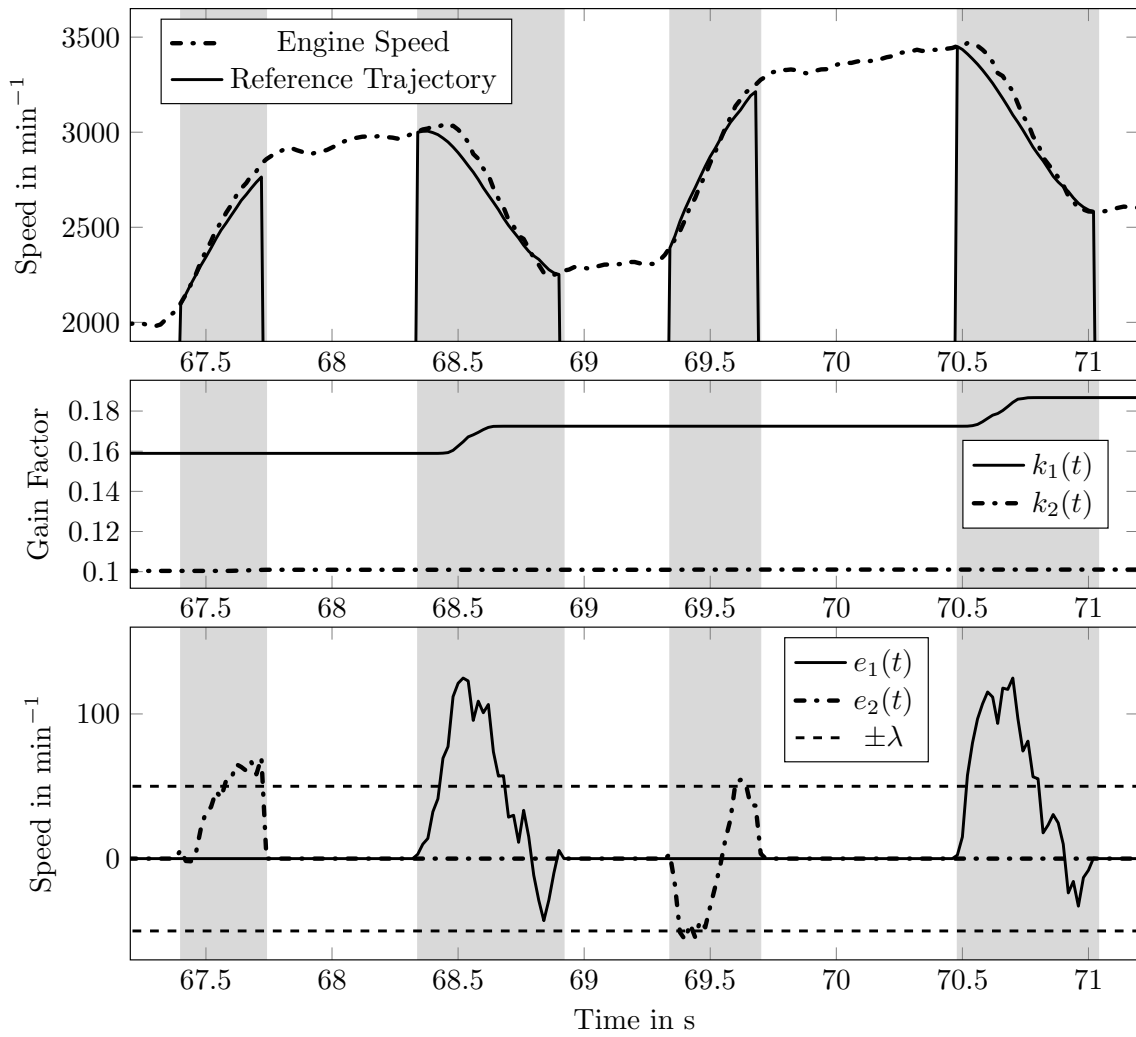


Figure 5.33: NAG3: Vehicle experiment of ④→③→④→③→④ maneuver, adaptive control

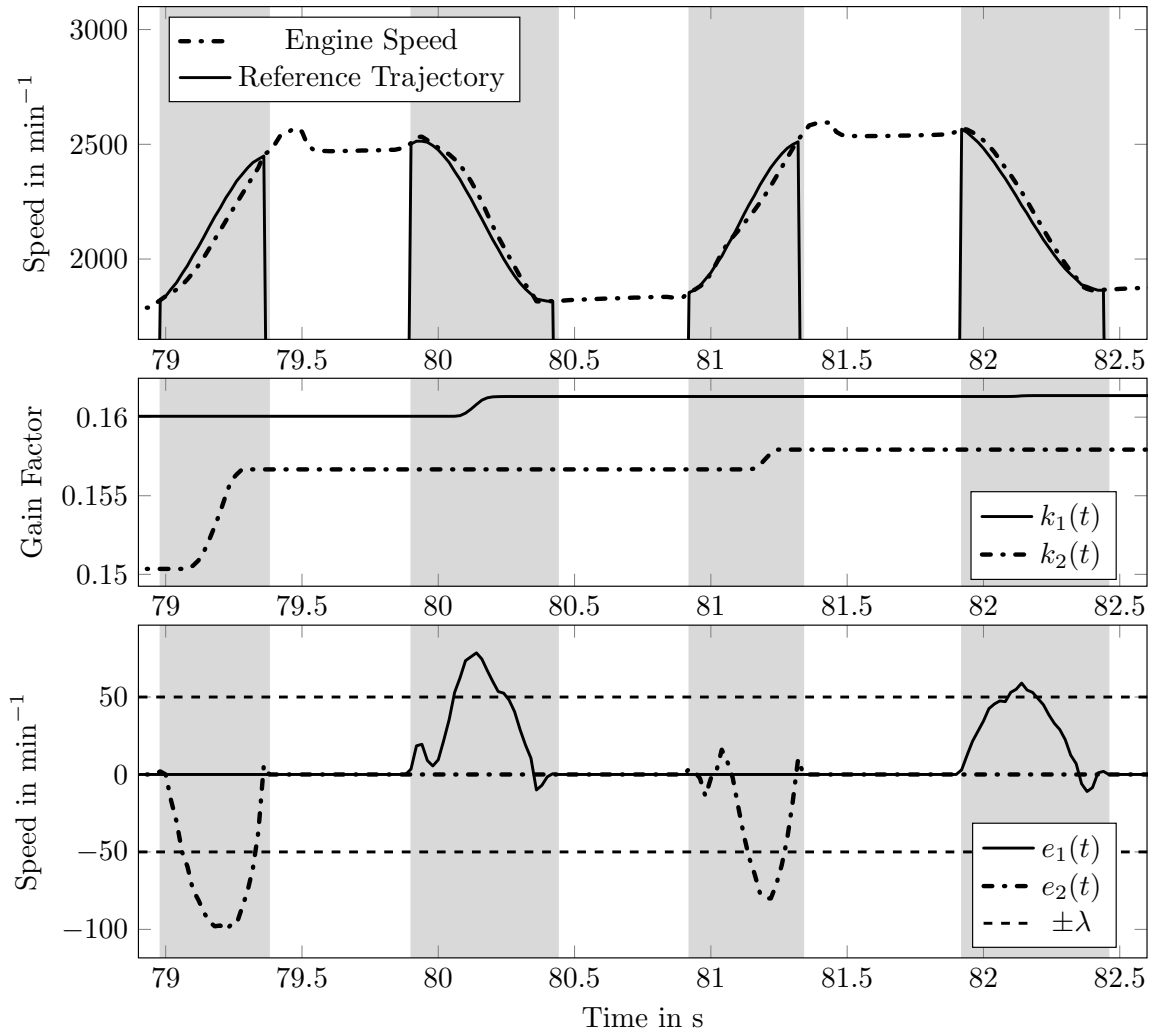


Figure 5.34: NAG3: SiL simulation of ⑤→④→⑤→④→⑤ maneuver, adaptive control

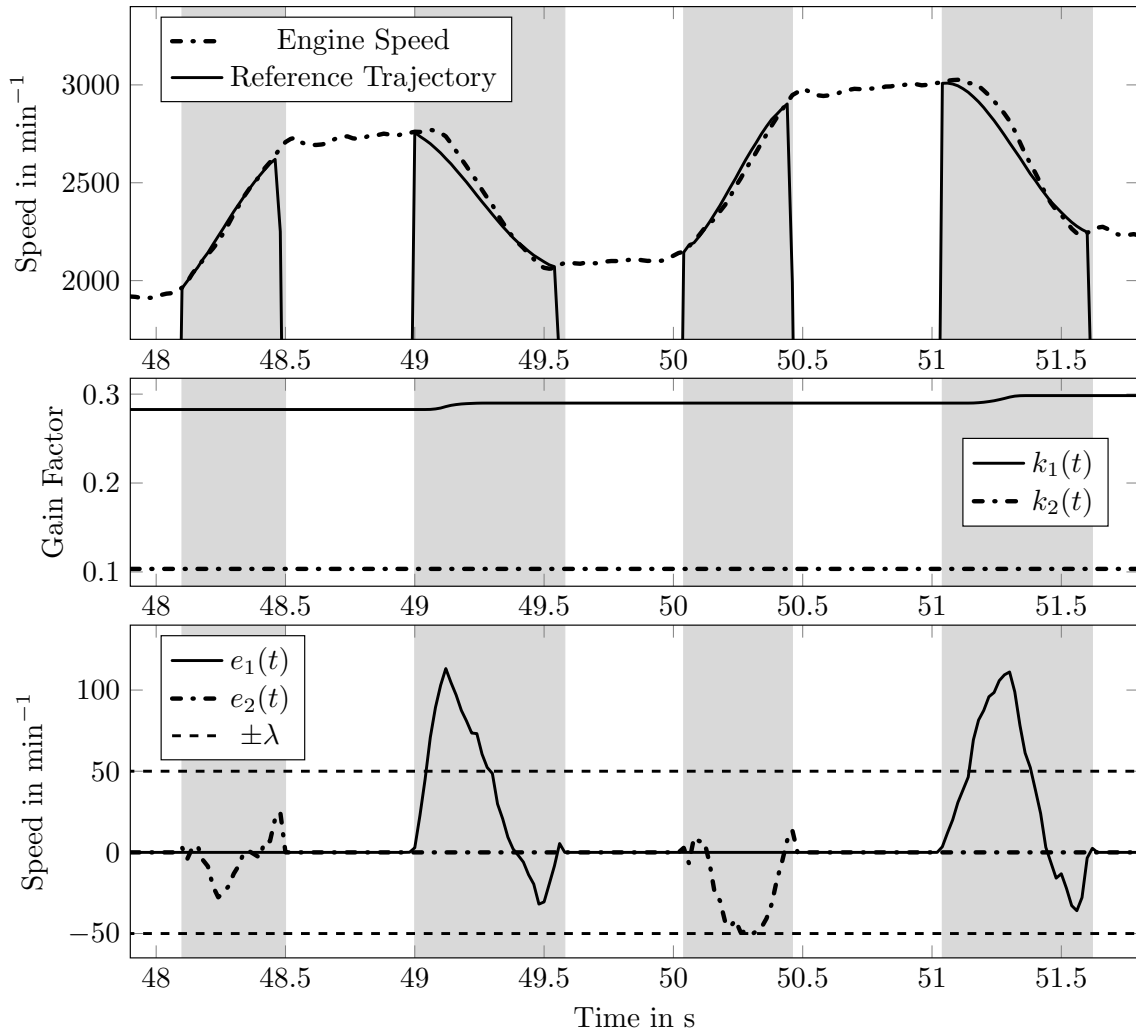


Figure 5.35: NAG3: Vehicle experiment of ⑤→④→⑤→④→⑤ maneuver, adaptive control

Discussion

During simulation and vehicle testing of three distinct driving maneuvers with the NAG3 transmission, the following findings were made:

- The quality of the simulation setup is adequate. During operation of the traditional clutch controller, the predictions made by the simulation are less reliable than with the adaptive controller, in terms of both shift speed and progression of the engine speed signal (see Table 5.3). The shift duration is the same in simulation and vehicle experiments, as far as adaptive control is considered. During traditional control, shift duration differs between simulation and vehicle experiment.
- A smooth form of the engine speed signal is achieved, except for minor oscillations caused by the adaptive controller, in both simulation and vehicle experiment.
- The adaptive controller achieves the same shift speed as the traditional controller, except for downshifts from 5th to 4th gear, where shifts are 0.1 s slower.

Table 5.3: Comparison of shift duration for NAG3 transmission

Traditional Control	Simulation	Vehicle
①→②→③→④	0.5 s – 0.7 s	0.6 s – 0.9 s
③→④	0.7 s	0.5 s
④→③	0.3 s	0.3 s
④→⑤	0.7 s	0.5 s
⑤→④	0.3 s	0.3 s
Adaptive Control		
①→②→③→④	0.7 s	0.7 s
③→④	0.5 s	0.5 s
④→③	0.3 s	0.3 s
④→⑤	0.5 s	0.5 s
⑤→④	0.4 s	0.4 s

- Tracking of the reference trajectory is far better with the adaptive controller. The resulting error signals are much smaller and are also reduced below λ at the end of the shift procedures.
- The waiting time of $t_d = 0.5$ s is never reached during the shifts considered here, since their duration is much shorter than in the FDCT transmission. It is advisable to reduce t_d accordingly to allow for a decrease of $k(\cdot)$.

In summary, the shift quality achieved by the traditional controller is matched by the adaptive control algorithm, except for some small oscillations in the engine speed signal. Tracking of the reference trajectory is improved and shift speed is the same in most cases.

5.2.3 Comparison of Shift Duration

Now, the traditional and adaptive clutch controllers in the NAG3 transmission are evaluated regarding shift speed performance.

Upshift Duration

First, upshifts are considered during vehicle pull away from standstill with an accelerator pedal value of $p_a = 40\%$.

The data for traditional clutch control is already depicted in Figs. 5.24 and 5.25. Upshift duration is therefore 0.5 s – 0.7 s in simulation and 0.6 s – 0.9 s in the vehicle.

For the adaptively controlled upshifts, shift durations of 0.7 s are achieved in both simulation and vehicle experiment, as depicted in Figs. 5.30 and 5.31. In these cases, the desired duration of the reference trajectory has also been set to $t_{dur,1} = 0.7$ s. In order to test if shorter shifts are possible, the desired shift time is reduced to $t_{dur,1} = 0.5$ s.

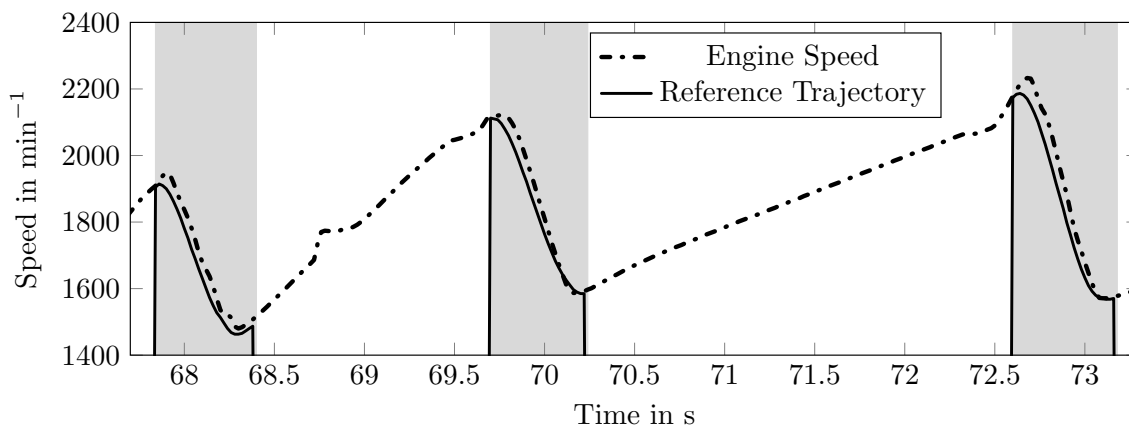


Figure 5.36: NAG3: SiL simulation of ①→②→③→④ maneuver, adaptive control, $t_{dur,1} = 0.5$ s

As shown in simulation (see Fig. 5.36) and in data obtained by vehicle experiment (see Fig. 5.37), upshifts are conducted successfully within a time span of 0.5 s. The form of the engine speed signal in the vehicle differs from the one in simulation in exhibiting minor oscillations.

The desired shift time is further reduced to $t_{dur,1} = 0.3$ s. Figures 5.38 and 5.39 show the

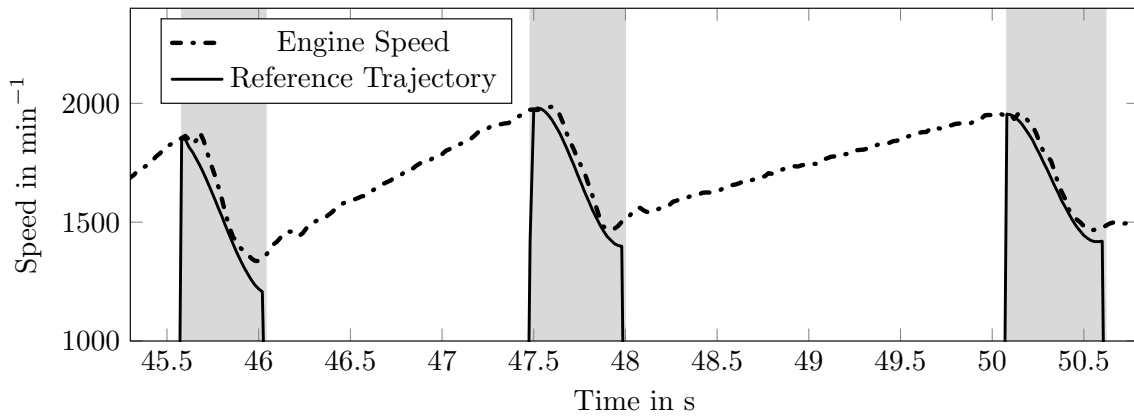


Figure 5.37: NAG3: Vehicle experiment of ①→②→③→④ maneuver, adaptive control, $t_{\text{dur},1} = 0.5$ s

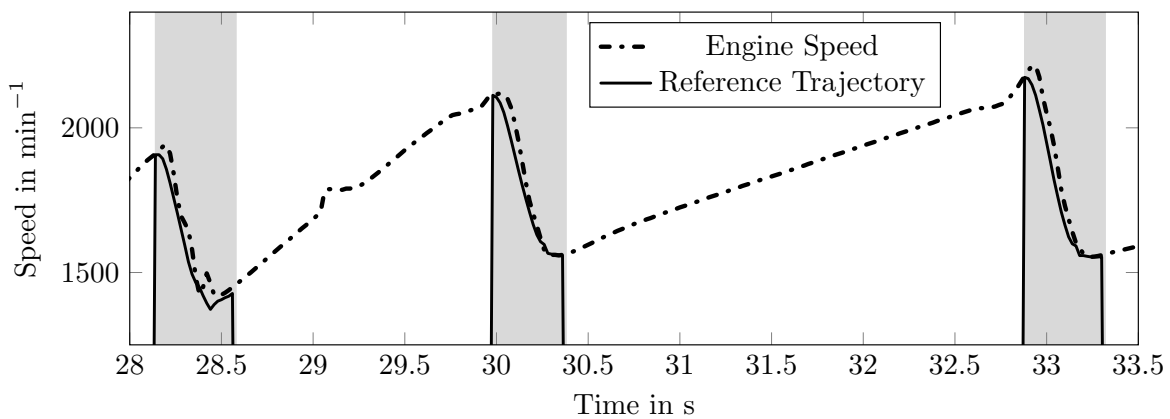


Figure 5.38: NAG3: SiL simulation of ①→②→③→④ maneuver, adaptive control, $t_{\text{dur},1} = 0.3$ s

resulting upshift procedures in simulation and vehicle experiment, respectively. Shifts are conducted successfully. However, oscillations occur during both simulation and vehicle experiment. Also, shift duration ranges from 0.3 s to 0.4 s. Therefore, the desired shift speed is not achieved in all cases. This suggests that the controller and the clutch system have reached their maximum performance here.

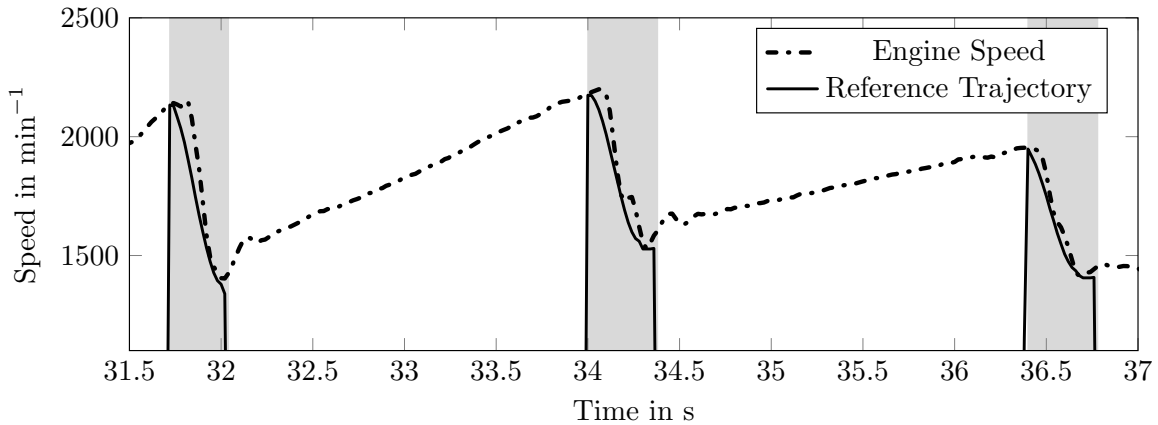


Figure 5.39: NAG3: Vehicle experiment of ①→②→③→④ maneuver, adaptive control, $t_{dur,1} = 0.3$ s

Downshift Duration

In order to investigate downshift performance, the vehicle is brought to a speed of $80 \text{ km} \cdot \text{h}^{-1}$ and put into 8th gear. Then, four consecutive downshifts are conducted with an accelerator pedal value of $p_a = 40\%$.

For comparison, the maneuver is carried out under traditional control operation. As

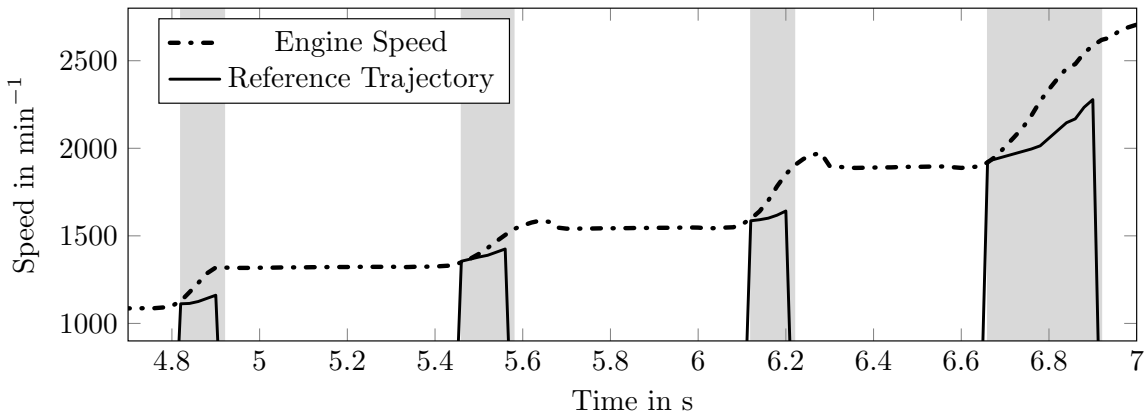


Figure 5.40: NAG3: SiL simulation of ⑧→⑦→⑥→⑤→④ maneuver, traditional control

depicted in Fig. 5.40, upshift duration under traditional control ranges from 0.1 s to 0.3 s during simulation. This is confirmed by the vehicle experiment (see Fig. 5.41). Note that during simulation, tracking of the reference signal is very poor, whereas the vehicle experiment data exhibits good tracking behavior of the traditional controller.

Now, the maneuver is carried out with the adaptive controller in operation. The desired shift duration is set to $t_{dur,2} = 0.3$ s in an attempt to reduce overall downshift duration and match the traditional control performance. As shown in the simulation results in

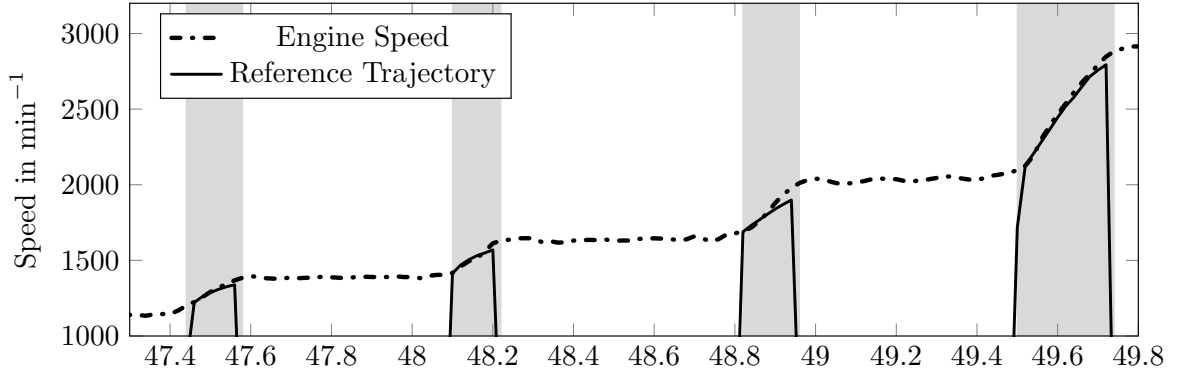


Figure 5.41: NAG3: Vehicle experiment of ⑧→⑦→⑥→⑤→④ maneuver, traditional control

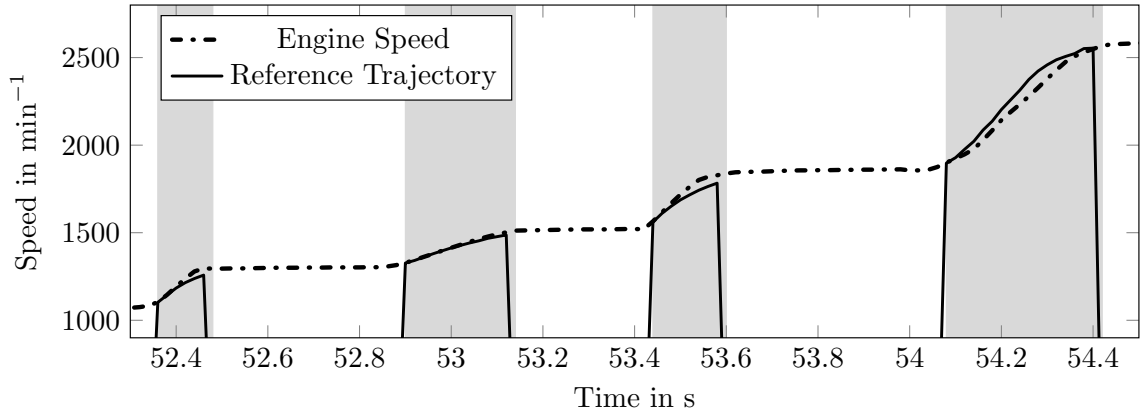


Figure 5.42: NAG3: SiL simulation of ⑧→⑦→⑥→⑤→④ maneuver, adaptive control, $t_{dur,2} = 0.3$ s

Fig. 5.42, the adaptively controlled downshifts are performed smoothly in the desired time frame, or even faster. Shift duration ranges from 0.1 s to 0.3 s. When considering the vehicle data shown in Fig. 5.43, shifts are conducted within 0.15 s to 0.4 s, which is a little slower than in simulation. The desired shift duration is further reduced to $t_{dur,2} = 0.2$ s in an attempt to match traditionally controlled shift speed. The results of the simulation are shown in Fig. 5.44, where smooth control operation is achieved with $t_{dur,2} = 0.2$ s. Again, shift duration ranges from 0.1 s to 0.3 s, which is no improvement compared to the previous setting of $t_{dur,2} = 0.3$ s. As shown in the vehicle experiment data in Fig. 5.45, downshifts are conducted in 0.15 s to 0.35 s. Thus, it is not possible to reduce shift duration below these values by setting a shorter desired shift duration $t_{dur,2}$. The adaptive controller's maximum performance is reached here. No improvement is achieved compared to the traditional controller.

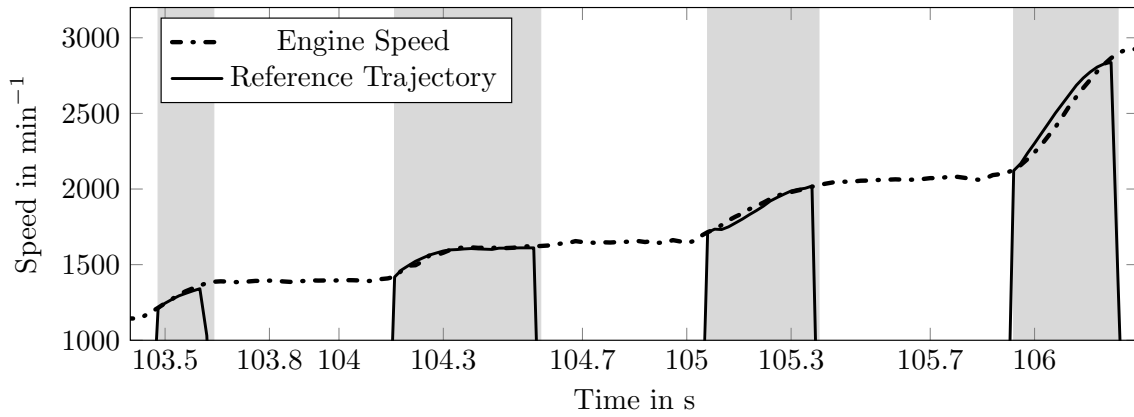


Figure 5.43: NAG3: Vehicle experiment of ⑧→⑦→⑥→⑤→④ maneuver, adaptive control, $t_{dur,2} = 0.3$ s

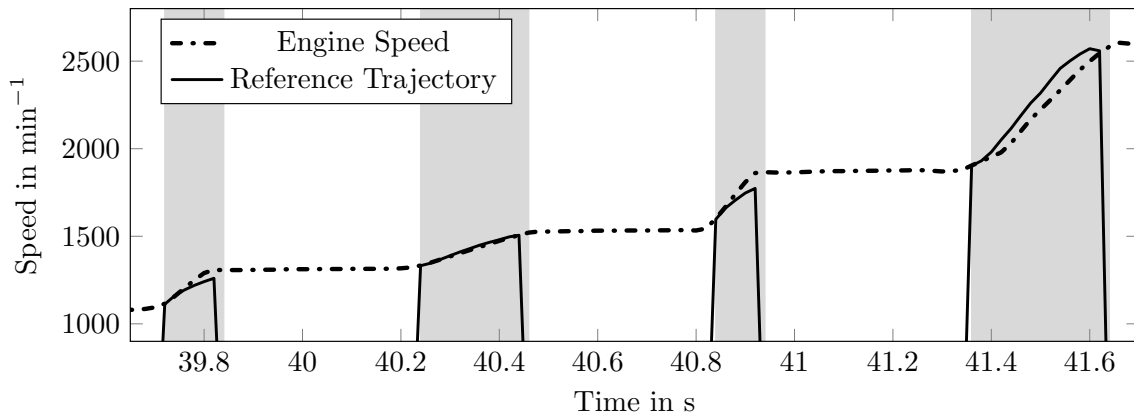


Figure 5.44: NAG3: SiL simulation of ⑧→⑦→⑥→⑤→④ maneuver, adaptive control, $t_{dur,2} = 0.2$ s

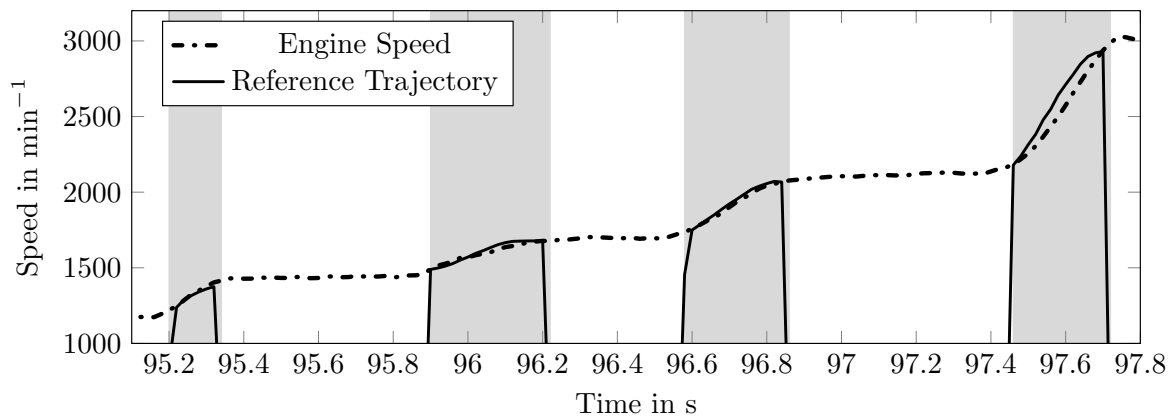


Figure 5.45: NAG3: Vehicle experiment of ⑧→⑦→⑥→⑤→④ maneuver, adaptive control, $t_{dur,2} = 0.2$ s

Discussion

The investigation of shift speed in the NAG3 transmission revealed that the adaptive controller is able to conduct most shifts as fast as the traditional controller, whereas upshifts are completed even faster. However, downshift procedures are completed ca. 0.05 s slower during adaptive control.

Table 5.4: Comparison of up- and downshift duration for NAG3 transmission

Traditional Control	Simulation	Vehicle
①→②→③→④	0.5 s – 0.7 s	0.6 s – 0.9 s
⑧→⑦→⑥→⑤→④	0.1 s – 0.3 s	0.1 s – 0.3 s
Adaptive Control		
①→②→③→④	0.3 s – 0.4 s	0.3 s – 0.4 s
⑧→⑦→⑥→⑤→④	0.15 s – 0.35 s	0.15 s – 0.35 s

The simulation is more reliable while the adaptive controller is in operation (see Table 5.4), where the results are confirmed by the vehicle experiment. In conclusion, the adaptive controller matches the traditional control performance with the NAG3 transmission concerning shift speed.

5.3 Exemplary Shifts during Coasting

So far, only powered shifts with an accelerator pedal value of $p_a > 0$ have been considered. Both constrained and release shifts are conducted with this setting. However, unpowered shifts with a negative engine torque can be performed by the adaptive controller as well. To demonstrate controller operation during some exemplary unpowered shifts, the vehicle is accelerated to $60 \text{ km} \cdot \text{h}^{-1}$ and put into 5th gear. The accelerator pedal is released and two consecutive downshifts are conducted. This maneuver may be initiated to facilitate engine braking, for example during downhill coasting.

The following figures show the results of simulation and vehicle experiments during traditional and adaptive control of the unpowered downshift maneuver with the FDCT transmission. As shown in Figs. 5.46 and 5.47, the traditionally controlled downshifts are conducted in a time frame of ca. 0.8 s in simulation and ca. 1.5 s in the actual vehicle. The control error is considerably larger during the vehicle experiment, and some oscillations are present in the engine speed signal as well. The control performance is compared to the adaptive controller in the following plots.

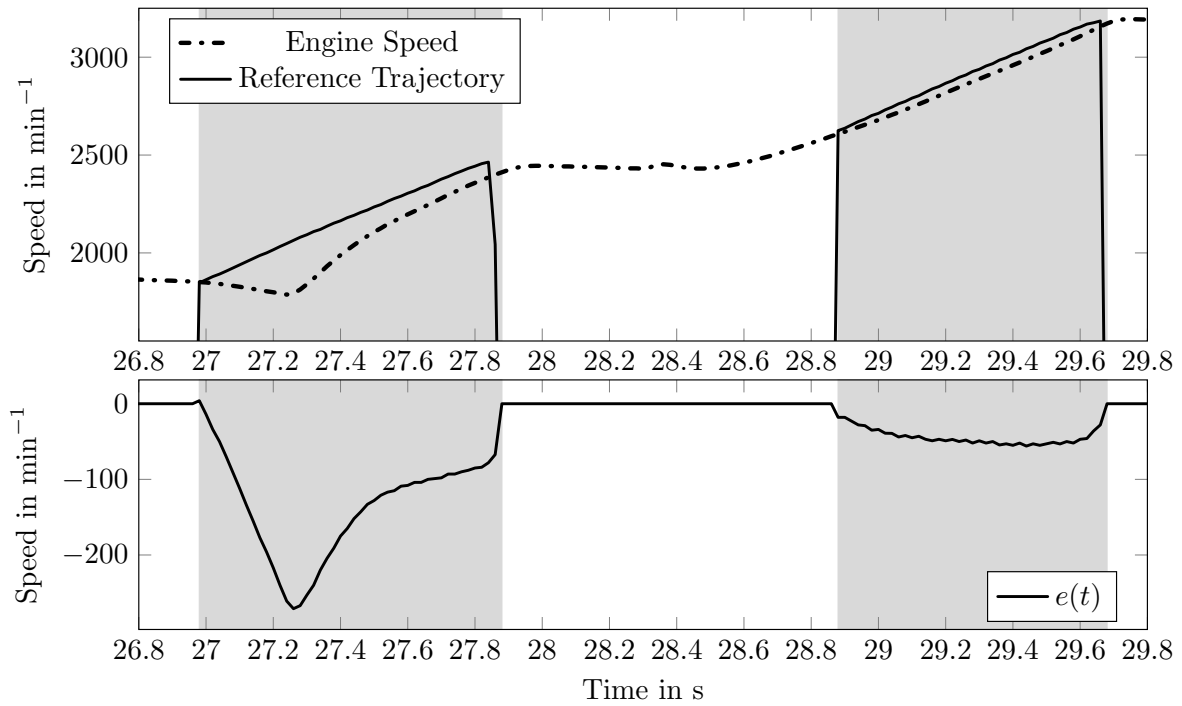


Figure 5.46: FDCT: SiL simulation of ⑤→④→③ maneuver, traditional control

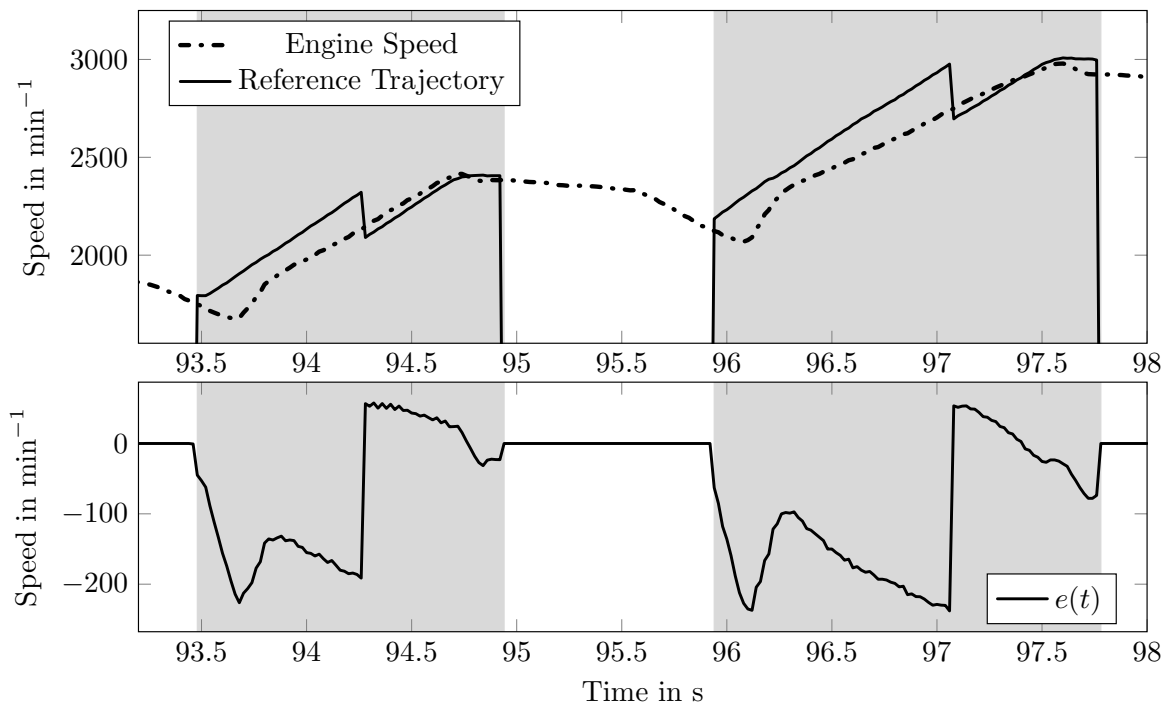


Figure 5.47: FDCT: Vehicle experiment of ⑤→④→③ maneuver, traditional control

The adaptive controller performs well in simulation (see Fig. 5.48) and in the vehicle experiment (see Fig. 5.49). However, some oscillations are present in the engine speed signal

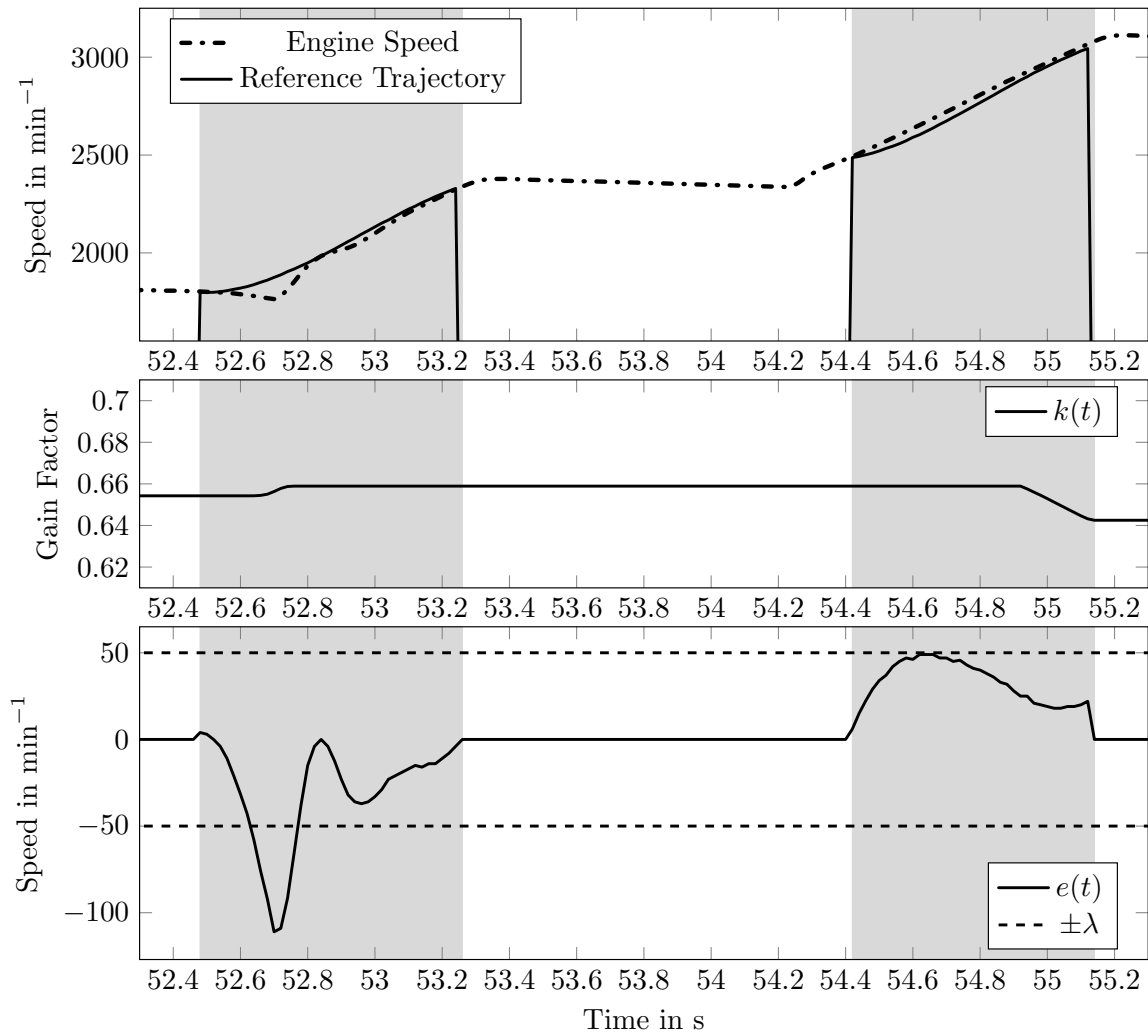


Figure 5.48: FDCT: SiL simulation of ⑤→④→③ maneuver, adaptive control

in the vehicle. The λ -neighborhood is left during the first downshift in simulation, but is obeyed almost all the time during vehicle experiment. Shift duration of the adaptively controlled unpowered downshifts is ca. 0.7s in simulation and ca. 0.8s in the vehicle, which is faster than with the traditional controller in operation.

This concludes the exemplary investigation of unpowered shifts. The general functionality of the adaptive controller with an accelerator pedal of $p_a = 0\%$ has been shown. Further analyses of unpowered shifts are not carried out, since the two types of constrained and release shifts have been investigated in previous sections.

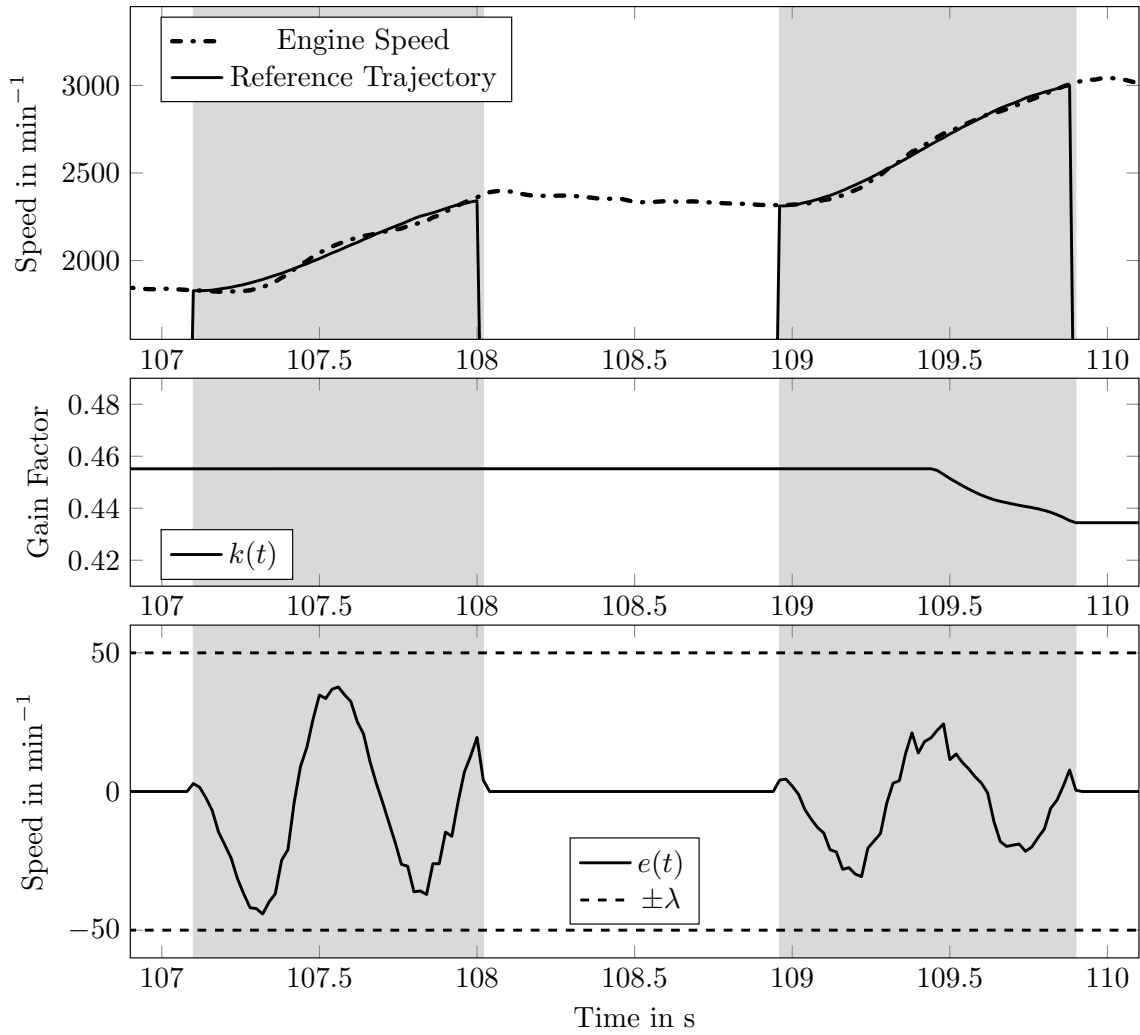


Figure 5.49: FDCT: Vehicle experiment of ⑤→④→③ maneuver, adaptive control

6 Discussion and Conclusions

This chapter concludes the thesis. The work is summarized, the results are discussed and conclusions regarding the feasibility of the control architecture are drawn. The control performance evaluation is followed by the considerations regarding the reduction of calibration efforts. An overview over future areas for research and improvement of adaptive λ -tracking control in clutch control systems for automatic transmissions is given.

6.1 Summary

This work was motivated by the increasing complexity in transmission control systems, driven by increased functionality and contribution of automatic transmissions to reduce fuel consumption in passenger cars. This development leads to a higher number of calibration parameters, which in turn results in increased calibration efforts. Various methods for coping with this issue have been indicated. Among them are the automation of the calibration process or the reduction of calibration efforts by means of simulation. In this thesis, a different approach has been taken: The goal was to reduce the need for calibration by reducing the number of calibration parameters. To achieve this, an adaptive feedback control architecture with λ -tracking that requires very few parameters has been implemented that is able to conduct its own calibration. Adaptive λ -tracking controllers are able to control systems with unknown and also with changing sets of parameters and can be designed without knowledge of system parameters. An adaption law is implemented that computes the feedback gains of an underlying PID-feedback controller by using information from the system output. Thus, the controller is able to adapt its parameters to the current system dynamics and the need for calibration is circumvented.

After introductory remarks and motivation of this work (see Chapter 1), an introduction into high-gain feedback control was given and the underlying principles have been outlined in Chapter 2. The stability criteria were discussed and the controller requirements have been derived. Following the theoretical analysis, a nonlinear system model of the electro-hydraulically actuated friction clutch in the automatic transmissions under consideration has been derived (see Chapter 3). It was used to investigate the high-gain

feedback stability of the system at hand. The investigation showed that the system is high-gain stabilizable and an adaptive λ -tracking controller can be applied to control the relative speed of friction clutches and is therefore able to control certain phases during a gearshift procedure. The speed control phase has been chosen for implementation of the adaptive controller, during which it controls the form of the engine speed signal that follows from the progression of the relative speed at the respective friction clutch.

The λ -tracking controller was implemented into the actual transmission control software running on a standard series production control unit and has been tested in a SiL simulation environment (see Chapter 4). Models of the respective vehicle, powertrain, transmission and control unit are incorporated into the simulation. Thus, the controller was designed and analyzed regarding its parameters and the resulting control performance. Gearshift procedures have been conducted and the control performance has been compared to the traditional control software in Chapter 5. The experiments have been carried out in vehicles on a test track using current series production powertrain hardware. The control performance predicted by simulation was confirmed by the vehicle experiments. The implementation of the adaptive controller in two distinct powertrains with entirely different transmissions mounted to different combustion engines shows the adaptive capability of the approach to successfully control systems with unknown parameters without the need for powerful prototyping control hardware. Instead, series production control hardware has been used.

6.2 Results

The goal of this thesis was to apply adaptive λ -tracking control during powered gearshifts in an attempt to reduce calibration parameters under the following conditions:

- stability of the resulting closed-loop control architecture has to be ensured,
- the control performance has to at least match the traditional control software,
- the control architecture has to be applicable to series production control hardware, and
- the number of calibration parameters has to be reduced.

6.2.1 Stability

In Chapter 3, an extensive stability analysis was conducted, based on a nonlinear mathematical model of the friction clutch system. It was shown that the system is high-gain stabilizable if a λ -tracking controller with a PD-feedback structure is implemented. Thus, the stability for the system class of electro-hydraulically actuated friction clutches has been established. This includes both the FDCT and NAG3 transmissions.

6.2.2 Control Performance

The adaptive controller devised in Chapter 4 has to at least match the control performance of the traditional controller, so that no disadvantages are introduced by the new control architecture. The control performance was evaluated by comparing shift speed and absence of oscillations in the engine speed signal while tracking the reference trajectory.

Oscillations

One of the control goals was to smoothly track the reference trajectory. Any oscillations or discontinuities present in the progression of the engine speed signal are unfavorable, as they cause poor shift quality by generating jerks in the powertrain and at the same time are perceived audibly by the passengers.

In case of the FDCT transmission, the adaptive controller achieved an overall smoother form of the engine speed signal with near to no oscillations. Hence, control performance was equal to, and in some cases even better than with the traditional controller.

For the NAG3 transmission, some oscillations are introduced in some of the investigated shift procedures. Generally, the adaptive controller achieved smooth control performance. To conclude, the adaptive controller is able to achieve a smooth control performance and thus contributes to shift quality.

Shift Speed

As discussed in Chapter 5, the adaptive controller is able to perform gearshifts mostly as fast as the traditional controller, for both the FDCT and the NAG3 transmission. In some cases, even faster shifts can be conducted. The downshift procedures in the NAG3 transmission take ca. 0.05 s longer than with the traditional controller. However, no assessment concerning shift comfort can be made. This was expressively excluded from this work, as discussed in Chapter 3. Thus, faster shifts, as achieved with adaptive control, may cause uncomfortable jerks in the powertrain, and this may be the reason why

traditionally controlled shifts tend to take longer. Nonetheless, this does not diminish the capabilities demonstrated by the adaptive controller. Hence, the goal of this thesis to match or even improve on the control performance of the clutch controller has been achieved.

6.2.3 Applicability to Series Production Hardware

One constraint for this work was to devise a control architecture that is able to be implemented into the existing setup of series production control units. This has been achieved by implementing the controller into the existing transmission control software. Moreover, the computational performance of the traditional TCU is sufficient to run the λ -tracking control algorithms. Additionally, only the speed sensors that are already present are used to create the control feedback loop.

In conclusion, no extensions or alterations of the control hardware have been made and the adaptive controller can be applied to the series production control units.

6.2.4 Reduction of Calibration Efforts

Another goal was to reduce calibration efforts by implementing adaptive λ -tracking controllers to reduce control software complexity while maintaining functionality. Thus, the reduction of calibration parameters is assessed.

First, consider the control software governing the gearshift procedures in the FDCT transmission. For traditional control, there is a total of 617 calibration parameters that are needed during the speed control phase of a gearshift. After implementing the adaptive λ -tracking controller, a total of 146 parameters becomes obsolete. However, the λ -tracking controller introduces 8 new parameters, so 138 parameters are saved in total. This constitutes a reduction of 22.4%.

When considering the NAG3 transmission, 646 calibration parameters are involved in the speed control phase of the gearshifts. The adaptive controller makes 250 parameters redundant while again introducing 8 new parameters on its own. Thus, a total of 242 parameters is saved, which is 37.5% of the original number.

Table 6.1: Number of calibration parameters

Transmission	Traditional control parameters	Adaptive control parameters	Reduction
FDCT	617	479	22.4%
NAG3	646	404	37.5%

The calibration parameters that are saved by replacing traditional control algorithms with adaptive λ -tracking control, are of the following types:

- control gains for open-loop controllers or gain matrices for gain scheduling controllers,
- time parameters to compute control value gradients,
- control values and control value matrices that are accessed by open-loop controllers,
- coefficients to influence control values depending on system state variables such as engine speed, torque, temperature and vehicle load and
- limit values of system state variables to trigger different behavior of open-loop controllers.

The saved parameters are characteristic for open-loop control strategies. They have been replaced by a feedback controller, which in turn only introduces a small number of new parameters and recomputes its own feedback gains by means of an adaption law. These new parameters can also be set by the designer in simulation, prior to vehicle testing. Thus, calibration of the adaptive control parameters is not costly.

Note that the additional parameters introduced by the adaptive controller are the same for both the FDCT and NAG3 transmissions. Despite different powertrain architectures, the controller is operational with the same set of parameters. This highlights the adaptive nature of the λ -tracking controller and demonstrates that the control parameters can be determined quickly with the help of simulations.

It is very difficult to assess the costs saved during development by reducing the discussed calibration parameters. No figures are available that express the work load required for calibrating a distinct set of parameters. Thus, the improvement achieved by reducing the number of calibration parameters is unquantifiable. However, if an even distribution of the calibration effort over all parameters is assumed, the work load is reduced by 22.4 % for the FDCT transmission and by 37.5 % for the NAG3 transmission. This constitutes a considerable reduction. Hence, the goal of reducing calibration efforts has been achieved.

6.3 Outlook

There are several aspects of this work that may be continued and modified in future projects regarding adaptive λ -tracking control in powertrain systems.

6.3.1 Adaptive Control Architecture

Various subjects concerning the structure of adaptive controllers may be investigated in the future.

- **MIMO Control Structure**

As discussed in Chapter 4, the focus on SISO control systems for clutch controllers may be insufficient in creating both comfortable and fast gearshift dynamics. The transient reduction or increase of engine torque during a gearshift has to be taken into account. In order to include the engine dynamics into the adaptive clutch control algorithm, a MIMO system design can be investigated. The first step may be to rely on the traditional engine intervention control algorithm while operating the gearshift clutches with the adaptive controller. However, the additional effect of the varying engine torque on the clutch dynamics has to be considered. This may be done by subtracting or adding a control value proportional to the engine intervention control signal.

Also, the second clutch that is active during a gearshift procedure may be incorporated into the control algorithm. This may prove to be another possibility to improve powertrain dynamics and shift quality.

- **Interaction of PID-feedback and Adaption Law Dynamics**

In Chapter 4, the unfavorable counteractive behavior of proportional and integral feedback terms and a fix to this problem has been discussed. However, different approaches may be taken to correct for unfeasible dynamics caused by the adaption law and the integral feedback. For instance, instead of muting the adaption law, it is conceivable to mute the integral feedback term. Thus, an adaptive λ -tracking PD-feedback controller would still be in operation.

It may be advantageous to further investigate the interaction of integral and adaption dynamics. So far, it was shown that the adaption law dynamics should not be dominant over the integral feedback dynamics.

- **Alternative Adaption Laws**

During this work, existing adaption laws proved to be sufficient in reaching the control goals. However, other adaptors are conceivable. If a decoupling of adaption and integral feedback dynamics can be devised, it may be incorporated into a new adaption law and thus avoid the counteracting behavior of proportional and integral feedback terms without the need for a correction term Δ .

- **Adaptive Feed-Forward Control**

The adaptive controller discussed in this thesis is operating without any feed-forward control term. The goal was to reduce calibration efforts, and as a result, no feed-forward control requiring calibration has been included. However, it may be feasible to devise an adaption law that generates a feed-forward control signal based on past gearshifts. Thus, the tracking error may be reduced further and the controller may become more dynamic.

- **Individual adaptive Gain Factors**

Currently, the same common gain factors $k_{1,2}(\cdot)$ are used for every upshift and downshift procedure, respectively. It may be advantageous to save individual gain factors for each individual gearshift in order to account for varying gearshift dynamics. Another possibility is to restart the adaption process from a low value of $k(\cdot)$ at the beginning of each gearshift and thus obtain a unique gain factor every time. This requires fast adaptive behavior while simultaneously achieving smooth control performance. However, the distinction between individually saved gain factors would become redundant.

- **Asymmetrical λ -Neighborhood**

The adaption law is currently designed with a symmetrical λ -strip, i.e., the adaptor does not distinguish between positive and negative values of $e(\cdot)$ regarding the λ -neighborhood. However, it may be useful to incorporate different values of λ relative to the sign of $e(\cdot)$. Thus, it is possible to allow for positive, but not for negative values of the error signal, for example. It is also conceivable to implement different adaptors depending on the sign of the error signal and thus generate individual adaption dynamics.

- **Control Hardware**

As discussed in Chapter 4, the adaptive controller would benefit from a shorter sampling time T of the digital control setup. The derivative feedback term would cause less noise and as a result, the coefficient κ may be increased. This would lead to a stronger damping of the PID-controller and would contribute to the avoidance of oscillations. The advantages of a faster digital controller may be investigated resulting in a recommendation for a future sampling time value.

It is also advisable to conduct extensive vehicle experiments under various environmental conditions, such as extreme temperatures. This way, the adaptive nature of the controller

can be evaluated by determining its ability to react to drastic changes in system parameters. Due to the lack of the required testing facilities, this could not be done in this thesis.

6.3.2 Other Components

The applicability of adaptive λ -tracking control is not limited to the speed control phase during gearshifts. Other possibilities and powertrain components are highlighted here.

- **Other phases during gearshift procedures**

The adaptive controller may be extended to be operated during other gearshift phases, for instance during the torque handover phase. The benefit would be an even further reduced number of calibration parameters.

- **Torque Converter Lock-up Clutch**

The lock-up clutch of the torque converter of the NAG3 transmission may also be outfitted with the adaptive λ -tracking controller to control the transmission input torque and clutch slippage.

- **Vehicle Pull Away Control**

In case of the FDCT transmission, vehicle pull away from standstill is controlled with the help of the clutch K1, that is also used during gearshifts. Hence, it is obvious that vehicle pull away may also be operated with the help of adaptive control. This may also lead to a reduction of calibration parameters for the transmission control software.

- **Engine Start during Hybrid Drive Mode**

Hybrid vehicles are equipped with an additional electric motor to propel the vehicle and recuperate electric energy during braking to be stored in the battery. The combustion engine is shut down as often as possible to maximize fuel saving. Thus, in a hybrid powertrain, the combustion engine has to be restarted frequently while the vehicle is in motion, whenever the power demand surpasses the means of the electric drive. This engine start-up procedure may also be controlled with the adaptive controller discussed in this thesis. However, it is likely that a MIMO system control approach has to be taken in order to implement the simultaneous control of engaging clutch, electric motor and combustion engine to achieve a smooth transition from electric drive mode to hybrid or conventional drive mode.

6.3.3 Evaluation of Calibration Efforts

As discussed above, the impact of the reduction of calibration parameters may be further investigated. One way to determine work load reduction is to analyze two complete calibration processes of the same powertrain: one transmission with the traditional control software and one with the adaptive controller. Then, the hours spent on both projects can be measured and compared and a figure conveying actual cost reduction can be found by assigning an hourly rate.

Also, an investigation of the complete calibration parameter set may reveal parts of the software that contribute disproportionately to the calibration efforts. The modules indicated may be investigated towards the applicability of adaptive control in an attempt to further reduce calibration parameters.

Bibliography

- [ÅsWi 89] ÅSTRÖM, K.J.; WITTENMARK, B.: *Adaptive Control*. Reading: Addison-Wesley, 1989
- [Adam 09] ADAMY, J.: *Nichtlineare Regelungen*. Berlin: Springer, 2009
- [BSEA 08] BAGOT, B.; SCHMIDT, A.; EBNER, T.; ALTENSTRASSER, H.: *Modellbasierte Methodik zur automatisierten Schaltqualitätsoptimierung von Automatikgetrieben*. In: ATZ - Automobiltechnische Zeitschrift (5) 2008, pp. 404 – 411
- [Behn 05] BEHN, C.: *Ein Beitrag zur adaptiven Regelung technischer Systeme nach biologischem Vorbild*. PhD Thesis, Ilmenau: Ilmenau University of Technology, 2005
- [BeLo 12] BEHN, C.; LOEPELMANN, P.: *Adaptive vs. Fuzzy Control of uncertain mechanical Systems*. In: International Journal of Applied Mechanics, 2012
- [BeSt 10] BEHN, C.; STEIGENBERGER, J.: *Experiments in Adaptive Control of Uncertain Mechanical Systems*. In: International Review of Mechanical Engineering (IREME) 4, 2010, pp. 886 – 898
- [BeSt 09] BEHN, C.; STEIGENBERGER, J.: *Improved Adaptive Controllers For Sensory Systems - First Attempts*. In: Modeling, Simulation and Control of Nonlinear Engineering Dynamical Systems, 2009
- [BeZi 06] BEHN, C.; ZIMMERMANN, K.: *Adaptive λ -tracking for locomotion systems*. In: Robotics and Autonomous Systems (54) 2006, pp. 529 – 545
- [Bull 00] BULLINGER, E.: *Adaptive λ -tracking for Systems with Higher Relative Degree*. PhD Thesis, Zurich: Swiss Federal Institute of Technology Zurich, 2000

- [BuAl 00] BULLINGER, E.; ALLGÖWER, F.: *Adaptive λ -tracking for Nonlinear Systems with Higher Relative Degree*. In: 39th IEEE Conference on Decision and Control 2000, pp. 4771 – 4776
- [ChAR 08] CHERNOUSKO, F.L.; ANANIEVSKI, I.M.; RESHMIN, S.A.: *Control of Nonlinear Dynamical Systems*. Berlin: Springer, 2008
- [Crew 07] CREWE, C.M.: *Development tools and techniques for automated transmissions*. SAE Technical Paper Series, 2007
- [Daim 13] *Technical Specifications of the NAG3 Transmission*. Internal Documentation, Daimler AG, 2013
- [Daim 11] *Technical Specifications of the FDCT Transmission*. Internal Documentation, Daimler AG, 2011
- [DGWJ 05] D’ANNA, T.; GOVINDSWAMY, K.; WOLTER, F.; JANSSEN, P.: *Aspects of Shift Quality With Emphasis on Powertrain Integration and Vehicle Sensitivity*. In: SAE 2005 Noise and Vibration Conference 2005
- [DAOGM 92] DOYLE, F.; ALLGÖWER, F.; OLIVIERA, S.; GILLES, E.; MORARI, M.: *On Nonlinear Systems with Poorly Behaved Zero Dynamics*. In: American Control Conference, Chicago 1992, pp. 2571 – 2575
- [DöHI 13] DÖRR, C.; HOMM, M.; INDLEKOFER, G.: *The new automatic transmission 9G-TRONIC from Mercedes-Benz*. In: 12th International CTI Symposium Automotive Transmissions, HEV and EV Drives, Berlin 2013, pp. 153 – 160
- [DrHa 99] DRAGAN, V.; HALANAY, A.: *Stabilization of Linear Systems*. Boston: Birkhäuser, 1999
- [FiJK 12] FISCHER, R.; JÜRGENS, G.; KÜÇÜKAY, F.: *Das Getriebebuch*. Vienna: Springer, 2012
- [Föll 98] FÖLLINGER, O.: *Nichtlineare Regelungen*. Munich: Oldenbourg, 1998
- [Föll 94] FÖLLINGER, O.: *Optimale Regelung und Steuerung*. Munich: Oldenbourg, 1994
- [Förs 91] FÖRSTER, H.J.: *Automatische Fahrzeuggetriebe*. Berlin: Springer, 1991

-
- [GaHS 93] GAUSCH, F.; HOFER, A.; SCHLACHER, K.: *Digitale Regelkreise, Ein einfacher Einstieg mit dem Programm μ LINSY*. Munich: Oldenbourg, 1993
- [GoWE 09] GOVINDSWAMY, K.; WELLMANN, T.; EISELE, G.: *Aspects of NVH Integration in Hybrid Vehicles*. In: SAE International Journal of Passenger Cars - Mechanical Systems 2009, pp. 1396 – 1405
- [Grim 13] GRIMM, J.: *Engine development trends in line with transmission demands*. In: 12th International CTI Symposium Automotive Transmissions, HEV and EV Drives, Berlin 2013, Vol. 2, pp. 245 – 253
- [HaES 08] HACKL, C.M.; ENDISCH, C.; SCHRÖDER, D.: *Funnel-Control in Robotics: An Introduction*. In: 16th Mediterranean Conference on Control and Automation, Ajaccio 2008, pp. 913 – 919
- [HaES 08] HACKL, C.M.; ENDISCH, C.; SCHRÖDER, D.: *Error Reference Control of Nonlinear Two-Mass Flexible Servo Systems*. In: 16th Mediterranean Conference on Control and Automation, Ajaccio 2008, pp. 1047 – 1053
- [IfJe 93] IFEACHOR, E.C.; JERVIS, B.W.: *Digital Signal Processing*. Harlow: Addison-Wesley, 1993
- [Ilch 91] ILCHMANN, A.: *Non-identifier-based adaptive control of dynamical systems: a survey*. In: IMA Journal of Mathematical Control and Information (8) 1991, pp. 321 – 366
- [IlRy 94] ILCHMANN, A.; RYAN, E.P.: *Universal λ -tracking for nonlinearly-perturbed systems in the presence of noise*. In: Automatica (30) 1994, pp. 337 – 346
- [IIsc 07] ILCHMANN, A.; SCHUSTER, H.: *PI-funnel control for two mass systems*. In: IEEE Transactions on Automatic Control, 2007
- [IIPL 97] ILCHMANN, A.; PAHL, M.; LUNZE, J.: *Adaptive regulation of a biogas tower reactor*. In: European Control Conference ECC '97, Brussels 1997
- [IIRS 02] ILCHMANN, A.; RYAN, E.P.; SANGWIN, C.J.: *Tracking with prescribed transient behaviour*. In: ESAIM: Control, Optimisation and Calculus of Variations (7) 2002, pp. 471 – 493
-

- [IoKo 83] IOANNOU, P.A.; KOKOTOVIC, P.V.: *Adaptive Systems with Reduced Models*. In: Lecture Notes in Control and Information Sciences, 1983
- [Isid 95] ISIDORI, A.: *Nonlinear Control Systems*. 3rd ed., Berlin: Springer, 1995
- [Kail 80] KAILATH, T.: *Linear Systems*. Englewood Cliffs: Prentice Hall, 1980
- [Khal 96] KHALIL, H.K.: *Nonlinear Systems*. Upper Saddle River: Prentice Hall, 1996
- [Koch 01] KOCH, J.: *Modellbildung und Simulation eines Automatikgetriebes zur Optimierung des dynamischen Schaltungsablaufs*. PhD Thesis, Stuttgart: University Stuttgart, 2001
- [Kuan 06] KUANG, M.L.: *An Investigation of Engine Start-Stop NVH in a Power Split Powertrain Hybrid Electric Vehicle*. In: 2006 SAE World Congress, Detroit 2006
- [KKAG 09] KÜÇÜKAY, F.; KASSEL, T.; ALVERMANN, G.; GARTUNG, T.: *Effiziente Abstimmung von automatisch schaltenden Getrieben auf dem Rollenprüfstand*. In: ATZ - Automobiltechnische Zeitschrift (3) 2009, pp. 216 – 223
- [LaZ 06] LANDAU, I.D.; ZITO, G.: *Digital Control Systems*. London: Springer, 2006
- [LaKr 10] LANG, K.; KROPINSKI, M.: *Virtual Powertrain Calibration at GM Becomes a Reality*. In: SAE International, 2010
- [LiTr 13] LIBERZON, D.; TRENN, S.: *The Bang-Bang Funnel Controller for Uncertain Nonlinear Systems With Arbitrary Relative Degree*. In: IEEE Transactions on Automatic Control (58) 2013, pp. 3126 – 3141
- [LoBä 13] LOEPELMANN, P.; BÄKER, B.: *High-Gain Feedback Stability of a nonlinear Drivetrain System*. In: European Control Conference ECC, Zurich 2013, pp. 908 – 913
- [LoBä 13] LOEPELMANN, P.; BÄKER, B.: *Aspects of adaptive λ -Tracking Control in Transmission Control Systems*. In: 12th International CTI Symposium Automotive Transmissions, HEV and EV Drives, Berlin 2013
- [LoBä 12] LOEPELMANN, P.; BÄKER, B.: *Towards adaptive Control of nonlinear Drivetrain Systems*. In: SDPS Conference, Berlin 2012

-
- [LoBä 12] LOEPELMANN, P.; BÄKER, B.: *A novel adaptive λ -Tracking Approach for automotive Transmission Control Systems*. In: Automotive Powertrain Control Systems, Berlin 2012, pp. 1 – 16
- [LoBe 11] LOEPELMANN, P.; BEHN, C.: *Various adaptive Control Strategies applied to a bio-inspired Receptor Model*. In: 56th International Scientific Colloquium, Ilmenau 2011
- [Löff00] LÖFFLER, J.: *Optimierungsverfahren zur adaptiven Steuerung von Fahrzeugantrieben*. PhD Thesis, Stuttgart: University Stuttgart, 2000
- [Lunz 10] LUNZE, J.: *Regelungstechnik 2*. Heidelberg: Springer, 2010
- [MaPo 96] MAREELS, I.; POLDERMANN, J.W.: *Adaptive Systems: An Introduction*. Boston: Birkhäuser, 1996
- [MVPI 99] MAREELS, I.; VAN GILS, S.; POLDERMANN, J.W.; ILCHMANN, A.: *Asymptotic Dynamics in Adaptive Gain Control*. In: Advances in Control: Highlights of ECC '99, 1999
- [Meye 11] MEYER, M.: *Signalverarbeitung*. Wiesbaden: Vieweg + Teubner, 2011
- [Mits 97] MITSCHKE, M.: *Dynamik der Kraftfahrzeuge*. Berlin: Springer, 1997
- [NaBL 07] NAUNHEIMER, H.; BERTSCHE, B.; LECHNER, G.: *Fahrzeuggetriebe*. Berlin: Springer, 2007
- [Niva 90] NIJMEIJER, H.; VAN DER SCHAFT, A.J.: *Nonlinear Dynamical Control Systems*. New York: Springer, 1990
- [Nuss 84] NUSSBAUM, R.D.: *Some remarks on a conjecture in parameter adaptive control*. In: Systems & Control Letters (3) 1984, pp. 243 – 246
- [RöBK 12] RÖHRLE, R.; BENTELE, H.; KRAUSS, F.: *Flexible, Configurable Control Unit: Optimization of data calibration*. In: Automotive Powertrain Control Systems, Berlin 2012, pp. 106 – 118
- [RöWa 95] RÖSCH, R.; WAGNER, G.: *Die elektronische Steuerung des automatischen Getriebes W5A 330/580 von Mercedes-Benz*. In: ATZ - Automobiltechnische Zeitschrift (97) 1995, pp. 736 – 748
-

- [ScKB 05] SCHOEGGL, P.; KRIEGLER, W.; BOGNER, E.: *Virtual Optimization of Vehicle and Powertrain Parameters with Consideration of Human Factors*. SAE Technical Paper Series 2005-01-1945, 2005
- [Schr 10] SCHRÖDER, D.: *Intelligente Verfahren - Identifikation und Regelung nichtlinearer Systeme*. Heidelberg: Springer, 2010
- [Schu 09] SCHUSTER, H.: *Hochverstärkungsbasierte Regelung nichtlinearer Antriebssysteme*. PhD Thesis, Munich: Munich University of Technology, 2009
- [Sont 98] SONTAG, E.D.: *Mathematical Control Theory - Deterministic Finite Dimensional Systems*. 2nd ed., New York: Springer, 1998
- [Stef 07] STEFFEN, B.: *Reproduzierbare Schaltpunkte und automatisierte Applikation von Pkw-Getrieben*. In: ATZ - Automobiltechnische Zeitschrift (7) 2007, pp. 632 – 638
- [TiRE 12] TIMMAN, M.; RENZ, M.; EISENHARDT, T.: *Start/Stop-systems and -strategies in conjunction with a 48V-system*. In: Automotive Powertrain Control Systems, Berlin 2012, pp. 215 – 230
- [Unbe 08] UNBEHAUEN, H.: *Regelungstechnik I*. Wiesbaden: Vieweg + Teubner, 2008
- [WiBy 84] WILLEMS, J.C.; BYRNES, C.I.: *Global adaptive stabilization in the absence of information on the sign of the high-frequency gain. Part I: analysis and optimization of systems*. In: 6th International Conference on Analysis and Optimization, 1984, pp. 49 – 57
- [WöBr 05] WÖRN, H.; BRINKSCHULTE, U.: *Echtzeitsysteme*. Berlin: Springer, 2005
- [WUDZ 04] WRONKA, C.M.; UHLMANN, A.; DUNNIGAN, M.W.; ZALZALA, A.M.: *Fast robust controllers for a MITSUBISHI PA-10 manipulator developed under QNX Neutrino*. In: Proceedings of the International Symposium on Robotics, Paris 2004
- [ZhTI 93] ZHAO, Z.; TOMIZUKA, M.; ISAKA, S.: *Fuzzy gain scheduling of PID controllers*. In: IEEE Transactions on Systems, Man and Cybernetics (23) 1993, pp. 1392 – 1398

List of Figures

1.1	Exemplary plot of clutch pressures versus time of a common powered upshift procedure, including some exemplary time constants $t_1 - t_4$ and pressure values $p_1 - p_3$ that are subject to calibration	3
2.1	Closed-loop control structure	10
2.2	Classification of control systems	12
2.3	Principle of λ -tracking	13
2.4	Principle of funnel control with limit functions $\pm \frac{1}{\varphi(t)}$ ([ILSc 07])	18
2.5	Root locus plot of an LTI system with feedback stabilization and different settings for the proportional feedback gain $k(\cdot)$	21
3.1	FDCT dual-clutch transmission ([Daim 11], © by Daimler AG)	30
3.2	NAG3 automatic transmission ([Daim 13], © by Daimler AG)	31
3.3	Clutch control system overview	34
3.4	Hydraulic control valve with inlets and outlets	35
3.5	Hydraulic clutch subsystem	37
3.6	Mechanical clutch subsystem	40
3.7	Splitting the system into a nonlinear and a linear subsystem	47
4.1	Exemplary constrained shift procedure	55
4.2	Release shift procedure	56
4.3	Software-in-the-Loop simulation setup	57
4.4	SiL simulation of exemplary downshift procedures without control initialization in FDCT transmission	59
4.5	SiL simulation of exemplary downshift procedures with control initialization of the integral feedback term in FDCT transmission	60
4.6	SiL simulation of an exemplary adaption of $k(\cdot)$ from 0 to ca. 4000 during upshift procedure with increase coefficient $\gamma = 0.5$	61
4.7	SiL simulation of an exemplary adaption of $k(\cdot)$ from 0 to ca. 0.4 during an upshift procedure, with increase coefficient $\gamma = 5 \cdot 10^{-5}$	62

4.8	SiL simulation of exemplary up- and downshift procedures with standard parameters from Table 4.2, FDCT transmission	65
4.9	Upshifts exhibiting strong control output oscillations due to noise amplification by derivative feedback term, $\kappa = 0.1$	66
4.10	Upshifts without control output oscillations due to reduced derivative coefficient $\kappa = 0.01$	67
4.11	Downshift procedures with integral gain coefficients of $\eta = \{0.1, 1, 2\}$	68
4.12	Upshift (top row) and downshift (bottom row) procedures with $\lambda = \{10, 20, 50\}$	69
4.13	Upshift procedures during vehicle pull away with $\sigma = 0.1$	71
4.14	Upshift procedures during vehicle pull away with $\sigma = 0.2$	71
4.15	Upshift procedures during vehicle pull away with $\sigma = 0.4$	72
4.16	Upshift procedures during vehicle pull away with initialization of common gain factor $k(\cdot)$	73
4.17	Upshift procedures during vehicle pull away with $\gamma = 1 \cdot 10^{-5}$	74
4.18	Upshift procedures during vehicle pull away with $\gamma = 2 \cdot 10^{-5}$	75
4.19	Upshift procedures during vehicle pull away with $\gamma = 4 \cdot 10^{-5}$	75
4.20	Simulation of long downshift procedure from 5th to 4th gear with counteracting proportional and integral feedback terms	77
4.21	Unwanted behavior of counteracting integral and proportional terms (left), and acceptable control behavior (right)	78
4.22	Simulation of downshift procedure from 5th to 4th gear with muted adaption law and no counteracting feedback terms	79
4.23	Simulation of exemplary shifts with fully exponential adaption law, FDCT transmission	83
4.24	Derivative feedback term during shift procedure without (top) and with (bottom) filter (4.41) applied; $\kappa = 1$	88
4.25	Exemplary simulation of traditional shift procedures with discontinuous steps in the set point trajectory $y_{\text{ref}}(\cdot)$	89
4.26	Generation of a C^∞ -continuous reference trajectory $y_{\text{ref}}(\cdot)$ in form of a 3rd-polynomial, with parameters $\omega_S, \dot{\omega}_S, \omega_E, \dot{\omega}_E, t_{\text{dur}}$	90
4.27	Exemplary simulation of adaptively controlled shift procedures with set point trajectory $y_{\text{ref}}(\cdot)$ as 3rd-order polynomial with $t_{\text{dur}} = 0.7\text{ s}$	90
4.28	SiL simulation of adaptively controlled upshifts without engine torque reduction in NAG3 transmission, $p_a = 30\%$	92
4.29	SiL simulation of adaptively controlled upshifts with engine torque reduction in NAG3 transmission, $p_a = 30\%$	94

5.1	Vehicle experimental setup	95
5.2	FDCT: SiL simulation of ①→②→③→④ maneuver, traditional control . . .	97
5.3	FDCT: Vehicle experiment of ①→②→③→④ maneuver, traditional control	98
5.4	FDCT: SiL simulation of ④→③→④→③→④ maneuver, traditional control .	99
5.5	FDCT: Vehicle experiment of ④→③→④→③→④ maneuver, traditional control	100
5.6	FDCT: SiL simulation of ⑤→④→⑤→④→⑤ maneuver, traditional control .	101
5.7	FDCT: Vehicle experiment of ⑤→④→⑤→④→⑤ maneuver, traditional control	101
5.8	FDCT: SiL simulation of ①→②→③→④ maneuver, adaptive control	102
5.9	FDCT: Vehicle experiment of ①→②→③→④ maneuver, adaptive control .	103
5.10	FDCT: SiL simulation of ④→③→④→③→④ maneuver, adaptive control . .	104
5.11	FDCT: Vehicle experiment of ④→③→④→③→④ maneuver, adaptive control	105
5.12	FDCT: SiL simulation of ⑤→④→⑤→④→⑤ maneuver, adaptive control . .	106
5.13	FDCT: Vehicle experiment of ⑤→④→⑤→④→⑤ maneuver, adaptive control	107
5.14	FDCT: SiL simulation of ①→②→③→④ maneuver, adaptive control with $t_{dur,1} = 0.7\text{ s}$	110
5.15	FDCT: Vehicle experiment of ①→②→③→④ maneuver, adaptive control with $t_{dur,1} = 0.7\text{ s}$	110
5.16	FDCT: SiL simulation of ①→②→③→④ maneuver, adaptive control with $t_{dur,1} = 0.5\text{ s}$	111
5.17	FDCT: Vehicle experiment of ①→②→③→④ maneuver, adaptive control with $t_{dur,1} = 0.5\text{ s}$	111
5.18	FDCT: SiL simulation of ⑦→⑥→⑤→④ maneuver, traditional control . . .	112
5.19	FDCT: Vehicle experiment of ⑦→⑥→⑤→④ maneuver, traditional control	112
5.20	FDCT: SiL simulation of ⑦→⑥→⑤→④ maneuver, adaptive control with $t_{dur,2} = 1\text{ s}$	113
5.21	FDCT: Vehicle experiment of ⑦→⑥→⑤→④ maneuver, adaptive control with $t_{dur,2} = 1\text{ s}$	113
5.22	FDCT: SiL simulation of ⑦→⑥→⑤→④ maneuver, adaptive control with $t_{dur,2} = 0.7\text{ s}$	114
5.23	FDCT: Vehicle experiment of ⑦→⑥→⑤→④ maneuver, adaptive control with $t_{dur,2} = 0.7\text{ s}$	114
5.24	NAG3: SiL simulation of ①→②→③→④ maneuver, traditional control . . .	116
5.25	NAG3: Vehicle experiment of ①→②→③→④ maneuver, traditional control	117
5.26	NAG3: SiL simulation of ④→③→④→③→④ maneuver, traditional control .	118

5.27	NAG3: Vehicle experiment of ④→③→④→③→④ maneuver, traditional control	119
5.28	NAG3: SiL simulation of ⑤→④→⑤→④→⑤ maneuver, traditional control .	119
5.29	NAG3: Vehicle experiment of ⑤→④→⑤→④→⑤ maneuver, traditional control	120
5.30	NAG3: SiL simulation of ①→②→③→④ maneuver, adaptive control	121
5.31	NAG3: Vehicle experiment of ①→②→③→④ maneuver, adaptive control .	122
5.32	NAG3: SiL simulation of ④→③→④→③→④ maneuver, adaptive control . .	123
5.33	NAG3: Vehicle experiment of ④→③→④→③→④ maneuver, adaptive control	124
5.34	NAG3: SiL simulation of ⑤→④→⑤→④→⑤ maneuver, adaptive control . .	125
5.35	NAG3: Vehicle experiment of ⑤→④→⑤→④→⑤ maneuver, adaptive control	126
5.36	NAG3: SiL simulation of ①→②→③→④ maneuver, adaptive control, $t_{dur,1} = 0.5$ s	128
5.37	NAG3: Vehicle experiment of ①→②→③→④ maneuver, adaptive control, $t_{dur,1} = 0.5$ s	129
5.38	NAG3: SiL simulation of ①→②→③→④ maneuver, adaptive control, $t_{dur,1} = 0.3$ s	129
5.39	NAG3: Vehicle experiment of ①→②→③→④ maneuver, adaptive control, $t_{dur,1} = 0.3$ s	130
5.40	NAG3: SiL simulation of ⑧→⑦→⑥→⑤→④ maneuver, traditional control .	130
5.41	NAG3: Vehicle experiment of ⑧→⑦→⑥→⑤→④ maneuver, traditional control	131
5.42	NAG3: SiL simulation of ⑧→⑦→⑥→⑤→④ maneuver, adaptive control, $t_{dur,2} = 0.3$ s	131
5.43	NAG3: Vehicle experiment of ⑧→⑦→⑥→⑤→④ maneuver, adaptive control, $t_{dur,2} = 0.3$ s	132
5.44	NAG3: SiL simulation of ⑧→⑦→⑥→⑤→④ maneuver, adaptive control, $t_{dur,2} = 0.2$ s	132
5.45	NAG3: Vehicle experiment of ⑧→⑦→⑥→⑤→④ maneuver, adaptive control, $t_{dur,2} = 0.2$ s	132
5.46	FDCT: SiL simulation of ⑤→④→③ maneuver, traditional control	134
5.47	FDCT: Vehicle experiment of ⑤→④→③ maneuver, traditional control . . .	134
5.48	FDCT: SiL simulation of ⑤→④→③ maneuver, adaptive control	135
5.49	FDCT: Vehicle experiment of ⑤→④→③ maneuver, adaptive control	136

List of Tables

3.1	Gearshift pattern of FDCT transmission	30
3.2	Gearshift pattern of NAG3 transmission	32
3.3	Sign of high-frequency gain	50
4.1	Classification of shift procedures	53
4.2	Standard set of adaptive control parameters	64
4.3	Adaptive control parameters for fully exponential adaption law	82
5.1	Comparison of shift duration for FDCT transmission	108
5.2	Comparison of up- and downshift duration for FDCT transmission	115
5.3	Comparison of shift duration for NAG3 transmission	127
5.4	Comparison of up- and downshift duration for NAG3 transmission	133
6.1	Number of calibration parameters	140

Acknowledgments

This thesis is the result of a three-year doctoral program at Daimler AG, Stuttgart, in cooperation with the Dresden Institute of Automobile Engineering (IAD) at Technische Universität Dresden. I would like to thank Univ.-Prof. Dr.-Ing. Bernard Bäker for his helpful remarks and for his thesis supervision.

Many friends and colleagues supported me, and I owe thanks to all of you. This work would not have been possible without you.

First of all, I would like to thank Mario Ott. His knowledge of automatic transmissions and transmission control software as well as his support during vehicle experiments provided invaluable help. I also thank my colleagues Bernd Boehmer, Patrick Damm, Nils Hirsemann and Daniel Schindler for their help in understanding the intricacies of transmission control software and my colleague Brian Douglas for his support in software generation. I thank Dr. Josef Steuer and Dr. Markus Kern for giving me the opportunity to work on this project at the department Hybrid-e-System at Daimler AG.

I would also like to thank Prof. Dr.-Ing. Stefan Halfmeier at Mannheim University of Applied Sciences for his profound insights into automotive engineering and for his interest in my work.

Special thanks go out to PD Dr.-Ing. habil. Carsten Behn at Ilmenau University of Technology for his continued interest in my research in adaptive control and for his fruitful remarks and discussions. His very high standards of scientific research have influenced me throughout the years of this thesis and I will continue to try to live up to them in the future.

A very big thank you goes to my girlfriend Julia, who kept me engaged and motivated and I thank her for being patient with me during stressful times.

Last but not least, I would like to thank my family and my friends Mirko and Ralf for their mental support.

”There is nothing so practical as a good theory.” – Kurt Lewin